Ex vivo gene therapy for β-hemoglobinpathies and metabolic disorders

Marine Laurent

THESE DE DOCTORAT

NNT : 2023UPASL006

université PARIS-SACLAY

Ex vivo gene therapy for β-hemoglobinopathies and metabolic disorders

Thérapie génique ex vivo pour les β-hémoglobinopathies et les maladies métaboliques

Thèse de doctorat de l'université Paris-Saclay

École doctorale n° 577, Structure et dynamique des systèmes vivants (SDSV)

Spécialité de doctorat : Biologie moléculaire et cellulaire

Graduate School : Life science and Health

Référent : Université d'Evry Val d'Essonne

Thèse préparée dans l'unité de recherche **Integrare research unit UMR_S951 (Université Paris-Saclay, Univ Evry, Inserm, Généthon)**, sous la direction du docteur **Mario Amendola, Chargé de recherche**

Thèse soutenue à Paris, le 16 février 2023, par

Marine LAURENT

Composition du Jury

Membres du jury avec voix délibérative

Sylvain FISSON Professeur des Universités, INSERM, Université d'Evry	Président du Jury
Erika BRUNET Directrice de recherche, INSERM, Imagine	Rapportrice & Examinatrice
Dagmar KRATKY Professeur des Universités, Institut de biologie moléculaire et de biochimie, Université médicale de Graz	Rapportrice & Examinatrice
Alessia CAVAZZA Chargée de recherche, Collège universitaire de Londres	Examinatrice

ABSTRACT

université PARIS-SACLAY | ÉCOLE DOCTORALE Structure et dynamique des systèmes vivants (SDSV)

Title : *Ex vivo* gene therapy for β-hemoglobinopathies and metabolic disorders

Keywords : β-hemoglobinopathies, lysosomal acid lipase deficiency, gene therapy, CRISPR-Cas9, HBA platform

Abstract : Monogenic disorder are inherited mutation(s) in a single gene that result in abnormal protein synthesis impairing normal cellular homeostasis and organ function that reduces patient life-pan. Recently autologous transplantation of genetically corrected patient's hematopoietic stem cells (HSCs) defined as *ex vivo* gene therapy (GT) has emerged as a promising curative approach for such genetic diseases. In *ex vivo* GT, targeted integration of a therapeutic transgene into a tolerant and safe locus appears to be a powerful approach to produce the therapeutic protein above physiological level in a broad type of hematopoietic cells using endogenous promoter (Morgan et al., 2017; Naldini, 2019). Such genome editing strategy relies on DNA double-strand break and delivery of a functional copy of the mutated gene in the locus of interest. Here, we exploited the α-globin locus (HBA) as a safe harbor locus for transgene integration to develop a universal platform for expression and secretion of therapeutic proteins into erythroid cells. In HSCs, we induced double-strand breaks (DSBs) in HBA locus with CRISPR-Cas9 and delivered a therapeutic transgene using AAV-6 to target integration by homology directed repair. Due to the abundance of erythroid cells in human ($5X10^6$ RBCs/microliter of blood) and the high HBA expression in erythroid population (around 1,5g/day), the HBA platform would require minimal transgene integration events in HBA locus to provide sufficient amount of therapeutic proteins reducing as consequence the potential off-target and toxicity due to editing and DNA donor delivery.

First, we applied the HBA platform for β-thalassemia : a genetic condition impairing the hemoglobin formation and triggering toxic α-globin chain precipitation. The genetic correction of β-thalassemia using our HBA platform results in 1 copy of α-globin gene deletion decreasing the α-globin chain precipitation while β-globin gene integration into HBA locus restore the normal hemoglobin formation. Then, we evaluated the HBA platform for erythroid-specific secretion of therapeutic proteins into bloodstream and, in particular,we focused on a genetic metabolic disorder: lysosomal acid lipase (LAL) deficiency caused by LIPA gene mutation(s) that lead to toxic lipid accumulation especially in liver. We achieved efficient expression and secretion of LAL enzyme that retained enzymatic activity and cross-corrected the lipid accumulation in patients' fibroblasts. We then focused on the optimization of LIPA cDNA transgene using lentiviral vectors (LVVs) to maximize the LAL expression and secretion. The optimized LIPA transgene will serve for LVV-based *ex vivo* GT and for our HBA targeted platform in the purpose of enhancing the LAL expression while minimizing the targeting integration events required to fully correct the disorder. Finally, to better characterize LAL-D phenotype and to evaluate the therapeutic potency of our GT strategy, we set-up a multimodal cytometry approach using flow cytometry and image flow cytometry. We evaluated this pipeline on mainly patient's fibroblasts and on peripheral mononuclear blood mononuclear cells (PBMCs) for LAL-D mouse model.

université PARIS-SACLAY
ÉCOLE DOCTORALE
Structure et dynamique des systèmes vivants (SDSV)

Titre : Thérapie génique *ex vivo* pour les β-hémoglobinopathies et les maladies métaboliques

Mots clés : β-hémoglobinopathies, déficience en lipase acide lysosomale, thérapie génique, CRISPR-Cas9, platforme HBA

Résumé : Les maladies monogéniques sont des mutations héréditaires d'un seul gène qui entraînent une synthèse anormale de protéines, altérant l'homéostasie cellulaire normale et la fonction des organes et réduisant la durée de vie des patients. Récemment, la greffe autologue de cellules souches hématopoïétiques (HSCs) de patients génétiquement corrigés appelée thérapie génique (TG) *ex vivo*, est apparue comme une approche curative prometteuse pour ces maladies. Dans la TG *ex vivo*, l'intégration ciblée d'un transgène thérapeutique dans un locus tolérant apparaît comme une approche puissante pour produire les protéines thérapeutiques à un niveau supérieur au niveau physiologique dans un large type de cellules hématopoïétiques en utilisant un promoteur endogène. Une telle stratégie d'édition du génome repose sur la cassure double brin d'ADN et la livraison d'une copie fonctionnelle du gène muté dans le locus d'intérêt. Ici, nous avons exploité le locus de l'α-globine (HBA) comme un locus tolérant pour l'intégration de transgènes afin de développer une plateforme universelle pour l'expression et la sécrétion de protéines thérapeutiques par les globules rouges (GR). Dans les HSCs, nous avons induit des cassures double brin dans le locus HBA avec CRISPR-Cas9 et délivré un transgène thérapeutique en utilisant un AAV-6 pour cibler l'intégration par réparation dirigée par l'homologie. En raison de l'abondance des globules rouges chez l'homme ($5X10^6$ globules rouges/microlitre de sang) et de la forte expression de HBA dans cette population (environ 1,5g/jour), la plateforme HBA nécessiterait un minimum d'événement d'intégration du transgène pour fournir une quantité suffisante de protéines thérapeutiques, réduisant ainsi les risques de toxicité et d'édition non spécifique induit par CRISPR-Cas9 ou l'AAV6.

Dans un premier temps, nous avons appliqué la plateforme HBA à la β-thalassémie : une condition génétique altérant la formation de l'hémoglobine (composé de 2 α-globine et 2 β-globine) et déclenchant la précipitation toxique de la chaîne α-globine. La correction génétique de la β-thalassémie à l'aide de notre plateforme HBA entraîne la délétion d'une copie du gène de l'α-globine, ce qui diminue la précipitation de cette chaîne, tandis que l'intégration du gène de la β-globine dans le locus HBA rétablit la formation normale d'hémoglobine. Ensuite, nous avons évalué la plateforme HBA pour la sécrétion spécifique de protéines thérapeutiques par les GRs dans la circulation sanguine et, en particulier, nous nous sommes concentrés sur un trouble métabolique génétique : la déficience en lipase acide lysosomale (LAL) causée par une ou plusieurs mutations du gène LIPA qui entraînent une accumulation toxique de lipides, notamment dans le foie. Nous avons obtenu une expression et une sécrétion efficaces de l'enzyme LAL qui a conservé son activité enzymatique et corrigé l'accumulation de lipides dans les fibroblastes des patients. Nous nous sommes ensuite concentrés sur l'optimisation du transgène LIPA en utilisant des vecteurs lentiviraux (LVVs) pour maximiser l'expression et la sécrétion de la LAL. Le transgène LIPA optimisé servira à développer une TG *ex vivo* basée sur les LVVs et à notre plateforme ciblée HBA dans le but d'améliorer l'expression de LAL tout en minimisant les événements d'intégration nécessaires pour corriger complètement la maladie. Enfin, pour mieux caractériser le phénotype la déficience en LAL et évaluer le pouvoir thérapeutique de notre stratégie de GT, nous avons mis en place une approche de cytométrie multimodale utilisant la cytométrie en flux et la cytométrie en flux d'images. Nous avons évalué ces techniques principalement sur les fibroblastes du patient et sur les cellules mononucléaires du sang périphérique (PBMCs) provenant de souris déficiente en LAL.

ACKNOWLEDGEMENT

I would like to thank my thesis jury members: **Dr. Dagmar Kratky** and **Dr. Erika Brunet** for examining my manuscript and providing their expertise on gene therapy and metabolism impairment in lysosomal acid lipase deficiency and **Pr. Sylvain Fisson** and **Dr. Alessia Cavazza** for being my thesis examiner. Thanks also to my thesis committee: **Dr. Annarita Miccio** and **MD-PhD François-Xavier Mauvais** for their helps and advice along my thesis journey. I would like to express my gratitude to my thesis supervisor, **Dr. Mario Amendola**, for his continuous support during my thesis, the confidence and freedom that he provides me along my time at Genethon.

I want to thank now the present and past Gene editing team members that permit by a way or another my thesis fulfilment. Thank to **Dr. Giulia Pavani** for her patience, enthusiasm, and motivation. I want to thank my former officemate **Fatima Amor** for her help and advises along my thesis, but even more for being a source of motivation and energy through all our talking, eating and evening. Big thanks to the LAL teams : **Christine Jenny** for her goodwill, constant backing and her good advices (scientific or not) during my master internship and my thesis; **Sarah Bayol** for her involvement in LAL project, her dynamism and genuineness; **Laurie Lacombe** for her flexibility, her enthusiasm and for being a support on the LAL development. I wish for both of you the best for your theses. **Anna Fabiano**, thanks you for being my teammate after the Lockdown and for all your support in the beginning of my thesis. **Dr. Alexandra Tachtsidi** and **Dr. Fetta Mazed**, I want to thank you for all our discussions and shared moments that I am sure will continue. **Dr. Davide Monteferrario** for your trust in the first place and for your scientific legacy that you transmit during my master internship. **Abdel Tounsi,** thanks you for being such a kind and smiling person. **Margaux Mombled**, **Maelle Ralu, Dr. Simon Guiraud** and **Aboud Sakkal** thanks you for the discussions and encouragements between 2 experimentations and lunch time.

During my time at Genethon, I meet great persons that make all this work possible. I would like

to thank **Dr. Jérémie cosette** for help on microscopy and Imagestream acquisition and analysis, but even more for his patience, his pedagogy as well as for imagering or piano or aromatherapy. I want to thank **Peggy Sanatine** for the complete formation and constant support on flow cytometer as well as your kindness along my Genethon experience. A big thanks to **Dr.Celine Rocca** and **Maxime Ferrrand** for their time and advices on HSCs transplantation, you have brought me closer to the goal ! I want to acknowledge the Bioexperimentation teams: **Dr. Nathalie Daniele**, **Laetitia Van Wittenberghe**, **Adeline Miranda**, **Beatrice Moreau,** and **Rayane Hamadache** for all their supports, advice, time, and experimentation that they invest on the project and on me. Thank to viral production team: **Guillaume Dubreuil** and **Noémie Pinault** to provide us all the vectors needed for the project. Thanks to the IMF's team: **Dr. Giuseppe Ronzitti**, **Dr. Tiziana La Bella**, **Pauline Vidal**, **Dr. Fanny Collaud**, **Dr. David-Alexandre Gross,** and **Dr. Berangère Bertin** you have been a precious for help along my thesis cruises!

Finally, I want to thank **Dr. Célia Sourd** for all these 5 years of adventures and shared moments. You have been all along these years a constant boost source. Thanks to **Pierre-Romain Le Brun** for having challenged my liver and for all our hallway chats. Big dedication to my "Chagoles" : **Ieva, Heloise, Julie** & **Marion** for all our playing and discussions nights, you make the lock-down supportable ! I want to thank **Fantin** for all our shares on the thesis journey and for your constant suggestion of taking vacation! More seriously, thanks you have been there when I doubted, I wishes you the best for the future. Thanks to my oldest friend, **Elisa** for being on me side since the beginning and making me a happiness godmother. Last but not least, I want to thank **Amine** for having open me to new culture, for his constant trust and communicative joy (except when you are playing FIFA).

Mes derniers et les plus importants remerciements reviennent à ma famille et particulièrement à mes parents, sans vous rien n'aurait été possible. Merci d'avoir cru en moi, de m'avoir soutenu pendant toutes ces années et m'avoir laissé réaliser mon rêve. Vous êtes mes supporteurs et sponsors officielles de la première heure, promis cette fois c'est fini les études.

Table of contents

Table of figures

Content of tables

ABBREVIATIONS :

A

AAV : Adeno-associated vectors
AAVS1 : AAV integration site 1
AAP : Assembly activated protein
ABE : Adenine base editors
ADA-SCID : Adenosine deaminase deficiency severe combined immunodeficiency
ALB : Albumin
ARSA : Arylsulfatase A
AS3 : Anti-sickling β-globin

B

BCL11A : B cell lymphoma/leukemia 11A
BE : Base editor
BFU-E : Blast-forming unit-erythroid
BM: Bone marrow
Bp : Base pairs

C

CBE : Cytosine base editor
CD : Cluster of differentiation
cDNA : Complementary DNA
CE : Cholesterol ester
CESD : Cholesterol ester storage disorder
CFU : Colony-forming unit
CFU-E : Colony-forming unit-erythroid
CFU-GEMM : Multipotential colony-forming unit
cHS4 : Chicken β-globin HS4
CMP : Common myeloid progenitor
CNS : Central nervous system
CRISPR-Cas : Clustered regularly interspaced short palindromic repeats (CRISP) associated (Cas) protein
crRNA : CRISPR RNA
CXCR4 : CXC chemokine receptor type 4

D

dCas9 : Dead Cas9
DDR : DNA damage response
DNA : Deoxyribonucleic acid
Ds : Double-strand
DSB : Double-strand break

E

EF : Elongation factor
EPO : Erythropoietin
ER : Endoplasmic reticulum
ERT : Enzyme replacement therapy

F

FA : Fatty acid
FC : Free cholesterol
FDA : Food and Drug Administration
FFA : Free fatty acid
Flt3 : Fms-like tyrosine kinase receptor 3

G

GAA : Acid α-glucosidase
GAG : Glycosaminoglycan
GAVHD : Graft-versus-Host disease
G-CSF : Granulocyte colony-stimulation factor
GLA : α-Galactosidase A
GMP : Granulocyte-monocyte progenitor
gRNA : Guide RNA
GT : Gene therapy

H

HA : Homology arm
Hb : Hemoglobin
HbA : Adult hemoglobin
HBA : α-globin gene
HBB : β-globin gene
HbF : Hemoglobin fetal
HbS : Hemoglobin S
HDAd5/35 ++ : Helper-dependent adenovirus
HDL : High-density lipoprotein
HDR : Homology-directed repair
HiFi : High Fidelity
HITI : Homology-independent targeted integration
HIV : Human immunodeficient virus
HMGA2 : High mobility group AT hook 2
HPFH : Hereditary persistence of fetal hemoglobin

HPLC : High-performance liquid chromatography
HRE : Heme Responsive Elements
HS : Hypersensitive site
HSCs : Hematopoietic stem cells
HSCT : Hematopoietic stem cells transplantation
HSPCs : Hematopoietic stem and progenitor cells
HUDEP-2 β0 : β-thalassemic HUDEP-2

I

IDL : Intermediated density lipoprotein
IdLV : Integration-defective lentiviral vector
IDUA : α-L-Iduronidase
IEM : Inborn error of metabolisms
IFC: Image flow cytometry
IL-3 : Interleukine-3
Indels : Integrations and/or deletions
ITR : Inverted terminal repeat

K

Kda : Kilodalton
KI : Knock-in
KO: Knock-out

L

LAMP : Lysosome-associated membrane protein
LAL : Lysosomal acid lipase
LAL -/- : LAL KO mouse
LAL-D : LAL-deficiency
LCR : Locus controlling region
LD : Lipid droplet
LDL : Low density lipoprotein
LDLR : Low-density lipoprotein receptor
LG : Lysogreen
LIPA : Lipase A gene
LSD : Lysosomal storage disorders
LSK : Lin- Sca-1+ c-kit+
LPL : Lipoprotein lipase
LT-HSCs : Long-term HSCs
LTR : Long terminal repeat
LVV : Lentiviral vector
LYNUS : Lysosomal nutrient-sensing machinery
γ-RV : γ-retroviral vector

M

MCOLN1 : Mucolipin 1
MDSCs : Myeloid derived suppressor cells
MEP : Megakaryocyte erythroid progenitor
MLD : Metachromatic leukodystrophy
MLV : Murine Leukemia virus
MMEJ : Microhomology-mediated end joining
MPP : Multipotent progenitor
M6P : Mannose 6 phosphate
M6P-R : Mannose 6-phosphate receptor
MSP : Mucopolysaccharidoses
mTOR : Mammalian target of rapamycin

N

nCas9 : Nickase Cas9
NHEJ : Non-homologous end joining
NR : Nile Red
Nts : Nucleotides

O

0_2 : Oxygen
ODN : Oligodeoxynucleotides

P

PAM : Protospacer adjacent motif
PB : peripheral blood
PBMCs : Peripheral blood mononuclear cells
PBS : Phosphate-buffered saline
PE : Prime editor
pegRNA : Prime editing guide RNA
PES : Polyethersulfone
PGK : Phosphoglycerate kinase promoter
PIC : Pre-integration complex
PITCH : Precise integration into target chromosome
PRT : Protein replacement therapy

R

rAAV : Recombinant AAV
RBCs : Red blood cells
RNA : Ribonucleic acid
RNP : Ribonucleoprotein
RT : Reverse transcription
RV : Retrovirus

RVD : Repeat Di-residues

S

scAAV : Self-complementary AAV
SCD : Sickle cell disease
SCF : Stem cell factor
SCID-X : X-linked severe combined immunodeficiency
SDF-1 : Stromal cell derived factor 1
SFSV : Spleen focus forming virus
SGSH : Sulfamidase
SH-HSCs : Short-term HSCs
SIN : Self-inactivated
Sp : *Streptococcus pyogenes*
SREBP : Sterol regulatory-element binding protein
SRT : Substrate reduction therapy
Ss : Single strand
ssAAV: Single stranded AAV
SSC : Side scatter
ssODN : Single stranded
ODN

T

TALE : Transcription activator–like effector
TALEN : Transcription activator–like effector nuclease
TG : Triglyceride
TPO : Thrombopoietin
TracRNA : Transactivating-CRISPR RNA
TSS : Transcription site

U

UTR : Untranslated region

V

VLDL : Very-low density lipoprotein
VSV-G : Vesicle vesicular stomatitis virus

W

WB : Western Blot
WBCs : White blood cells
WD : Wolman disease

Z

ZFN : Zing-finger nuclease
ZFP : Zinc finger protein

Introduction

1 *EX VIVO* GENE THERAPY TO TREAT MONOGENIC DISORDER

Gene therapy (GT) is defined as a genetic modification -introduction, removal, or change- into patient genome in the attempts to treat or cure a disease, e.g. either correct a genetic defect in inherited disorders or activate the immune response for cancer therapy. The two main GT approaches are: i) *ex vivo* GT that consists in genetic correction/modification of patient's hematopoietic stem or differentiated blood cells, such as T lymphocytes, outside the body and their transplantation back into patients; ii) *in vivo* GT that relies on the direct injection into patient's body of vectors encoding the therapeutic sequence (Alnasser, 2021). Nowadays, GT is applied for a wide range of monogenic disorders from metabolic diseases to neuromuscular diseases (Figure 1) (Arabi et al., 2022).

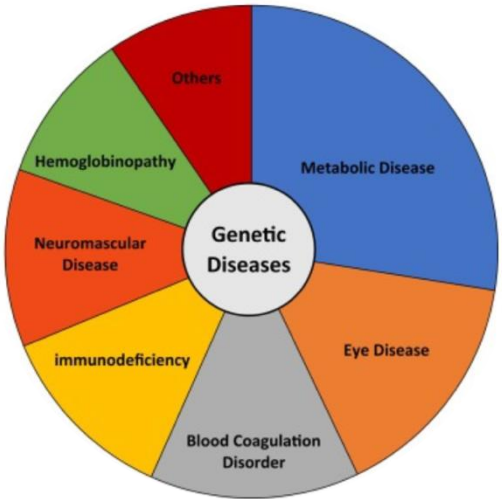

Figure 1) Representation of monogenic disease treated with gene therapy in clinical trials from 2010 to 2020 (Arabi et al., 2022).

1.1 LENTIVIRAL-BASED *EX VIVO* GENE THERAPY FOR MONOGENIC DISORDER

1.1.1 Monogenic disorder

Monogenic disorders are rare inherited mutations in a single gene leading to morbidity and reduce patient lifespan. While the description of hereditary phenotype began in XIX century by Mendel (Mendel, 1886) providing the first basis for genetics, it is only upon double-strand deoxyribonucleic acid (DNA) discovery by Watson & Crick in XX century (Watson and Crick, 1953) that precise hereditary unit called gene was described as coding protein region involved in the normal cellular

function. Now, around 5000-8000 monogenic diseases have been identified including cysticfibrosis, sickle cells anemia, Duchenne muscular dystrophy … (Prakash et al., 2016). All these disorders result in abnormal protein synthesis that impairs normal cellular homeostasis and organ function. The understanding and treatment of monogenic disorders have been the subject of major scientific research over the past decade. The development of genome sequencing allows to identify the mutated gene(s) and therefore the impaired cellular mechanism. Overtime therapeutic options have been developed to counterbalance the morbidity phenotype as organs transplantation, blood transfusion or allogenic hematopoietic stem cells transplantation (HSCTs). HSCTs shown successful disease management improving the life quality or lifespan in a wide broad of monogenic disorders such as hemoglobinopathies and metabolic disorders. The treatment involves replacing the patient's own hematopoietic stem cells (HSCs) with healthy cells from a donor (Copelan, 2006). HSCs are multipotent cells able to reconstitute a healthy blood system that can deliver the missing proteins to the affected tissues (Figure 2). In human, hematopoietic stem and progenitor cells (HSPCs) are located in bone marrow (BM) microenvironment called niches. The BM niche offers the proper environment for HSCs differentiation or self-renew. HSPCs are composed of long-term HSCs (LT-HSCs), short-term HSCs (ST-HSCs) and multipotent progenitor (MPP) (Figure 2). The LT-HSCs are the multipotent stem cells able to generate all the blood-lineage population : white bloods cells (WBCs) as myeloid and lymphoid lineages, red blood cells (RBCs) and platelets, and of self-renewing their own population. Whereas ST-HSCs and MPP have differential potential but no self-renewal capacity (Skulimowska et al., 2021; Hawley et al., 2006).

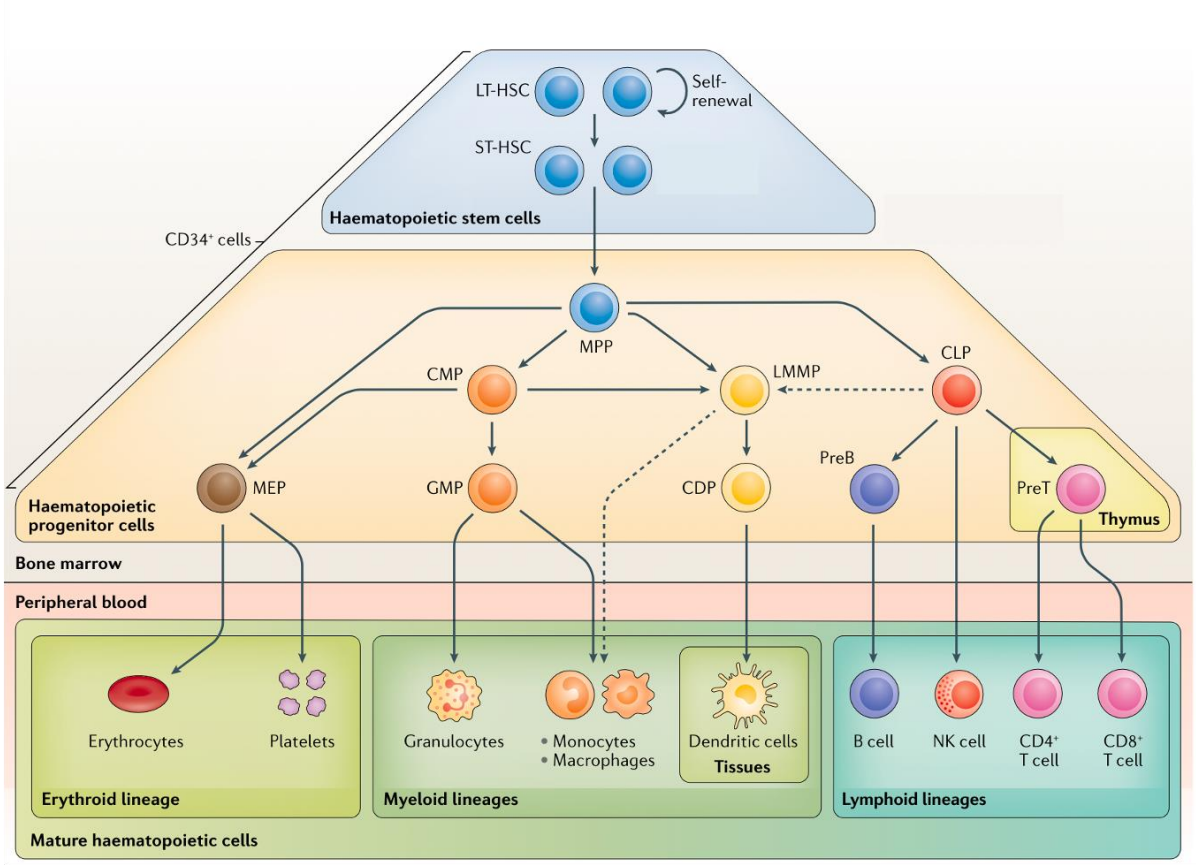

Figure 2) HSCs are located in BM niche and divided in LT-HSC, ST-HSC and MPP able to provide the entire blood cells. LT-HSC is the only HSCs population able to self-renew (adapted from G. Ferrari et al., 2021).

Although therapeutic for some monogenic disorders, HSCTs are limited by availability of suitable donor and the immune reaction induced by donor lymphocytes against the recipient (Graft-versus-host disease, GAVHD) (Skulimowska et al., 2021; Hawley et al., 2006). Recently autologous transplantation of genetically corrected patient's HSCs defined as *ex vivo* GT has emerged as a promising curative alternative. In fact, *ex vivo* GT bypasses the requirement of a well-matched donor and therefore provides the potential to treat virtually all patients (Morgan et al., 2017).

1.1.2 Principle of *ex vivo* gene therapy

In *ex vivo* GT, patient's own HSCs are recovered and isolated from peripheral blood (PB) or BM (Figure 3.1-3, described in Introduction Part 1.1.3), genetically modified (Figure 3.4, described in Introduction Part 1.2) and transplanted back into patients (Figure 3.5, described in Introduction Part 1.1.4). Upon engraftment, modified HSCs will be able to restore healthy hematopoietic system that can produce the therapeutic proteins above physiological level in a broad type of hematopoietic cells from WBCs (lymphocytes, monocytes, natural killer cells), platelets and RBCs (Morgan et al., 2017; Naldini, 2019). Correction of HSCs can take different forms from the insertion of a functional copy of mutated gene (described in Introduction Part 1.1.5) to the editing of the underlaying mutation(s) using nuclease (described in Introduction Part 1.2). Both strategies involve modification of patient's HSCs genome and require the transport of DNA sequence into the nucleus using viral vector as retrovirus (described in Introduction Part 1.1.5) or non-viral-vectors as nanoparticle (described in Introduction Part 1.2.4).

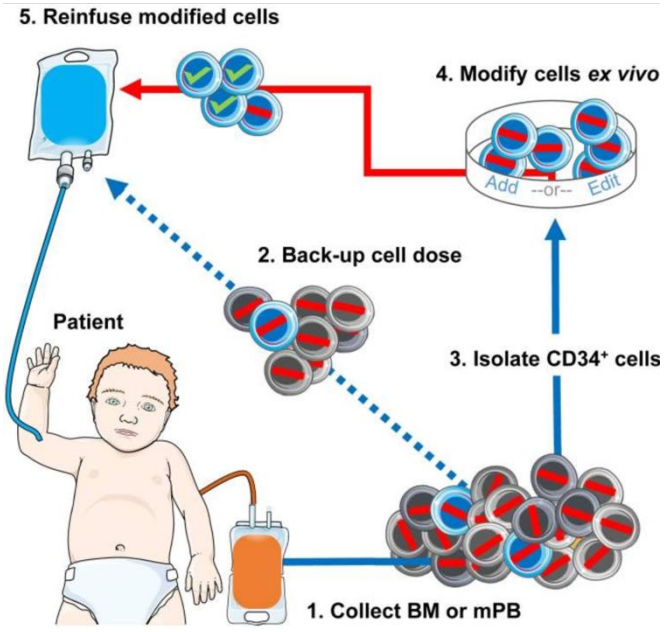

Figure 3) Principle of gene therapy (adapted from Morgan et al., 2017). Patient's HSCs are collected, isolated, and corrected prior re-transfusion

Nowadays, *ex vivo* GT is under clinical evaluation for a wide range of genetic disorders as metabolic disorders or hemoglobinopathies (Arabi et al., 2022).

1.1.3 Recovering and culturing of HSCs

Originally, HSCs were harvested directly from the patient's BM in the iliac crests by syringe aspiration, but the amount of cells recovered was small and the process was quite painful and could lead to infections. This technique is now only used in case of poor mobilization by chemical agents. Nowadays, HSCs harvesting is mainly performed via leukapheresis after HSCs PB mobilization with chemical agents as granulocyte colony-stimulation factor (G-CSF) and/or Plerixafor. G-CSF is a pro-inflammatory cytokine that promotes the maturation and proliferation of myeloid stem cells as well as their migration from BM into the blood (Morris et al., 2014). Although, G-CSF enhances by 6-7 fold the HSCs cells in circulation (Grigg et al., 1995), it appears to be ineffective for 5-30% of patient (Skulimowska et al., 2021). The combination of Plerixafor and G-CSF enhances the mobilization compared to the single used of G-CSF by 10-fold and becomes a gold standard protocol of HSCs mobilization. Plerixafor (as called ADM3100) is a selective inhibitor of CXC chemokine receptor 4 (CXCR4) receptors preventing the binding of its ligand the stromal derived cell factor 1 (SDF-1) produced by BM stromal cells to retain HSCs in the niches. Therefore, blocking the SDF-1/CXCR4 axis facilitates the migration of HSCs from BM to bloodstream (Fricker, 2013). Nevertheless, developing new mobilizing agents remains necessary for patient poorly mobilized with G-CSF. Recently, new compounds have been analyzed such as Ixazomib that modulate the VLA4/VCAM1 axis involved in the adherence of HSCs to the BM niche (Ghobadi et al., 2014, 2018), Groβ an CXCR2 agonist for neutrophil mobilization (Hoggatt et al., 2018) or an inhibitor of Cdc42 involved in the exit of HSCs from the niche (Skulimowska et al., 2021)…

During leukapheresis, HSCs are enriched via their cluster of differentiation (CD) 34+ marker using magnetic beads. Other cell surface markers have been tested as CD34+ CD38- population in order to isolate LT-HSCs with higher purity. The amount of CD34+ CD38- cells recovered is lower than with the CD34+ marker alone, but it is enriched in LT-HSC (self-renewing HSC population) and therefore would require less reagents and culture volume for their modification/correction prior transplantation, simplifying scale-up and reducing costs (Naldini, 2019). After purification, CD34+ cells are modified and cultivated in a well-defined medium containing cytokines (human Thrombopoietin (TPO), human interleukine-3 (IL3), human stem cell factor (SCF), human Fms-like

tyrosine kinase receptor 3 (Flt3)) to maintain their stemness prior re-transplantation into patients (Gentner et al., 2021; Kohn et al., 2021). Overtime, new molecules have been tested to improve the HSCs culture medium such as StemRegin-1 (Boitano et al., 2010) which is described to enhance the expansion of HSCs. However, a protocol for expanding *ex vivo* LT repopulating HSCs from BM or PB mobilized is still missing, even if some progress has been done recently on murine HSCs (Naldini, 2019; Wilkinson et al., 2019). In addition, some research aims to improve *ex vivo* culture to replicate as closely as possible the BM niche to maintain HSC self-renewal. For instance, co-culture of CD34+ cells with mesenchymal stromal cells enhances the survival and proliferation of cord-blood progenitor cells and results in an significant improvement of engraftment (de Lima et al., 2012). To provide more HSCs, some groups are working on the HSCs generation via pluripotent stem cells (Sugimura et al., 2017) and endothelial cells (Lis et al., 2017).

1.1.4 Mobilization and re-infusion of HSCs

After modification, HSCs is transplanted back into patient by intravenous injection (Figure 3). To assure a successful engraftment, patient BM niches should be emptied in order to let the space for corrected HSCs. Therefore, prior transplantation, patients must undergo myeloablation. Overtime, different methods have been used to clear the BM niches from lethal irradiation to chemical agent as Busulfan (Ciurea and Andersson, 2009). Total body irradiation was abandoned due to the severe morbidity and mortality on patients for the benefit of chemical myeloablation. Busulfan have been initially employed as chemotherapy but is now also used a myeloablation agent due to immunosuppressive effect on BM and microglia (Ciurea and Andersson, 2009). New depleting agents are currently under evaluation such as monoclonal antibody directed on a specific BM cells population (for instance : anti-c-kit alone (Czechowicz et al., 2007, NCT02963064) or associated with CD47 blocking agent (Chhabra et al., 2016), or combined strategy with immunotoxin as Saporin to inactive ribosome thus blocking protein synthesis (Bergamaschi et al., 1996; Skulimowska et al., 2021).

Nevertheless, myeloablation suffers from several short and long-term side effects as fatal infections caused by immunosuppression or BM niches architecture modification that could alter HSCs engraftment. Alternative treatments without myeloablation have been tested on mouse model to

assure good engraftment while removing the conditioning toxicity. One strategy involves in increasing the amount of HSCs via *ex vivo* expansion prior transplantation (Wilkinson et al., 2019) and another one used the competitive advantage of corrected cells over non-corrected one to reinforce the engraftment (Omer-Javed et al., 2022).

1.1.5 Lentiviral-based correction of HSCs

Ex vivo GT has been initially developed using viral vectors to deliver therapeutic gene. Among all viruses, retroviruses have been mainly and successfully employed as viral vehicle. Retroviruses (RV) are enveloped single-strand (ss)-Ribonucleic acid (RNA) virus belonging to Retroviridaea family composed of 7 genera: α-, β-,γ-, δ-, ε-retroviridae, spumaviridae and lentiviridae. Lentiviral vector (LVV) coming from Human immunodeficient virus (HIV) and γ-retroviral vector (γ-RV) coming from Murine Leukemia virus (MLV) are the main viral vectors used for *ex vivo* GT in clinical trials due to their abilities to integrate double-strand (ds)-DNA into host genome and their high transgene packaging ability (7-10kb) (Worgall and Crystal, 2014; Poletti and Mavilio, 2018).

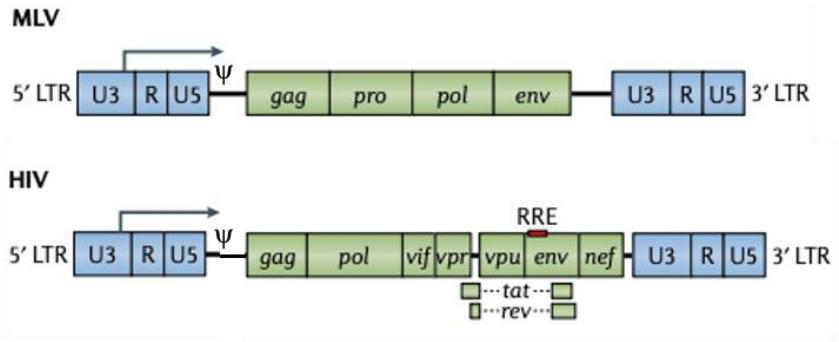

Figure 4) Structure of MVL and HIV virus (adapted from G. Ferrari et al., 2021) encoding essential genes as gag, pro, pol and env; long terminal repeat (LTRs) and Psi sequence.

Both HIV and MLV viral genomes contain 4 essential genes (*gag, pro, pol* and *env*) and important non-coding sequences, such as the long terminal repeat (LTRs) sequences, which are involve in the initiation and termination of transcription, and the *Psi* sequence (ψ), the packaging signal essential for encapsulating the viral genome (Figure 4). The *gag* gene codes for the primary structural poly-protein involved in the assembly of non-infectious and immature viral-like particle. The *pro* gene

encodes a protease responsible of maturation of viral particles. The *pol* gene includes the reverse transcriptase, RNase H and integrase. The *env* gene encodes for the envelope proteins of retrovirus. The HIV genome contains additional specific accessory proteins (*vif, vpr, vpu* and *nef)* involved in the infectious cycle and in the pathology (G. Ferrari et al., 2021; Ghosh et al., 2020). The mechanism of infection of RV is described in the figure 5.

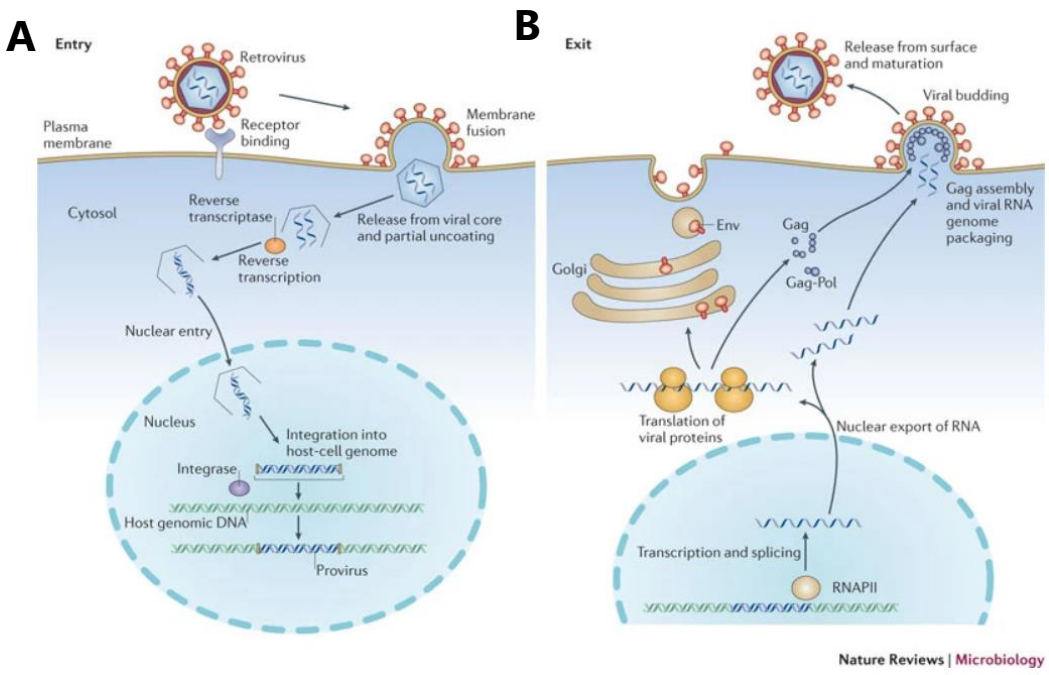

Figure 5) Mechanism of infection of RV (from Stoye, 2012) **A**: Upon virus entry, the viral ss-RNA is released, reverse transcribed in ds-DNA and integrated into host genome. **B**: Viral genome uses the host machinery to produce new viral particles.

In Retroviridaea family, the viral entry is receptor recognition dependent. Upon host cells infection, the genetic material is released and reverse transcriptase results in the synthesis of ds-complementary DNA (cDNA) and its assembly into a pre-integration complex (PIC) that can be targeted to the nucleus. The integration of ds-cDNA into host genome occurs via integrase enzyme present in the retrovirus particle. Upon integration, viral genome uses the host transcription and translation machineries to produce new viral particles that can be released in extracellular matrix and infected other cells (Yi et al., 2011; Poletti and Mavilio, 2018; Stoye, 2012). The main differences between LVV and γ-RV vectors come from their infecting target cells and their viral integration. In fact, γ-RV virus infects

dividing cells while LVV infect both non-dividing and dividing cells. To enhance LVV HSCs infection, the culturing medium changes the cell phase from G0 (non-dividing phase) to G1 (dividing phase) as HSCs are slowly dividing cells. Moreover the integration of γ-RV occurs into promoters, enhancers or around transcription site (TSS) while LVV integrates into active gene bodies (G. Ferrari et al., 2021; Poletti and Mavilio, 2018).

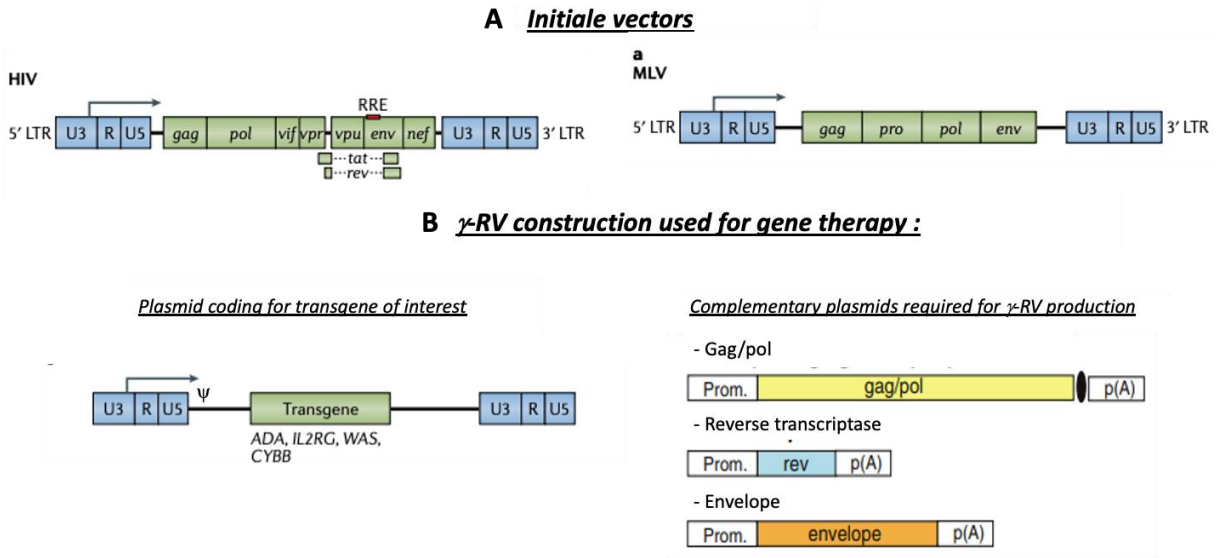

Figure 6) ***A*** *: Initial structure of γ-RV (adapted from G. Ferrari et al., 2021) and* ***B*** *: the γ-RV construction used in GT with the complementary plasmids required for viral formation (adapted from G. Ferrari et al., 2021 and Sinn et al., 2005).*

In order use viral vector as vehicle for transgene delivery, replicative machinery of retrovirus genome has been removed in order to avoid any replication and spreading of the modified vectors (Figure 6). In this attempt, several optimizations have been performed first by removing env protein and accessories genes (*vif, vpr, vpu* and *nef*) (Figure 6A), in order to reduce the virulence and the replication of the γ-RV construction, and then by eliminating the *transactivator* gene (*tat*) and by splicing *gag, pol* and *rev* genes in 2 different plasmids to reduce the potential vector recombination (Figure 6B) (Sinn et al., 2005). Since HIV can naturally infect only lymphocyte T, the viral *env* gene was replaced with the spike G glycoproteins of vesicle vesicular stomatitis virus (VSV-G) from rhabdovirus vesicular stomatitis virus (figure 8). This new VSV-G envelope broads vector tropism to transduce a

wide range of cells types including CD34+ HSCs and is more stable than original envelope, therefore easier to produce and concentrate in order to increase vector titer (Okimoto et al., 2001), and lacks pre-existing human immunity (Hastie et al., 2013). The non-replicative γ-RV developed was used in clinical trial to treat deficiency X-linked severe combined immunodeficiency (SCID-X) caused by a deficiency of Interleukin 2 receptor resulting in immunodeficiency in patient. Although *ex vivo* GT was successful for restoring immunity in patient, 25% of them develop leukemia caused by γ-RV transactivation of pro-oncogene (Fischer et al., 2010; G. Ferrari et al., 2021). Even with limitations, clinical trials continue with γ-RV (NCT01129544) and the first γ-RV treatment Strimvelis for adenosine deaminase deficiency severe combined immunodeficiency (ADA-SCID) was approved by Food and Drug Administration (FDA) in 2016 (NCT04959890).

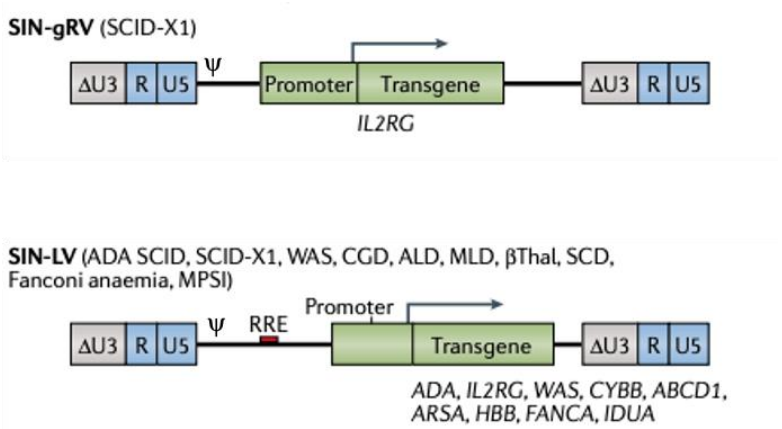

Figure 7) LV and γ-RV SIN construction containing inactive U3 promoter, Psi sequence, exogenous promoter and therapeutic transgene used for GT (G. Ferrari et al., 2021)

Nonetheless, this unwanted event leads to the development of self-inactivated (SIN) vectors in which the natural retrovirus promoter U3 has been deleted in both 5' and 3' LTR to prevent pro-oncogene transactivation (Figure 7) (Sinn et al., 2005; Hacein-Bey-Abina et al., 2014). The removing of U3 structure requires the use of exogenous promoter that must be added before transgene sequence. Moreover, LVV appears to be less genotoxic than γ-RV, therefore LVV are preferentially used now in *ex vivo* GT (G. Ferrari et al., 2021).

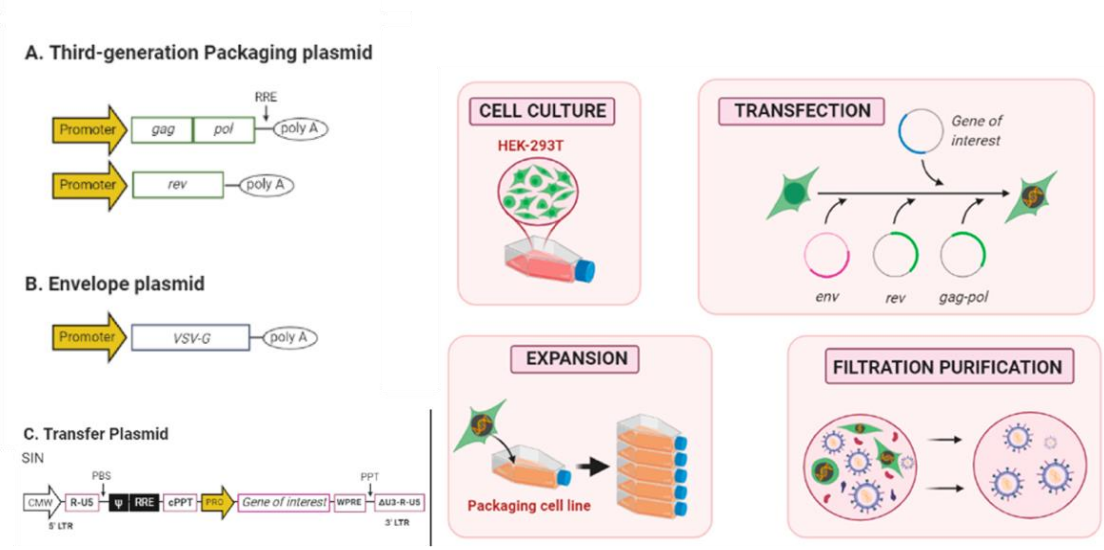

Figure 8) SIN-LVV and γ-RV production in HEK293T cells adapted from (Martínez-Molina et al., 2020). 4 different plasmids (A, B & C) are co-transfected in HEK-293T cell line. After cell expansion, supernatant is filtrated, concentrated, and titrated.

The production of SIN-RV is based on the co-transfection, in a producer cell line HEK293-T, of 4 plasmids: 1 plasmid encoding *gag* and *pol* genes, 1 plasmid encoding the reverse transcriptase (*rev* gene), 1 plasmid encoding the envelope protein, 1 plasmid encoding the transgene of interest under control of an exogenous promoter. Upon viral production, the supernatant is filtrated, concentrated, and titrated (Figure 8). Although the process of viral production is the same for LVV and γ-RV, the isoforms of *gag* and *pol* as well as LTR sequences differ (Martínez-Molina et al., 2020). The SIN-LV transduction and integration can be improved in CD34+ HSCs by using chemical drugs as Cyclosporine A, H, prostaglandine-2, protamine sulfate or LentiBoost (Naldini, 2019; Jang et al., 2020). The *ex vivo* GT results in a stable and safe long-term hematopoietic engraftment able to reconstitute the complete blood system while producing the therapeutic protein for a wide range of disorder as hemoglobinopathies (described in Introduction Part II) and metabolic defects (described in Introduction Part III) (Naldini, 2019; G. Ferrari et al., 2021).

1.2 GENE EDITING OF HSCS FOR MONOGENIC DISORDERS

Precise modification of genome in order to insert a specific DNA sequence takes different forms overtime. It started in 1980 and relied on DNA microinjection into cell nuclei to integrate the gene into the locus of interest upon homologous recombination or in a random site. Unfortunately, such strategy was very inefficient and was mostly used to generate mouse embryonic stem cells containing desired mutation(s) or gene insertion to create a murine model to study gene function or a particular phenotype (Capecchi, 2005). Nowadays, genome editing using nuclease is the holy gray in GT as it allows to perform precise modification of the patient underlying mutation(s) or efficient targeted integration of functional gene into specific locus. Editing of the genome requires 2 sequential events : nuclease cleavage at the locus of interest and precise DNA reparation to introduce the desired modification. In this attempt, three generations of programmable nucleases (ZFNs, TALENs, and CRISPR-Cas system) have been developed and are now evaluated in clinical trials (Shamshirgaran et al., 2022).

1.2.1 Zing-finger nuclease (ZNF) and Transcription activator–like effector nuclease (TALEN)

1.2.1.1 ZNF

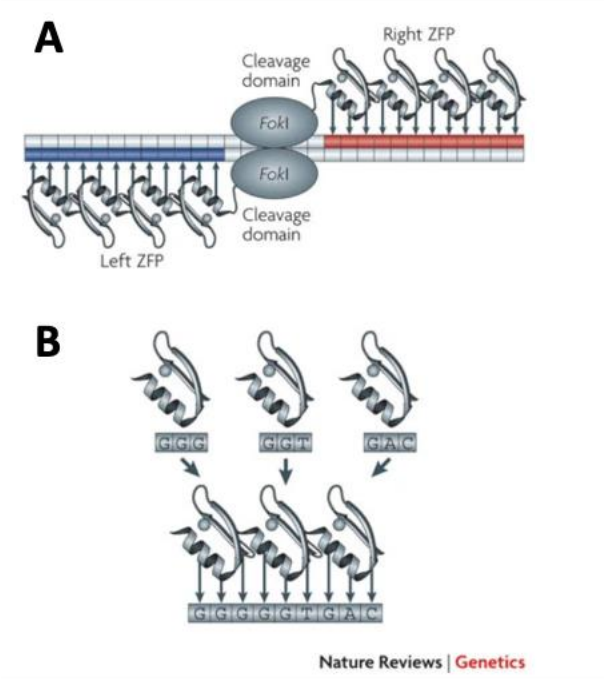

*Figure 9) Representation of ZFN strategy **A** : Zing finger protein (ZFP) recognizes the DNA sequence of interest and FokI induce double-strand break (DSB). **B** : Array of ZFP must be proper design to recognize the correct DNA pattern (adapted from Urnov et al., 2010).*

Zing-finger nuclease (ZFN) are artificial endonucleases composed of a succession of Zinc finger protein (ZFP) fused to the *FokI* nuclease (Figure 9). The 30 amino acid ZFP is able to bind DNA via Cys2-His2 fingers and each ZPF recognize individual 3-base pairs (bps) of nucleic acid. Therefore, the combination of 3 to 6 Zinc finger motifs allows the recognition and the binding of a specific DNA sequence. The DNA double-strand break (DSB) occurs only upon dimerization of FokI on the ZFP-targeted sequence that particularity increases the specificity of editing (Urnov et al., 2010). Nonetheless, DSB requires the engineering of each ZFP to bind one nucleotide triplet of interest and the design of 2 different ZFNs for both DNA strands, therefore developing 30 amino acid ZFP to recognize 3 nucleotides and a functional ZFP array to target a sequence of interest is quite difficult and time consuming and limits the use of this editing technology (Shamshirgaran et al., 2022). When properly designed, ZNF is quite specific and efficient with low immunogenicity both *in vitro* and *in*

vivo (Li et al., 2011; Ou et al., 2019), and has been developed as *ex vivo* GT for genetic blood disorders (Sickle cells disease and β-thalassemia, Mullard, 2020).

1.2.1.2 TALEN

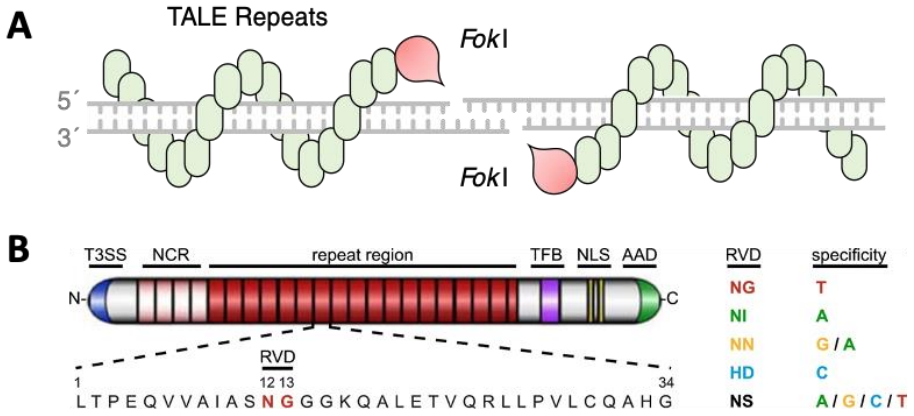

Figure 10) ***A*** *: Representation of the TALEN system (adapted from Shamshirgaran et al., 2022)* ***B*** *: TALE repeat sequences recognize the locus of interest that is cleaved by FokI upon TALEN dimerization. The engineering of RVD domain of TALE results in the recognition of a unique nucleotide (adapted from Becker and Boch, 2021)*

TALENs are based on a similar strategy that ZFN : tandem of DNA-binding protein and *FokI* nuclease except that DNA-binding occurs via Transcription activator–like effector (TALE) from bacterium *Xanthamonas* causing plant disease (Becker and Boch, 2021). Each TALE differs on 2 amino acid residues called Repeat Di-residues (RVD) able to recognize a single nucleotide and the array of TALE allows to construct a DNA recognition protein. The dimerization of TALEN on the targeted DNA sequences results in DSB via *FokI* nuclease (Shamshirgaran et al., 2022) TALEN technology has been used in a clinical trial for immunotherapy against cancer (Mullard, 2020). Although TALEN offers higher DNA binding specify in an easier way to design, the system suffers from the same limitation than ZNF technology namely the difficulty to design.

1.2.2 CRISPR

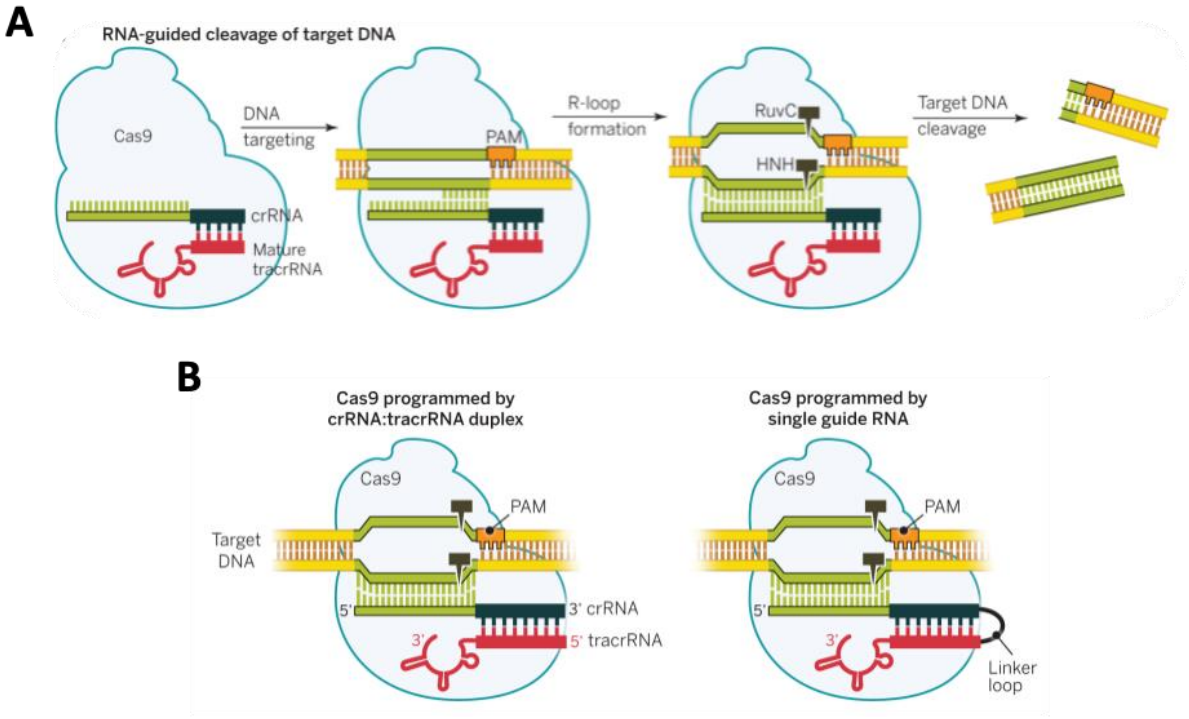

*Figure 11) Mechanisms of DSB with CRISPR-cas9 system **A** : A RNA duplex (crRNA:tacrRNA) complex with Cas9 are able to recognize the sequence of interest via proto-spacer-adjacent motif (PAM) and cleaves the dsDNA. **B** : The strategy has been simplified using a single guide RNA (gRNA) instead of the RNA duplex (adapted from Doudna and Charpentier, 2014)*

While ZFN and TALEN require protein engineering for DNA interaction, CRISPR-Cas system is RNA-guided DNA endonuclease and requires only a change in RNA sequence to target different genomic locus. CRISPR-Cas system originates from prokaryote immune system that cleaves foreign DNA from viruses or plasmids. CRISPR-Cas system has been divided in 2 classes : the class 1 is composed type I, III and V using multi-Cas proteins to cleave foreign DNA while the class 2 including type II, V and VI using a single Cas protein for DSB. The most spread CRISPR-Cas system is a class II, the Cas9 nuclease from *Streptococcus pyogenes* (SpCas9). Cas9 nuclease is composed of 2 nuclease domains : HNH and RuVC able to respectively cleave RNA targeted strand and the complementary one to induce DSB (Figure 11.A). Initially, the CRISPR-Cas system consisted of a spCas9 protein coupled with RNA duplex of transactivating-CRISPR RNA (tracrRNA) and CRISPR RNA (crRNA) (tracrRNA:crRNA) (Figure 11.A). The 5' sequence of crRNA is composed of 20 nucleotides (nts) RNA sequence (spacer

sequence) complementary to the DNA target site and the 3′ sequence contains CRISPR repeat sequences able to base pair with the 5′ sequence of tracrRNA. Therefore, tracrRNA:crRNA duplex forms a guide RNA structure able to recognize DNA sequence, spacer, and recruit the Cas9 enzyme, via the 3′ tracrRNA scaffold , to perform DSBs at the target site (Jiang and Doudna, 2017). Currently, a fused guide RNA (gRNA) was engineered with 5′ RNA complementary sequence for DNA target site (20 nucleotides spacer) and a Cas9-RNA binding structure in 3′ (Figure 11.B). For cutting the intended DNA, the Cas9/gRNA complex needs to find the 20 nts sequence complementary to the g-RNA, flanked to its 5′ by a short 3 nts, proto-spacer-adjacent motif (PAM) sequences, which is fixed and depends on the specific Cas used, for SpCas9 the NGG motif (N = A, T, C, or G). Once the DNA target sequence is recognized, the Cas9 nuclease induces a blunt-end DSB 3bps upstream of PAM sequence (Figure 11.A) (Doudna and Charpentier, 2014; Liu et al., 2022). CRISPR-Cas9 system can be employed with a gRNA or multiplex gRNA to target multiple locus or to induce large DNA deletion.

1.2.3 DNA repair

Upon DSB, 3 main pathways of DNA repair can take place (Figure 12) :

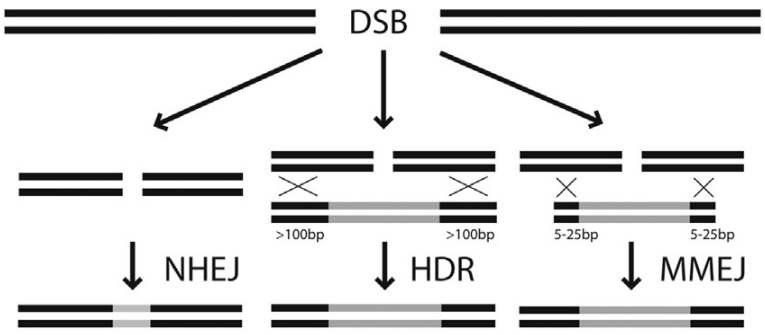

Figure 12) The 3 way of DNA reparation upon DSB adaptated from (Yanik et al., 2018). NHEJ : Non-homologous end joining, HDR : Homology-directed repair, MMEJ : Microhomology-mediated end joining.

Non-homologous end joining (NHEJ) is an error prone pathway resulting in insertion and/or deletion (indels) of few nts at the cleavage site. It could result in a reading frame shift or a premature stop codon insertion that disrupt the normal gene function and is mainly used to knock-out (KO) genes.

Homology-directed repair (HDR) aims at targeted insertion of sequence of interest or correct a specific gene via homologous recombination. In fact, HDR relies on a template DNA containing large homology arm (HA) surrounded cleavage site to precisely insert a DNA sequence. Upon CRISPR-cas9 editing, single-stranded oligodeoxynucleotides (ssODNs) or double-strand DNA, delivered via viral vectors, non-viral vectors, or transfection methods, can be used as template DNA in the targeted genomic locus.

Microhomology-mediated end joining (MMEJ) results also into DNA sequence integration or correction, but required minimal HA (5-25bps) around the cutting site and results in indels generation at the targeted site (Yanik et al., 2018).

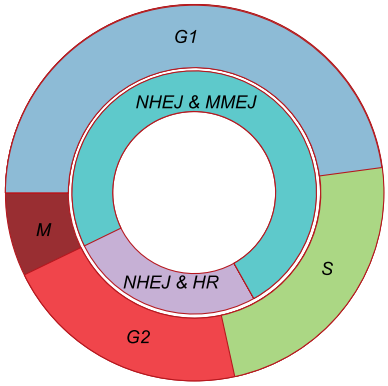

Figure 13) Mechanisms of DNA reparation depends on the cell cycle (adapted from Taleei and Nikjoo, 2013). S : DNA replication phase, M : Mitosis, G1 & G2 : interphase

The mechanism of cells reparation upon DSB depends on the cell cycle phase that is composed of 4 phases : the S phase corresponding to the DNA replication phase, Mitosis (M) phase leading to cells division and 2 interphases : G1 & G2 (Figure 13). NHEJ is mainly active during interphase, while HDR is preferentially used during S and G2 phases explaining the low HDR events in non-dividing cells such as HSCs. Finally, the MMEJ reparation mechanism is involved during G1 and S phases (Figure 13) (Taleei and Nikjoo, 2013).

CRISPR-Cas 9 technology has a wide range of application from disruption of gene to study its function or insertion of DNA sequence into the break site via HDR or MMEJ reparation. The last one represent one of the promising approach to treat monogenetic disorder (S. Ferrari et al., 2021).

1.2.4 Targeted integration

To treat monogenic disorder, a functional copy of the mutated gene can be targeted either into its natural locus under the control of its physiological promoter (Figure 14.A) or under the control of a superactive promoter (Figure 14.B) or into a tolerant to integration locus (Figure 14.C) (Pavani and Amendola, 2020). All together, these strategies aim to produce strong and efficient therapeutic proteins at a physiological or supraphysiological level to correct the monogenic disorder.

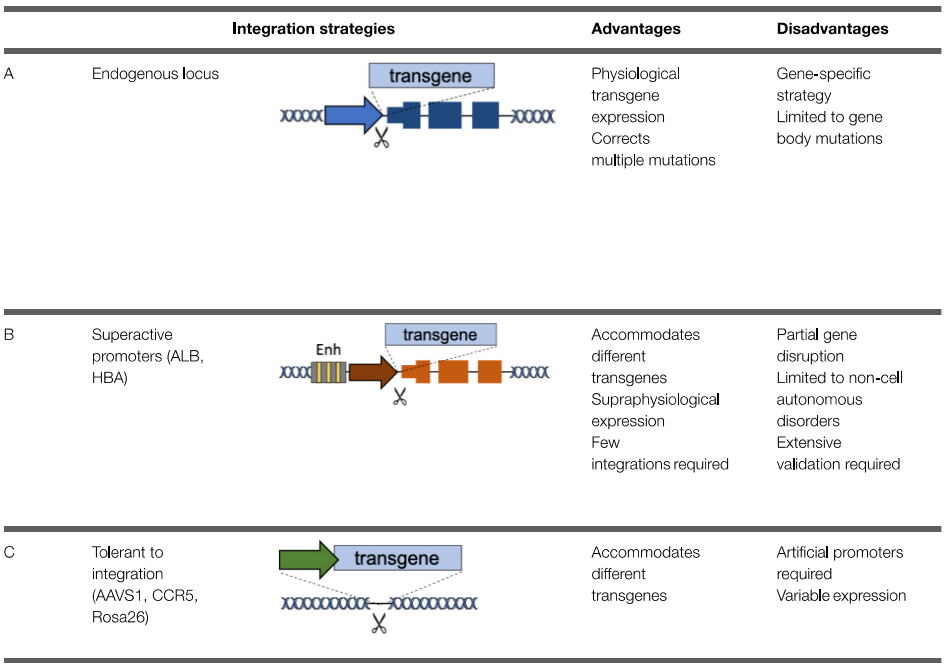

Figure 14) The different integration strategies and their advantages/disadvantages (adapted from Pavani and Amendola, 2020)

Developing such strategies in *ex vivo* GT requires both efficient editing in the targeting locus and delivery of DNA template into HSCs nucleus. The most adopted method for *ex vivo* editing consists of electroporation of Cas9 and gRNA Ribonucleoprotein (RNP) complex that results in efficient editing with a reasonable cytotoxicity in HSCs (Lattanzi et al., 2019). Polymer-based nanoparticles have recently emerged as new delivery system for nuclease in HSCs resulting a lower toxicity and a better LT-HSCs reconstruction (El-Kharrag et al., 2022). The DNA template delivery methods upon DSBs are based on 2 approaches : Viral or non-viral and mostly rely on HDR-based integration (Drysdale et al., 2021).

1.2.4.1 Viral based HDR strategy

Viral based HDR-method mainly relies on the transduction of HSCs with Adeno associated virus (AAV) or Integrative deficient LV (IdLV). AAVs has been discovered as contaminant of Adenovirus preparation. In fact, AAVs belong to the family of *Parvoviridae* and requires co-infection with a helper virus as adenovirus for its replication. AAV genome is 4,7 kbp ss-DNA flanked by Inverted Terminal Repeats (ITRs), essential for virus replication and packaging signal, and encodes 2 genes : *rep* and *cap* respectively for viral replication and capsid subunits. The *cap* gene determines the viral tropism and encodes also for the assembly activating protein (AAP) involved in the virus assembly. 12 natural serotypes have been identified with different tissue tropism, e.g., AAV-2 targeting especially brain, eyes, and liver. Moreover, human presents a high seroprevalence of AAVs ranging from 15% to 90% depending on serotypes without cause any disorder (Wang et al., 2019; Meier et al., 2020).

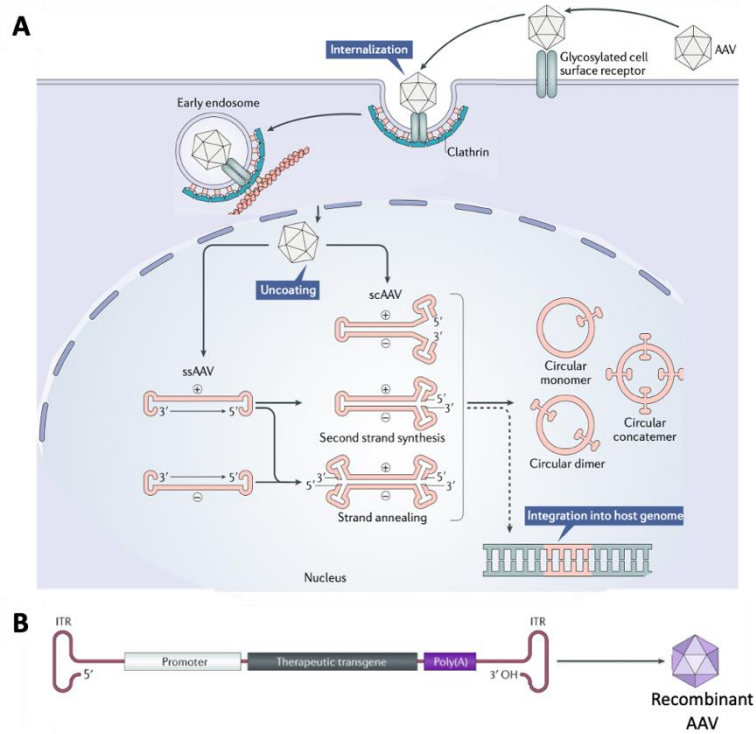

*Figure 15) **A**: Representation of AAV infection into eukaryote cells (adapted from Wang et al., 2019) Upon virus entry, the viral ss-DNA is released and could be converted into ds-DNA (ssAVV) or not (scAAV). ITR sequences lead to viral genome circularization **B** : Structure of AAV construction used for gene integration must contain a therapeutic transgene that may be expressed either by an exogenous or endogenous promoter upon targeted integration (from Li and Samulski, 2020)*

The cell infection with AAV depends on recognition of glycosylated cell surface receptor that result in virus endocytosis. Cytoskeletal system traffics viral endosome through nucleus to deliver viral genome (Figure 15A). Upon AAV infection, viral genome can integrate in *AAV integration site 1 (AAVS1)* locus due to homology of ITR and *Rep* gene for this locus (Wang et al., 2019). To be used as vectors of gene therapy, AAVs have been engineered to avoid viral replication by removing from their genome *replicative* and *capsids* genes. Only ITRs sequences have been conserved as they are mandatory for viral production and transgene expression (Figure 15.B)(Li and Samulski, 2020). There are 2 types of recombinant AAVs (rAAV) : single stranded AAV (ssAAV) and self-complementary AAV (scAAV). The ssAAV are transcriptionally inactive and must be converted to dsDNA in the nucleus to be transcribed. Whereas scAAVs are designed to be dsDNA and can be directly transcribed. ITR sequences result in circularization of rAAV that can persist into the nucleus. The removal of *rep* gene decreases the genome integration of AAVs in *AAVS1* (Wang et al., 2019). In *ex vivo* GT, AAV6 capsid provides the highest tropism for HSCs and has been employed to target insertion of gene of interest. To assure efficient HDR, AAV6 has been designed to encode transgene of interest with long homology arms (~ 300-800bps) for the targeted locus (Azhagiri et al., 2021). The expression of the transgene depends on the promoter (Figure 15). AAV6 HDR-donor has been tested to correct X-SCID (Rai et al., 2020) and metabolic defects (Gomez-Ospina et al., 2019; Scharenberg et al., 2020). Nonetheless, AAV6 infection results in cytotoxicity reducing the LT-HSCs repopulation and limiting their employment (Romero et al., 2019). Besides, AAV ITRs remain the most integrated sequence into the targeted locus in HSCs and are transcriptionally active suggesting possible gene transactivation around integration site (Ferrari et al., 2022). Therefore, other safer delivery templates are currently under investigation among them IdLV vector.

IdLVs are integrase defective lentiviral vector due to mutations disrupting reverse transcriptase enzymatic activity or interaction with key cellular cofactors (Qamar Saeed et al., 2014) and have been developed initially to avoid insertional mutagenesis (Banasik and McCray, 2010; Azhagiri et al., 2021). The IdLV generation and production are similar of LV in the exception that for the production the pol plasmid encoding the mutated integrase must be used (Vijayraghavan and Kantor, 2017). IdLVs are used in HDR strategy due to cargo potential up to ~ 10kbs. Romero et al., 2019 compares IdLV and AAV6 donor templates after ZNF or CRISPR-Cas9 editing on sickle cell disease (SCD) and shown

that IdLV is less cytotoxicity with a limited HDR efficiency compared to AAV6. Besides, improvement of IdLV transduction has been shown to enhance HDR frequency in LT-HSCs with less genotoxicity compared to AAV vector (Ferrari et al., 2022). Thus, AAV or IdLV HDR-method could integrate concatemer of full or partial viral transgene into the CRISPR-Cas 9 DSBs affecting the safety of the strategy (Hanlon et al., 2019; Wang et al., 2017) and, therefore, required better safety assessment and development of alternative technology.

1.2.4.2 Non-viral HDR based method

One of the non-viral HDR based method relies on ssODN delivery into the desired locus. ssODN is a short oligo (~ 200 nts) flanked by two homology arms (HA) of 30-60 nts allowing insertion into the locus of interest. ssODNR-HDR based method is easier to design and implement and results in efficient HDR in HSCs but it is limited by its small DNA size that can correct only precise mutated portion of gene (Azhagiri et al., 2021). Plasmid based method has been also used to provide DNA template upon nuclease cleavage. For instance, the homology-independent targeted integration (HITI) using NHEJ reparation machinery. In the strategy, plasmid encoding transgene of interest is flanked with the same gRNA sequences that is used to delete the gene targeted. Upon nuclease, both the genomic DNA and plasmid are cleaved generating DNA deletion in the locus of interest that could be repaired via NHEJ machinery using plasmid as template. With this method, the orientation of the transgene is mediated with gRNA direction (Suzuki et al., 2016). The HITI strategy has been recently employed in murine HSCs and result in a rescue of X-SCID phenotype (Byambaa et al., 2021) offering a non-viral based method to deliver a full functional gene. More recently, CRISPR-HITI has been adapted for AAVs *in vivo* delivery in retina and liver. It requires co-delivery of an AAV encoding spCas9 and an AAV coding the cassette of interest flanked by two gRNA targets similar to the one targeting the genomic DNA for *in vivo* linearization. Upon cutting, NHEJ reparation induces stop codon on the endogenous gene and the precise integration of the start codon and transgene results in expression of the inserted sequence (Tornabene et al., 2022). A similar strategy, precise integration into target chromosome (PITCH), has been employed using MMEJ reparation machinery in which the plasmid contains gene of interest surrounded with small homology arms for the targeted locus. The system has been used *in vitro* into human and animal cells (Nakade et al.,

2014 ; Sakuma et al., 2015) and *in vivo* in *Fah-/-* mice to integrate Fah donor sequence into its natural locus (Yao et al., 2017).

1.2.5 CRISPR drawbacks

An important drawback of CRISPR-cas9 system is the off-target editing than can occur out of the locus of interest. In fact, gRNA can tolerate few mismatch and therefore can target non-desired DNA sequence affecting its expression (Cullot et al., 2019; Kosicki et al., 2018). Nowadays, online software such as CRISPOR used for gRNA selection provides prediction of potential off-target sites (Concordet and Haeussler, 2018). Off-target editing could be evaluated *in vitro* using Digenome-seq or SITE-seq technique: purified genomic DNA is CRISPR/Cas9 cleaved with gRNA of interest. After cutting, a library of fragmented sequences is next generation sequenced and aligned with a reference genome. The identification of off-target sequence(s) is based on the detection of Indels into the fragmented DNA compared to the genome of reference (Atkins et al., 2021).

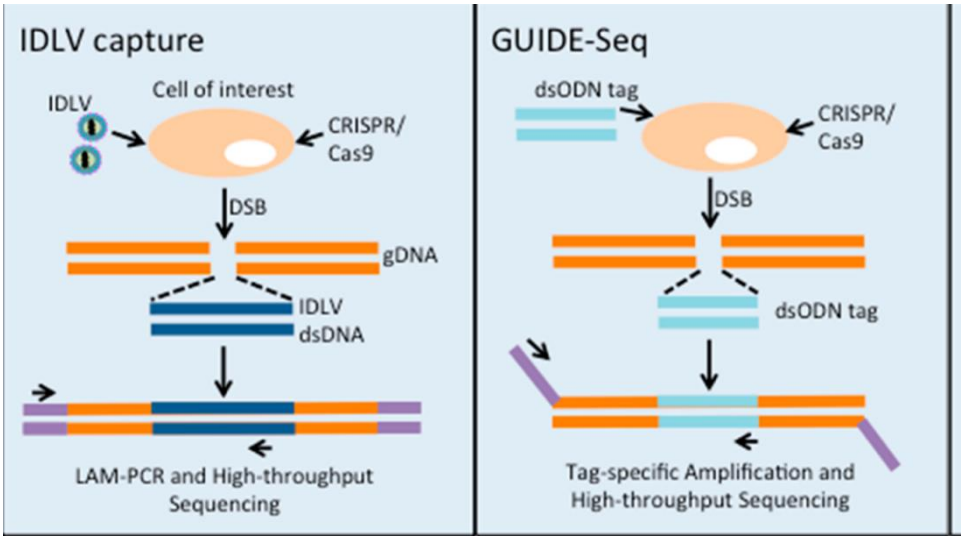

Figure 16) Representation of IdLV capture and GUIDE-seq for the experimental determination of gRNA off-target (adapted from Tasan and Zhao, 2017).

The *in cellulo* identification of off-target site is based on capturing of either ds-ODN (GUIDE-seq Tsai et al., 2015) or IdLV into the DSB sites induced by the nucleases (Gabriel et al., 2011; Wang et al., 2015). Then, the site(s) of integration are amplified and sequenced with next-generation sequencing

(Figure 16) (Tasan and Zhao, 2017). The sequencing data are mapped on the human genome to identify the locus of insertion thus the off-target nuclease site(s) (Gabriel et al., 2011; Wang et al., 2015). In order minimize off-target events and maximize the on-target edition, new Cas9 orthologes have been studied with different PAM recognition sequences such as Cas 12 (type V CRISPR-cas) or Cas13 (Type VI) (Cebrian-Serrano and Davies, 2017; Gasiunas et al., 2020) and High Fidelity (HiFI) Cas 9 was also engineered (Vakulskas et al., 2018).

CRISPR-Cas9 editing has been reported to induce on-target chromosomal re-organization as large deletion, loss of allele heterozygosity, chromothripsis or chromosome loss which could result in cancer development and therefore require careful evaluation (Cullot et al., 2019; Wen and Zhang, 2022).

In addition, DSBs result in the activation of p53-mediated DNA damage response (DDR) that induces cell growth arrest and the apoptosis of edited cells. AAV-mediated delivery of DNA template triggers a cumulative effect of p53 activation in HSCs and results in a decrease of cell proliferation and engraftment efficiency (Schiroli et al., 2019). Temporary inhibition of P53 was reported to increase the percentage of editing (Haapaniemi et al., 2018) and HDR-mediated DSB repair. Finally, pre-existing humoral response with anti-Cas9 antibodies was found in human serum as well as anti-Cas9 T cells in human donor blood limiting the *in-vivo* delivery of CRISPR-Cas9 system (Charlesworth et al., 2019; Wagner et al., 2019).

1.2.6 Alternative to CRISPR-Cas9 systems

The inactivation of one of the two active domains of Cas9 nuclease results in nickase Cas9 (nCas9): D10A that cleaves the targeted DNA strand or H840A cleaving the gRNA complementary DNA sequence. nCas9 gives raise to base (BE) and prime editor (PE) technologies to precisely edit gene of interest without inducing DSB. Also, nCas9 offers the advantage to reduce indels at off-targets and chromosomal rearrangement (Cullot et al., 2019).

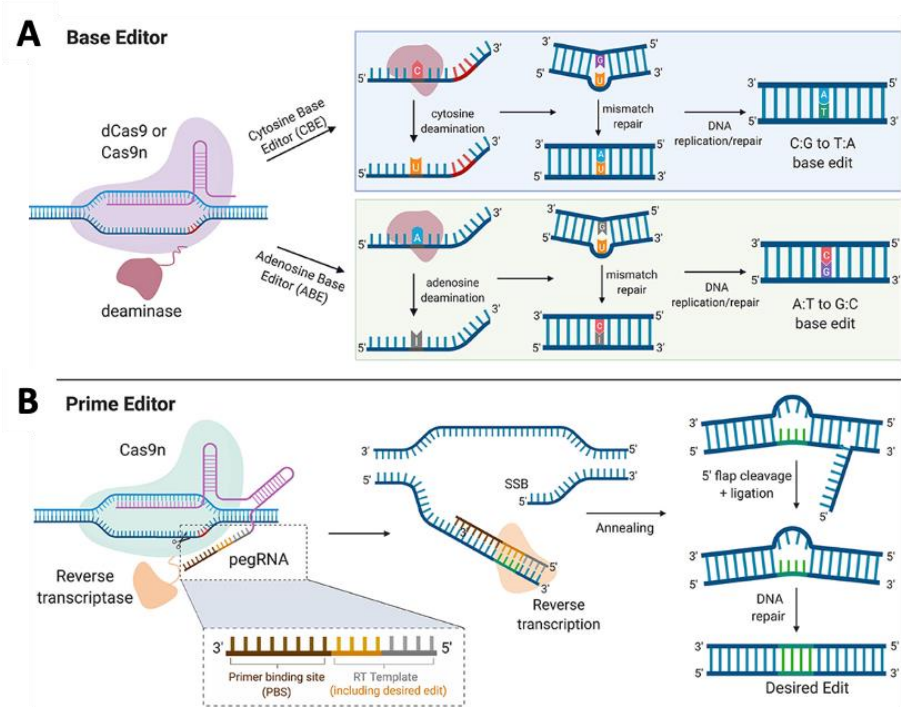

Figure 17) Base editor and prime editor strategies to precisely edited a locus of interest without inducing DSB (adapted from Uddin et al., 2020). ***A****: Base editor is composed of cytosine base editor (CBE) inducing C to T conversion and adenine base editor (ABE) inducing A to G modification.* ***B:*** *Prime editor uses pegRNA to insert a small nucleotide sequence (up to 44 nucleotides) upon reverse transcription.*

BE consists of nCas9 fusion with either deaminase such as Cytosine base editor (CBE) changing C:G to T:A and Adenine base editor (ABE) editing A:T to G:C (Figure 17.A) (Uddin et al., 2020). PE instead consists of nCas9 fused with a reverse transcriptase complex with a prime editing guide (peg) RNA. The pegRNA is a template for insertion of the desired modification via reverse transcription (RT). It is composed of primer binding site to initiate the RT and a template containing the desired edit. The reverse transcriptase synthetizes complementary DNA from template containing the desired modification on the targeted site. Upon RT, the 5′ flip DNA containing the non-desired mutation is cleaved during DNA reparation (Figure 17.B) (Uddin et al., 2020). Contrary to BE that modify a single base, PE could tolerate insertion up to 44 bp of desired genetic modification (Anzalone et al., 2019).

Whereas the inactivation of the 2 nuclease domains of Cas9 results in dead Cas9 (dCas9) able to bind DNA on a targeted locus without inducing cleavage. dCas9 can be fused to different enzymes such as transcriptional repressor (CRISPR interference) or activator (CRISPR activator), methylase, demethylase in order to regulate gene expression by altering transcription or chromatin context (Kanafi and Tavallaei, 2022).

2 HEMOGLOBINOPATHIES

2.1 ERYTHROCYTES

2.1.1 From HSCs to erythrocytes

Erythrocytes are a major blood component involved in the oxygen transport via their tetrameric protein : hemoglobin (Hb). In human, RBCs circulate in bloodstream with a lifespan of 120 days and everyday ≅ 200 billons of RBCs are produced from HSCs differentiation called erythropoiesis (Hattangadi et al., 2011; Caulier and Sankaran, 2022).

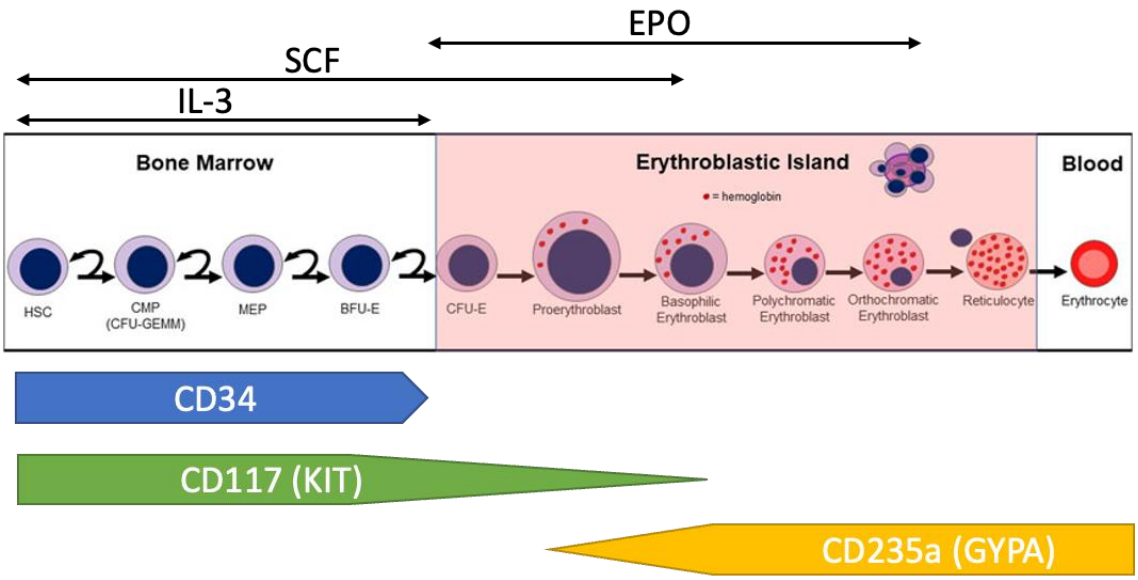

Figure 18) Erythroid differentiation from HSCs with the cytokines involved and the cell marker surface (adapted from Caulier and Sankaran, 2022; Munley et al., 2022). CMP : common myeloid progenitor, CFU-GEMM : multipotential colony-forming unit; MEP : megakaryocyte erythroid progenitor; BFU-E : blast-forming unit-erythroid; CFU-E: colony-forming unit-erythroid

The different steps of erythropoiesis are represented in the Figure 18. In brief, this 14-days differentiation results in massive Hb production, nucleus condensation and enucleation in reticulocytes. The early phase of differentiation occurs in the BM niches and result in erythroid-committed progenitors. While the late phase of differentiation takes place in erythroblastic island in

BM composed of macrophages able to phagocyte nuclei from erythroid-precursors enucleation (Figure 18) (Dzierzak and Philipsen, 2013; Caulier and Sankaran, 2022). Erythropoiesis requires cytokines to control and activate downstream regulatory pathways among them : IL-3 is involved in the proliferation of early erythroid-committed progenitors, SCF to enhance the proliferation and survival of BFU-Es and CFU-Es and the kidney-derived cytokine erythropoietin (EPO) to promote the expansion of mature precursors from CFU-E to orthochromatic reticuloblast (Hattangadi et al., 2011; Caulier and Sankaran, 2022). The final maturation into erythrocytes occurs into the blood circulation. Along with differentiation, cell surface markers change and allow to follow erythroid-cell population by flow cytometry and to enrich for a population of interest (Caulier and Sankaran, 2022; Munley et al., 2022) .

2.1.2 Hemoglobin

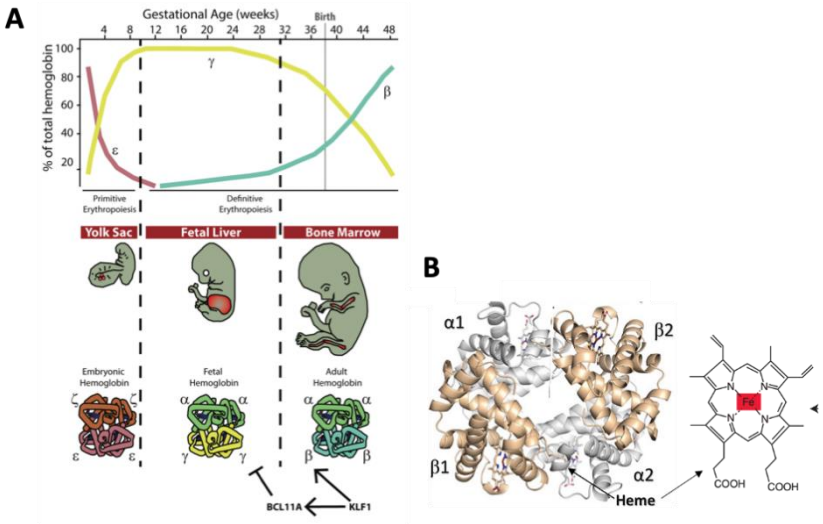

*Figure 19) **A**: Representation of globin synthesis in function of gestational ages (adapted from Cantú and Philipsen, 2014) and **B:** adult hemoglobin (HbA) structure (adapted from Ahmed et al., 2020; Dailey and Meissner, 2013)*

The oxygen-carrier protein hemoglobin in adults is composed of 2 pairs of globin-like chains : α associated with β-like chains either β or δ or γ-chains. Each globin chain contains a heme acting as a cofactor. In embryo, erythroid cells from the yolk sac produce embryonic Hb composed of the pre-α chains : ξ and β-like chains : ε or γ-chains (Figure 19.A). At 12 week of gestation, fetal hemoglobin

(HbF) composed of α- and γ-globin chains (α2γ2) is expressed from erythroid cells located in spleen and liver. After birth, the adult Hb (HbA) is predominant (95%) and is composed of 2 α-chains coupled with 2 β-chains ($\alpha_2\beta_2$), while the HbF decreases to reach only 1% of total Hb 6-month after birth (Figure 19. A) (Cantú and Philipsen, 2014; Clarke and Higgins, 2000; Dzierzak and Philipsen, 2013). Heme is synthetized during erythroid differentiation from proerythroblast following 8 enzymatic reactions. It consists of a porphyrin ring with iron atom Fe2+ able to bind 1 oxygen (O_2) molecule (Figure 19.B). HbA contains 4 heme and therefore carries 4 molecules of O_2 (Ahmed et al., 2020; Dailey and Meissner, 2013; Pittman, 2011) to be delivered into organs and tissues. Also, heme regulates the transcription of different genes upon *cis* Heme Responsive Elements (HRE) binding or to modulate its own production or others erythroid specific proteins (Chiabrando et al., 2014).

2.1.3 Globin expression

The α-globin gene are located in the chromosome 16, while β-globin like genes are found in a cluster on the chromosome 11. Diploid cells encode for 4 α-globin genes and 2 β-globin genes. The expression of the different of β-like globin chains are closely regulated by the locus controlling region (LCR) that contains chromatin opening and DNA enhancer elements as 5 DNase hypersensitive sites (HSs) within 200-400 bps size and separated from each other by 2-4 kbps (Liang et al., 2008).

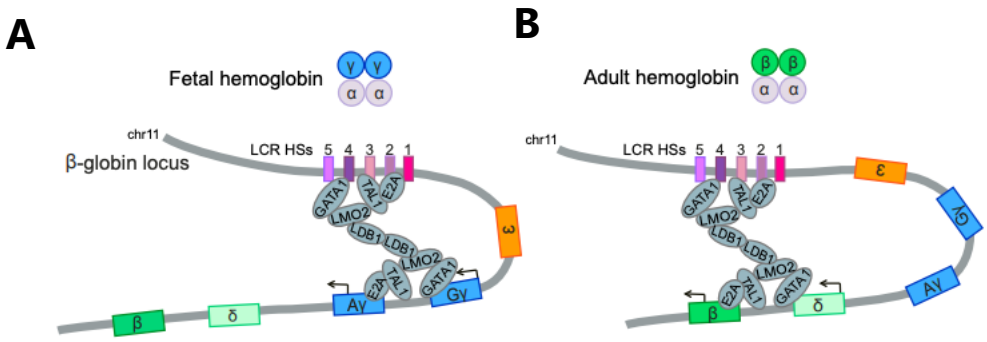

Figure 20) Representation of the transcriptional loop of α and γ-globin synthesis (adapted from Cavazzana et al., 2017). ***A****: The fetal hemoglobin is composed of the 2 γ- and 2 α chains.* ***B****: The adult hemoglobin results in the switch of globin expression from γ- toβ- globin chains and is therefore composed of the 2 β- and 2 α-chains.*

The LCR forms a regulatory loop able to interact with β-globin chains via a pentametric structure composed of 2 transcriptional activators : GATA1 and E2A, a transcription co-factor : TAL-1, a transcriptional regulator element : LMO2 and loop formation and stabilization protein : LDB1 (Figure 20) (Brandt and Koury, 2009; Kim and Dean, 2012; Katsumura et al., 2013). GATA1 is a master regulator of Hb subunit expression and heme biosynthesis and is involved in megakaryocytes, eosinophils, and mast cells maturation. The GATA1 recognition DNA motif consists of (A/T)GATA(A/G) sequence present in the *cis*-regulatory elements of globin promoter. Upon LCR binding, GATA1 recruits the RNA polymerase II to initiate transcription (Katsumura et al., 2013).

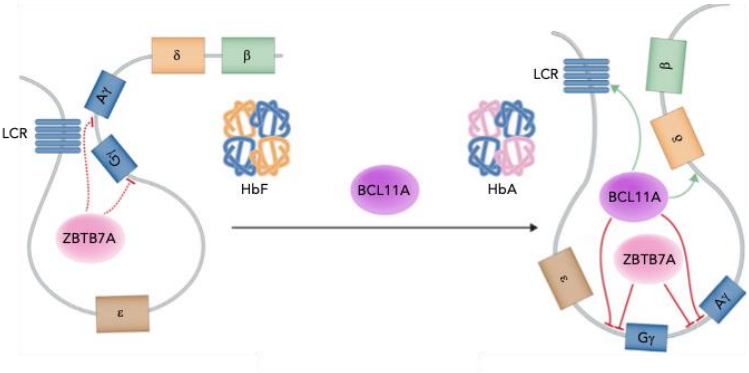

Figure 21) Representation of BCL11A and ZBTB7A inhibition of γ-globin synthesis resulting in the fetal to adult hemoglobin switch (from Caulier and Sankaran, 2022). Both transcriptional factors bind γ-globin promoter and recruit actors of DNA condensation to inhibit the γ-globin chains expression.

The formation of a pentameric complex composed of the transcriptional co-regulator B cell lymphoma/leukemia 11A (BCL11A) and ZBTB7A (called also LRF), a transcriptional factor, on the β-globin locus prevents γ-globin expression and is responsible of the switch from fetal to adult HbA (Figure 21). In fact, BCL11A and ZBTB7A transcriptional factors bind γ-globin promoter and recruit the chromatin remodeling complex NuRD that condensate chromatin and block the γ-globin expression (Cavazzana et al., 2017; Caulier and Sankaran, 2022). Natural mutation(s) in the γ-globin promoter removes the γ-globin repression and results in a persistent expression of HbF described as hereditary persistence of fetal hemoglobin (HPFH) (Cavazzana et al., 2017; Caulier and Sankaran, 2022).

2.2 HEMOGLOBINOPATHIES

The 2 main β-hemoglobinopathies are sickle cells disease (SCD) and β-thalassemia, both of them result in patient anemia and represent each year 400 000 affected births (Frati and Miccio, 2021).

2.2.1 Sickle cell disease

The SCD is caused by a A-to-T point mutation in the β-globin gene resulting in a E6V amino acid substitution in β-globin chains (β^S) forming Hemoglobin S (HbS). SCD is mainly found in sub-Saharan Africa, the Mediterranean basin, the Middle East, and India due to the malaria protective effect of the HbS. Migration flux increases the spread of the disorder in the world.

In deoxygenated condition, HbS polymerizes since in β^S chain the residue V6 can connect the phenylalanine and leucine residues in positions 85 and 88 of adjacent HbS (Cavazzana et al., 2017). This polymerization damages erythrocytes by forming an inflexible sickle RBCs. As consequence, sickled RBCs cause hemolytic anemia and vaso-occlusion that result in ischemic damage to tissues triggering pain and organs failure such as acute chest syndrome. Overtime, chronic complications can occur as vasculopathy (pulmonary hypertension, cerebral vascular disease …) or progressive organs dysfunction (liver damage, renal failure …).

The severity of SCD depends on the polymerization of HbS that correlate with the amount of Hb in RBCs. Patient suffering from SCD could have different hemoglobin traits improving their phenotype as α-thalassemia traits or as expression of HbF caused by HPFH due to mutation in γ-globin promoter. In α-thalassemia, 1 or 2 copies out of the 4 α-globin genes are deleted decreasing α-globin production and thus Hb formation. The reduction of Hb in SCD patient presenting α-thalassemia traits could decrease HbS polymerization and severity of the disorder and increase patient survival (Belisário et al., 2010; Rumaney et al., 2014; Piel et al., 2017). Moreover, the production of HbF caused by disruption of BCL11A or ZBTB7A γ-globin repression reduces also HbS polymerization.

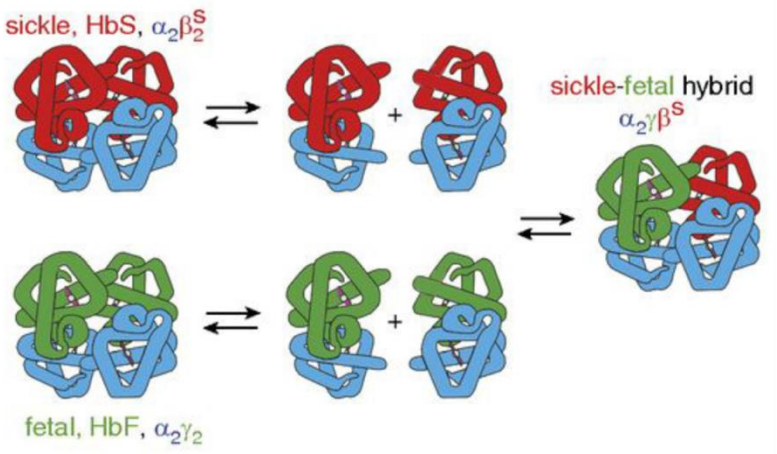

Figure 22) Representation of the HbS, HbF and hybride HBF/HbS structure, (from Eaton and Bunn, 2017).

In fact, γ-globin chains can form hybrid Hb (Figure 22) : ($\alpha_2\gamma\beta^S$) that can polymerize less efficiently with HbS due to the glutamine at position of 87 of γ-globin chains which is less favorable of lateral contact with Valine 6 of β^S-chains (Eaton and Bunn, 2017).

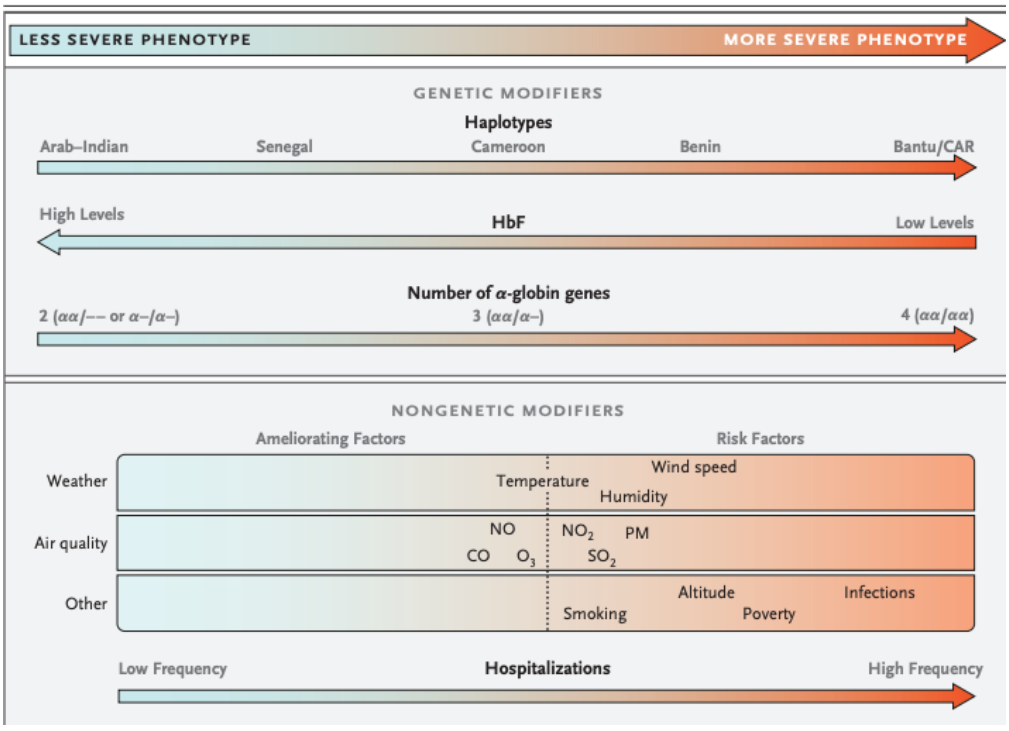

Figure 23) Genetic and nongenetic factors influencing the severity of SCD (from Piel et al., 2017). The severity of the phenotype depends on the levels of HbF and the number copy of α-globin gene and could also be influenced by non-genetic conditions as the humidity, the altitude and the infections

Others environmental factors have been described to influence HbS polymerization such as climatic and meteorologic factors, air quality and infectious disease (Figure 23). Current treatments consist of hydroxyurea that relies on increase HbF and prevents patient from acute pain and chest syndrome, on penicillin prophylaxis in children, and on blood transfusion. Allogenic HSCT represents a curative option SCD patient. In fact, 20% of donor granulocyte chimerism is sufficient to produce 100% of normal RBCs thus correct the SCD phenotype (Drysdale et al., 2021). Nevertheless, HSCT suffers from severe limitations such as the availability of suitable donors and remains quite expensive especially for lower-income countries.

2.2.2 β-thalassemia

β-thalassemia results in a wide range of mutations in the β-globin genes from single point mutation to large deletions affecting 1,5% of worldwide population. Mutation in β-globin genes triggers a decrease of β-globin production thus amount HbA. As for SCD, the β-thalassemia are mainly found in from Africa to south Europe and middle East toward Southeast Asia. The severity of the phenotype relies on the underlying mutation: β^+ indicates a mild mutation(s) with a relative decrease of β-globin chains expression; β^0 corresponds to a severe mutation(s) resulting in complete abrogation of β-globin chains synthesis. Absence of β-globin chains causes α-globin chains precipitation in erythroid precursors and erythrocytes which are associated with impairs erythropoiesis and hemolysis (Cavazzana et al., 2017; Taher et al., 2021).

3 forms of disease have been described :

- β-thalassemia minor, an asymptomatic form, resulting from heterozygous mutation(s) of the β-globin gene that is associated with no hematologic impairment (β-thalassemia silent carriers).
- β-thalassemia intermediate results in mild anemia and symptoms that occurs later in life and are transfusions independent although they may undergo blood transfusion occasionally (pregnancy, surgery, during infection or childhood …)

- β-thalassemia major suffers from severe anemia and symptoms in earlier life-stage that require lifelong treatment and are transfusion-dependent for their survival

β-thalassemia intermediate and major forms are caused by either heterozygous or homozygous mutations in β-globin genes. The diagnosis of patients is based on physical examination, family history and on hemoglobin electrophoresis or high-performance liquid chromatography (HPLC) (Taher et al., 2021).

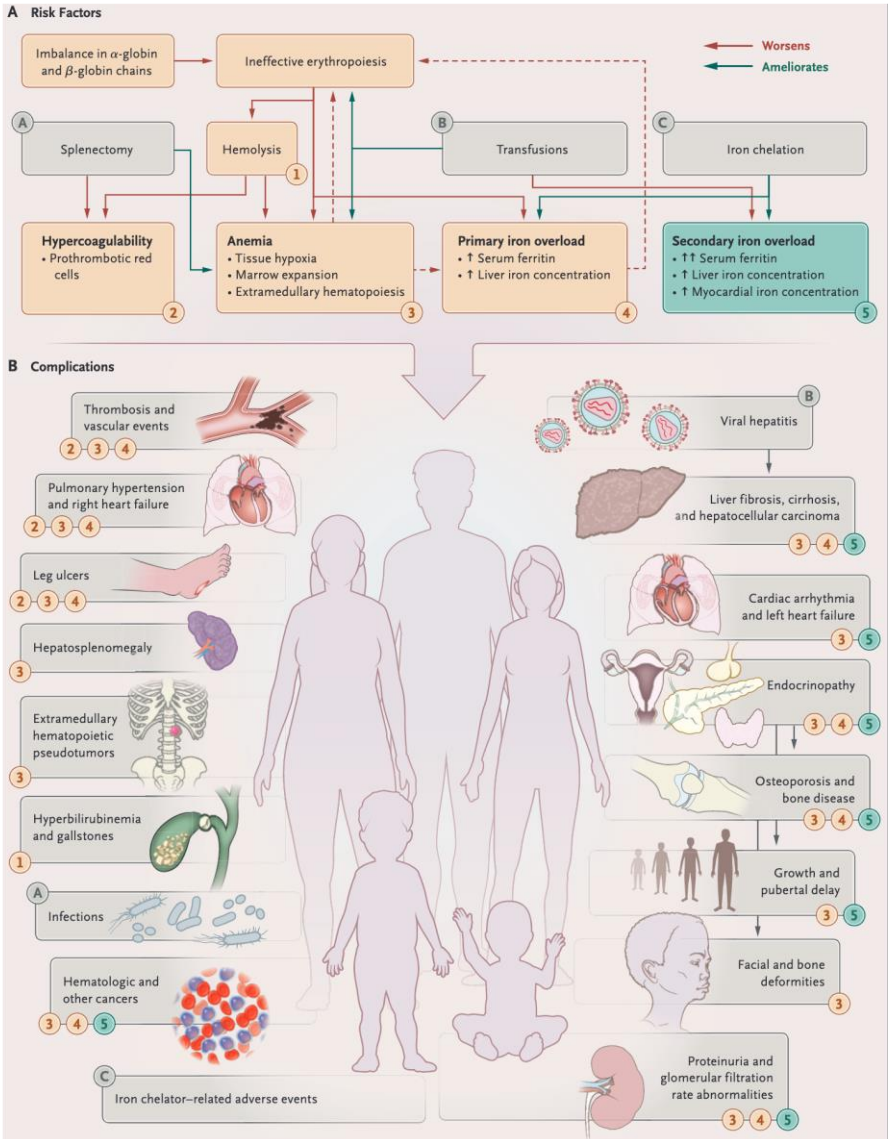

Figure 24) Representation of the phenotype of thalassemia patients, (from Taher et al., 2021). ***A****: Represent the risk factors of β-thalassemia patient that could suffer from anemia caused by hemolysis induced by α-globin precipitation.* ***B****: Represent all the complications that could develop β-thalassemia patient*

As consequence of impaired Hb, β-thalassemic patients suffer from hypercoagulability, anemia, primary iron overload that result in complications such as thrombosis, hepatomegaly, liver fibrosis (Figure 24). The ineffective erythropoiesis induced by β-thalassemia results in blockage in the erythroid differentiation in polychromatic erythroblasts and in erythroid precursors death (Taher et al., 2021).

In SCD, two condition can reduce the amount of free α-globin chains : i) α-thalassemia trait, which decreases the severity of the disease caused by α-globin chains precipitation; ii) expression of γ-globin chains which replaces the β-globin and reduces the imbalance between α-globin chains and β-globin chains and ameliorates the phenotype (Taher et al., 2021; Magrin et al., 2019; Cavazzana et al., 2017). The management of the disorder not only relies on blood transfusion but also on iron chelation and splenectomy. The treatment of transfusion-dependent β-thalassemia relies on drug administration as luspatercept therapy and on allogenic HSCs transplantation. Luspatercept therapy consists of injection of a recombinant protein able to increase the erythroid maturation, but it required frequent injections and long-term efficiency is still under evaluation. Allogenic HSCT results in 90% of disease free-survival in children transfusion dependent, but are limited by availability of suitable donors and its cost (Taher et al., 2021).

In order to offer a curative treatment for both SCD and β-thalassemia, ex vivo GT approaches have been developed and mainly focus on the insertion of a functional β-globin gene or enhancement the HbF synthesis.

2.3 *EX VIVO* GENE THERAPY FOR HEMOGLOBINOPATHIES

2.3.1 Lentiviral-based gene therapy

Insertion of a functional copy of healthy β-globin gene (HBB) in patient's HSCs offers the opportunity to produce heathy β-globin chains correcting the HbS precipitation in SCD and adjusting the normal HbA synthesis in β-thalassemia. Long-term HBB insertion takes advantage of SIN-LVV transduction to deliver therapeutic transgene into HSCs (Cavazzana et al., 2017; Drysdale et al., 2021).

Overtime, several constructions have been tested in clinical trials (described in https://clinicaltrials.gov/) to maximize the β-globin chains production while reducing LVV insertional mutagenesis (Figure 25).

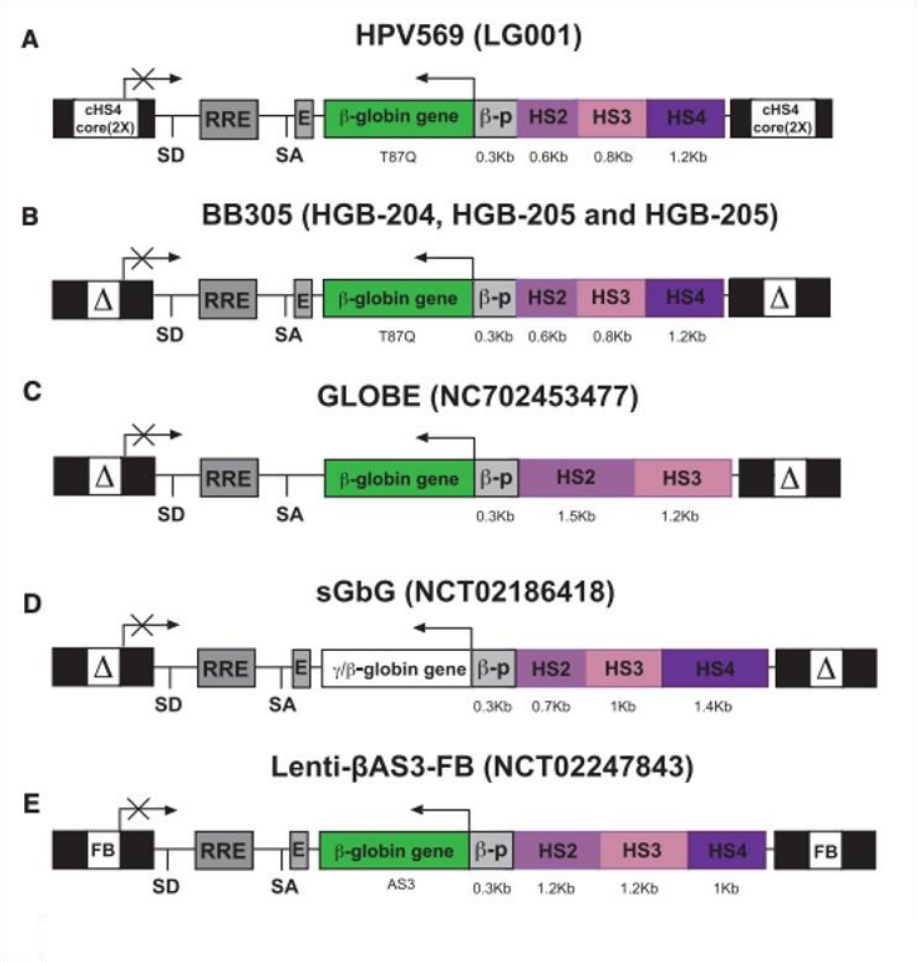

Figure 25) Representation of different LV constructions used to treat β-thalassemia in clinical trials (adapted from Cavazzana et al., 2017; Drysdale et al., 2021)

In 2007, a HPV569 LVV construction encoding a modified HBB gene with anti-sickling property induced by T87Q substitution in β-globin chains has been tested in clinical trial in France for β-thalassemia. The βT87Q-globin gene was inserted under control of 3 LCR HS site from β-globin promoter (HS2, HS3, HS4, Clinical trial : LG001 phase 1/2) using chicken β-globin HS4 chromatin insulator (cHS4) to reduce the neighboring gene transactivation upon genome integration. The β-thalassemic patient becomes transfusion independent 1 years after GT, but insertion analysis reveals a clonal dominance of integration in high mobility group AT hook 2 (HMGA2) gene (Cavazzana-Calvo

et al., 2010). In 2013, a France (NCT02151526) and international (NCT01745120) clinical trials started for both β-thalassemia and SCD with SIN-LVV BB305 encoding βT87Q-globin. The BB305 vector developed contains 5'LTR cytomegalovirus promoter and the cHS4 was removed due to its low viral production and transduction efficiency as well as its ability to induce vector rearrangement (Cavazzana et al., 2017; Drysdale et al., 2021). The GT in β-thalassemic patient results in reduction or abrogation of blood transfusion without development of integration clonal dominance (Thompson et al., 2018). In SCD patient treated in the French clinical trial an increase of Hb 15 months after GT has been described but with a modest clinical benefit (Ribeil et al., 2017). Improvement on the CD34+ mobilization by using Plerixafor alone instead of BM harvest and myeloablation with Busulfan provide better outcome in SCD patient with an absence of blood transfusion and severe SCD complications (Kanter et al., 2019). SIN-LV BB305 are now under evaluation in a phase 3 clinical trials for SCD open for younger pediatric patient (NCT04293185) (Drysdale et al., 2021).

In 2015, GLOBE SIN-LV clinical trial (NC702453477) started in Italy with vector encoding WT HBB under control of β-globin promoter and only 2 LCR HSs from β-globin promoter (HS2 and HS3) (Miccio et al., 2008). In the GT trial, patients undergo treosulfan and thiotepa myeloablation conditioning and corrected CD34+ were injected directly in the BM cavity. Pediatric patients undergo successful HSC engraftment with a stable vector integration and become transfusion independent after GT (Marktel et al., 2019).

In order to reach a curative level of hemoglobin in SCD, a β-globin chain able to overcompete the affinity for α-globin chain of the β^S-globin chain is required (Levasseur et al., 2004). Therefore, alternative therapeutic transgenes have been proposed as the γ-globin transgene (NCT02186418) or anti-sickling β-globin (AS3) transgene containing 3-point mutations leading to T87Q, E22A and G16D substitutions (NCT02247843) that have higher affinity for α-globin that β^S-globin as consequent inhibit HbS formation. The two LVs strategies show successful engraftment and therapeutic benefice for patient. Consequently, HBB addition with LVV transduction of patient HSCs provides a clear therapeutic benefit for SCD and β-thalassemia patients.

2.3.2 Gene editing-based gene therapy

Alternative HSCs corrections have been proposed based on gene editing to enhance HbF production or correction of the underlying β-globin mutation.

2.3.2.1 HDR-correction on underlying SCD mutation :

HDR correction of the pathologic β-globin locus relies on the delivery of exogenous DNA donor template containing homology arm (HA) for the targeted locus (β-globin gene). The donor sequence can be carried by ssODN, or viral vectors as IdLV or rAAV6.

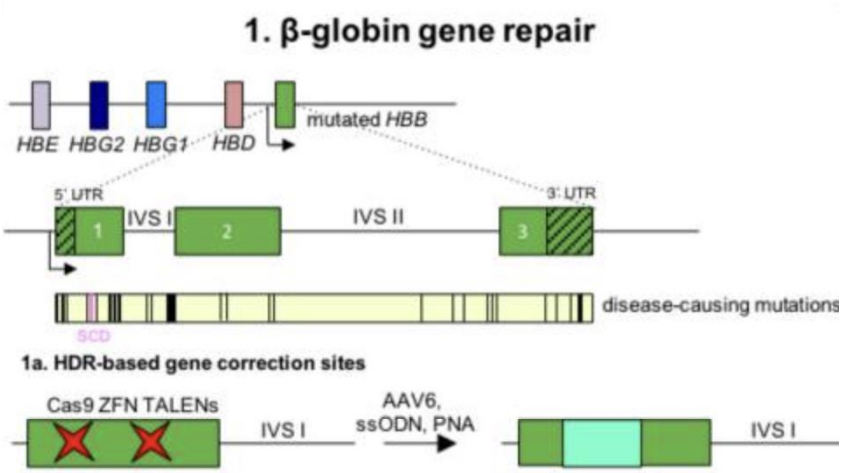

Figure 26) Representation of the β- globin gene repair consisting of replacement of mutated portion of β-globin gene (adapted from Frati and Miccio, 2021).

HDR-based correction has been developed in SCD using RNP complex targeting β-globin locus in the E6V point mutation and HBB template delivered (Figure 26) with ssODN (DeWitt et al., 2016) or AAV6 (Dever et al., 2016). In SCD HSCs cells, the implementation of HDR correction results in a sufficient production of HbA improving SCD RBCs phenotype. In xenotransplantation, the HDR corrected population declines suggesting that HDR is less efficient in LT-repopulation HSCs (DeWitt et al., 2016). Recently, HDR-modified CD34+ using RNP electroporation and ssODN has been evaluated in SCD rhesus macaque and shown successful engraftment of edited CD34+ in PB at 3-4 months but the required therapeutic threshold (20%) wasn't reached due to low HDR (around 1%)

ratio (Uchida et al., 2021, 2019). HDR-based therapy has been evaluated for β-thalassemia in patient-derived iPSCs and concentrated on disease-causing point mutation (Frati and Miccio, 2021).

2.3.2.2 Strategies to restore γ-globin expression :

Both for SCD and β-thalassemia, the expression of HbF ameliorates the disease phenotype. To restore the synthesis of γ-globin, CRISPR and ZNF based technologies have been designed to delete the GATA1 binding site of BCL11A erythroid specific-enhancer thus disrupting its expression. In fact, BCL11A is a repressor of γ-globin synthesis, therefore blocking the expression of BCL11A by disrupting its GATA1 transcription factor binding site will restore the expression of γ-globin in erythroid cells. The CRISPR-based therapy gives rise to 2 clinical trials for SCD (NCT03745287) and β-thalassemia (NCT03655678) started in 2018. One year after treatment, the patients treated show successful engraftment of modified CD34+ with a high level of editing (80 % and 60%, respectively). Both patient produce HbF and become transfusion independent with a elimination of vaso-occlusion events for SCD patient (Frangoul et al., 2021).

In 2018, a clinical trial with ZNF-based strategy (NCT03432364) started for β-thalassemia. All 5 patients undergo successful autologous transplantation of edited CD34+ that result in on-target indel generating a BCL11A KO, disrupting BCL11A expression in any blood cells and increasing HbF synthesis in erythroid population. Nonetheless after 1 to 2 years of GT, the level of HbF drop down by 64% requiring blood transfusion resumption (Smith et al., 2019; Walters et al., 2021).

Both CRISPR-Cas9 and ZNF nuclease induce DSB that remains quite toxic for cells and could result in chromosomal rearrangement. Moreover, off-target editing could be also observed with CRISPR-cas9 systems that is a major concern for β- hemoglobinopathies gene editing due to strong sequence homology among β-like globin locus. Therefore, base editing strategy for β-hemoglobinopathies are now under investigation to precisely modified a desired sites without inducing DSB (Antoniou et al., 2021; Frati and Miccio, 2021).

Base editing can be applied to reactivate the HbF by generating HPFH mutations or by disrupting erythroid-specific enhancer of BCL11A. Different point mutations have been tested to mimic HPFH modifications at position : -115 & -114, -198, or -175 of the γ-globin promoter 1/2 using optimized ABE and lead to respectively 20%, 50% and 58% of modifications able to restore a strong γ-globin expression. Moreover, precise edition of GATA1 binding site in BCL11A enhancer using ABE to convert 2 A>G sites leads to strong editing (90%) and restores HbF up to 32% in erythroid differentiated SCD HSCs improving erythropoiesis in β-thalassemic patient (Antoniou et al., 2021).

2.3.2.3 Base editors to correct the SCD mutation :

Base editor has been proposed as a new strategy to correct the underlying mutation in SCD. The current A>T mutation cannot be corrected with BE in SCD. Nonetheless, ABE can be applied to generate a Makassar allele (HbG) described to be non-pathologic by converting GTG codon to GCG triplet coding for Alanine. New engineering ABE nuclease was able to correct 45 to 80% of SCD allele in SCD HSCs and produced 52 to 72% of HbG in erythroid differentiated cells rescuing the SCD phenotype (Brendel and Williams, 2020; Antoniou et al., 2021).

Base editor represents a promising therapeutic approach for SCD but some challenges remain as BE delivery and possible off-target activity. Prime editing could offer another therapeutic benefit since it manages to correct the SCD mutation in HEK293T cells (Anzalone et al., 2019).

3 LYSOSOMAL STORAGE DISORDER AND GENE THERAPY

3.1 ROLE OF LIVER AND INBORN ERROR OF METABOLISM

3.1.1 The liver

The liver is one of the largest human organs with a weight around 1,4 kg in adults and is divided in 2 functional units called lobules. The liver plays a central role to maintain body homeostasis via the synthesis, the degradation, and the metabolism of a wide range of complex molecules. Basically, liver is able to convert the nutrients absorbed from gut into useable substances for the body. It manages the storage of these substances and their release upon body request. Liver is also the organ of detoxification as is able to degrade toxic compounds in harmless substances that can be, further later, eliminated. The liver synthetizes the bile that is delivered in the digestive tract via the bile duct aiming to digest lipids. Liver plays a role in the coagulation as it produces factors of clotting and in the degradation of old RBCs. In fact, the liver is responsible of 85% of synthesis of the circulating protein volume (Trefts et al., 2017).

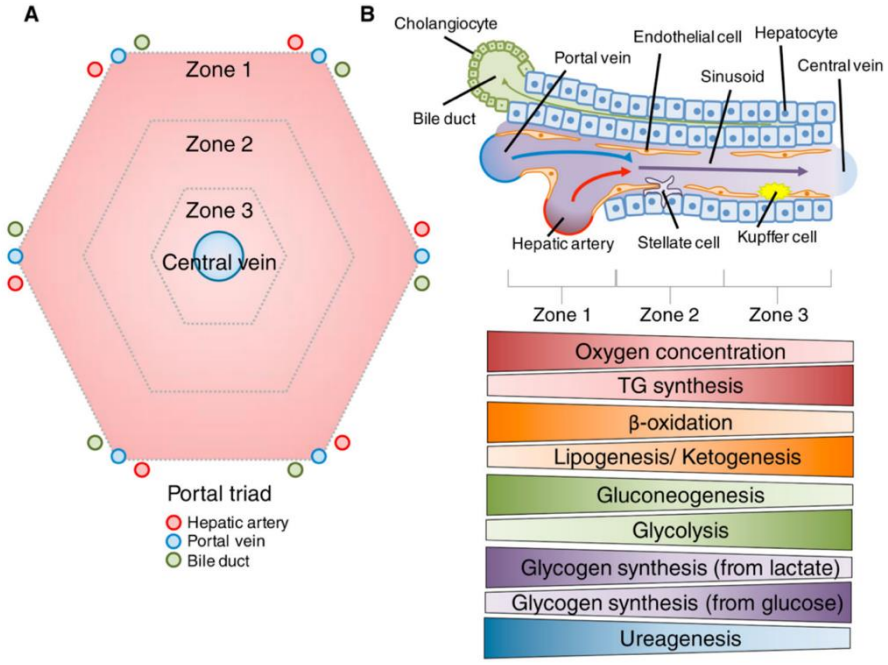

Figure 27) Structure of the liver with the 3 zones and all different cell types involved in liver function as hepatocytes, stellate or Kupffer cells aiming to degrade and synthetize organic compounds (adapted from Trefts et al., 2017).

Liver is composed of different cell types as hepatocytes, sinusoidal endothelial cells, stellate cells (storage of vitamin A), and macrophages as Kupffer cells. Hepatocytes are primary epithelial cells involved in the metabolic activity of the liver (Figure 27). The sinusoidal endothelial cells are located between blood circulation and hepatocytes and form pores to allow the exchanges of proteins and particles between plasma and liver cells. Meanwhile, macrophages eliminate pathogens, endotoxins and contribute to the clearance of cellular debris via their phagocytosis ability (Trefts et al., 2017). Each liver lobule is composed of 3 zones, the blood circulation in liver is driven be a sinusoid network in which the oxygen-rich blood from the hepatic artery is mixed with nutrient-rich blood from portal circulation Then blood progress through the 3 zones to reach the central vein, during blood flowing oxygen is absorbed and the hepatocytes process with the different metabolism activities (Figure 27). In fact, Zone 1 is involved in oxidative metabolism : gluconeogenesis, bile formation, and cholesterol formation while the zone 3 plays a role in detoxification, lipogenesis and glycogen synthesis (Kalra et al., 2022). The metabolic activity of hepatocytes differs in function of the lobules zones and is tightly regulated by the gene expression activation.

3.1.2 Lipids metabolism

3.1.2.1 Lipid's structure and transporters

Lipids are essential macromolecules degraded by hepatocytes. They act as source of energy production and are involved in the synthesis of vitamins, hormones, bile acid, cellular membranes, and cell signaling.

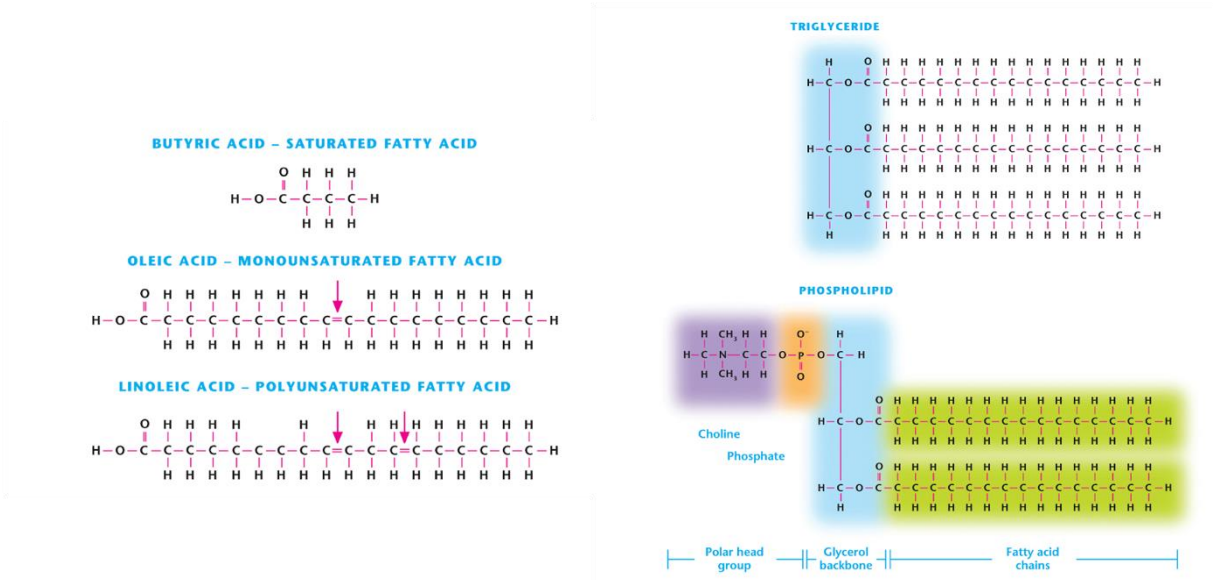

Figure 28) Representation of the 3 main lipids in human : Fatty acid saturated or unsaturated, triglycerides and phospholipids (adapted from Chandel, 2021).

The 4 main lipids in human are fatty acid (FA), cholesterol, phospholipids, and triglycerides (TG). FAs are organized in function of the number of carbon bonds and the presence (mono or poly-unsaturated FA) or not (saturated FA) of double bonds (Figure 28). Phospholipids and triglycerides derive from FA. In fact, phospholipids are 2 FAs linked with glycerol, a glucose derived product, and a polar molecule as choline while TG are FAs combined with glycerol (Figure 28). The hydrolysis of TG into FAs and glycerol is mediated by lipase enzyme and called β-oxidation. It occurs only in the liver and remains a large source of energy when blood level of glycose is low. In contrary, the FA synthesis is regulated by metabolites from glycolysis as citrate and palmitoyl-CoA, by hormones or posttranslational modification of enzymes. Cholesterol is a precursor of vitamins D and steroid

hormones as testosterone or estrogen. Cholesterol and phospholipid are essential components of membranes within the cell. Cholesterol could also be synthetized in liver by the enzyme : HMG-CoA reductase from Acetyl-coA ,a metabolite of glycolysis (Nguyen et al., 2008; Chandel, 2021).

Mainly, lipids are coming from the digestion and are transported in circulation by 4 types of lipoproteins (Figure 29), all of them differing by their level of protein, phospholipid, cholesterol and triglyceride or by their functions (Callahan et al., 2020).

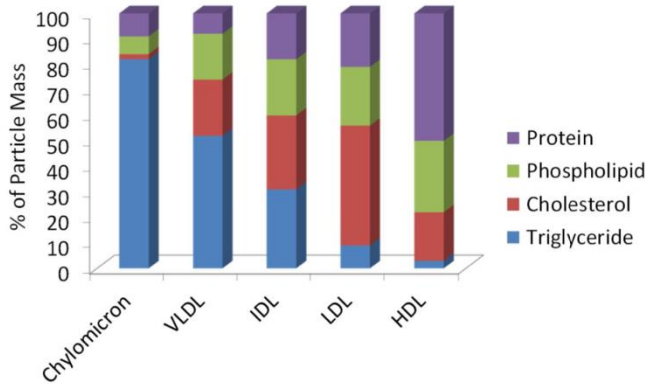

Figure 29) Composition of the different lipoproteins to transport lipids from digestion through liver or tissues (adapted from Callahan et al., 2020). VLDL : very-low density lipoprotein, IDL : intermediated density lipoprotein, LDL : low density lipoprotein HDL

3.1.2.2 Lipids absorption and degradation

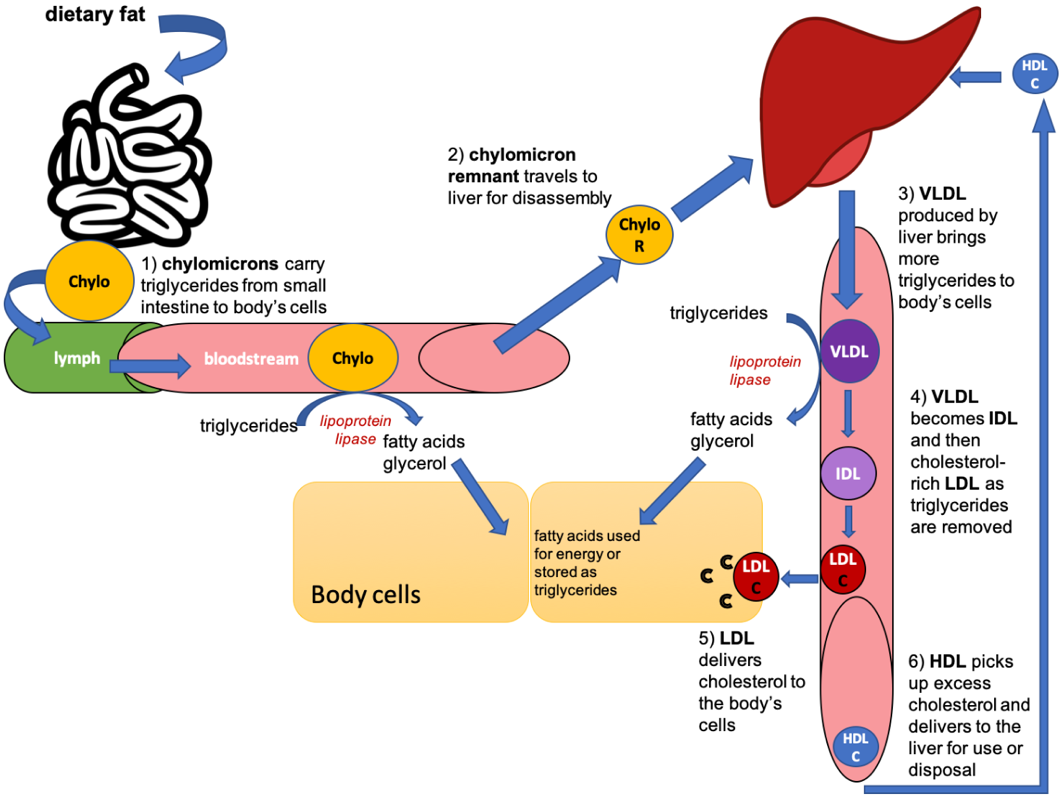

Figure 30) Representation of transport of lipids from intestine to tissue cells with the different lipoproteins involved (adapted from Callahan et al., 2020).

The transport of lipids from intestine to tissue is schematized in Figure 30. Initially, the transport of lipids from the digestive tract are mediated by chylomicron. In enterocytes, FAs are converted into TGs while cholesterol is esterified to form cholesterol-esters (CEs) and both are packaged into chylomicrons. Chylomicrons are then released into the lymph and further later in the bloodstream to be uptake by skeletal tissues or adipocyte. The tissues lipoprotein lipase (LPL) degrades TG from chylomicron into FAs and glycerol that can be used as energy sourced or stored. Hydrolysis of TGs results in a size decrease to form chylomicron remnant enriched of CE. Chylomicron remnants are then captured by liver and CEs are used to form very-low-density- lipoproteins (VDHL), bile acid or hormones. VDHL transports TGs and CEs into peripheral tissues that degrade TG into FAs while CEs are concentrated in intermediated density lipoprotein (IDL) particle, then in low density lipoprotein (LDL). LDLs continue to circulate in bloodstream and deliver cholesterol and TG into peripheral

tissues. The production rate of LDLs is regulated by cholesterol content of hepatocytes and by the LDL-receptor (LDL-R) activity in the liver that mediate the internalization of LDL: High activity due to high level of LDLs in circulation reduced the LDLs production. In peripheral tissues, the release of cholesterol reduces the activity of HMG-CoA reductase and the production of LDL-receptor. In fact, cholesterol from LDL is delivered in the lysosome and move toward endoplasmic reticulum (ER) to inhibit the production of LDL-receptor. As the level of cholesterol is already high in hepatocytes and peripheral tissues, there is no need to further increase the amount of cholesterol into cells by LDL-uptake. Excess of circulated LDL leads to atherosclerosis.

Finally, high density lipoprotein (HDL) is produced by peripheral tissues when cholesterol is in excess and corresponds to reverse cholesterol transporter require to transport excess of cholesterol into the liver. Macrophages play a central role in this HDL formation and maturation. Thus, HDL delivered in the liver serves to bile formation or are released into bile (Feingold, 2000; Callahan et al., 2020).

3.1.3 Inborn error of metabolisms

Inborn error of metabolisms (IEMs) is caused by genetic defect on a metabolic pathway resulting in an impairment on metabolic function disrupting homeostasis. IME was first described in 1909 by Sir Garrod, but it was not until the discovery in 1948 by Beadle and Tatum that biochemical systems are regulated by specific genes and that metabolic dysfunctions were associated with genetic mutations in the corresponding gene. Nowadays, around 1000 IEMs have been described with a cumulation incidence around 1/800. IEMs are classified based on the group of enzyme defectives, the accumulated toxic substrates or affected organelles. Therefore, IEMs are heterogenous groups of disease including amino acid disorders, fatty acid oxidation diseases, mitochondrial dysfunctions, lipid storage diseases and lysosomal storage disorders (LSD). The genetic defect can be caused by point mutations, deletions, insertions, or chromosomal rearrangements that lead to either a loss of active enzyme, or transporter or co-factor triggering dysfunction on the metabolic pathway or toxic accumulation of metabolites. Disease burden depends on the residual enzymatic activity and clinical manifestation may start from birth to adulthood. Therefore, the diagnosis relies on genetic tests and enzymatic assays that are available as newborn screening or prenatal diagnosis. Management of

IEMs includes specific diet, enzyme replacement therapy (ERT), substrate inhibition or even organs transplantation (Mak et al., 2013; Ezgu, 2016).

3.2 LYSOSOMAL STORAGE DISORDERS

3.2.1 Lysosome

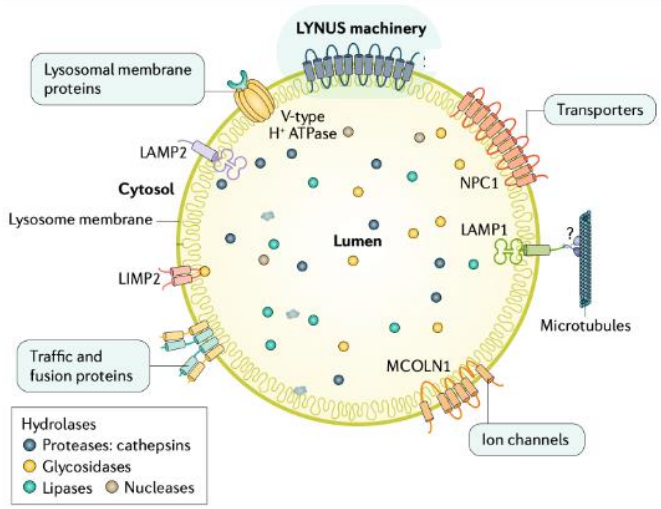

Figure 31) Structure and composition of lysosome (adapted from Platt et al., 2018)

Lysosomes are intracellular acidic organelles (pH 4.5-5.5) playing a central role in cellular homeostasis performing complex molecule degradation and cell signaling. Lysosomes are composed of a single phospholipid membrane including membrane proteins, transporters, and ion channels. Among them, transporters as lysosome-associated membrane protein 2 (LAMP2) allow the transport of substrates from cytoplasm to lysosome; ion channels as mucolipin 1 (MCOLN1) fine-tune the ion concentration in lysosomes; the lysosomal nutrient-sensing machinery (LYNUS) is responsible for the sensing of nutrient environment within lysosome (Figure 31). The mobility of lysosomes in the cytoplasm is mediated via microtubules that interact with the lysosome-associated membrane protein 1 (LAMP1) and their acidification is driven by a ATP proton pump (V-type H^+ ATPase) (Platt et al., 2018; Lawrence and Zoncu, 2019). The lysosomal lumen contains around 100 lysosomal proteins, mainly hydrolases that are activated in acidic environment and able to degrade lipids, nucleic acids, proteins, and carbohydrates. Lysosomes degrade products from endocytosis, phagocytosis, or autophagy of

cytoplasmic compound as ERs, mitochondria or other lysosomes and export the digestive products to serve as new building blocks. Nonetheless, the role of lysosome is not limited to degradation and recycling, as it is involved also in cells signaling and in energy or amino acid sensing (Lawrence and Zoncu, 2019; Yang and Wang, 2021). Lysosomes can interact also with other cytoplasmic organelles as mitochondria or ERs to mutually regulate homeostasis. Lysosome biogenesis is closedly linked to intra- and extra- cellular signals to conserve their own homeostasis. The generation of new lysosomal vescicle by fission requires hydrolase synthesis and post-translational modification adding an oligosaccharide group phosphorylated : mannose 6-phophate (M6P) that can be specifically recognized via Mannose 6-phosphate receptor (M6P-R) present into early-endosome. Early-endosome are then maturated to late-endosome and later in lysosomes (Platt et al., 2018; Yang and Wang, 2021).

3.2.2 Lysosomal storage disorders

LSD are subfamily of IEMs, that cause around 70 monogenic diseases mainly autosomal recessive or X-linked inherited. LSDs are the result of mutation(s) in gene encoding lysosomal proteins (nucleases, lipases, glucosidases …) or membrane transporters that generate accumulation of toxic substrates (lipids, proteins, carbohydrates) impairing the normal function of the lysosome. Due to its role in complex molecules degradation, the liver is often affected by LSDs even if the severity of the impairment depends on the deficient gene product. Macrophages (Knupfer cells in liver or microglia cells in the central nervous system (CNS)) play also a central role in clearance of cells debris and impaired metabolic products resulting in a dysfunction on this immune population in LSD that can trigger inflammation and worsen disease progression (Parenti et al., 2021; Platt et al., 2018; Ezgu, 2016). Overall, the incidence of LSD is around 1:5000 live births, but taking individually the monogenic disorders incidence are rare : 1:50000 - 1:250 000 live births. Although the LSD prevalence increases in some ethnicities due to founder effect (Platt et al., 2012, 2018). The most common LSDs are represented in the table 1.

Disorders (gene)		Deficient enzyme	Compound accumulated	Main affected tissues	CNS involvement
Sphingolipidoses	Fabry disease (GLA)	α-Galactosidase A	Globotriaosylceramide	Kidney, heart	-
	Gaucher disease (GBA)	β -Glucocerebrosidase	Glucocerebroside and glucosylsphingosine	Spleen/liver, bone marrow	+
	Metachromatic leukodystrophy (ARSA and PSAP)	Arylsulfatase A and prosaposin	Sulfatides	CNS	+
	Niemann–Pick disease types A and B (SMPD1)	Sphingomyelin phosphodiesterase	Sphingomyelin	Liver	+
Mucopolysaccharidoses	MPS I: Hurler syndrome (IDUA)	α-L-Iduronidase	Dermatan sulfate and heparan sulfate	Bone, heart	+
Glycogen storage disease	GSD II: Pompe disease (GAA)	Lysosomal α-glucosidase	Glycogen	Skeletal muscle, heart	+/-
Lipid storage diseases	Lysosomal Acid lipase deficiency (LAL-D): Wolman disease and cholesterol ester storage disease (LIPA)	Lysosomal acid lipase	CE, TG	Liver	-

Table 1) List of the major LSDs with the corresponding deficient enzyme, compound accumulated, and main tissues affected with or without CNs involvement (adapted from Platt et al., 2018)

LSDs are heterogenous disorders, but common clinical phenotypes have been described in LSD patients as hepatomegaly and splenomegaly. Other phenotypes can be observed according to the nature of toxic accumulation as cardiac involvement in Pompe disease or CNS dysfunction in Hurler syndrome or metachromatic leukodystrophy. The severity of the disease depends mainly on the mutation(s) that cause either an early onset of the disease in pediatric patients (severe form) or a late onset in young people or adults (mild to asymptomatic form) (Platt et al., 2018; Ezgu, 2016). In LSD

caused by deficiency of hydrolase (Table 1), the severity of the disease corresponds with the residual enzymatic activity.

The diagnosis of LSD is based on clinical symptoms, on determination of toxic compound accumulation as measure of glycosaminoglycans in the urine for Mucopolysaccharidoses (MSP). The final diagnosis consists in enzymatic activity assays in peripheral blood mononuclear cells (PBMCs) and single gene sequencing (Parenti et al., 2021; Platt et al., 2018). Nonetheless, diagnosis of late-onset form remains delayed due to the non-specific clinical symptoms which are weakness or abnormal movement or ataxia or mild muscular impairment for Pompe disease (Platt et al., 2018). Alternative approaches have been tested to better understand the LSD phenotype such a transcriptomic analysis, genome-wide association studies (Parenti et al., 2021). In order to decrease the incidence of LSD, carrier screening to identify couple that carries a mutation(s) for the same metabolic gene could be applied. Also newborn screening would increase the efficiency of the treatment but, it is performed only for disorders that have a suitable treatment (Platt et al., 2018). For LSD, there are 5 main therapeutic strategies :

- Enzyme replacement therapy (ERT) is a common treatment for LSD caused by hydrolase deficiency (Table 1) and consists of an intravenous injection of the recombinant missing enzyme aiming to degrade the lysosomal toxic accumulation. In patient, enzyme delivered by bloodstream could be uptake via M6P-R receptor present on the surface of many cell types and targeted to the lysosomes to replace the missing enzymatic function. Nowadays, all diseases presented in the Table 1 have a corresponding ERT. The treatment improves the patient clinical phenotype and increases lifespan but remains quite expensive and required weekly administration throughout the patient's lifetime. ERT is limited by the development of immune response against the recombinant enzyme that can decrease the treatment efficiency and lead to anaphylactic shock. Thus, ERT is also not able to cross the blood brain barrier to correct the neurological impairment and is inaccessible for certain organs as cardiovascular sys-

tems or ocular function (Platt et al., 2018). In order to improve the targeting or pharmacokinetic of ERT, second generation of enzymes have been build up as glycoengineered GAA for Pompe disease (Parenti et al., 2021).

HSCT : The principle is similar than ERT instead of enzyme injection, healthy cells will produce the missing protein. Upon HSCT, BM-derived cells from healthy donor can produce functional enzyme that can correct affected tissues via cross-correction. While improving clinically features, the production of missing enzyme upon HSCT remains low and doesn't reach a corrective level for patients. For Hurler syndrome, HSCT remains the standard care treatment as it prevent neurological impairment that cannot be corrected with ERT (Nagree et al., 2019; Platt et al., 2018).

- Substrate reduction therapy (SRT) consists of the use of chemical molecule to prevent from substrate toxic accumulation. For now, SRT has been approved only for Sphingolipidoses (Hurler syndrome and Niemann–Pick disease) and inhibit the glycosphingolipid biosynthesis. SRT is easier to employ as its orally administrated and doesn't induce immune response, but patients may undergo adverse effects due to drug metabolization. Thus, SRT requires to well understood the underlying metabolic pathways to find the proper reaction to block. Other SRTs have currently under clinical trials for Fabry disease or MSPIII (Platt et al., 2018). For some LSDs as LAL-D, diet management can prevent substrate absorption and therefore its accumulation.

- Liver transplantation : The transplantation of healthy liver from donor could be an alternative option for LSD to reduce the hepatic and peripheric organs burden (Liu et al., 2019). Nonetheless, due to the multisystemic defect of LSD, liver transplantation doesn't prevent from disease progression and therefore not provide a long-term curative treatment for some LSDs (Ramakrishna et al., 2022).

- *Ex vivo* GT : Correction of patient's HSCs represents an promising approach to treat LSD since they could lead to supraphysiological expression of lysosomal enzyme and cross-correct affected tissues. Modification of patient's HSCs prevent GAVHD and allows to treat patient with no-matched donor. Thus, expression of enzyme by HSC-derived cells should be less immunogenic than ERT (Saif et al., 2012).

The development of new therapeutic options can also take advantage of cell-based screening to identify candidate molecules for LSD (Parenti et al., 2021). Drug screening in Niemann-Pick type C patient fibroblasts by cell image-based quantification of lysosomes with specific marker as LAMP-1 or toxic accumulated products as cholesterol with Filipin staining resulted in the discovery of new chemical drugs improving the cellular homeostasis (Pugach et al., 2018). Using such cell-based assay to quantify lysosomes and them content using specific probes has been employed in other LSDs in order to find therapeutic treatments or to follow the disease phenotype (Xu et al., 2012; Aguisanda et al., 2017). Cell image-based vesicle quantification can also take advantage of newly developed image flow cytometry (IFC) to further enhance the specificity and the precision of the measurement. In fact, IFC combines flow cytometry that allows the single cell analysis of fluorescence signal or scatter light from cells in suspensions with microscopy imaging that take a real image of the acquired cells. Finally, the localization and the number of the fluorescence events into acquired cells can be visualized and quantified with IFC algorithm. IFC has been recently employed for macrophage phagocytosis analysis (Mochalova et al., 2022), or extracellular vesicles analysis in human plasma (Woud et al., 2022) paving the way to use IFC as diagnosis or drug discovery pipeline for LSD.

3.2.3 Lysosomal acid lipase (LAL) deficiency

The lysosomal acid lipase (LAL) is an enzyme involved in the degradation of TGs and CEs in the lysosomes in almost all cell types, especially macrophages and hepatocytes. LAL is activated by acidic pH and hydrolyzes CE and TG into free cholesterol (FC) and free fatty acid (FFA) that serve as source of energy by fatty acid oxidation, membrane formation or biosynthesize of cholesterol-derived compounds (Li and Zhang, 2019).

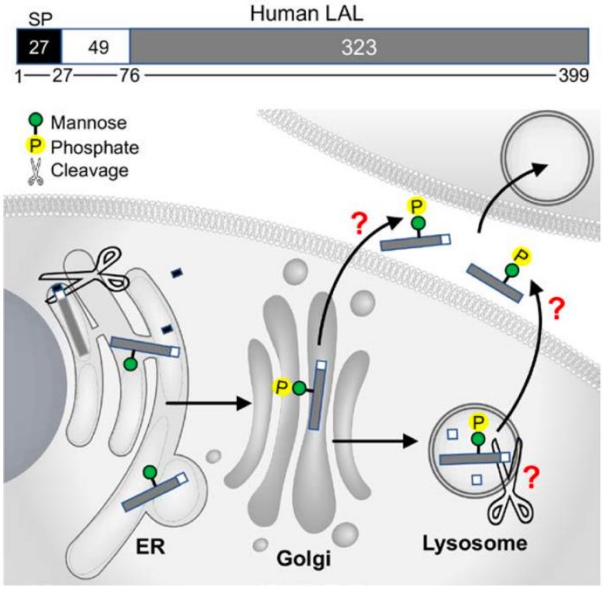

Figure 32) Representation of the LAL enzyme as a prepropeptide and LAL export, post-translational modification, lysosomal activation and extracellular secretion (adapted from Li and Zhang, 2019).

LAL hydrolase is a 399 amino acids prepropeptide. To be active, post-translational glycosylation of LAL enzyme is required. Protein gel electrophoresis of LAL purified results in 2 protein bands at 41 and 56 kilodalton (kda). The 56 kda represents the propeptide with the elimination of the 27 amino acids signal peptide. The signal peptide is cleaved in the lumen of the ER and then LAL traffics through the Golgi apparatus to undergo post-translational modification especially M6P modification that is present in all soluble LAL form. The 41 kda corresponds to the LAL enzyme without it 49 amino acid of propeptide sequence that is cleaved in the lysosomes (Ameis et al., 1994; Zschenker, 2004; Braulke and Bonifacino, 2009). As other lysosomal enzyme, LAL could be secreted in small amount and uptake via M6P-R, even if the mechanism of LAL secretion is not clear (Figure 32) (Li and Zhang, 2019).

The LAL is encoded by the lipase A (*LIPA)* gene (10q23.2–23.3, 10 exons, NCBI entry : 3988). 120 *LIPA* mutations have been identified and are associated with LAL deficiency (LAL-D), an autosomal recessive LSD. LAL-D triggers CEs and TGs accumulation in tissues and organs especially in the liver, spleen, intestine, and macrophage, resulting in multi-organs failure. The severity of the disorder depends on the remaining amount of functional enzyme. 2 forms have been characterized : cholesterol esters storage disorder (CESD, prevalence 1/40 000 live births), less severe with later-onset, with around 2-12% of functional enzyme; Wolman disease (WD prevalence 1/100 000 live births), severe form of the disorder with early-onset, with less than 2% of functional LAL enzyme. The diagnosis of LAL-D is based on the clinical phenotype, residual LAL activity from blood spot and on the sequencing of the underlying mutation(s) (Witeck et al., 2022; Vijay et al., 2020; Li and Zhang, 2019). LAL-D patients suffer from hepatomegaly, splenomegaly, and hyperlipidemia without CNS involvement (Table 1). WD patients undergo difficulty to thrive, intestinal malabsorption and adrenal gland calcification, all of them leading to a premature death in first year after birth without treatment. CESD patients present a milder clinical feature with premature atherosclerosis and cardiac affection that could result in death in childhood or adolescence if not treated (Witeck et al., 2022).

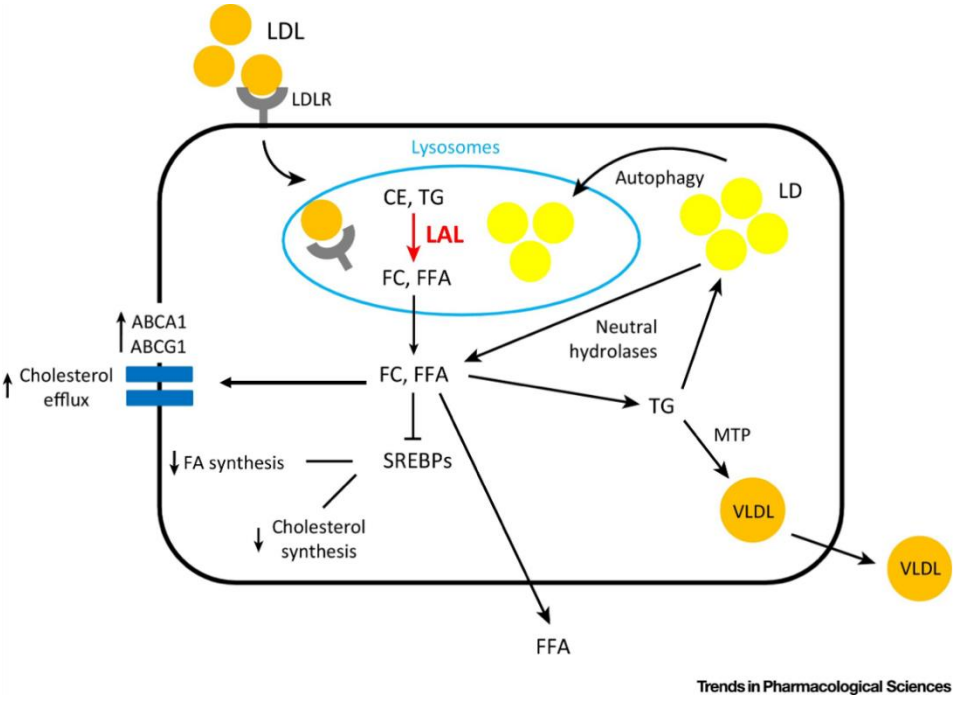

Figure 33) Representation of the LAL function into healthy cells (adapted from Gomaraschi et al., 2019).

In healthy cells, LDLs delivered into cytoplasm via endocytosis are targeted to the lysosomes and transported CEs and TGs are then hydrolyzed to FC and FFA (Figure 33). The high FCs amount inactivate transcription factors, as sterol regulatory element-binding proteins (SREBPs) that regulates FA and cholesterol synthesis, cholesterol efflux or LDL uptake by controlling the LDL-R expression. CEs and TGs are stored in lipid droplet (LD) that are degraded by LAL upon autophagy. In adipocytes, FFAs are released in bloodstream or stored as TG while in hepatocytes, TGs are packaged into VLDL to be delivered in all tissues. In immune cells, LAL enzyme plays a central role in cell proliferation and activation due to the energy requirement for those process (Gomaraschi et al., 2019; Li and Zhang, 2019). In hepatocytes, LAL-D results in an increase of VLDL secretion and the decrease of FCs activate SREBP promoting lipid synthesis and blocking cholesterol efflux and HDLs synthesis. In the liver, the lipid accumulation occurs both in hepatocytes and Kupfer cells (Gomaraschi et al., 2019). `

To further understand the LAL mechanism of action, a LAL-deficiency mouse (LAL -/-) model has been generated (Du, 1998). LAL-/- mouse undergoes massive lipid accumulation in liver, spleen, small intestine resulting in hepatomegaly, splenomegaly. The LAL-/- model mimics the CESD phenotype in terms of survival (7-8 months) but the lipid accumulation resembles to the severe form of the disease: WD (Du, 1998). In this model, the decrease of cholesterol efflux and the increase of cholesterol content result in macrophage activation and myeloproliferation with an increased tissue infiltration of myeloid derived suppressor cells (MDSCs) (Ding et al., 2014). Moreover, accumulation of lipids impairs also the T-cell maturation in thymus and spleen leading to decrease of circulating mature T-cells (Qu et al., 2009; Li and Zhang, 2019; Gomaraschi et al., 2019). LAL-/- model adapts to lipid homeostasis disruption by promoting the use of glucose as energy source and results in plasma glucose reduction, as well as reduced liver glucose and glycogen (Du et al., 2001). Deficiency of LAL causes also respiratory inflammation and modification of alveolar structure (Lian et al., 2004).

ERT is the standard care after LAL-D diagnosis and consists of weekly intravenous administration of recombinant LAL enzyme called Sebelipase (Kanuma®, Alexion Pharmaceuticals, Inc.). This non-curative treament improves the lifespan of patients and the clinical features mainly the liver function. Nonetheless, ERT has be associated with the development of antibodies against the recombinant

enzyme in 9% of treated patient, remains very costly and its long-term efficacy is still under evaluation (Burton et al., 2022; Vijay et al., 2020). HSCT could be also used for LAL-D and shows normalization of liver function but is associated with high procedure morbidity and is quite limited by the donor suitability or GAVHD (Tolar et al., 2009; Potter et al., 2021). Liver transplantation from healthy donor has been also employed in LAL-D patient but it is not sufficient to prevent from disease progression (Bernstein et al., 2018).

3.3 GENE THERAPY FOR LSD

To treat LSD, there are several GT strategies that target either hepatocyte via *in vivo* GT or HSCs upon *ex vivo* GT. Both strategies are based on classical gene replacement, addition or correction using LVVs, AAVs, or genome editing. The main advantage of GT for LSD comes from the ability of the produced enzyme by corrected cells to be secreted and uptake via M6P-R to correct even non-modified cells and cross-correct affected tissues.

LVV-based *ex vivo* GT was first developed for metachromatic leukodystrophy (MLD) (Biffi et al., 2013) and is now under clinical trials (Phase 1/2 : NCT01560182, Phase 2 : NCT03392987, Phase 3 : NCT04283227). MLD is caused by arylsulfatase A (ARSA) deficiency and results in severe neurological impairment due to toxic accumulation of sulfatides in central and peripheral nervous tissues that lead to neuroinflammation and demyelination. The GT consists of recovering CD34+ from early-onset to late juvenile MLD patient, transduction with LVV particle encoding ARSA cDNA under the control of the ubiquitous human phosphoglycerate kinase promoter (PGK) and re-infusion of corrected HSCs after busulfan myeloablation. The conditioning and the transplantation allow to replace the pathologic microglia in brain by ARSA overexpressing microglia aiming to improve the neurological function in MLD patient. Recent data from the NCT01560182 clinical trial shown a stable HSCs engraftment and an efficient ARSA expression (up to 18-fold) that improve early-onset of MLD. GT results in a motor skill acquisition and normal cognitive development especially in patient treated before symptoms appearance. No clonal dominance was observed, but 4 patients out of 26 alive developed transient antibodies against the ARSA enzyme (Fumagalli et al., 2022).

Different *ex vivo* GT have applied for other LSDs using different promoter to drive the expression of the therapeutic transgene in cell specific population as macrophage or erythroid population or both. In fact, the Mucopolysaccharidosis Type IIIA, a neurogenerative LSD caused by the deficiency of sulfamidase, was initially treated with a spleen focus forming virus (SFFV) promoter encoding the lysosomal enzyme sulfamidase (SGSH) gene but results in a low correction of the behavior abnormalities compared to standard HSCT in MSPIIIA mouse model (Langford-Smith et al., 2012). The employment of myeloid-specific CD11b promoter results instead in an efficient correction of the neurological impairment in mouse model and put in light the fundamental aspect of using the proper cell type to treat LSD (Ellison et al., 2019).

This LVV construction is currently under investigation in phase 1/2 clinical trial (NCT04201405). *Ex vivo* GT under clinical trials evaluation (Table 2) mainly relies on the expression of therapeutic lysosomal enzyme via specific as myeloid promoter for MSPIIIA or ubiquitous promoter as elongation factor 1α (EF1α) for Fabry disease: NCT02800070, (Huang et al., 2017; Khan et al., 2021), PGK for MLD and Mucopolysaccharidosis Type I (Hurler syndrome, deficiency of IDUA) : NCT03488394 (Gentner et al., 2021).

Disease	Gene cDNA	promoter	Clinical trials	Phase	Clinical data
Fabry disease	GLA	EF1α	**NCT02800070**	I	Khan et al., 2021
Metachromatic leukodystrophy (MLD)	ARSA	PGK	**NCT01560182**	I/II	Fumagalli et al., 2022
			NCT03392987	II	
			NCT04283227	III	
Hurler syndrome	IDUA	PGK	**NCT03488394**	I/II	Gentner et al., 2021
Mucopolysaccharidosis Type IIIA (MSPIIIA)	SGSH	CD11b	**NCT04201405**	I/II	

Table 2) Sum-up of ongoing clinical trials for LSD with the promoter used and the clinical trials and references of data

Meanwhile, other promoters have been tested to maximize the expression and secretion of functional enzyme to cross-correct tissues. Among them, erythroid specific expression of enzyme has been tested for Hurler syndrome, a LSD caused by deficiency of IDUA and affected heart and liver function (Wang et al., 2009). Erythroid lineage restricted expression of transgene could decrease the risk of oncogenes activation and results in a strong secretion in bloodstream of the therapeutic enzyme without interfering with the hemoglobin synthesis. Finally, RBCs delivery would reduce the immunological response against the therapeutic enzyme (Grimm et al., 2015). In fact, for hurler syndrome the erythroid secreted IDUA results in supraphysiological production of enzyme able to correct Hurler phenotype even in the CNS. Authors claims that even with low gene transfer (<1%), the erythroid secretion of enzyme would provide a clinical benefit for patient. Lastly, a combined promoter with β-Globin LCR and EF1α short promoter provides a strong erythroid expression while conserving the white blood cells expression. Such promoter associates the production of therapeutic enzyme in bloodstream with the production by other HSC derived cell as macrophage to provide local enzyme into affected tissues (Montiel-Equihua et al., 2012). LVV-based HSCs correction using β-Globin LCR-EF1α promoter has been recently applied for Pompe disease. Pompe disease is caused by deficiency in acid α-glucosidase (GAA) that results in glycogen accumulation impairing the heart and skeletal muscle function. The transplantation in a mouse model of LVV β-Globin LCR-EF1α expressing GAA results in stable engraftment and GAA expression correcting the cardiac and muscle phenotype (Piras et al., 2020).

Alternative of blood re-infusion of the LVV corrected HSCs, an intracerebroventricular injection has been evaluated by injecting LV-ARSA CD34+ into immunosuppressed mouse model to replace microglia by overexpression ARSA microglia without required BM transplantation. It results in extensive and quicker repopulation of microglia in brain with more ARSA expressing microglia compared to conventional blood ARSA corrected CD34+ re-infusion (Capotondo et al., 2017). Intracerebroventricular injection would be helpful for LSD with neurological impairment by increasing the enzyme producing microglia.

Genome editing strategy has been also tested for Hurler syndrome by integrating the IDUA cDNA into the CCR5 safe-harbor locus. In this strategy, human HSCs were edited with RNP complex targeting the CCR5 locus and then transduced with AAV6 particle encoding IDUA cDNA under the control of PGK promoter. Then corrected cells were transplanted in IDUA-/- immunocompromised mice. Authors achieve efficient gene knock-in : 44 % in peripheral-blood HSCs resulting in IDUA expression especially in liver and spleen leading to a decrease of toxic glycosaminoglycans (GAG) accumulation, but no IDUA were found in the brain (Gomez-Ospina et al., 2019). This gene editing paves the ways of universal platform for LSD genetic correction.

4 THESIS INTRODUCTION AND OBJECTIVES

In *ex vivo* GT, targeted integration of a functional copy of a mutated gene into a safe harbor locus provides a suitable therapy to treat wide range of monogenic disorder. In this context, we exploited the α-globin locus (HBA) as a safe harbor locus to develop a universal platform for expression and secretion of therapeutic proteins into erythroid cells. In fact, HBA locus expressed high α-globin chain (around 1,5g/day) and the loss of 3 out of 4 HBA genes is asymptotic (Vichinsky, 2013). Therefore, hijacking the HBA promoter should result in high transgene expression without interfering with the normal Hb formation. LV- correction of HSCs using erythroid promoter demonstrated the ability of erythroid cells to produce β-globin chains (described introduction Part 2.2.1) and to support the secretion of functional proteins as clotting factor (Chang et al., 2006) or metabolic enzyme as IDUA for Hurler syndrome (described Introduction part 3.3 , (Wang et al., 2009)). Due to the abundance of erythroid cells in human ($5X10^6$ RBCs/microliter of blood) and the high HBA expression in erythroid population, HBA targeted platform would require minimal editing and integration events to maximize the protein production reducing potential off-target and toxicity due to editing and DNA donor delivery.

My two main thesis objectives were i) the evaluation of the therapeutic potency of hijacking the HBA promoter for both β-globin chain expression in β-thalassemia context and metabolic enzyme secretion for erythroid delivery of the missing protein for metabolic diseases and ii) characterization of LAL-D and development of LV-based *ex vivo* gene therapy for the disease.

During my thesis, I participated in the evaluation of CRISPR-based knock-in (KI) in HBA locus for β-thalassemia which combined reduction the α-globin expression caused by HBA deletion and insertion of β-globin gene into HBA locus to restore the α/β imbalance (Described Result Part 6.1). Then, we applied the HBA targeted platform for erythroid expression and secretion in bloodstream of therapeutic proteins as clotting factors IX responsible of Hemophilia B and different lysosomal enzymes as α-galactosidase (GLA) responsible of Fabry disease, Iduronidase (IDUA) responsible of Mucopolysaccharidosis and Lysosomal acid lipase (LAL) responsible of Wolman disease (WD)

(Described Result Part 6.2). We then focused on the optimization of LIPA cDNA transgene to enhance the LAL expression and secretion (Described Result Part 6.3.1). For this purpose, I developed LVVs encoding LIPA cDNA under erythroid promoter to produce LAL in mature erythroid cells. The optimized LIPA transgene will serve for LVV-based *ex vivo* GT for LAL-D treatment and for our HBA targeted platform in the purpose of enhancing the LAL expression while minimizing the targeting integration events required to fully correct the LAL-D. Finally, we set-up a multimodal cytometry approach using flow cytometry and image flow cytometry (IFC) to better characterize LAL-D phenotype and to evaluate the therapeutic potency of GT. We evaluated this pipeline on WD patient's fibroblasts, on LIPA KO engineered Jurkat cells and on PBMCs for LAL-D mouse model (Described Result Part 6.3.2). This approach could be applied as a follow-up pipeline for LAL-D patient or to assess therapeutic effect of viral construction or production slot.

.

Materials and methods

5 MATERIALS AND METHODS

5.1 CLONING AND LENTIVIRAL PRODUCTION

5.1.1 Cloning of LIPA transgenes into plasmids

Genscript (https://www.genscript.com) performed the LIPA cloning in plasmids encoding an erythroid promoter (HS2HS3 β-globin LCR). All the LIPA transgenes have been synthetized and cloned in pCCL_HS2HS3_β-globin_GFP_WPRE by removing GFP sequence and integration of LIPA transgenes using restriction enzymes: PspLI and XhoI. The sequence of LIPA cDNA without signal peptide and with HA-Tag was:

GGGAAACTGACAGCTGTGGATCCTGAAACAAACATGAATGTGAGTGAAATTATCTCTTACTGGGGATTCC
CTAGTGAGGAATACCTAGTTGAGACAGAAGATGGATATATTCTGTGCCTTAACCGAATTCCTCATGGGAG
GAAGAACCATTCTGACAAAGGTCCCAAACCAGTTGTCTTCCTGCAACATGGCTTGCTGGCAGATTCTAGTA
ACTGGGTCACAAACCTTGCCAACAGCAGCCTGGGCTTCATTCTTGCTGATGCTGGTTTTGACGTGTGGATG
GGCAACAGCAGAGGAAATACCTGGTCTCGGAAACATAAGACACTCTCAGTTTCTCAGGATGAATTCTGGG
CTTTCAGTTATGATGAGATGGCAAAATATGACCTACCAGCTTCCATTAACTTCATTCTGAATAAAACTGGC
CAAGAACAAGTGTATTATGTGGGTCATTCTCAAGGCACCACTATAGGTTTTATAGCATTTTCACAGATCCCT
GAGCTGGCTAAAAGGATTAAAATGTTTTTTGCCCTGGGTCCTGTGGCTTCCGTCGCCTTCTGTACTAGCCCT
ATGGCCAAATTAGGACGATTACCAGATCATCTCATTAAGGACTTATTTGGAGACAAAGAATTTCTTCCCCA
GAGTGCGTTTTTGAAGTGGCTGGGTACCCACGTTTGCACTCATGTCATACTGAAGGAGCTCTGTGGAAATC
TCTGTTTTCTTCTGTGTGGATTTAATGAGAGAAATTTAAATATGTCTAGAGTGGATGTATATACAACACATT
CTCCTGCTGGAACTTCTGTGCAAAACATGTTACACTGGAGCCAGGCTGTTAAATTCCAAAAGTTTCAAGCC
TTTGACTGGGGAAGCAGTGCCAAGAATTATTTTCATTACAACCAGAGTTATCCTCCCACATACAATGTGAA
GGACATGCTTGTGCCGACTGCAGTCTGGAGCGGGGGTCACGACTGGCTTGCAGATGTCTACGACGTCAAT
ATCTTACTGACTCAGATCACCAACTTGGTGTTCCATGAGAGCATTCCGGAATGGGAGCATCTTGACTTCAT
TTGGGGCCTGGATGCCCCTTGGAGGCTTTATAATAAAATTATTAATCTAATGAGGAAATATCAGGGAGGG
AGCGGCTATCCCTATGACGTGCCTGATTACGCCGGCACAGGATCCTACCCCTATGATGTGCCTGACTACG
CTGGCAGCGCCGGATACCCTTATGATGTGCCTGATTATGCTTAA

With the Stop codon in red and HA-tag highlighted in yellow. All sequences started with Kozac sequence: CACC

Signal peptide (SP)	Abbreviation	DNA sequences of signal peptide	Ref
WT LIPA	SP1	ATGAAAATGCGGTTCTTGGGGTTGGTGGTCTGTTTGG-TTCTCTGGACCCTGCATTCTGAGGGGTCTGGA	Uniprot
a-1 antitrypsin	SP2	ATGCCGTCTTCTGTCTCGTGGGGCATCCTCCTGCTGGCAGGCCTGTGCTGCCTGGTCCCTGTCTCCCTGGCT	(Puzzo et al., 2017)
Iduronate 2-sulfatase	SP6	ATGCCGCCACCCCGGACCGGCCGAGGCCTTCTCTGGCTGGG-TCTGGTTCTGAGCTCCGTCTGCGTCGCCCTCGGA	
Chymotrypsinogen B2	SP7	ATGGCTTTCCTCTGGCTCCTCTCCTGCTGGGCCCTCCTGGGTAC-CACCTTCGGC	
Plasma protease inhibitor	SP8	ATGGCCTCCAGGCTGACCCTGCT-GACCCTCCTGCTGCTGCTGCTGGCTGGGGATAGAGCCTCCTCA	
Serum albumin preprotein	SP9	ATGAAGTGGGTAACCTTTATTTCCCTTCTTTTTCTCTT-TAGCTCGGCTTATTCC	(Kober et al., 2013)
Azurocidin preprotein	SP10	ATGACCCGGCTGACAGTCCTGGCCCTGCTGGCTGG-TCTGCTGGCGTCCTCGAGGGCC	

Table 3) The DNA sequences and related genes of signal peptides used for LIPA constructions

The plasmids were analysed by digestion profile using restriction enzymes and by sequencing. To increase the amount of plasmids Maxiprep were performed according to the manufacturing protocol (*Nucleobond Xtra Maxi EF, Macherey-nagel).*

The codon optimizations of SP8 LIPA construction have generated using 3 softwares :

Software	Online link
IDT	https://eu.idtdna.com/pages/tools/codon-optimization-tool
Genescript	https://www.genscript.com/codon-opt.html?page_no=1&position_no=2&sensors=googlesearch
Thermofisher	https://www.thermofisher.com/fr/fr/home/life-science/cloning/gene-synthesis/geneoptimizer.html

Table 4) Software used for codon optimization

The sequences of LIPA optimization are presented in the patent : EP 20 306524.8

5.1.2 Lentiviral production

The production of SIN-LVV vectors was performed by transient transfection of HEK 293T with packaging plasmid : pMDLg/p.RRE, plasmid encoding reverse transcriptase : pK.REV, and with VSV-G pseudotyped envelope plasmid, and with our plasmid encoding LIPA transgene. 24h after transfection, cell medium was changed, and LVVs were recovered at 48h and 72h. Then, LVVs were filtrated with 0.22 µm Polyethersulfone (PES) membrane (Corning) and concentrated using ultracentrifugation 19 000 rpm for 2h (Beckman, LE-80K Ultracentrifuge). After ultracentrifugation, the supernatant was removed, and LVVs were resuspended in X-Vivo 20 (Lonza) and stored at -80°C. LVVs were titrated in HCT116 cells and HIV-1 Gag p24 content was quantified using ELISA (Perkin-Elmer) according to manufacturer's instructions.

5.2 CELL CULTURE

5.2.1 K562

K562 (ATCC® CCL-243) cells were maintained in a RPMI 1640 medium supplemented with 2 mM glutamine (Gibco by Life Technology), 10% fetal bovine serum (FBS, BioWhittaker, Lonza), 10 mM HEPES, 1 mM sodium pyruvate (Gibco) and penicillin and streptomycin (100U/ml each, LifeTechnologies).

5.2.2 CD34+ HSCs

hHSCs cells were recovered from cord blood provided by Centre Hospitalier Sud-Francilien (CHSF, Evry, France). CD34+ were isolated by immunomagnetic selection with AUTOMACS PRO (Miltenyi Biotec, Paris, France) after immunostaining with CD34 MicroBead Kit (Miltenyi Biotec) and stored in -80°C in FBS+10% DMSO solution. CD34+ were defrosted in a solution of 10 mL HBSS (Gibco) supplemented with 10% of human serum AB male heat inactivated (Biowest) and equilibrated at room temperature for 10 min prior centrifugation at 400g for 7 minutes. Then, CD34+ cells were pre-stimulated in a StemSpan medium (Stemcell technologies) containing 300 ng/mL of hSCF (Miltenyi Biotec), 300 ng/mL of hFlt3 (Miltenyi Biotec), 100 ng/mL of hIL-3 (Miltenyi Biotec), 750 nM of StemRegenin-1 (Stemcell technologies), 350 µM of UM 171 (Stemcell technologies) and penicillin and streptomycin (100U/ml each, LifeTechnologies). StemRegenin-1 and UM 171 were added just prior used. CD34+ were erythroid differentiated for 14 days either with an erythroid specific medium or in semisolid Methocult Medium. The liquid culture erythroid differentiation was initiated using a Stem Span medium (Stemcell technologies) containing 20 ng/mL of hSCF (Miltenyi Biotec), 5 ng/mL of hIL-3 (Miltenyi Biotec), 1ng/mL of EPO (EPEX syringe, Janssen), 2ng/mL of Dexamethasone (Sigma Aldrich), 1ng/mL of β-oestradiol (Sigma Aldrich), and penicillin and streptomycin (100U/ml each, LifeTechnologies). The colony-forming cells (CFC) assay (H4435, StemCell Technologies) was performed by seeded 1000 CD34+ in 3 mL methylcellulose that are further divided in 2 petri dishes. Then, colonies were count and identified manually according to morphological criteria (BFU-E, CFU-G/GM, and CFU-GEMM).

5.3 LENTIVIRAL TRANSDUCTIONS AND VECTOR COPY NUMBERS DETERMINATION

5.3.1 LV transduction in K562

K562 were transduced at a MOI of 10 with LV particles. For the transduction, K562 were spin down at 600g for 5 min, and re-suspended in 400 µL of medium supplemented with polybren (8µg/mL, Sigma Aldrich). The proper volume of vector was added onto cells and the transduction occurs overnight at 37°C 5% CO2. The day after, K562 were washed once in a volume of phosphate-buffered saline (PBS) and re-suspended in the culturing medium. K562 were cultivated for 14 days.

5.3.2 LV transduction in CD34+ HSCs

Prior CD34+ transduction, a 12-well plate were coated with Retronectin (5 µg/well, Takara) at 4°C overnight. CD34+ were transduced 1 days after pre-stimulation at a MOI of 30. CD34+ were washed once with a volume PBS and spin down at 400 g for 5 min. Then, CD34+ were re-suspended in 300 µL of pre-stimulation medium supplemented with 4µg/mL protamine sulfate (Sigma Aldrich) and disposed into retronectin-coated plate. Then the corresponding volume of LV was added and CD34+ were transduced overnight at 37°C 5% C02. The day after, cells were washed once in PBS and re-suspended in erythroid medium.

5.3.3 Measurement of vecors copy number (VCNs)

The LV integration was measured by qPCR on DNA. The DNA extraction was performed on 50 000 cells using QuickExtract™ DNA Extraction Solution (Lucigen, Middelton, WI, USA) according to manufacturer's instructions. The extracted DNA was diluted in 1/25 in distilled water (Gibco). The vector quantification was performed on PSI sequence and normalized with Albumin (ALB) sequence (Table 4). The qPCR was performed with 6 µL of qPCR mix and 4µL of diluted DNA. A standard was used to determine the vector copy number of PSI and ALB in function of Ct.

Name of primer	Sequences	Reaction (µM)
PSI Forward	CAGGACTCGGCTTGCTGAAG	0.1
PSI Reverse	TCCCCCGCTTAATACTGACG	0.1
PSI Probe (FAM)	CGCACGGCAAGAGGCGAGG	0.1
ALB Forward	GCTGTCATCTCTTGTGGGCTGT	0.3
ALB Reverse	ACTCATGGGAGCTGCTGGTTC	0.3
ALB Probe (VIC)	CCTGTCATGCCCACACAAATCTCTCC	0.25

Table 5) Primer sequences and quantity (µM) for mix reaction for VCNs qPCR

The qPCR was run a LightCycler device (Roche) with the following protocol:

- Pre-incubation 95°C, 15min
- Amplification (45 cycles) : 95°C, 15s ; 60°C, 1min
- Cooling 40°C, 30s

The Copy number of Alb and Psi were determined from the standard curve equation. The VCN is calculated by a ratio between $\frac{\text{Copy number of PSI}}{\text{Copy of ALB}}$ X 2

5.4 LAL TRANSGENE EXPRESSION MEASUREMENT

5.4.1 Western Blot

To detect intracellular proteins, cells were lysed in RIPA buffer (Sigma-Aldrich) supplemented with protease inhibitor (Roche) freezed/thawed twice and centrifuged 10 minutes at 14 000 rcf at 4 °C. Total protein was quantified using BCA assay (Thermo-Fisher Scientific). Between 10-20 µg of protein or 5-10µL of supernatant were denatured at 90 °C for 10 minutes, run under reducing conditions on a 4–12% Bis-tris gel and transferred to a nitrocellulose membrane using iBlot2 system (Invitrogen). After Ponceau staining (Invitrogen), membranes were blocked for 2 h with Odyssey blocking buffer

(Odyssey Blocking buffer (PBS)) and incubated for 1 h with primary antibodies: mouse anti-hLAL (Thermofisher, 9G7F12, 7G6D7, dilution 1:2000) or mouse anti-HA-tag (Eurogentec, 16B12, dilution 1:1000) followed by specific secondary antibodies in PBS:Blocking buffer respectively: goat anti-mouse IgG (H+L) at 800CW or donkey anti-mouse IgG (H+L) at 680LT (Li-Cor Biosciences, dilution 1:15 000). β-tubulin (Li-Cor Biosciences, rabbit polyclonal, dilution 1:15 000) was used as loading control and revelled with secondary antibodies in PBS:Blocking buffer : goat anti-rabbit IgG (H+L) at 680CLT (Li-Cor Biosciences, dilution 1:15 000). Blots were imaged at 169 µm with Odyssey imager and analysed with ImageStudio Lite software (Li-Cor Biosciences, Lincoln, NE, USA). After image background subtraction (average method, top/bottom), band intensities were quantified and normalized with β-tubulin signal or with the volume of supernatant.

5.4.2 LAL activity

Protein activity was detected in supernatants as previously described (Aguisanda et al., 2017; Hamilton et al., 2012) with some modifications. Samples were incubated 10 minutes at 37 °C with 42 µM Lalistat-2 (Sigma-Aldrich), a specific competitive inhibitor of LAL, or with water. Samples were then transferred to a Optiplate 96 F plate (PerkinElmer) where fluorimetric reactions were initiated with 75 µl of substrate buffer (340 µM of 4-Methylumbelliferyl phosphate (4-MUP, Cayman chemicals), 0.9% Triton X-100 (Sigma Aldrich) and 220 µM cardiolipin (Sigma Aldrich) in 135mM acetate buffer pH 4.0). After 10 minutes, fluorescence was recorded (35 cycles, 30 seconds intervals, 37 °C) using SPARK TECAN Reader (Tecan, Austria). Kinetic parameters (average rate, RFU/min) were calculated using Magellan Software and the relative LAL activity was calculated as follow:

$$Relative\ LAL\ activity = \frac{Signal\ \ without\ Lalistat}{Signal\ \ with\ Lalistat}$$

5.4.3 HA-tag RNA expression with RT-qPCR

5.4.3.1 RNA extraction & cDNA synthesis

RNA was extracted using RNeasy Micro kit (Qiagen) from 200 000 cells and 40 ng of RNA were

reverse transcribed in cDNA using the Transcriptor First Strand cDNA Synthesis Kit (Roche) with oligo(dT) probe. The cDNA was diluted in 1/25 prior qPCR in distilled water (Gibco).

5.4.3.2 HA-tag qPCR

The SYBR Green (Maxima SYBR GREEN/ Rox qPCR, thermofisher) qPCR mix was prepared with 0.3 µM of primers for GAPDH and HA-taq. Then 4µL of the diluted cDNA were loaded to 6µL of mix qPCR in a 384-well plate.

Name of primer	Sequences
GAPDH Forward	CTTCATTGACCTCAACTACATGGTTT
GAPDH Reverse	TGGGATTTCCATTGATGACAAG
HA-taq Forward	TGATTACGCCGGCACAG
HA-tag Reverse	ATCAGGCACATCATAAGGGTATC

Table 6) Primer sequences for HA-taq RT-qPCR

The qPCR was run a LightCycler device (Roche) with the following protocol:

- Pre-incubation 95°C, 15min
- Amplification (40 cycles) : 95°C, 15s ; 60°C, 1min
- Cooling 40°C, 30s

The level of HA-tag expression was expressed as $2^{-(Ct\ GAPDH - Ct\ HA\ taq)}$.

Results

6 RESULTS:

The result section is subdivided in 2 main parts :

In the first part, we developed a HDR based genome editing strategy to provide a treatment for β-thalassemia. In this attempt, we combined deletion of α-globin gene (HBA) using CRISPR-Cas9 nuclease to mimic α-thalassemia trait and targeted integration of β-globin (HBB) cDNA into HBA locus via HDR repair mechanism to achieve robust expression of β-globin chains and restore HbA formation. HBA locus was selected as a safe harbour locus due both to its high and erythroid-lineage specific (~1.5 g/day) expression allowing β-globin synthesis under physiological condition and its asymptomatic deletion of 3 out the 4 α-globin genes in diploid cells. Using this HBA targeting approach, we were able to restore the α/β imbalance that led to significant HbA formation (described in part 6.1). Then, we applied the CRISPR-based KI platform in HBA locus for erythroid expression and bloodstream secretion of therapeutic proteins (described in part 6.2). In fact, hijacking the HBA promoter to express therapeutic protein in erythroid population provides a universal platform for monogenic disorders that require supplementation of the missing protein with a particular interest for LAL. Due to the abundance of erythroid cells in human ($5X10^6$ RBCs/microliter of blood) and the high HBA expression in erythroid population, HBA targeted platform would require minimal editing and integration events to maximize the protein production reducing potential off-target and toxicity due to editing and DNA donor delivery.

In the second part, we optimized the LIPA cDNA to further enhance the expression and erythroid secretion of the therapeutic LAL enzyme to reach optimal correction of LAL-D phenotype. In this context, we developed LVVs encoding LIPA cDNA under GLOBE promoter (Miccio et al., 2008) resulting in erythroid expression and secretion of the LAL enzyme in erythroid differentiated CD34+ populations (described in part 6.3.1). This study would allow us both to establish a curative LV-based *ex vivo* GT for LAL-D and to develop an optimized LIPA transgene suitable for HBA targeting platform that will minimize further the integration events on HBA locus require to reach therapeutic level therefore the toxicity on CRISPR KI platform. Finally, we developed multimodal cytometry tools using

flow cytometry and IFC to better characterize the lipid accumulation of LAL-D and evaluate *in vitro* the proper uptake and therapeutic potential of erythroid secreted LAL enzyme or LVV construction (described in part 6.3.2).

6.1 HBA TARGETING APPROACH FOR *EX VIVO* GT TREATMENT OF β-THALASSEMIA (PAVANI ET AL., 2021)

Introduction :

β-thalassemia is caused by mutation(s) in HBB gene that lead to a decrease or abruption of β-globin chains synthesis thus result in a reduction HbA and α-globin precipitation. Deletion of α-globin gene has been already described to reduce the severity β-thalassaemic phenotype. Here, we exploited a CRISPR-Cas9 technology for HBA locus to reduce α-globin precipitation by deletion of HBA copy and target insertion of functional and optimized HBB gene into HBA locus in a thalassaemic HUDEP-2 cells model and CD34+ HSCs.

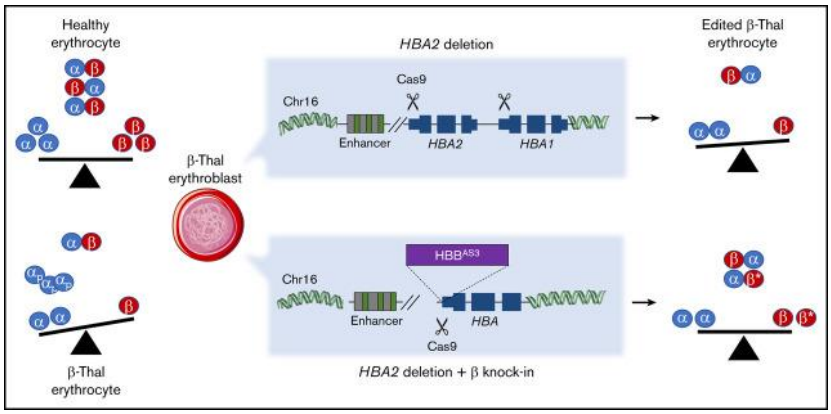

Figure 34) Representation of HBA-targeted platform for HBB expression (Pavani et al., 2021) that combined α-globin gene deletion and β-globin gene insertion under control of the endogenous α-globin promoter to restore the $\frac{\alpha}{\beta}$ imbalance.

Edited CD34+ cells were transplanted in immunocompromised mice to assure the proper engraftment and multilineage potency of corrected HSCs. Then, we measured the therapeutic effects of the platform in β-thalassaemic patients HSCs on the HbA formation by using HPLC. Finally, we tested Nickase Cas9 complex with our HBA gRNA to increase the safety and decrease the cell toxicity upon DSBs.

Contribution : In this paper, I participated on the experimentation and on the data analysis of HBA 2 deletion in HUDEP cells and of the targeting integration of β-globin transgenes into HBA locus in HUDEP cells.

REGULAR ARTICLE

blood advances

Correction of β-thalassemia by CRISPR/Cas9 editing of the α-globin locus in human hematopoietic stem cells

Giulia Pavani,[1] Anna Fabiano,[1,*] Marine Laurent,[1,*] Fatima Amor,[1] Erika Cantelli,[1] Anne Chalumeau,[2,3] Giulia Maule,[4,5] Alexandra Tachtsidi,[1] Jean-Paul Concordet,[6] Anna Cereseto,[4] Fulvio Mavilio,[7] Giuliana Ferrari,[8] Annarita Miccio,[2,3] and Mario Amendola[1]

[1]Integrated Genetic Approaches in Therapeutic Discovery for Rare Diseases (INTEGRARE), Genethon, Unité Mixte de Recherche (UMR) S951 INSERM, University Evry, University Paris-Saclay, Evry, France; [2]Imagine Institute, UMR 163 INSERM, Paris, France; [3]Paris Descartes, University Sorbonne Paris Cité, Paris, France; [4]Centre for Integrative Biology (CIBIO), University of Trento, Trento, Italy; [5]Institute of Biophysics, National Research Council, Trento, Italy; [6]National Museum of Natural History, UMR_1154 INSERM, UMR_7196 CNRS, University Sorbonne, Paris, France; [7]Department of Life Sciences, University of Modena and Reggio Emilia, Modena, Italy; and [8]Vita-Salute San Raffaele University, San Raffaele Telethon Institute for Gene Therapy (SR-TIGET), IRCCS San Raffaele Scientific Institute, Milan, Italy

Key Points

- *HBA2* gene deletion in human HSPCs reduces α-globin precipitates in erythroblasts and ameliorates β^{+}-thalassemia phenotype.
- Synergistic *HBA2* gene deletion and *HBB* gene replacement in HSPCs ameliorate β^{0}-thalassemia phenotype

β-thalassemias (β-thal) are a group of blood disorders caused by mutations in the β-globin gene (*HBB*) cluster. β-globin associates with α-globin to form adult hemoglobin (HbA, $\alpha_2\beta_2$), the main oxygen-carrier in erythrocytes. When β-globin chains are absent or limiting, free α-globins precipitate and damage cell membranes, causing hemolysis and ineffective erythropoiesis. Clinical data show that severity of β-thal correlates with the number of inherited α-globin genes (*HBA1* and *HBA2*), with α-globin gene deletions having a beneficial effect for patients. Here, we describe a novel strategy to treat β-thal based on genome editing of the α-globin locus in human hematopoietic stem/progenitor cells (HSPCs). Using CRISPR/Cas9, we combined 2 therapeutic approaches: (1) α-globin downregulation, by deleting the *HBA2* gene to recreate an α-thalassemia trait, and (2) β-globin expression, by targeted integration of a β-globin transgene downstream the *HBA2* promoter. First, we optimized the CRISPR/Cas9 strategy and corrected the pathological phenotype in a cellular model of β-thalassemia (human erythroid progenitor cell [HUDEP-2] β^{0}). Then, we edited healthy donor HSPCs and demonstrated that they maintained long-term repopulation capacity and multipotency in xenotransplanted mice. To assess the clinical potential of this approach, we next edited β-thal HSPCs and achieved correction of α/β globin imbalance in HSPC-derived erythroblasts. As a safer option for clinical translation, we performed editing in HSPCs using Cas9 nickase showing precise editing with no InDels. Overall, we described an innovative CRISPR/Cas9 approach to improve α/β globin imbalance in thalassemic HSPCs, paving the way for novel therapeutic strategies for β-thal.

Introduction

Adult hemoglobin consists of 2 pairs of globin subunits ($\alpha_2\beta_2$), whose production is strictly regulated to ensure their balanced expression in erythroid cells. Disorders in hemoglobin synthesis cause thalassemia, a severe anemia requiring lifelong supportive treatments.[1] β-thalassemia is the most common and severe form of thalassemia, with >70 000 new patients per year worldwide, caused by mutations in the β-globin gene (*HBB*) cluster, which result in reduced or absent synthesis of β-globin chain.[2] As a consequence, the free α-globin in excess forms toxic precipitates that cause intramedullary apoptosis of erythroid precursors (ineffective erythropoiesis) and death of mature

Submitted 6 April 2020; accepted 4 January 2021; published online 26 February 2021. DOI 10.1182/bloodadvances.2020001996.

*A.F. and M.L. equally contributed to this work.

GUIDE-seq datasets are available in the BioProject online repository (ID PRJNA676022; http://www.ncbi.nlm.nih.gov/bioproject/676022).

Requests for original data should be sent to Giulia Pavani (gpavani@genethon.fr).

The full-text version of this article contains a data supplement.

red blood cells (hemolysis). Healthy individuals carry 4 α-globin genes per cell (αα/αα), 2 genes in *cis* on each chromosome 16 (*HBA1* and *HBA2*), which often undergo genomic rearrangements and *HBA2* gene loss because of their sequence homology (96.67%, GRCh38). Clinical data have shown that the severity of β-thalassemia directly correlates with the number of α-globin genes, with *HBA* deletions having a beneficial effect for patients.[3] This positive effect is especially pronounced in patients with hemoglobin variant E (HbE) β-thalassemia, where the HbE allele still allows residual expression of β-globin chain (~50% of all β-thalassemia patients).[4-7]

Current clinical management of β-thalassemia patients relies on regular blood transfusion and iron chelation therapy, required to reduce organ damage and iron overload, respectively.[8] Allogeneic hematopoietic stem cell (HSC) transplantation is a definitive cure, but it is limited by the availability of compatible donors.[9-12]

Two alternative strategies have been proposed to counteract the α/β globin imbalance in β-thal. The first consists in the expression/induction of β-globins or β-like globins, such as γ-globin, to complex with the α-globins in excess and produce adult or fetal hemoglobin.[13-18] In particular, ex vivo HSC gene therapy with lentiviral vectors (LV) encoding for *HBB* transgene significantly ameliorates or resolves β^+-thalassemia in patients, where the residual endogenous *HBB* expression contributes to the clinical benefit; however, its effects are less pronounced for β^0-thalassemia (no residual *HBB* expression).[13,14] The second approach to treat β-thalassemia aims at reducing α-globin expression to avoid the formation of toxic precipitates in erythroid cells.[3,19,20]

Here, we propose to use the CRISPR/Cas9 system to combine these 2 strategies: (1) α-globin chain reduction by recreating the natural α-thalassemia trait ($-\alpha^{3.7}$ deletion, -α/αα or -α/-α) and (2) targeted integration and expression of a *HBB* transgene under the control of the endogenous *HBA* promoter. Concomitant downregulation of α-globin and upregulation of β-globin allows successful amelioration of α/β globin imbalance in both β^+ and β^0 thalassemia cells.

Methods

Plasmids

We designed 2 different cassettes for the expression of *HBB* (gene ID: 3043): (1) the first cassette contains a β-globin complementary DNA (cDNA), with 3 antisickling point mutations (β^{AS3}),[21] followed by a woodchuck posttranscriptional regulatory element and a SV40polyA; and (2) the second cassette contains the whole β^{AS3} gene with introns and its original 3′ untranslated region (UTR) and polyA (pA) site, with 3 antisickling point mutations.

Each cassette, followed by a green fluorescent protein (GFP) reporter gene under the control of the constitutive human phosphoglycerate kinase 1 promoter with an SV40 pA, was flanked by arms of homology (250 bp each) and cloned in a standard AAV vector backbone (AAV2) in sense orientation with respect to its inverted terminal repeat.

To generate the double reporter AAV, we substituted the β^{AS3} gene with the human low-affinity nerve growth factor receptor cDNA. Each cassette was synthetized by Genscript (Piscataway, NJ).

The LV encoding the β^{AS3} gene under the control of the erythroid specific β-globin enhancer/promoter was already described.[22]

All reagents and detailed sequence information are available upon request.

Vector productions

All recombinant single-stranded AAV2/6 used in this study were produced using a triple transfection protocol and purified by 2 sequential cesium chloride density gradients or chromatography, as described earlier.[23] The vector titer of each preparation was determined by real-time quantitative polymerase chain reaction (qPCR)–based titration method using primers and probe corresponding to the inverted terminal repeat region of the AAV genome.[24]

LV were produced by transient transfection of 293T using third-generation packaging plasmid pMDLg/p.RRE and pK.REV and pseudotyped with the vesicular stomatitis virus glycoprotein G envelope. LV were titrated in HCT116 cells and HIV-1 Gag p24 content was measured by enzyme-linked immunosorbent assay (PerkinElmer, Waltham, MA) according to the manufacturer's instructions.

Cell culture and reagents

K562 cells (ATCC CCL243) were maintained in RPMI 1640 medium containing 2 mM glutamine and supplemented with 10% fetal bovine serum (Lonza, Basel, Switzerland), 10 mM *N*-2-hydroxyethylpiperazine-*N*′-2-ethanesulfonic acid, 1 mM sodium pyruvate, and penicillin and streptomycin (100 U/mL each; Gibco, Waltham, MA).[25]

HUDEP-2 β^0 cells were derived from a HUDEP-2[26] clone where both β-globin alleles were knocked out using CRISPR/Cas9 and a guide RNA (gRNA) targeting *HBB* exon 1 (HBB gRNA), as previously described.[17] Both HUDEP-2 and HUDEP-2 β^0 cells erythroid differentiation was performed in presence of doxycycline in 2 phases, with and without stem cell factor to promote erythroid maturation.[27]

HUDEP-2 β^0 single cell clones with different *HBA2* copy number were obtained by limiting dilution.

Streptococcus pyogenes Cas9 protein (with 2 SV40 nuclear localization signals) was provided by J.P. Concordet and was expressed and purified as previously described.[28] *Streptococcus pyogenes* Cas9 D10A protein (Alt-R S.p. Cas9 D10A Nickase V3; with 3 SV40 nuclear localization signals) was purchased from Integrated DNA Technologies (Coralville, IA).

Chemically modified single guide RNA were purchased from Synthego (with protospacer adjacent motif):

HBB gRNA: TCTGCCGTTACTGCCCTGT(GGG)

5′ UTR (HBA15) gRNA: GGGUUCUCUCUGAGUCUGUG(GGG)

HBA knockout (KO) gRNA: GUCGGCAGGAGACAGCACCA(TGG)

HBA20 gRNA: CATAAACCCTGGCGCGCTCG(CGG)

Primer and probes for PCRs were purchased from Sigma-Aldrich (St Louis, MO) and Integrated DNA Technologies (Coralville, IA).

$CD34^+$ cell culture, transfection, and transduction

Human umbilical cord blood (UCB) samples were provided by Centre Hospitalier Sud-Francilien (CHSF; Evry, France) and processed according to France bioethics laws (Declaration

DC-2012-1655 to the French Ministry of Higher Education and Research). CD34$^+$ cells were selected from patients affected by β-thalassemia as described[29] upon signed informed consent approved by the Ethical Committee of the San Raffaele Hospital (Milan, Italy).

CD34$^+$ cells were purified by immunomagnetic selection with AUTOMACS PRO (Miltenyi Biotec, Paris, France) after immunostaining with CD34 MicroBead Kit (Miltenyi Biotec). Mobilized peripheral blood (MPB) and UCB CD34$^+$ were also purchased from Cliniscience (Nanterre, France).

MPB- or UCB-derived HSPCs were thawed and cultured in prestimulation media for 48 hours (StemSpan, Stemregenin-1 0.75 μM, UM171 0.35 μM; StemCell Technologies, Vancouver, BC, Canada; rhSCF 300 ng/mL, rhFlt3-L 300 ng/mL, rhTPO 100 ng/mL, and rhIL-3 20 ng/mL; CellGenix, Freiburg, Germany).

Single guide RNA (sgRNA) was diluted following the manufacturer's instruction and ribonucleoprotein complexes were formed with 30 pmol of spCas9 (ratio 1:1.5). A total of 2.5×10^5 hematopoietic stem/progenitor cells (HSPCs) per condition were transfected with ribonucleoprotein (RNP) using a P3 Primary Cell 4D-Nucleofector Kit (CA137 program).[25] In knock-in experiments, 10 minutes after transfection, HSPCs were transduced with AAV6 for 6 hours (multiplicity of infection, 10 000-30 000), washed, and left in prestimulation media for additional 24 to 48 hours.

Lentiviral transduction was performed as previously described.[25]

After manipulation, HSPCs were cultured in erythroid differentiation medium (StemSpan, StemCell Technologies; rhSCF 20 ng/mL, rhEpo 1 U/mL, IL3 5 ng/mL, dexamethasone 2 μM and beta-estradiol 1 μM; Sigma-Aldrich) or in semisolid MethoCult medium (colony-forming cells [CFC] assay, H4435; StemCell Technologies) for 14 days. Colonies were counted and identified according to morphological criteria (burst-forming units-erythroid [BFU-E], colony-forming unit-granulocyte/granulocyte macrophage, and colony-forming unit-granulocyte, erythrocyte, monocyte, megakaryocyte). In some experiments, BFU-E were picked and cultured in erythroid progenitor expansion medium, as previously described.[30]

Flow cytometry

Cells were fixed and/or permeabilized using Cytofix/Cytoperm (BD Bioscience, San Jose, CA) according to the manufacturer's instructions. For live cell analysis, viability was assessed using Zombie Yellow dye (BioLegend, San Diego, CA) per manufacturers' instructions to exclude dead cells from the analysis. Negative controls were obtained by staining cells with isotype control antibodies. For engraftment studies, an Fc Receptor Binding Inhibitor antibody was used to block unspecific binding of mouse antibody to human cells, as per manufacturers' instructions. Cells were analyzed using CytoFLEX S (Beckman Coulter, Pasadena, CA) or SP6800 Spectral Analyzer (Sony, Tokyo, Japan); data were elaborated with CytExpert (Beckman Coulter) or FlowJo software (Tree Star, Woodburn, OR).

We used MoFlocell sorter (Beckman Coulter) to select live GFP$^+$ cells.

See supplemental Table 1 for the antibodies list and supplemental Figure 3A for gating strategy of human engrafted cells.

DNA analysis

Genomic DNA was extracted with QIAamp DNA Micro Kit, AllPrep DNA/RNA 96 Kit (Qiagen, Hilden, Germany) or QuickExtract DNA Extraction Solution (Lucigen, Middleton, WI).

Quantification of editing efficiency (InDels). Fifty nanograms of genomic DNA were used to amplify the region that spans the cutting site of each gRNA using KAPA2G Fast ReadyMix (Kapa Biosystem, Wilmington, MA). After Sanger sequencing (Genewiz, Takeley, United Kingdom), the percentage of insertions and deletions (InDels) was calculated using TIDE[31] and ICE (Synthego) softwares. See supplemental Table 2 for primer sequences.

ddPCR. Digital droplet PCR (ddPCR) was performed according to manufacturer's instruction using ddPCR Supermix for Probes No dUTP (BioRad, Hercules, CA) and 1 to 50 ng of genomic DNA digested with *Hin*dIII (New England Biolabs, Ipswich, MA). Droplets were generated using AutoDG Droplet Generator and analyzed with a QX200 Droplet Reader; data analysis was performed with QuantaSoft (BioRad).

To quantify *HBA2* copy number, primers and probes were designed on the 3′UTR of *HBA2* gene because it differs significantly from *HBA1*.

To quantify on-target transgene integration events, primers and probes were designed spanning the donor DNA-genome 3′ junction. Human albumin (*ALB*) or *ZNF843* genes were used as reference for copy number evaluation (assay ID: dHsaCP2506312, BioRad). See supplemental Table 2 for primer and probe sequences.

RNA extraction and reverse transcription-qPCR

Total RNA was purified using RNeasy Micro Kit or, in case of individual BFU-E colonies, AllPrep DNA/RNA 96 Kit (Qiagen). RNA was reverse-transcribed using Transcriptor First Strand cDNA Synthesis Kit (Roche, Basel, Switzerland). qPCR was performed using Maxima Syber Green/Rox (Life Scientific, Thermo Fisher Scientific, Waltham, MA). Primers and probe were optimized using the standard curve method to reach 100% ± 5% efficiency. The expression of each target gene was normalized using human *GAPDH* as a reference gene (NM_002046.6) and represented as $2^{\Delta Ct}$ for each sample or as fold changes ($2^{\Delta\Delta Ct}$) relative to the control. See supplemental Table 2 for primer sequences.

Off-target analyses

GUIDE-seq. GUIDE-Seq experiments were designed as previously described.[32] Human embryonic kidney 293T/17 cells (2.5×105) were transfected using Lipofectamine 3000 (Life Scientific, Thermo Fisher Scientific) with 750 ng of SpCas9-coding and 250 ng of sgRNA-coding plasmid or an empty pUC19 vector (background control), 10 pmol of the bait double-stranded oligonucleotide containing phosphorothioate bonds at both ends and 50 ng of a pEGFP-IRES-Puro plasmid, expressing both enhanced GFP and the puromycin resistance genes. One day after transfection, cells were replated and selected with puromycin (1 μg/mL) for 48 hours to enrich for transfected cells.

Genomic DNA extraction was performed using DNeasy Blood and Tissue Kit (Qiagen) following manufacturer's instructions. Genomic DNA was sheared using a Covaris S200 sonicator to an average length of 500 bp and subsequently end-repaired. Library preparation was performed using adapters and primers previously described[32] and

quantified with Qubit double-stranded DNA High Sensitivity Assay Kit (Life Scientific, Thermo Fisher Scientific). The sequencing reaction was performed with MiSeq sequencing system (Illumina) using an Illumina Miseq Reagent Kit V2 - 300 cycles (2 × 150 bp paired-end) and raw sequencing data (FASTQ files) were analyzed using the GUIDE-Seq computational pipeline.[33] Briefly, after demultiplexing, putative PCR duplicates were consolidated into single reads and mapped to the human reference genome GrCh37. Reads with a mapping quality lower than 50 were filtered out. Upon identification of the genomic regions integrating double-stranded oligonucleotides in aligned data, off-target sites were identified if, at most, 7 mismatches against the target were present and if absent in the background controls. GUIDE-Seq datasets are available in the BioProject online repository (ID PRJNA676022; http://www.ncbi.nlm.nih.gov/bioproject/676022).

Amplicon-sequencing. A total of 200 ng of genomic DNA of RNP-edited HSPCs were used to amplify top 3 off-targets identified with Guide-Seq using Phusion High-Fidelity polymerase (New England Biolabs). After checking the correct amplification by Sanger sequencing (Genewiz), amplicons were purified using NucleoSpin Gel and PCR Clean-up Kit (Macherey-Nagel, Hoerdt, France), and 500 ng of DNA were used for library preparation. Illumina-compatible barcoded DNA amplicon libraries were prepared using TruSeq DNA PCR-Free Kit (Illumina). PCR amplification was then performed using 1 ng of double-stranded ligation product and Kapa Taq polymerase reagents (KAPA HiFi HotStart ReadyMix PCR Kit; Sigma-Aldrich). After purification (Ampure XP beads; Beckman Coulter), libraries were pooled and sequenced with Illumina NovaSeq 6000 (paired-end sequencing 100 × 100 bases). Data were analyzed using CRISPResso2.[34]

See supplemental Table 2 for primer sequences.

HPLC analysis of globin chains and tetramers

HPLC analysis was performed using a NexeraX2 SIL-30AC chromatograph (Shimadzu, Kyoto, Japan) and analyzed with LC Solution software. HSPC-derived erythroblasts were lysed in water and globin chains were separated using a 250 × 4.6-mm, 3.6-μm Aeris Widepore column (Phenomenex, Torrance, CA). Samples were eluted with a gradient mixture of solution A (water/acetonitrile/trifluoroacetic acid, 95:5:0.1) and solution B (water/acetonitrile/trifluoroacetic acid, 5:95:0.1), monitoring absorbance at 220 nm. Hemoglobin tetramers were separated by HPLC using a cation-exchange column (PolyCAT A; PolyLC, Columbia, MD). Samples were eluted with a gradient mixture of solution A (20 mM bis Tris, 2 mM KCN; pH 6.5) and solution B (20 mM bis Tris, 2 mM KCN, 250 mM NaCl; pH 6.8). The absorbance was measured at 415 nm.

In vivo experiments

NOD.Cg-Prkdc^{scid}Il2rg^{tm1Wjl}/SzJ (NSG) mice were purchased from The Jackson Laboratory, Bar Harbor, ME (strain 005557) and maintained in specific-pathogen-free conditions. This study was approved by Ethical Committee CEEA-51, and conducted according to French and European legislation on animal experimentation (APAFiS#16499-2018071809263257_v4).

Forty-eight hours after editing, 5 to 7 × 10^5 CD34$^+$ cells were injected intravenously into 8-week-old female NSG mice after sublethal irradiation (150 cGy). Human cell engraftment and knockin (KI) levels were monitored at different time points in peripheral blood by flow cytometry using anti-human CD45 and HLA-ABC antibodies (supplemental Table 1). Sixteen weeks after transplantation, blood, bone marrow, and spleen were harvested and analyzed. Peripheral blood was stained and red blood cells lysed during sample fixation (VersaLyse Lysing Solution and IOTest3 Fixative Solution; Beckman Coulter).

Cell purification and enrichment

Human CD34$^+$ or CD45$^+$ cells were purified from mouse peripheral blood or bone marrow by immunomagnetic selection with CD34 or CD45 MicroBead Kit UltraPure in combination with AUTOMACS PRO (PosselD2 Separation Program; Miltenyi Biotec).

Statistical analyses

Statistical analyses were performed using GraphPad Prism, version 6.00, for Windows (GraphPad Software, La Jolla, CA). One- or 2-way analysis of variance (ANOVA) with Tukey's multiple comparison posttest for 3 or more groups was performed as indicated. Values are expressed as mean ± standard deviation (SD) as otherwise indicated, with "n" indicating the number of independent biological replicates used in each group. Differences were considered significant at $*P < .05$ $**P < .01$, and $***P < .001$.

Results

Deletion of HBA2 gene reduces α-globin precipitates in a β^0 adult erythroid cell line

Clinical data suggest that a reduction of α-globin to 75% to 25% of its physiological levels is safe and beneficial to patients with β-thalassemia.[3,35] The most common natural mutations affecting α-globin synthesis are gene deletions that remove a single *HBA* gene from 1 or both chromosomes generating -α/αα or -α/-α genotypes (-$\alpha^{3.7}$ and -$\alpha^{4.2}$deletions[36]) (Figure 1A). To mimic these beneficial deletions with *Streptococcus pyogenes* (*Sp*)Cas9 nuclease, we designed a single gRNA that cuts both *HBA1 and HBA2* alleles removing 1 *HBA2* gene per chromosome. To minimize the possibility of generating a α-globin KO, the sgRNA was designed to target the 5′UTR (HBA15) of *HBA1* and *HBA2* (Figure 1A), where the presence of InDels resulting from double-strand breaks (DSBs) does not affect α-globin production.[37] As a β^0-thalassemia cell model, we used immortalized HUDEP-2, which can differentiate and express adult hemoglobin (supplemental Figure 1A-B), and we knocked out β-globin genes (HUDEP-2 β^0) (supplemental Figure 1C).

We transfected both wild-type HUDEP-2 and HUDEP-2 β^0 with RNP targeting *HBA* and we achieved efficient editing (83.1% ± 12.1 and 77.3% ± 18.2, respectively, n = 3; Figure 1B) and genomic deletion of *HBA2* gene (0.9 ± 0.2 and 0.9 ± 0.1 *HBA2* copy per cell, n = 3; Figure 1C), which resulted in a decrease of α-globin messenger RNA (mRNA) expression upon erythroid differentiation (Figure 1D). To establish a correlation between α-globin expression and number of *HBA* genes, we generated multiple cell clones with mono- or biallelic *HBA2* deletions (-α/αα and -α/-α, respectively, n = 3 per genotype) and we showed a significant amelioration of the α/β-like globin imbalance upon deletion of *HBA2*, with the -α/-α clones being indistinguishable from wild-type HUDEP-2 cells (Figure 1D; supplemental Figure 1D). Importantly, our *HBA2* deletion strategy reduced but did not abolish

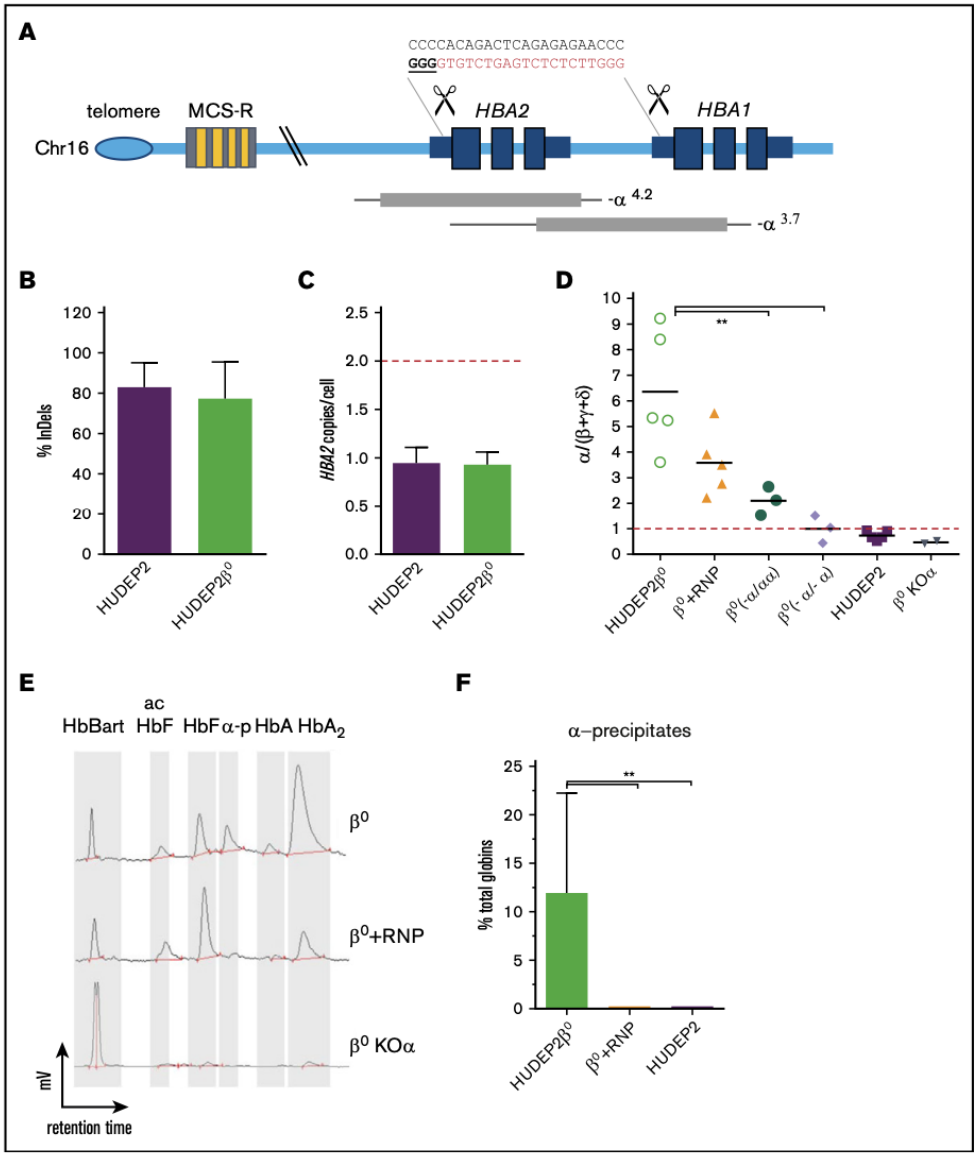

Figure 1. Deletion of *HBA2* reduces α-globin precipitates in HUDEP-2 β^0 cells. (A) Schematic representation of the α-globin locus. *HBA1* and *HBA2* genes are located in the subtelomeric region of chromosome (Chr) 16. Expression is regulated by 4 erythroid-specific enhancers (multispecies conserved elements [MCS-R]) located 10 to 50 kb upstream. Common occurring deletions are shown as gray bars and thin lines indicate regions of uncertainty of the breakpoints (adapted from Harteveld and Higgs[98]). gRNA cutting sites are indicated as scissors. gRNA nucleotide sequence is indicated on top (in bold/underlined the protospacer adjacent motif sequence). (B) Editing efficiency in HUDEP-2 cells is expressed as percentage of modified HBA alleles. Bars represent mean ± SD (n = 3). (C) HBA2 copies in edited cells in panel B. Red dashed line indicates the number of expected HBA2 alleles in normal cells. (D) Reverse transcription-qPCR quantification of α/β-like globin mRNA ratios in HUDEP-2 β^0 (n = 3-5) and in single-cell clones with monoallelic (α-/αα; n = 3) or biallelic (α-/α-; n = 3) *HBA2* deletions. β^0 + RNP = HUDEP2 β^0 bulk population edited with gRNA HBA15/Cas9. β^0 KOα = HUDEP2 β^0 bulk population edited with gRNA HBB/Cas9 to induce α-globin KO. Red dashed line indicates the physiological α/β-like ratio of 1. Bars represent mean ± SD (**$P < .01$, ANOVA, Tukey test). (E) Representative HPLC chromatograms of globin tetramer analysis in edited HUDEP-2 β^0. γ_4, Hb Bart; acHbF, acetylated fetal hemoglobin; HbF, fetal hemoglobin ($\alpha_2\gamma_2$); α-p, α-precipitates; HbA, adult hemoglobin ($\alpha_2\beta_2$). (F) Quantification of α-precipitates. Every tetramer is reported as percent of total hemoglobins; bars show mean ± SD (n = 3; **$P < .01$; ANOVA, Tukey test).

α-globin production, as observed in α-globin KO control cells obtained with a gRNA targeting the coding sequence within the first exon of *HBA1* and *HBA2* genes (Figure 1D).

We also measured the relative abundance of the different hemoglobin forms by HPLC analysis. In the absence of β-globin, a portion of the α-globin pool complexes with β-like globins, such as γ- and δ-globins (to form HbF and HbA2, respectively), whereas the excess precipitates in insoluble aggregates (α-precipitates). Remarkably, RNP deletion of *HBA2* genes significantly reduced α-precipitates without affecting hemoglobin synthesis (Figure 1E-F). This is in sharp contrast with α-globin KO cells, where the predominant hemoglobin observed was the toxic HbBart (γ-globin tetramers), typical of severe forms of α-thalassemia (Figure 1E). This result clearly indicates that only a controlled reduction of α-globin results in a beneficial effect.

Targeted integration of β^{AS3} transgene restores HbA expression in a β^0 adult erythroid cell line

To treat β^0-thalassemia patients, it is essential to express β-like globin chains; however, reaching expression levels to balance the endogenous α-globin has proven very challenging.[14] Therefore, we aim to lower the therapeutic threshold of β-globin expression by reducing α-globin abundance. For this purpose, we combined *HBA2* deletion with the KI of a β-globin transgene under the control of the endogenous *HBA* promoter. The same gRNA that deletes the *HBA2* gene will facilitate the integration of the β-globin transgene at this locus, whereas the endogenous *HBA* promoter will provide strong erythroid β expression, as previously suggested.[38-40] To discriminate exogenous vs endogenous β-globin expression, we used an *HBB* transgene containing 3 antisickling point mutations (β^{AS3}).[21]

To optimize β^{AS3} expression, we designed 2 DNA donor cassettes: (1) a β^{AS3} cDNA followed by a posttranscriptionally regulatory element[41] and SV40 polyadenylation signal (β^{AS3} cDNA); and (2) a β^{AS3} transgene that includes full-length *HBB* introns and the endogenous 3′UTR and polyadenylation signal (β^{AS3} full). Both cassettes were cloned in an AAV6 vector with a GFP reporter gene under the control of a constitutive promoter and flanked by homology arms to favor homologous DNA recombination (HDR)[42] (Figure 2A).

To perform KI HUDEP-2 β^0 cells were transfected with RNP, transduced with AAV6, and then GFP sorted to enrich for β^{AS3} integration (Figure 2B). A specific ddPCR confirmed on-target integration at molecular level (~0.8 β^{AS3} on-target copies per cell), in good agreement with GFP expression (~95% GFP positive cells after sorting) (Figure 2C).

Analysis of β^{AS3} mRNA expression in sorted cells showed an upregulation of about 100-fold for both cassettes upon erythroid differentiation, as expected from the endogenous α-globin promoter (Figure 2D). Although RNA levels were similar, we could detect β^{AS3} globin protein only with the β^{AS3} full, but not with the β^{AS3} cDNA cassette (Figure 2E-F). This observation was further confirmed by hemoglobin tetramer analysis, in which only β^{AS3} full cassette successfully restored ~40% of HbA ($\alpha_2\beta_2$) (Figure 2G-H). Overall, these results demonstrate that KI of β^{AS3} full cassette under the endogenous *HBA* promoter can restore HbA expression in β^0 thalassemic cells.

HSPCs can be efficiently edited and retain long-term and multilineage engraftment potential

To evaluate this strategy in clinically relevant cells, we transfected human umbilical cord blood HSPCs with RNP and then transduced with AAV, as described for HUDEP-2 cells (Figure 3A). Without any selection, we achieved robust genome cutting (Figure 3B), with an InDel pattern consisting mostly of 1 T nucleotide insertion (supplemental Figure 2A-C), together with efficient *HBA2* deletion and donor DNA KI (Figure 3C-D).

Upon differentiation, HSPC-derived erythroblasts expressed β^{AS3}-mRNA, which accounted for ~15% (14.2 ± 9.4, n = 6) of total β globin RNA (Figure 3E-F).

We then plated HSPCs in methylcellulose containing cytokines supporting erythroid and myeloid differentiation (CFC assay), and we confirm that modified progenitors retained their multilineage potential, although some toxicity was observed (supplemental Figure 2D-E).

Single BFU-E genotyping showed that the majority of colonies had *HBA2* deletion (Figure 3G) and β^{AS3} KI (Figure 3H) and 41% of them harbored both modifications (Figure 3I; supplemental Figure 2F).

Both *HBA2* deleted and β^{AS3} KI HSPCs were then transplanted in immunodeficient NOD/SCID/γ (NSG) mice[43] to evaluate their in vivo homing, engraftment, and multilineage potential (Figure 4A). Both edited HSPCs showed successful engraftment in bone marrow, spleen and blood, and multilineage differentiation (Figure 4B; supplemental Figure 3B). Because NSG mice do not support human erythroid differentiation,[44] we confirmed differentiation by CFC assay of isolated human $CD34^+$ cells from bone marrow of engrafted mice (supplemental Figure 3C).

In addition, the percentage of InDels, as well as the extent of *HBA2* deletion in RNP-treated HSPCs, remained similar ex vivo and in vivo, confirming a similar efficiency in both stem and progenitor cells (Figure 4C-D).

β^{AS3}KI HSPCs (GFP^+) were present at different time points (Figure 4E) in different lineages (supplemental Figure 3D); however, their engraftment was lower compared with unedited or *HBA2*-deleted HSPCs (Figure 4B,E), in accordance with previous reports describing AAV toxicity in HSPCs[45,46] and less efficient KI in noncycling HSCs.[47] Overall, these data show that we can achieve efficient *HBA2* deletion and β^{AS3} KI in HSPCs while preserving their in vivo long-term engraftment.

Editing patients' HSPCs ameliorates β^+- and β^0-thalassemia phenotype

To test our strategy in therapeutic conditions, we assessed correction of globin imbalance in patients' HSPCs. In particular, we tested the *HBA2* deletion approach in β^+ cells and the combination of the α-deletion and β^{AS3} KI strategy in β^+- and β^0-thalassemic HSPCs (supplemental Figure 4A-B).

HSPCs were transfected with RNP and transduced with AAV as described previously (Figure 3A). As positive control, HSPCs were transduced with a LV encoding for a β^{AS3} transgene under the control of the β-globin gene promoter and its mini-locus control region, currently in clinical trial for thalassemia (LV β^{AS3}).[13,48]

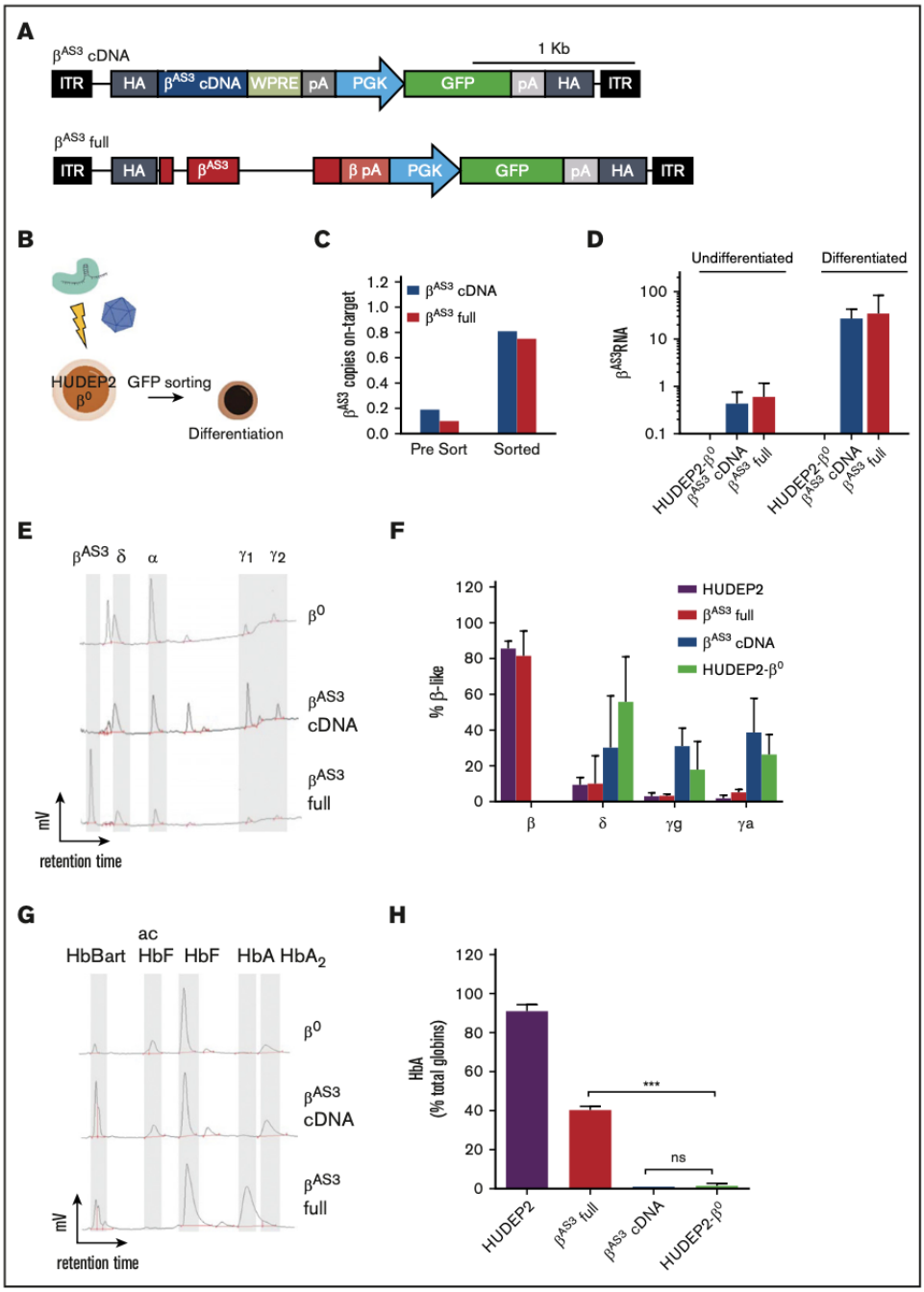

Figure 2. Targeted integration of a β^{AS3} transgene in the α-globin locus corrects thalassemic phenotype in HUDEP-2 β^0 cells. (A) AAV6 donors used for KI experiments. Both vectors contain a promoterless β^{AS3} transgene, followed by a phosphoglycerate kinase (PGK) promoter with a GFP reporter and simian virus pA. This cassette is flanked by 250-bp homology arms (homology) to gRNA genomic target. ITR, inverted terminal repeats. Top: β^{AS3} cDNA followed by the woodchuck posttranscriptionally regulatory element (WPRE) and SV40 pA (β^{AS3} cDNA); bottom: β^{AS3} transgene that includes endogenous introns, 3′UTR and pA (β^{AS3} full). A 1-kb scale bar is indicated at top. (B) Schematic representation of HUDEP-2 β^0 targeting experiments. (C) KI efficiency of β^{AS3} cDNA (blue) or β^{AS3} full (red) in HUDEP-2 β^0 cells measured by

RNP transfection was very efficient both in erythroid liquid culture and CFC in generating InDels (90.5% ± 7.1 for RNP and 90.4% ± 9.0 for RNP+AAV, mean ± SD; Figure 5A), *HBA2* deletion (0.95 ± 0.06 *HBA2* copies/cell for RNP and 0.77 ± 0.15 for RNP+AAV, mean ± SD; Figure 5B) and β^{AS3} KI (0.80 ± 0.21 copies/cell for RNP+AAV, mean ± SD; Figure 5C).

Globin expression was monitored during erythroid differentiation. mRNA globin imbalance (measured as α/β-like globins ratio) was ameliorated in all conditions (Figure 5D), with β^{AS3} KI cells performing better than *HBA2*-deleted erythroblasts because of β^{AS3} expression (Figure 5E; supplemental Figure 4C). Of note, modified HSPCs retained proper erythroid differentiation (supplemental Figure 4D) and multilineage potential (CFC assay; supplemental Figure 4F), although we observed some toxicity associated with the editing procedure (supplemental Figure 4E). Globin mRNA analysis of single BFU-E colonies derived from β^0- and β^+-edited HSPCs showed that α/β imbalance was improved in all conditions, in accordance with the reduced number of *HBA2* genes (supplemental Figure 4G) and with the stronger effect resulting from the concomitant α downregulation and β^{AS3} expression (Figure 5F).

Overall, these data show that we can modify β-thalassemia HSPCs and reduce their α/β globin balance, without affecting HSPCs potential.

Cas9 nickase represents a safe tool for HSPC editing

To reduce HSPC toxicity associated with nuclease-induced DSBs, we evaluated the use of Cas9 D10A nickase (Cas9 D10A). Because nicked genomic DNA is corrected by the endogenous base-excision repair pathway,[49] Cas9 D10A is expected to have minimal genotoxicity.[50,51]

To compare the efficiency of *HBA2* deletion and transgene targeted integration with single vs *trans* paired nicking of genomic DNA,[52] we selected another gRNA targeting α-globin 5′UTR (HBA20; supplemental Figure 5A-C) to combine with gRNA HBA15. K562 erythroleukemia cells were transfected with 1 or both gRNA complexed with Cas9 or Cas9D10A (RNP D10A) and transduced with a dual-reporter AAV vector to detect HDR (via a promoterless low-affinity nerve growth factor receptor) and non-HDR (via a phosphoglycerate kinase 1-GFP) integrations (supplemental Figure 5D). We first confirmed that gRNA HBA20 was comparable to HBA15 in generating InDels and *HBA2* deletions when complexed with wild-type Cas9 (RNP) (supplemental Figure 5E-F). When using RNP D10A, we observed that, without inducing any InDels (supplemental Figure 5E), both single and dual gRNA induced efficient HBA2 deletion and HDR integration, although to a lower extent compared with RNP (supplemental Figure 5F-H). Finally, we confirmed that RNP and RNP D10A gave the same ratio of HDR and non-HDR-mediated DNA integration (supplemental Figure 5I). Single gRNA generating 2 in *cis* nicks could induce genomic deletion by strand displacement, possibly facilitated by the homology of *HBA1* and *2* genes, whereas nick induced AAV integration can proceed via genome-AAV alignment, followed by Holiday junction resolution and completion of homologous recombination.[53] Because we did not observe any difference between HBA15 and dual gRNA RNP D10A, we decided to continue on HSPCs using only HBA15.

HSPCs were transfected with RNP or RNP D10A and then transduced with the AAV6 β^{AS3} donor DNA. In both conditions, we observed *HBA2* deletion, β^{AS3} KI and, upon erythroid differentiation, β^{AS3} mRNA upregulation (Figure 6A-D), although on-target InDels were observed only with Cas9 as a result of DSB repair (Figure 6E). The lower number of DSBs could also explain the reduced toxicity observed in CFC edited with Cas9 D10A (Figure 6F-G).

By genotyping single BFU-E colonies, we observed that most of RNP D10A-edited BFU-E had 1 *HBA2* deletion, followed by 1 *HBA2* deletion and 1 β^{AS3} KI (Figure 6H; supplemental Figure 6A-B). In addition, we performed Sanger sequencing of PCR products spanning deletion junctions and observed that, whereas Cas9 left a composite pattern of InDels, Cas9 D10A deletions were seamless, suggesting absence of exonuclease processing (Figure 6I).

Last, in bulk populations of RNP and RNP D10A edited HSPC, deep sequencing of 3 top-scoring off-targets identified by GUIDE-Seq[32] in 293T cells (supplemental Figure 6C) showed low to undetectable off-target activity for both Cas9 and Cas9 D10A (supplemental Figure 6D). This analysis, together with our previous off-target analyses,[37] confirms the target specificity of the selected gRNA HBA15 sequence.

Overall, these data indicate that Cas9 D10A performs *HBA2* deletion and β^{AS3} KI, although less efficiently than Cas9, with no InDels and lower cellular toxicity, representing a promising alternative strategy for HSPC editing.

Discussion

In this study, we demonstrated the possibility of correcting α/β globin imbalance in β-thalassemia cells using the CRISPR/Cas9 system. In particular, we showed an amelioration in both β^+- and β^0-thalassemia patients' HSPC-derived erythroblasts by combining 2 approaches: α-globin reduction by deleting *HBA2* gene to mimic α-thalassemia (-α/αα or -α/-α) and concomitant targeted integration and expression of a *HBB* transgene under the control of the endogenous *HBA* promoter. Because edited HSPCs retained engraftment and multilineage differentiation potential in vivo, the proposed strategy has clear potential for future clinical testing.

Inspired by clinical data showing that α-thalassemia ameliorates β-thalassemia,[3] several groups have proposed artificial down-regulation of α-globin expression as potential treatment of β^+-thalassemia, where residual β-globin expression guarantees sufficient hemoglobin formation (such as HbE, about one-half of all β-thalassemias).[3]

Figure 2. (continued) on-target ddPCR before and after sorting. (D) β^{AS3} transcript upregulation in targeted HUDEP-2 β^0 upon erythroid differentiation (qPCR, n = 2, mean ± SD). (E-F) HPLC analysis of globin monomers in differentiated HUDEP-2 β^0. Representative chromatograms (E) and relative quantification (F) of β-like subunits are shown; (mean ± SD; n = 3). (G-H) HPLC analysis of globin tetramers in differentiated HUDEP-2 β^0. Representative chromatograms (G) and HbA ($\alpha_2\beta_2$) quantification (H) are shown (mean ± SD, n = 3; $^{**}P < .01$; ANOVA, Tukey test). ns, not significant.

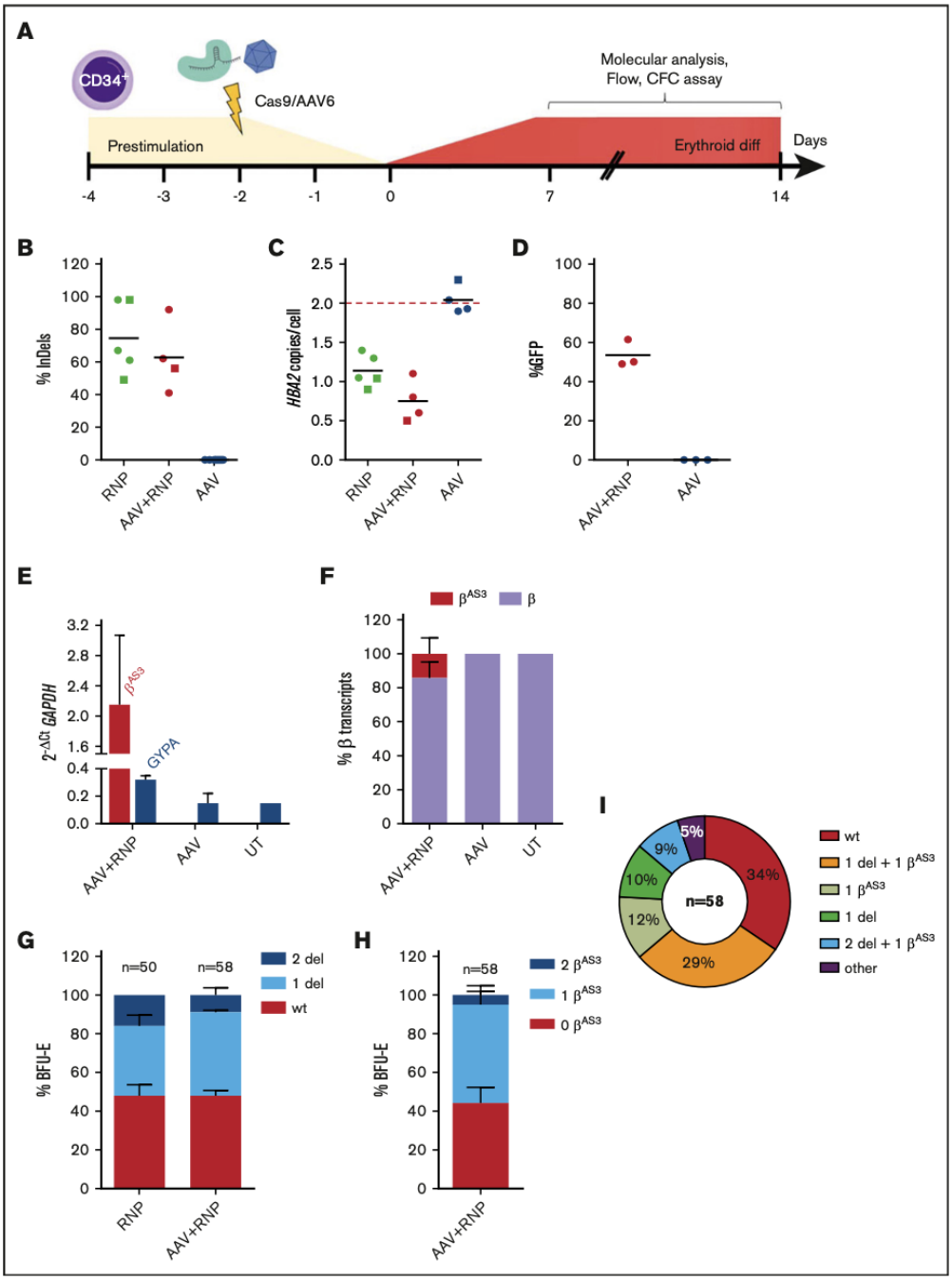

Figure 3. *HBA2* deletion and β^{AS3} integration efficiency in HSPCs. (A) Schematic representation of HSPC targeting experiments. (B) Editing efficiencies in HSPCs at day 12 of erythroid differentiation. Lines represent mean. *HBA2* copies (C) and KI efficiency (D) in edited HSPCs in erythroid liquid culture (●) or in BFU-E (■). Black lines represent mean; red line indicates the number of expected *HBA2* alleles in untreated HSPCs. (E) β^{AS3} and glycophorin A (GYPA) transcripts in HSPC-derived erythroblasts (qPCR, n = 2, mean ± SD). (F) Relative abundance of endogenous β and KI-β^{AS3} mRNA at day 12 of erythroid liquid culture (n = 6, mean ± SD). *HBA2* deletion (G) and β^{AS3} integration (H) pattern in single BFU-E. Bars represent mean ± SD (colonies derived from 2 independent experiments); no integration (0), monoallelic (1), and biallelic (2) KI or deletion (del). (I) Genotypes distribution of single KI-β^{AS3} BFU-E. Percentages are indicated (n = 58).

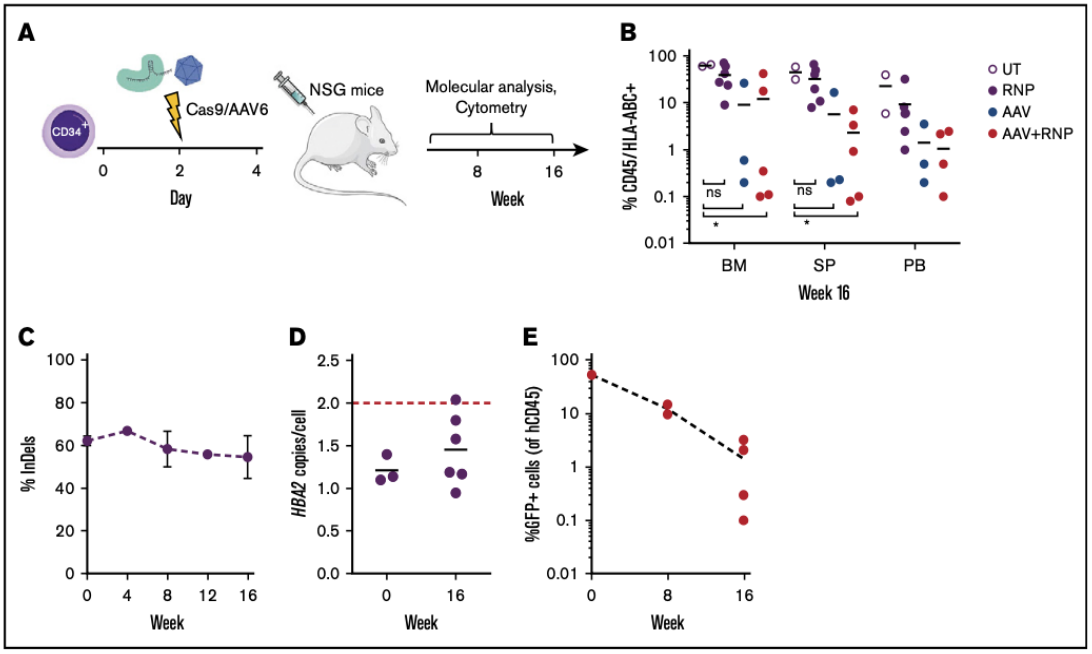

Figure 4. *HBA2*-deleted and β^{AS3} KI HSPCs engraft NSG mice and maintain their multilineage potential. (A) Schematic representation of engraftment experiments. (B) Percentage of human $CD45^+$/$HLA\text{-}ABC^+$ cells in hematopoietic organs of mice. BM, bone marrow; PB, peripheral blood; SP, spleen. Black lines indicate mean. (C) InDel efficiency in PB of RNP-engrafted mice at different timepoints (mean ± SD; n = 2-4). (D) *HBA2* copies in RNP-treated HSPCs at day 0 (injection) and in BM of engrafted mice at week 16. Black lines indicate mean; red line indicates the number of expected HBA2 alleles in untreated HSPCs. (E) GFP^+ cells in PB of transplanted mice over time. GFP is expressed as percentage of $CD45^+$ cells; line indicates mean.

Using a single gRNA targeting the 5′ untranslated region of both α-globin genes, we achieved efficient α-globin reduction by deleting 1 α-globin gene (*HBA2*), which corrected α/β imbalance and reduced α-precipitates in HUDEP-2 β^0. Because *HBA1* and *HBA2* are similarly expressed,[54] removal of 1 or 2 *HBA2* genes should reduce α-globin expression to ~75% to 50% of its normal level, thus falling in the therapeutic window to benefit β-thal.[3] This α-globin reduction strategy could be used to treat moderate β^+-thalassemia or to complement pharmacological treatment aimed at increasing expression of β-like globin in severe β^+ or β^0 patients.[55-57] To treat β^0-thalassemia, where there is no residual β-globin expression, we combined α-globin reduction with β-globin replacement. We optimized, delivered, and integrated an AAV6 β^{AS3} expression cassette under the control of the endogenous *HBA* promoter by HDR using the same gRNA deleting *HBA2* gene. Remarkably, the expression of 1 β^{AS3} transgene was sufficient to reestablish almost one-half of normal hemoglobin level in HUDEP-2 β^0.

Hijacking the endogenous *HBA* promoter for the expression of β^{AS3} transgene has 2 main advantages: (1) it does not require the genomic insertion of an exogenous promoter, which could result in transactivation of neighboring genes; and (2) compared with *HBB* gene correction strategies, it is a viable approach also for point mutations and deletions that inactivate regulatory elements in the *HBB* promoter.[58]

We confirmed that this "double" editing is feasible and efficient in primary human HSPCs from healthy donors and β^+- or β^0-thalassemia patients and does not affect erythroblast differentiation. Both *HBA2* deletion and β^{AS3} KI improved α/β globin imbalance to levels that were comparable or better than current *HBB* gene addition strategy based on LV. Additional experiments will be performed to systematically compare these 2 gene therapy strategies; however, our encouraging results support the development of a CRISPR/Cas9-based gene therapy approach. In addition, by transplanting HSPCs in humanized NSG, we demonstrated that both *HBA2* deletion and β^{AS3} KI occur in long-term HSCs and that edited HSCs can give rise to multiple progenitors and differentiated hematopoietic lineages.

The idea of downregulating the expression of α-globin alone or in combination with increased expression of β-globin has already been proposed by several groups in mice and human cells with mixed outcomes.[19,59,60] The only test on thalassemic patient's HSPCs was performed using a foamy viral vector encoding an *HBB* transgene and a short hairpin against α-globin mRNA[61]; however, this approach is hindered by limitations of this RNA interference technology[62-64] and the mutagenic potential of semi-random integrating viral vector.[65,66]

Alternatively, α-globin mRNA downregulation was obtained in HSPCs with epigenetic drugs, such as broad-spectrum histone demethylase or deacetylase inhibitor; nevertheless, the effect on α-globin protein was not established and drug specificity, toxicity, and mechanism of action still need to be assessed.[67-69]

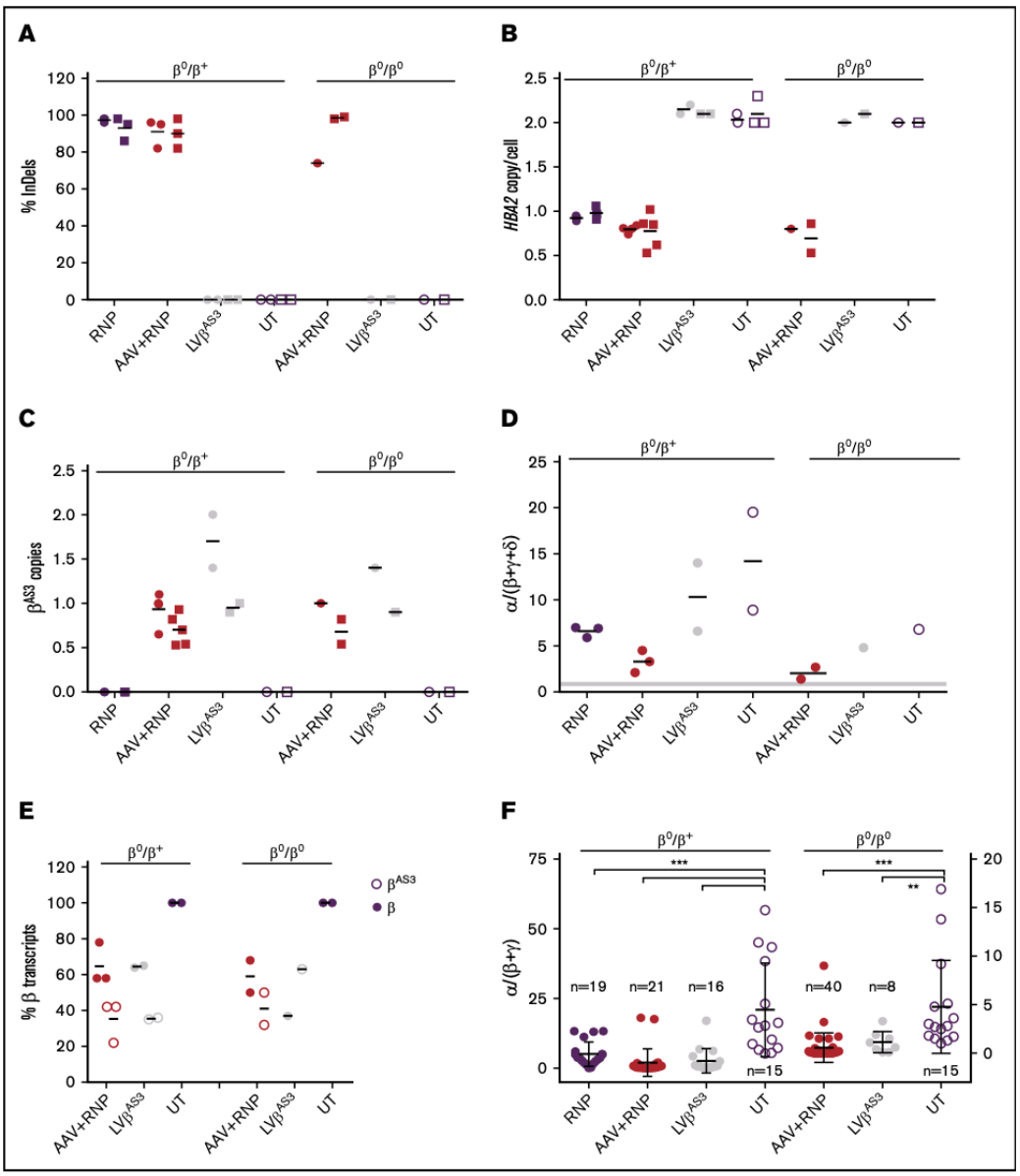

Figure 5. Genome editing of the α-globin locus ameliorates globin balance in thalassemic HSPCs. InDels (A), *HBA2* copies (B), and β^{AS3} integrated copies (C) quantification in edited thalassemic HSPCs in erythroid liquid culture (●) or in BFU-E (■). Black lines represent mean. HSPCs from 1 patient of each genotype were used. (D) α/β-like globin mRNA ratios in edited thalassemic erythroblasts at day 12. Black lines indicate mean; gray line shows the range of α/β-like globin ratio in healthy donor MPB and UCB HSPCs (n = 5). (E) Relative abundance of endogenous β and integrated β^{AS3} mRNA at day 12 of erythroid liquid culture. Black lines represent mean. (F) α/β-like globin mRNA ratios in edited thalassemic BFU-E. β^0/β^+ colonies (n = 71) are plotted on the left axis, β^0/β^0 (n = 63) on the right axis. Each dot represents a single colony. Black lines indicate mean ± SD (***$P < .001$; **$P < .01$; ANOVA, Tukey test). HSPCs derived from 1 patient of each genotype were used for this figure.

Using genome editing tools, Mettananda et al elegantly demonstrated the possibility of reducing α-globin expression in HbE patients' cells by deleting a powerful α-globin enhancer.[20] Although promising, this modification is beneficial only for β^+ patients and requires plasmid transfection combined with GFP-sorting enrichment, a strategy that is not suited for clinical translation.[25] Finally, the need for

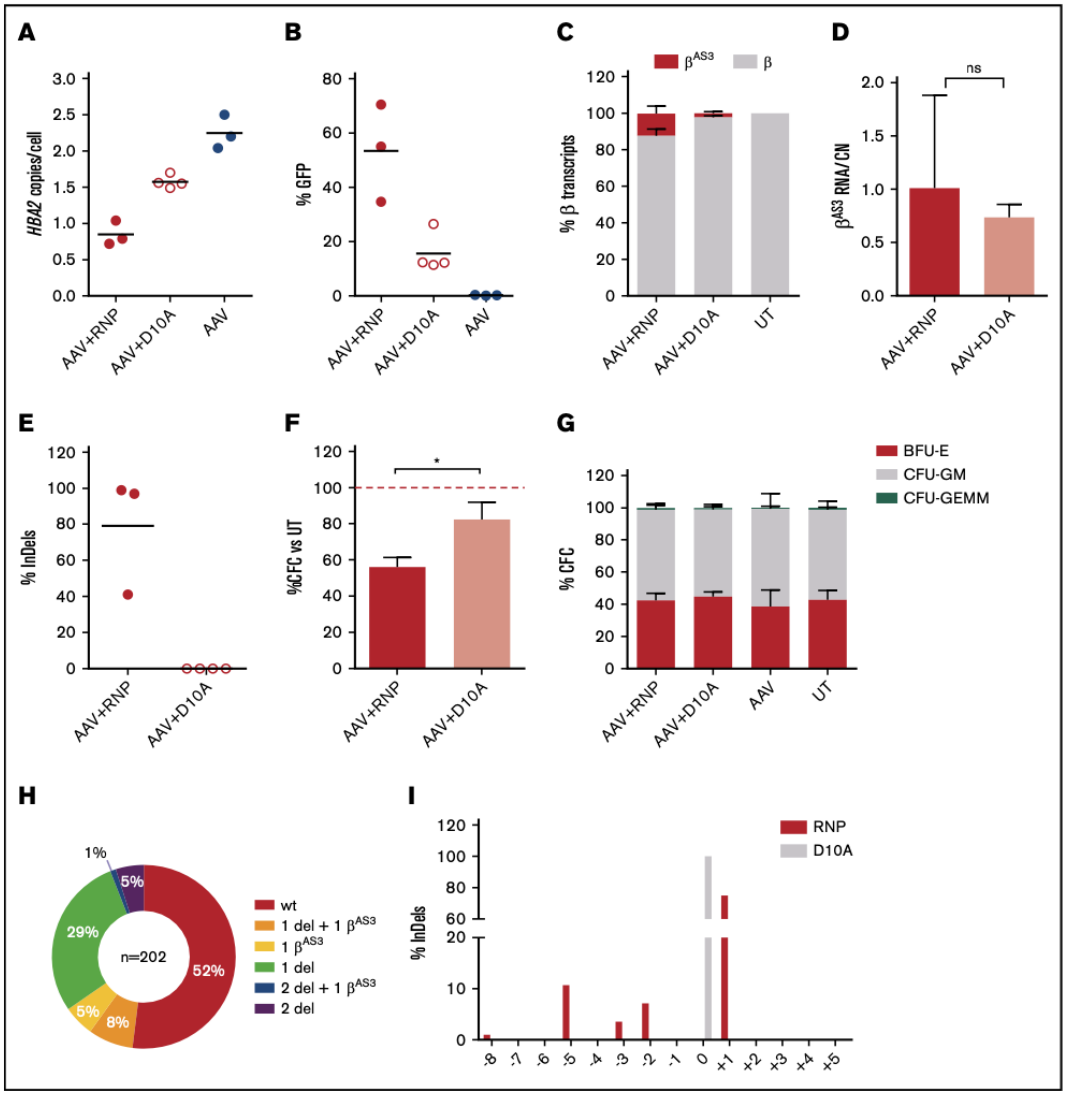

Figure 6. Cas9 nickase editing results in seamless *HBA2* deletion and reduced HSPCs toxicity. (A-B) *HBA2* copies (A) and KI efficiency (B) in Cas9 (RNP) or Cas9 nickase (RNP D10A) edited HSPCs in erythroid liquid culture. Black lines represent mean. (C) Relative abundance of endogenous β and KI-β^{AS3} mRNA at day 12 of erythroid liquid culture (mean ± SD, n = 3-4). (D) expression of β^{AS3} transcripts normalized by copy number (CN) in Cas9- or Cas9 nickase-treated erythroblasts (mean ± SD, n = 4-5). (E) InDel quantification at gRNA target site in edited HSPCs. Black lines represent mean. (F) CFC number expressed as percentage of untreated control (UT). Bars represent mean ± SD (n = 3-4); red dashed line indicates 100%. (G) CFU frequency in edited HSPCs. BFU-E, burst-forming unit-erythroid; CFU-GM, CFU-granulocyte, macrophage. Colony-forming unit-granulocyte, erythroid, macrophage, megakaryocyte; Bars represent mean ± SD (n = 2-4). (H) Genotypes of BFU-E (n = 202) derived from RNP D10A + AAV HSPCs. Percentages are indicated. (I) Frequency of different InDel patterns in HBA2 deleted BFU-E treated with Cas9 (RNP, red; n = 28) or Cas9 nickase (RNP D10A, gray; n = 96). Editing was measured across HBA2 deletion junctions.

2 gRNAs to perform enhancer deletion increases the risk of on- and off-target side effects and can be technically challenging.

Our approach has the advantage of combining α reduction with β expression to restore α/β-globin balance and increase hemoglobin level to treat both β^0- and β^+-thalassemia patients' HSPCs. Technically, we deliver Cas9/gRNA as RNP, which allows efficient HSPC modification without any selection and is already used in clinical trials (eg, NCT03164135, NCT03655678). In addition, our strategy requires only 1

gRNA, thus minimizing the possibility of on- and off-target side effects.

To further reduce this risk and general cellular toxicity associated with Cas9-induced DSB, we investigated the use of Cas9 D10A nickase.[51,70-72] Inspired by Metzger et al, who demonstrated that site-specific nicking enzymes can induce HDR with an AAV-delivered template in 293 cells,[53] we showed for the first time that a single Cas9 D10A/gRNA RNP can be used in HSPCs to achieve seamless genomic deletion and AAV targeted integration, without generating any InDels. Because the efficiency of targeted integration obtained with Cas9 D10A is lower than with Cas9, we will further optimize this approach by improving RNP transfection with nanoparticles,[73] reducing AAV donor size,[74] and using Cas9 nickase variants[75] and drugs affecting cellular DNA repair.[76,77] Further in vivo studies will be performed with this strategy to demonstrate effective editing of repopulating HSPCs.

By performing GUIDE-Seq analysis,[32] we verified the target specificity of the selected gRNA HBA15, confirming our previous off-target analyses.[37] However, additional safety aspects need to be carefully evaluated before clinical translation of this HSPC gene therapy platform. It will be particularly challenging to qualitatively and quantitatively assess all the possible on-target editing outcomes, especially low-frequency ones. We quantified *HBA2* deletions, but we could not detect any *HBA2* inversion by PCR analysis of edited HSPCs, although inversions are reported to be a frequent side product when generating CRISPR genomic deletions.[17,78] This observation could be a true negative result, as previously reported for *HBG* editing in HSPCs,[79,80] or because of technical difficulties associated with amplification of repetitive inverted sequences with high GC content present in the α-globin locus.[81] In addition, on-target cleavage can generate undesired chromosomal alterations,[70,82-84] whereas integration of AAV donor DNA can occur via HDR as well as via partial HDR or non-homologous end joining with or without the *HBA2* deletion.[85-87] A combination of whole genome sequencing,[88] long-range PCR,[89] long-read sequencing,[90] next-generation mapping,[91] and/or directional sequencing[92] will help to address these concerns by unraveling the full spectrum of editing outcomes.

In summary, we describe a novel CRISPR strategy to correct α/β globin imbalance in thalassemic HSPCs by α-globin downregulation with or without *HBB* transgene expression. Future experiments will elucidate the therapeutic potential of this strategy for treating β^{+}- and β^{0}-thalassemia and, eventually, sickle cell disease, where lower α-globin levels reduce HbS polymerization and sickle hemoglobin concentration and β^{AS3} compete with β sickling for binding α-globin.[21,93-97]

Acknowledgments

The authors thank Chiara Antoniani for the generation of HUDEP-2 β^{0} cells, Anna De Cian for Cas9 protein production, Samantha Scaramuzza for help with patients HSPCs, Fanny Collaud, Genethon "Vector Core Facility" for AAV production, Genethon "Imaging and Cytometry Core Facility" for image analysis and fluorescence-activated cell sorting, Genethon "Functional Evaluation Facility" for help with mice experimentation, and the Imagine "Genomic Platform" for amplicon sequencing. The authors also thank the entire M.A. laboratory, Marina Cavazzana, Anne Galy, and Ronzitti for fruitful discussion. In addition, the authors thank Ryo Kurita and Yukio Nakamura for proving HUDEP-2 cells under a material transfer agreement with Genethon. The authors gratefully acknowledge the Conseil Général de l'Essonne (ASTRES) and Genopole Research in Evry for financial help for the purchase of equipment and are grateful to consenting mothers and to L. Rigonnot and staff of the Maternity at the Centre Hospitalier Sud-Francilien (CHSF; Evry, France) for providing umbilical cord blood samples.

This work was supported by grants from Bayer Hemophilia Awards Program (G.P.) and AFM-Telethon, INSERM, Genopole Chaire Fondagen and the Agence Nationale de la Recherche (ANR-16-CE18 STaHR) (M.A.). G.P. was supported by European Union's Horizon 2020 (SCIDNET No 666908).

Authorship

Contribution: G.P. conceived the study, designed and performed experiments, analyzed data, and wrote the manuscript; A.F. performed experiments and analyzed data on HSPCs; M.L. performed experiments and analyzed data on HUDEP-2 β^{0} cells; F.A. performed experiments and analyzed data on Cas9 (D10A); E.C. performed experiments and analyzed data on HSPCs; A.C. performed HPLC analyses; G. M. and A.C. performed and analyzed GUIDE--Seq experiments; A.T. performed molecular analyses; J.-P.C. provided purified SpCas9 protein; F.M. provided scientific advice and financial support; G.F. provided β-thalassemia HSPCs; A.M. provided HUDEP-2 β^{0} cells, performed and analyzed HPLC, and edited the manuscript; and M.A. conceived the study, designed experiments, analyzed data, and wrote the manuscript.

Conflict-of-interest disclosure: G.P. and M.A. are the inventors of a patent describing this HSC-based gene therapy strategy for treating β-thalassemia (correction of β-thalassemia phenotype by genetically engineering hematopoietic stem cell; EP19305484.8). The remaining authors declare no competing financial interests.

ORCID profiles: G.P., 0000-0002-2522-2684; A.F., 0000-0002-7604-6967; G.M., 0000-0002-7770-5688; A.T., 0000-0003-2155-6078; F.M., 0000-0003-0459-4320; G.F., 0000-0003-0790-3133; M.A., 0000-0002-1188-8856.

Correspondence: Mario Amendola, INTEGRARE, Genethon, UMR S951 INSERM, University Evry, University Paris-Saclay, 1 bis, Rue de l'Internationale, 91000 Evry, France; e-mail: mamendola@genethon.fr.

References

1. Cao A, Galanello R. Beta-thalassemia. *Genet Med*. 2010;12(2):61-76.
2. Weatherall DJ. The challenge of haemoglobinopathies in resource-poor countries. *Br J Haematol*. 2011;154(6):736-744.
3. Mettananda S, Gibbons RJ, Higgs DR. α-Globin as a molecular target in the treatment of β-thalassemia. *Blood*. 2015;125(24):3694-3701.

4. Sharma V, Saxena R. Effect of alpha-gene numbers on phenotype of HbE/beta thalassemia patients. *Ann Hematol*. 2009;88(10):1035-1036.

5. Fucharoen S, Weatherall DJ. The hemoglobin E thalassemias. *Cold Spring Harb Perspect Med*. 2012;2(8):a011734.

6. Sripichai O, Munkongdee T, Kumkhaek C, Svasti S, Winichagoon P, Fucharoen S. Coinheritance of the different copy numbers of alpha-globin gene modifies severity of beta-thalassemia/Hb E disease. *Ann Hematol*. 2008;87(5):375-379.

7. Charoenkwan P, Teerachaimahit P, Sanguansermsri T. The correlation of α-globin gene mutations and the XmnI polymorphism with clinical severity of Hb E/β-thalassemia. *Hemoglobin*. 2014;38(5):335-338.

8. Allali S, de Montalembert M, Brousse V, Chalumeau M, Karim Z. Management of iron overload in hemoglobinopathies. *Transfus Clin Biol*. 2017;24(3):223-226.

9. Besse K, Maiers M, Confer D, Albrecht M. On modeling human leukocyte antigen-identical sibling match probability for allogeneic hematopoietic cell transplantation: estimating the need for an unrelated donor source. *Biol Blood Marrow Transplant*. 2016;22(3):410-417.

10. Chandrakasan S, Malik P. Gene therapy for hemoglobinopathies: the state of the field and the future. *Hematol Oncol Clin North Am*. 2014;28(2):199-216.

11. Saber W, Opie S, Rizzo JD, Zhang MJ, Horowitz MM, Schriber J. Outcomes after matched unrelated donor versus identical sibling hematopoietic cell transplantation in adults with acute myelogenous leukemia. *Blood*. 2012;119(17):3908-3916.

12. Sadelain M, Boulad F, Galanello R, et al. Therapeutic options for patients with severe beta-thalassemia: the need for globin gene therapy. *Hum Gene Ther*. 2007;18(1):1-9.

13. Marktel S, Scaramuzza S, Cicalese MP, et al. Intrabone hematopoietic stem cell gene therapy for adult and pediatric patients affected by transfusion-dependent ß-thalassemia. *Nat Med*. 2019;25(2):234-241.

14. Thompson AA, Walters MC, Kwiatkowski J, et al. Gene therapy in patients with transfusion-dependent β-thalassemia. *N Engl J Med*. 2018;378(16):1479-1493.

15. Wu Y, Zeng J, Roscoe BP, et al. Highly efficient therapeutic gene editing of human hematopoietic stem cells. *Nat Med*. 2019;25(5):776-783.

16. Martyn GE, Wienert B, Yang L, et al. Natural regulatory mutations elevate the fetal globin gene via disruption of BCL11A or ZBTB7A binding. *Nat Genet*. 2018;50(4):498-503.

17. Antoniani C, Meneghini V, Lattanzi A, et al. Induction of fetal hemoglobin synthesis by CRISPR/Cas9-mediated editing of the human β-globin locus. *Blood*. 2018;131(17):1960-1973.

18. Traxler EA, Yao Y, Wang YD, et al. A genome-editing strategy to treat β-hemoglobinopathies that recapitulates a mutation associated with a benign genetic condition. *Nat Med*. 2016;22(9):987-990.

19. Xie SY, Ren ZR, Zhang JZ, et al. Restoration of the balanced alpha/beta-globin gene expression in beta654-thalassemia mice using combined RNAi and antisense RNA approach. *Hum Mol Genet*. 2007;16(21):2616-2625.

20. Mettananda S, Fisher CA, Hay D, et al. Editing an α-globin enhancer in primary human hematopoietic stem cells as a treatment for β-thalassemia. *Nat Commun*. 2017;8(1):424.

21. Levasseur DN, Ryan TM, Reilly MP, McCune SL, Asakura T, Townes TM. A recombinant human hemoglobin with anti-sickling properties greater than fetal hemoglobin. *J Biol Chem*. 2004;279(26):27518-27524.

22. Weber L, Poletti V, Magrin E, et al. An optimized lentiviral vector efficiently corrects the human sickle cell disease phenotype. *Mol Ther Methods Clin Dev*. 2018;10:268-280.

23. Ayuso E, Mingozzi F, Bosch F. Production, purification and characterization of adeno-associated vectors. *Curr Gene Ther*. 2010;10(6):423-436.

24. Rohr UP, Wulf MA, Stahn S, Steidl U, Haas R, Kronenwett R. Fast and reliable titration of recombinant adeno-associated virus type-2 using quantitative real-time PCR. *J Virol Methods*. 2002;106(1):81-88.

25. Lattanzi A, Meneghini V, Pavani G, et al. Optimization of CRISPR/Cas9 delivery to human hematopoietic stem and progenitor cells for therapeutic genomic rearrangements. *Mol Ther*. 2019;27(1):137-150.

26. Kurita R, Suda N, Sudo K, et al. Establishment of immortalized human erythroid progenitor cell lines able to produce enucleated red blood cells. *PLoS One*. 2013;8(3):e59890.

27. Vinjamur DS, Bauer DE. Growing and genetically manipulating human umbilical cord blood-derived erythroid progenitor (HUDEP) cell lines. *Methods Mol Biol*. 2018;1698:275-284.

28. Ménoret S, De Cian A, Tesson L, et al. Homology-directed repair in rodent zygotes using Cas9 and TALEN engineered proteins. *Sci Rep*. 2015;5(1):14410.

29. Lidonnici MR, Aprile A, Frittoli MC, et al. Plerixafor and G-CSF combination mobilizes hematopoietic stem and progenitors cells with a distinct transcriptional profile and a reduced *in vivo* homing capacity compared to plerixafor alone. *Haematologica*. 2017;102(4):e120-e124.

30. Wen J, Tao W, Hao S, Zu Y. Cellular function reinstitution of offspring red blood cells cloned from the sickle cell disease patient blood post CRISPR genome editing. *J Hematol Oncol*. 2017;10(1):119.

31. Brinkman EK, Chen T, Amendola M, van Steensel B. Easy quantitative assessment of genome editing by sequence trace decomposition. *Nucleic Acids Res*. 2014;42(22):e168.

32. Tsai SQ, Zheng Z, Nguyen NT, et al. GUIDE-seq enables genome-wide profiling of off-target cleavage by CRISPR-Cas nucleases. *Nat Biotechnol*. 2015;33(2):187-197.

33. Tsai SQ, Topkar VV, Joung JK, Aryee MJ. Open-source guideseq software for analysis of GUIDE-seq data. *Nat Biotechnol*. 2016;34(5):483.

34. Clement K, Rees H, Canver MC, et al. CRISPResso2 provides accurate and rapid genome editing sequence analysis. *Nat Biotechnol*. 2019;37(3): 224-226.

35. Badens C, Joly P, Agouti I, et al. Variants in genetic modifiers of β-thalassemia can help to predict the major or intermedia type of the disease. *Haematologica*. 2011;96(11):1712-1714.

36. Mettananda S, Higgs DR. Molecular basis and genetic modifiers of thalassemia. *Hematol Oncol Clin North Am*. 2018;32(2):177-191.

37. Pavani G, Laurent M, Fabiano A, et al. Ex vivo editing of human hematopoietic stem cells for erythroid expression of therapeutic proteins [published correction appears in *Nat Commun*. 2020;11(11):4146]. *Nat Commun*. 2020;11(1):3778.

38. Morianos I, Siapati EK, Pongas G, Vassilopoulos G. Comparative analysis of FV vectors with human α- or β-globin gene regulatory elements for the correction of β-thalassemia. *Gene Ther*. 2012;19(3):303-311.

39. Moreau-Gaudry F, Xia P, Jiang G, et al. High-level erythroid-specific gene expression in primary human and murine hematopoietic cells with self-inactivating lentiviral vectors. *Blood*. 2001;98(9):2664-2672.

40. Papanikolaou E, Georgomanoli M, Stamateris E, et al. The new self-inactivating lentiviral vector for thalassemia gene therapy combining two HPFH activating elements corrects human thalassemic hematopoietic stem cells. *Hum Gene Ther*. 2012;23(1):15-31.

41. Huang ZM, Yen TS. Role of the hepatitis B virus posttranscriptional regulatory element in export of intronless transcripts. *Mol Cell Biol*. 1995;15(7): 3864-3869.

42. Wang J, Exline CM, DeClercq JJ, et al. Homology-driven genome editing in hematopoietic stem and progenitor cells using ZFN mRNA and AAV6 donors. *Nat Biotechnol*. 2015;33(12):1256-1263.

43. Ishikawa F, Yasukawa M, Lyons B, et al. Development of functional human blood and immune systems in NOD/SCID/IL2 receptor gamma chain(null) mice. *Blood*. 2005;106(5):1565-1573.

44. Hu Z, Van Rooijen N, Yang YG. Macrophages prevent human red blood cell reconstitution in immunodeficient mice. *Blood*. 2011;118(22): 5938-5946.

45. Romero Z, Lomova A, Said S, et al. Editing the sickle cell disease mutation in human hematopoietic stem cells: comparison of endonucleases and homologous donor templates. *Mol Ther*. 2019;27(8):1389-1406.

46. Schiroli G, Conti A, Ferrari S, et al. Precise gene editing preserves hematopoietic stem cell function following transient p53-mediated DNA damage response. *Cell Stem Cell*. 2019;24(4):551-565.e8.

47. Genovese P, Schiroli G, Escobar G, et al. Targeted genome editing in human repopulating haematopoietic stem cells. *Nature*. 2014;510(7504): 235-240.

48. Miccio A, Cesari R, Lotti F, et al. In vivo selection of genetically modified erythroblastic progenitors leads to long-term correction of beta-thalassemia. *Proc Natl Acad Sci USA*. 2008;105(30):10547-10552.

49. Caldecott KW. Single-strand break repair and genetic disease. *Nat Rev Genet*. 2008;9(8):619-631.

50. Cong L, Ran FA, Cox D, et al. Multiplex genome engineering using CRISPR/Cas systems. *Science*. 2013;339(6121):819-823.

51. Ran FA, Hsu PD, Lin CY, et al. Double nicking by RNA-guided CRISPR Cas9 for enhanced genome editing specificity [published correction appears in *Cell*. 2013;155(2):479-480]. *Cell*. 2013;154(6):1380-1389.

52. Chen X, Janssen JM, Liu J, et al. In trans paired nicking triggers seamless genome editing without double-stranded DNA cutting. *Nat Commun*. 2017; 8(1):657.

53. Metzger MJ, McConnell-Smith A, Stoddard BL, Miller AD. Single-strand nicks induce homologous recombination with less toxicity than double-strand breaks using an AAV vector template. *Nucleic Acids Res*. 2011;39(3):926-935.

54. Molchanova TP, Pobedimskaya DD, Huisman TH. The differences in quantities of alpha 2- and alpha 1-globin gene variants in heterozygotes. *Br J Haematol*. 1994;88(2):300-306.

55. Bradai M, Abad MT, Pissard S, Lamraoui F, Skopinski L, de Montalembert M. Hydroxyurea can eliminate transfusion requirements in children with severe beta-thalassemia. *Blood*. 2003;102(4):1529-1530.

56. Biswas S, Ray R, Roy K, Bandyopadhyay A, Ghosh K, Bhattacharyya M. Alpha globin gene mutation: a major determinant of hydroxyurea response in transfusion-dependent HbE-β-thalassaemia. *Acta Haematol*. 2019;142(3):132-141.

57. Thein SL. The emerging role of fetal hemoglobin induction in non-transfusion-dependent thalassemia. *Blood Rev*. 2012;26(Suppl 1): S35-S39.

58. Thein SL. The molecular basis of β-thalassemia. *Cold Spring Harb Perspect Med*. 2013;3(5):a011700.

59. Xie SY, Li W, Ren ZR, Huang SZ, Zeng F, Zeng YT. Correction of β654-thalassaemia mice using direct intravenous injection of siRNA and antisense RNA vectors. *Int J Hematol*. 2011;93(3):301-310.

60. Voon HP, Wardan H, Vadolas J. siRNA-mediated reduction of alpha-globin results in phenotypic improvements in beta-thalassemic cells. *Haematologica*. 2008;93(8):1238-1242.

61. Amendola M, Giustacchini A, Gentner B, Naldini L. A double-switch vector system positively regulates transgene expression by endogenous microRNA expression (miR-ON vector). *Mol Ther*. 2013;21(5):934-946.

62. Martin JN, Wolken N, Brown T, Dauer WT, Ehrlich ME, Gonzalez-Alegre P. Lethal toxicity caused by expression of shRNA in the mouse striatum: implications for therapeutic design. *Gene Ther*. 2011;18(7):666-673.

63. Grimm D, Streetz KL, Jopling CL, et al. Fatality in mice due to oversaturation of cellular microRNA/short hairpin RNA pathways. *Nature*. 2006;441(7092):537-541.

64. Manjunath N, Wu H, Subramanya S, Shankar P. Lentiviral delivery of short hairpin RNAs. *Adv Drug Deliv Rev*. 2009;61(9):732-745.

65. Rothe M, Modlich U, Schambach A. Biosafety challenges for use of lentiviral vectors in gene therapy. *Curr Gene Ther*. 2013;13(6):453-468.

66. Cavazzana-Calvo M, Payen E, Negre O, et al. Transfusion independence and HMGA2 activation after gene therapy of human β-thalassaemia. *Nature*. 2010;467(7313):318-322.

67. Mai A, Jelicic K, Rotili D, et al. Identification of two new synthetic histone deacetylase inhibitors that modulate globin gene expression in erythroid cells from healthy donors and patients with thalassemia. *Mol Pharmacol*. 2007;72(5):1111-1123.

68. Mettananda S, Fisher CA, Sloane-Stanley JA, et al. Selective silencing of α-globin by the histone demethylase inhibitor IOX1: a potentially new pathway for treatment of β-thalassemia. *Haematologica*. 2017;102(3):e80-e84.

69. Mettananda S, Yasara N, Fisher CA, Taylor S, Gibbons R, Higgs D. Synergistic silencing of α-globin and induction of γ-globin by histone deacetylase inhibitor, vorinostat as a potential therapy for β-thalassaemia. *Sci Rep*. 2019;9(1):11649.

70. Cullot G, Boutin J, Toutain J, et al. CRISPR-Cas9 genome editing induces megabase-scale chromosomal truncations. *Nat Commun*. 2019;10(1):1136.

71. Chen X, Tasca F, Wang Q, et al. Expanding the editable genome and CRISPR-Cas9 versatility using DNA cutting-free gene targeting based on in trans paired nicking. *Nucleic Acids Res*. 2020;48(2):974-995.

72. Hyodo T, Rahman ML, Karnan S, et al. Tandem paired nicking promotes precise genome editing with scarce interference by p53. *Cell Rep*. 2020;30(4):1195-1207.e7.

73. Nguyen DN, Roth TL, Li PJ, et al. Polymer-stabilized Cas9 nanoparticles and modified repair templates increase genome editing efficiency. *Nat Biotechnol*. 2020;38(1):44-49.

74. Pavel-Dinu M, Wiebking V, Dejene BT, et al. Gene correction for SCID-X1 in long-term hematopoietic stem cells [published corrections appear in *Nat Commun*. 2019;10(1):2021 and 2019;10(1):5264]. *Nat Commun*. 2019;10(1):1634.

75. Rees HA, Yeh WH, Liu DR. Development of hRad51-Cas9 nickase fusions that mediate HDR without double-stranded breaks. *Nat Commun*. 2019;10(1):2212.

76. Metzger MJ, Stoddard BL, Monnat RJ Jr.. PARP-mediated repair, homologous recombination, and back-up non-homologous end joining-like repair of single-strand nicks. *DNA Repair (Amst)*. 2013;12(7):529-534.

77. Vriend LE, Krawczyk PM. Nick-initiated homologous recombination: protecting the genome, one strand at a time. *DNA Repair (Amst)*. 2017;50:1-13.

78. Li J, Shou J, Guo Y, et al. Efficient inversions and duplications of mammalian regulatory DNA elements and gene clusters by CRISPR/Cas9. *J Mol Cell Biol*. 2015;7(4):284-298.

79. Métais JY, Doerfler PA, Mayuranathan T, et al. Genome editing of HBG1 and HBG2 to induce fetal hemoglobin. *Blood Adv*. 2019;3(21):3379-3392.

80. Li C, Psatha N, Sova P, et al. Reactivation of γ-globin in adult β-YAC mice after ex vivo and in vivo hematopoietic stem cell genome editing. *Blood*. 2018;131(26):2915-2928.

81. Flint J, Tufarelli C, Peden J, et al. Comparative genome analysis delimits a chromosomal domain and identifies key regulatory elements in the alpha globin cluster. *Hum Mol Genet*. 2001;10(4):371-382.

82. Kosicki M, Tomberg K, Bradley A. Repair of double-strand breaks induced by CRISPR-Cas9 leads to large deletions and complex rearrangements [published correction appears in *Nat Biotechnol*. 2018;36:899]. *Nat Biotechnol*. 2018;36(8):765-771.

83. Zuccaro MV, Xu J, Mitchell C, et al. Allele-specific chromosome removal after Cas9 cleavage in human embryos. Cell. 2020;183(6):1650-1664.

84. Adikusuma F, Piltz S, Corbett MA, et al. Large deletions induced by Cas9 cleavage. *Nature*. 2018;560(7717):E8-E9.

85. Nelson CE, Wu Y, Gemberling MP, et al. Long-term evaluation of AAV-CRISPR genome editing for Duchenne muscular dystrophy. *Nat Med*. 2019;25(3):427-432.

86. Hanlon KS, Kleinstiver BP, Garcia SP, et al. High levels of AAV vector integration into CRISPR-induced DNA breaks. *Nat Commun*. 2019;10(1):4439.

87. Canaj H, Hussmann JA, Li H, et al. Deep profiling reveals substantial heterogeneity of integration outcomes in CRISPR knock-in experiments. *bioRxiv*. 2019:841098. </prpt>

88. Zuo E, Huo X, Yao X, et al. CRISPR/Cas9-mediated targeted chromosome elimination. *Genome Biol*. 2017;18(1):224.

89. Dolan AE, Hou Z, Xiao Y, et al. Introducing a spectrum of long-range genomic deletions in human embryonic stem cells using type I CRISPR-Cas. *Mol Cell*. 2019;74(5):936-950.e5.

90. Bi C, Wang L, Yuan B, et al. Long-read individual-molecule sequencing reveals CRISPR-induced genetic heterogeneity in human ESCs. *Genome Biol*. 2020;21(1):213.

91. Barseghyan H, Tang W, Wang RT, et al. Next-generation mapping: a novel approach for detection of pathogenic structural variants with a potential utility in clinical diagnosis. *Genome Med*. 2017;9(1):90.

92. Stangl C, de Blank S, Renkens I, et al. Partner independent fusion gene detection by multiplexed CRISPR-Cas9 enrichment and long read nanopore sequencing. *Nat Commun*. 2020;11(1):2861.

93. Rumaney MB, Ngo Bitoungui VJ, Vorster AA, et al. The co-inheritance of alpha-thalassemia and sickle cell anemia is associated with better hematological indices and lower consultations rate in Cameroonian patients and could improve their survival. *PLoS 1*. 2014;9(6):e100516.

94. Higgs DR, Aldridge BE, Lamb J, et al. The interaction of alpha-thalassemia and homozygous sickle-cell disease. *N Engl J Med*. 1982;306(24):1441-1446.

95. Raffield LM, Ulirsch JC, Naik RP, et al; NHLBI Trans-Omics for Precision Medicine (TOPMed) Consortium, Hematology & Hemostasis, Diabetes, and Structural Variation TOPMed Working Groups. Common α-globin variants modify hematologic and other clinical phenotypes in sickle cell trait and disease. *PLoS Genet.* 2018;14(3):e1007293.

96. Serjeant GR, Vichinsky E. Variability of homozygous sickle cell disease: the role of alpha and beta globin chain variation and other factors. *Blood Cells Mol Dis.* 2018;70:66-77.

97. Levasseur DN, Ryan TM, Pawlik KM, Townes TM. Correction of a mouse model of sickle cell disease: lentiviral/antisickling beta-globin gene transduction of unmobilized, purified hematopoietic stem cells. *Blood.* 2003;102(13):4312-4319.

98. Harteveld CL, Higgs DR. Alpha-thalassaemia. *Orphanet J Rare Dis.* 2010;5(1):13.

Supplementary information

Supplemental Table 1 : antibodies for flow cytometry

Name	Fluorochrome	Clone	Company	Catalog Number
human Fc Receptor binding inhibitor polyclonal antibody			eBioscience	16-9161-73
anti-human Fetal Hemoglobin	APC		Life Technologies	MHF05
anti-human Hemoglobin β	PE	37-8	Santa Cruz Biotechnology	sc-21757
anti-human HLA-ABC	PE	G46-2.6	BD Bioscience	555553
anti-human CD36	FITC	C836	BD Bioscience	555454
anti-human CD235a (GYPA)	PE-Cy7	GA-R2	BD Bioscience	563666
anti-human CD71	APC	M-A712	BD Bioscience	551374
anti-human CD45	APC	HI30	BD Bioscience	555485
anti-human CD33	BV421	P67.6	BD Bioscience	744761
anti-human CD19	BV605	HIB19	BD Bioscience	740394
anti-human CD3	BB700	SK7	BD Bioscience	566575
anti-human CD271 (NGFR)	APC	ME20.4-1.H4	Miltenyi Biotec	130-113-418
anti-human CD34	PE	AC136	Miltenyi Biotec	130-113-179
IgG1, κ isotype control	APC		Life Technologies	MG105
IgG1, κ isotype control	APC		BD Bioscience	550854
IgG1, κ isotype control	FITC		BD Bioscience	555748
IgG1, κ isotype control	BV421		BD Bioscience	562438
IgG1, κ isotype control	BV605	X40	BD Bioscience	562652
IgG1, κ isotype control	BB700	X40	BD Bioscience	566404
IgG2a, κ isotype control	APC	G155-178	BD Bioscience	551414
IgG2a, κ isotype control	PE		BD Bioscience	555574
IgG2a, κ isotype control	PE	S43.10	Miltenyi Biotec	130-113-272
IgG2b, κ isotype control	PE-Cy7		BD Bioscience	560542

All antibodies were mouse monoclonal antibodies, unless differently specified.

Supplemental Table 2: primer list

PCR		
Gene/amplicon	**name**	**sequence**
HBA 1/2	3820 F	TATCGCCAGAGGGAAAGGGA
	4870 R	CTTGAAGTTGACCGGGTCCA
HBA1/2 sequencing	894 R	TAGGTCTTGGTGGTGGGGAA
HBA2	611 F	GCACTCTTCTGGTCCCCAC
	1512R	GCAGAGAGGTCCTTGGTCTG
HBA1	HBA EX1F	CCGACAAGACCAACGTCAA
	5614 R	CTCTAGGGTCCAGCGTTTTTCC
AAVS1	MA359	CAGCTCAGGTTCTGGGAGAG
	MA360	CTTGTAGGCCTGCATCATCA
HBA1/del	3820 F	TATCGCCAGAGGGAAAGGGA
	5614 R	CTCTAGGGTCCAGCGTTTTTCC
HBB	F7895	AGGCCATCACTAAAGGCACC
	R8327	AGTCAGGGCAGAGCCATCTA
HBB promoter	HBB9 F	CTGTCTCCACATGCCCAGTT
	HBB9 R	GGAGACGCAGGAAGAGATCC
Off Target 1	OT1-F	CCTCTGCTGGCAGGATTT
	OT1-R	AGCAAGGGTAAGAATCTGTCTC
Off-Target 2	OT2-F	TCTCACAATTCAAGAGGCCAGA
	OT2-R	TCAGACACACACAGGGAGAG
Off-Target 3	OT3-F	GTTCTCCAGCAGCCTTTCA
	OT3-R	AGCACTTCCAAAGGGTTGT
ddPCR		
On-target 3'junction	3'HBA INT F	TGGACAAACCACAACTAGAATGC
	3'HBA INT 3 R	AAGTGCGGGAAGTAGGTCTT
	3'HBA INT PRB	56-FAM/CTGTCTCCTGCCGACAAGACCAAC
HBA2	HBA2 3' F	GCCCTTCCTGGTCTTTGAATA
	HBA2 3' R	ACCTCCATTGTTGGCACAT
	HBA2 3' PRB	56-FAM/TGTGTGTGCCTGGGTTCTCTCTAT
ALB	ALB F	GCTGTCATCTCTTGTGGGCTGT
	ALB R	ACTCATGGGAGCTGCTGGTTC
	ALB P	CCTGTCATGCCCACACAAATCTCTCC
qPCR		
GAPDH	GAPDH F	CTTCATTGACCTCAACTACATGGTTT
	GAPDH R	TGGGATTTCCATTGATGACAAG
HBA1/HBA2	HBA F	CGGTCAACTTCAAGCTCCTAA
	HBA R	ACAGAAGCCAGGAACTTGTC
HBB	HBB F	GCAAGGTGAACGTGGATGAAGT
	HBB R	TAACAGCATCAGGAGTGGACAGA
HBB AS3	HBBAS3 F	AAGGGCACCTTTGCCCAG
	HBBAS3 R	GCCACCACTTTCTGATAGGCAG
HBG1/HBG2	HBG1 2 F	CCTGTCCTCTGCCTCTGCC
	HBG1 2 R	GGATTGCCAAAACGGTCAC
HBD	HBD F	CAAGGGCACTTTTTCTCAG
	HBD R	AATTCCTTGCCAAAGTTGC
GYPA	hGYPA F	GGTGGCAATGCACACTTCAA
	hGYPA R	ACCCTTTCTCCGGTTTCCTC

F=forward; R=reverse, PRB=probe.

Supplementary data

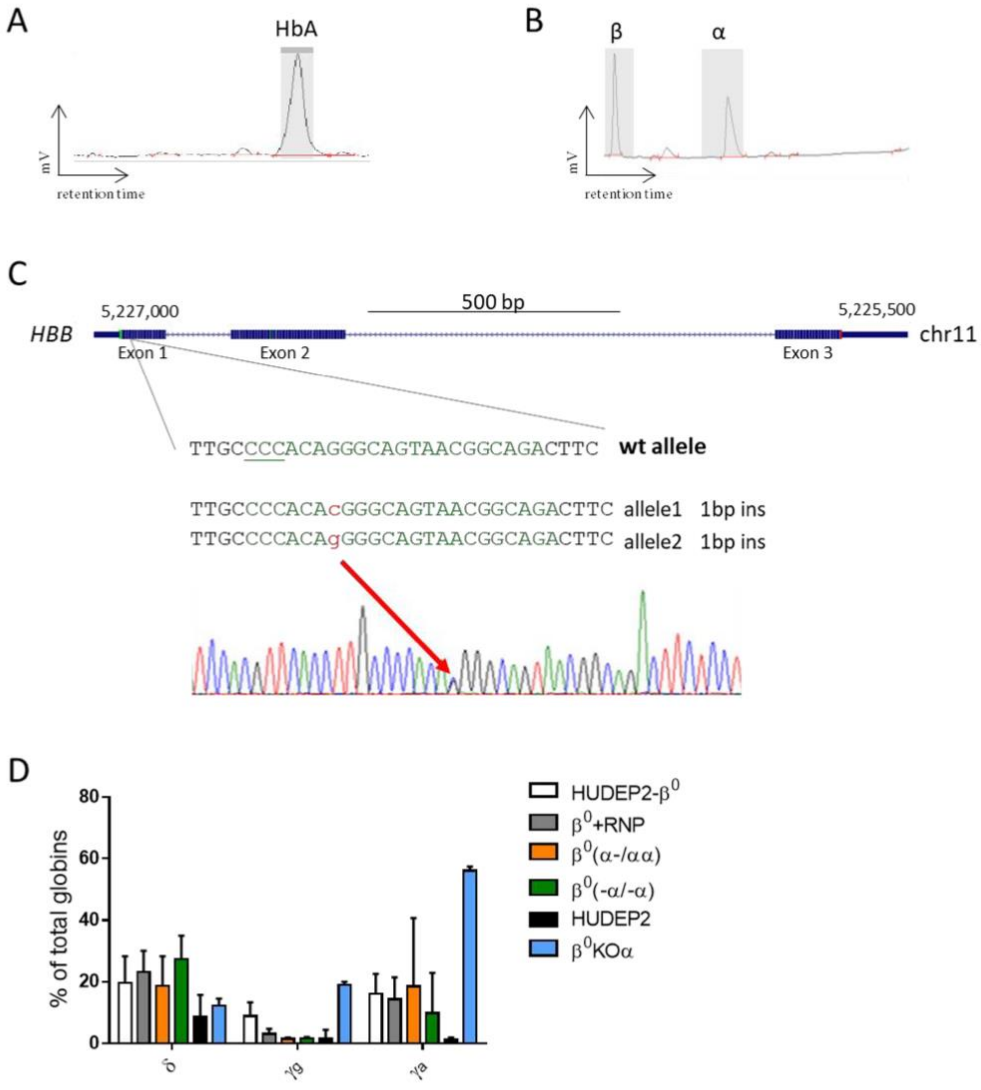

Supplementary figure 1. Genotype of HUDEP-2 β^0

(**A-B**) Representative HPLC chromatograms of globin tetramer (**A**) and b-like subunits (**B**) analysis. HbA, adult hemoglobin ($\alpha_2\beta_2$). (**C**) Schematic representation of the β-globin gene (*HBB*; hg38). Reference allele (wt) is shown above HUDEP-2 β^0 Sanger sequencing profiles. Frameshift disruption occur at leucine 15. gRNA target site is shown in green, PAM sequence is underlined and +1 insertions are shown in red. (**D**) RT-qPCR quantification of β-like globin mRNA ratios in HUDEP-2 β^0 (n=3-5) and in single cell clones with monoallelic (α-/αα; n=3) or biallelic (α-/α-; n=3) *HBA2* deletions. β^0 + RNP = HUDEP2 b^0 bulk population edited with gRNA HBA15/Cas9. β^0 KOa= HUDEP2 β^0 bulk population edited with gRNA HBB/Cas9 to induce a-globin KO. Bars represent mean±SD (n=3; ** p<0.01, ANOVA, Tukey's test).

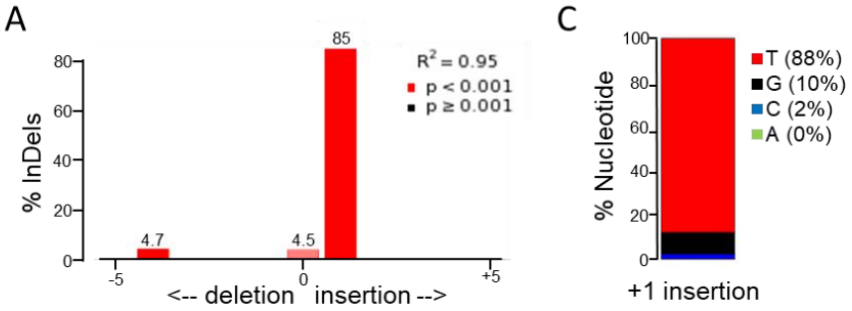

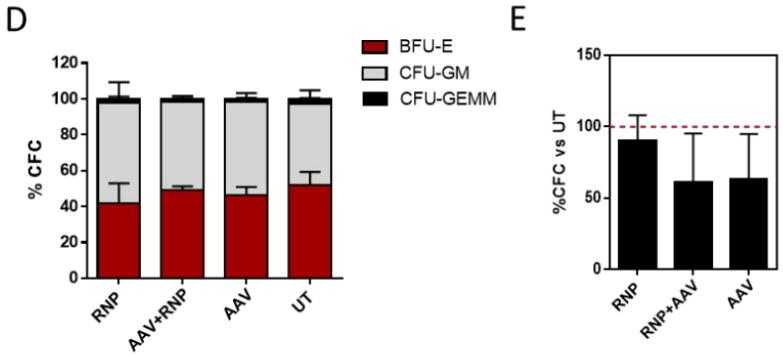

F

	wt	1 β^{AS3}	2 β^{AS3}	**Tot**
wt	20	7	1	28
1 del	6	17	2	25
2 del	0	5	0	5
Tot	26	29	3	

Supplemental Figure 2. *Ex vivo* characterization of edited HSPCs.

(**A-C**) Representative InDel spectrum (A), sequence (B) and 1+ nucleotide insertion probability (C) for gRNA HBA15. In (B) Red line: gRNA sequence; blue line: PAM sequence. (**D**) Colony formation unit (CFU) frequency in edited HSPCs. CFU-GEMM, granulocyte, erythroid, macrophage, megakaryocyte; BFU-E, burst-forming unit-erythroid; CFU-GM, granulocyte, macrophage. Bars represent mean ±SD (n=3-5). (**E**) CFC number expressed as percentage of untreated control (UT). Bars represent mean ±SD (n=3-5), red dashed line indicates 100%. (**F**) Colony genotypes shown in Figure 3I.

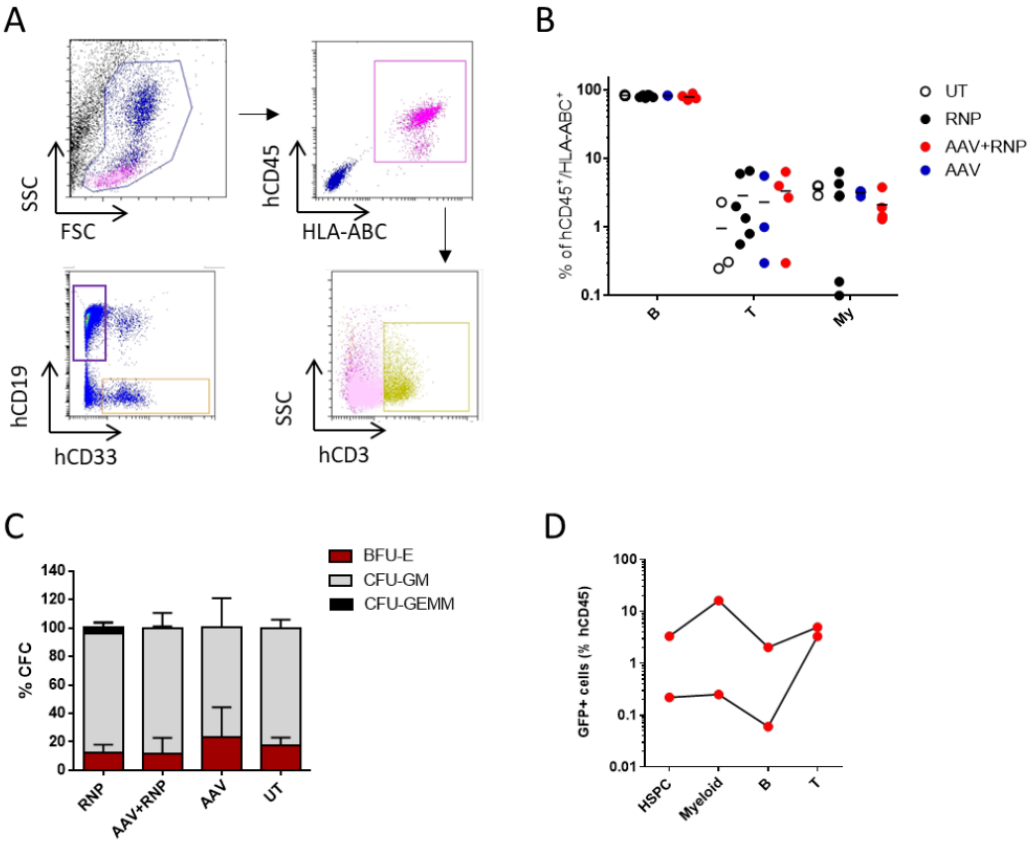

Supplemental Figure 3. *In vivo* characterization of edited HSPCs.

(**A**) Gating strategy to analyze engraftment levels and cell lineages of human xenografts in NSG mice. Representative plots for quantification of human hematopoietic (CD45+/HLA-ABC+), human B (CD19+), human myeloid (CD33+) and human T (CD3+) cells. (**B**) Immunophenotyping of human xenografts in bone marrow of NSG mice. Each dot represents one animal, lines indicate mean. (**C**) Colony formation unit (CFU) frequency in bone marrow-derived CD34. CFU-GEMM, granulocyte, erythroid, macrophage, megakaryocyte; BFU-E, burst-forming unit-erythroid; CFU-GM, granulocyte, macrophage. Bars represent mean ±SD (n=2-4). (**D**) GFP positive cells in HSPCs (CD34), myeloid (CD33), B (CD19) and T (CD3) cells in BM of transplanted mice. Each line represents one animal.

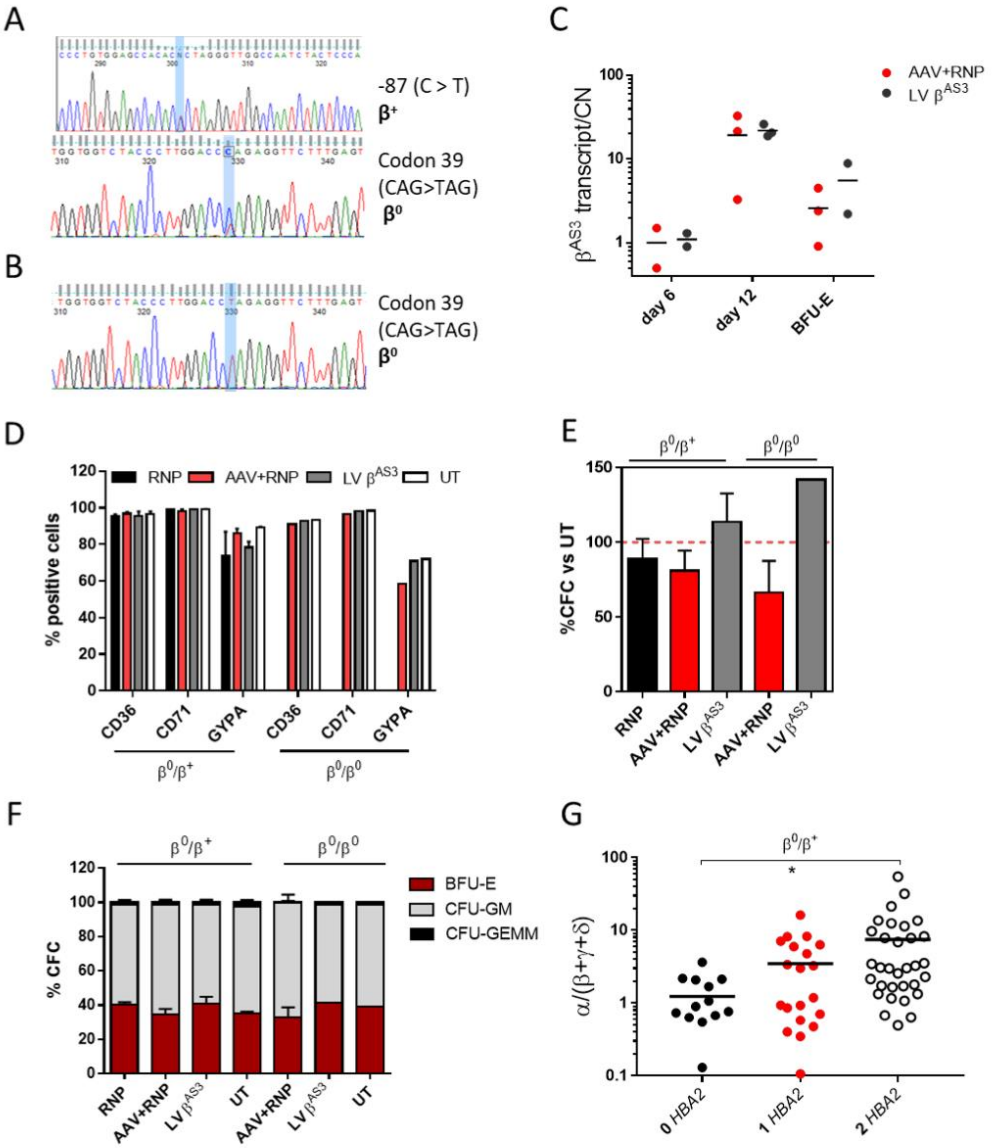
A
-87 (C > T)
β+
Codon 39
(CAG>TAG)
β0
B
Codon 39
(CAG>TAG)
β0
C
AAV+RNP
LV βAS3
βAS3 transcript/CN
day 6
day 12
BFU-E
D
RNP
AAV+RNP
LV βAS3
UT
% positive cells
CD36
CD71
GYPA
β0/β+
β0/β0
E
β0/β+
β0/β0
%CFC vs UT
RNP
AAV+RNP
LV βAS3
F
β0/β+
β0/β0
BFU-E
CFU-GM
CFU-GEMM
% CFC
RNP
AAV+RNP
LV βAS3
UT
G
β0/β+
α/(β+γ+δ)
0 HBA2
1 HBA2
2 HBA2

Supplemental figure 4. Characterization of edited thalassemic HPSCs.

(**A**-**B**) Sanger sequencing of *HBB* gene in patients' HSPCs. Patient 1 carries the -87 C>T β^+ mutation in heterozygosis with the codon 39 (CAG>TAG) β^0 mutation (A). Patient 2 is homozygous for the codon 39 (CAG>TAG) β^0 mutation (B). Blue boxes highlight the mutated nucleotides. (**C**) β^{AS3} RNA expression during erythroid differentiation in β^+ erythroblasts. Values are normalized per copy number (CN). Black lines indicate mean. (**D**) Flow-cytometry analysis at day 12 of erythroid differentiation of edited HSPCs. Results are shown as mean ±SD (n=1-3). (**E**) CFC numbers expressed as percentage of untreated control (UT). Red dotted line indicates 100%; bars represent mean ±SD (n=1-3). (**F**) Colony-forming cell (CFC) frequency in edited HSPCs (mean ±SD). CFU-GEMM, granulocyte, erythroid, macrophage, megakaryocyte; BFU-E, burst-forming unit-erythroid; CFU-GM, granulocyte, macrophage. (**G**) α/β-like globin mRNA ratios in edited thalassemic BFU-E (n=67) are plotted. 2 HBA2 colonies come from untreated and wt edited BFUE. Each dot represents a single colony. Black lines indicate mean (n= ;*, $p<0.01$; 1 way ANOVA, Dunn's test).

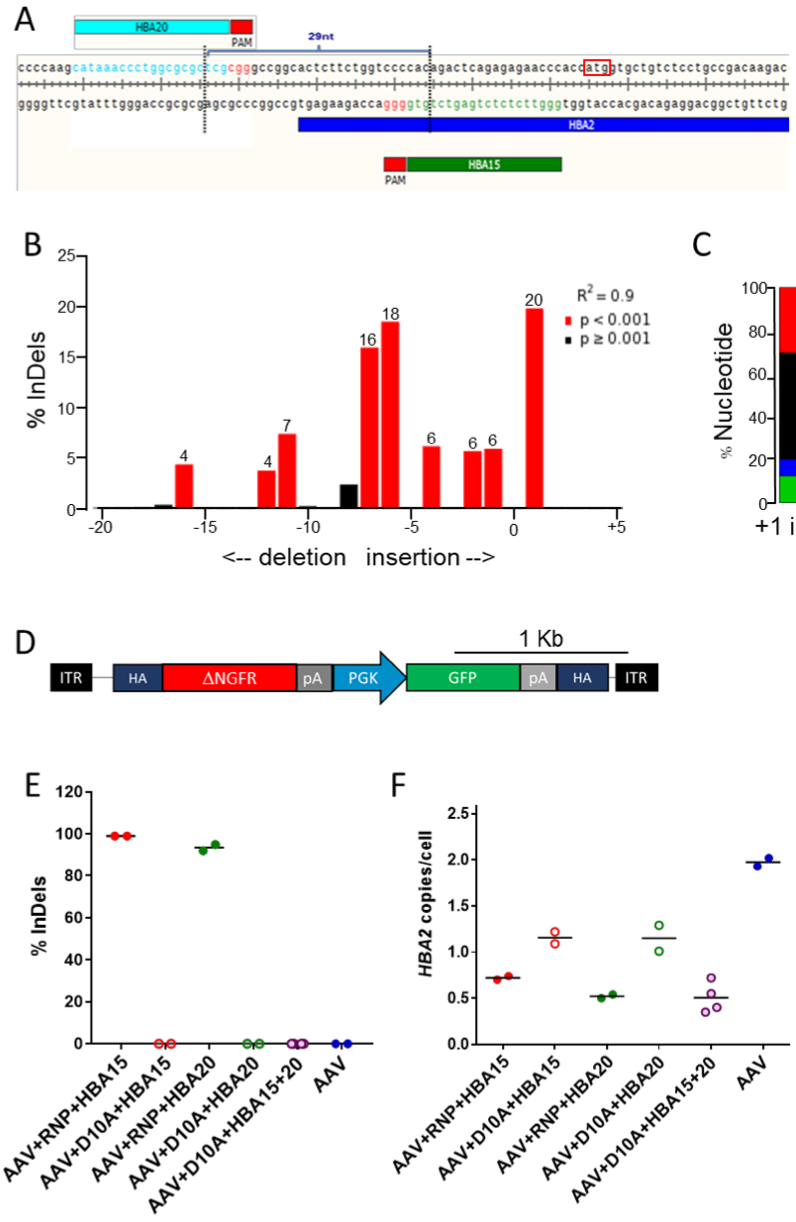
A
HBA20
PAM
29nt
HBA2
HBA15
PAM
B
% InDels
$R^2 = 0.9$
p < 0.001
p ≥ 0.001
<-- deletion insertion -->
C
% Nucleotide
T (30.3%)
G (49.5%)
C (7.6%)
A (12.5%)
+1 insertion
D
1 Kb
ITR
HA
ΔNGFR
pA
PGK
GFP
pA
HA
ITR
E
% InDels
AAV+RNP+HBA15
AAV+D10A+HBA15
AAV+RNP+HBA20
AAV+D10A+HBA20
AAV+D10A+HBA15+20
AAV
F
HBA2 copies/cell
AAV+RNP+HBA15
AAV+D10A+HBA15
AAV+RNP+HBA20
AAV+D10A+HBA20
AAV+D10A+HBA15+20
AAV

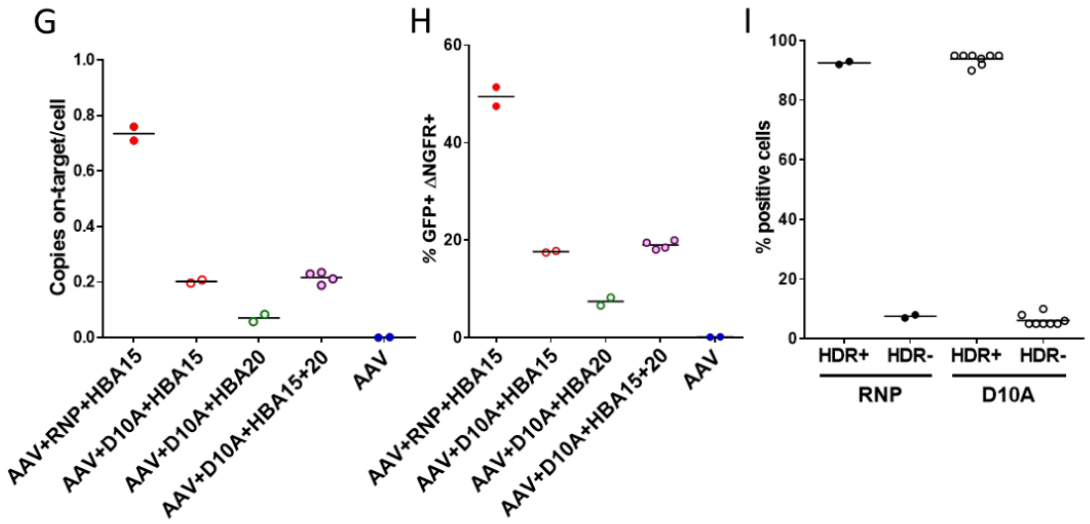

Supplemental figure 5. Single vs dual nick editing of K562

(**A**) Genomic location of HBA15 and HBA20 gRNAs. The distance between the two cutting sites is indicated. Red rectangle: HBA start codon. (**B**-**C**) Representative InDel spectrum (A) and 1+ nucleotide insertion probability (B) for HBA20. (**D**) AAV6 donor used for KI experiments. Vector contains a promoterless transgene encoding for the truncated inactive form of the human low affinity nerve growth factor receptor (ΔNGFR), followed by a phosphoglycerate kinase (PGK) promoter with a GFP reporter and simian virus polyA (pA). This cassette is flanked by 250 bp homology arms (homology) to gRNA genomic target. ITR, inverted terminal repeats. 1KB scale bar is indicated on top. (**E**-**F**) InDels (E) and *HBA2* copies (F) quantification in edited K562 cells. Black lines represent mean. (**G**-**H**) AAV knock-in efficiency in term of on-target DNA integration (G) and NGFR/GFP expression (H). Black lines represent mean. (I) Percentage of cells with HDR or not HDR mediated DNA targeted integration (same data of H). HDR+ = (GFP+ DNGFR+ / GFP+) * 100; HDR- = 100 - HDR+. Black lines represent mean.

A

	wt	1 β^{AS3}	2 β^{AS3}	Tot
wt	105	11	0	116
1 del	58	16	0	74
2 del	10	2	0	12
Tot	173	29	0	

B

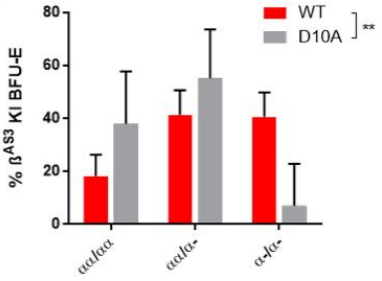

C

		Reads	Position (hg19)	Strand	Type	Gene
ON TARGET	G G G T T C T C T C T G A G T C T G T G N G G	329	Chr16_222886/226690	-	Exon	HBA2
OT-1	· A · · · · C · · · G · · · · · · · · · · ·	320	Chr3_141179078	-	Intergenic	
OT-2	· · · · · · C · · · · · · · G · · · · · · ·	135	Chr9_77688205	-	Intron	NMRK1
OT-3	· · · C · · · · C · · · · · · A · · · · A · ·	75	Chr8_143095162	+	Intergenic	
OT-4	· · · · · · · · C · C A T · · · · · · · · · ·	29	Chr4_66205583	-	Intron	EPHA5
OT-5	A · A · · · · · C · · · · · A · · · · · · · ·	28	Chr5_2859208	-	Intergenic	
OT-6	· · · C · · · · · · · · · · G · · · · A · · ·	20	Chr20_38984675	-	Intergenic	
OT-7	A · · G · · · · · · · · · · · · C T · · · · ·	16	Chr10_43101518	-	Intron	ZNF33B
OT-8	· · · · · A · · · C · A · · · · · · A · · · ·	13	Chr12_117293884	+	Intergenic	
OT-9	A · · G · · · · A · · · · · · · · · G · · · ·	11	Chr17_26110678	+	Intron	NOS2
OT-10	· · · G · · · G · · · · T · · · · · · · · · ·	10	Chr22_22683405	+	Intergenic	
OT-11	A A · · · · · G · · · · · · A · · · · · · · ·	8	Chr2_217147479	+	Intron	MARCH4
OT-12	· · · · · · C · · · · A · · G · · · · · · · ·	5	Chr11_70355141	-	Intron	SHANK2
OT-13	· · · · · · · · · · · C · · · · · · · · · · T	4	Chr6_24657192	-	Intron	TDP2
OT-14	C · · · · · · · · · · · · · · · · A · · · A ·	4	Chr6_169440547	-	Intergenic	
OT-15	A · · C · · C · · · · · · · · · · · · · · · A	3	Chr2_227599376	-	Exon	IRS1

D

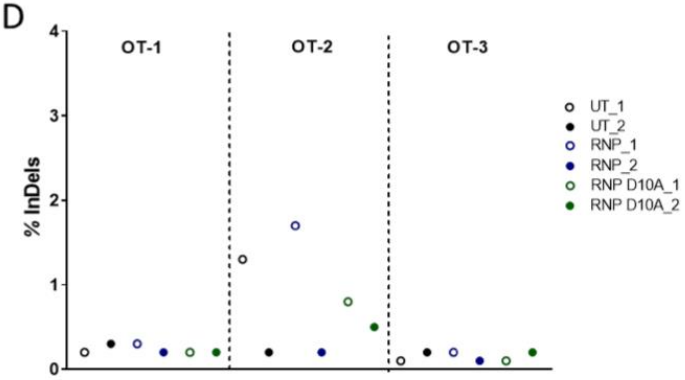

Supplemental figure 6. CFC and off-target analysis

(**A**) Colony genotypes shown in Figure 6H. (**B**) Genotype of CFC with β^{AS3} transgene integration using Cas9 (WT, gray; n=121) or Cas9 nickase (D10A, red; n=29). Bar represent frequency ±confidence intervals (**, $p < 0.01$; Chi-square test). (**C**) GUIDE-Seq analysis. The on-target sequence and PAM motif are shown in the top line. Off-targets and their mismatches to the on-target site (highlighted in color), sequencing read counts, chromosomal position (hg19), strand and type of genomic region are reported. The majority of off-targets map to intergenic regions or introns except OT-15, which lays in exon 2 of the IRS1 gene that is not expressed in the hematopoietic system. (**D**) InDel quantification by deep-sequencing of top 3 off-target sites identified by GUIDE-Seq in erythroblasts derived from control and edited HSPCs (n=2 different healthy donors). On-target InDels were 92 and 98% (TIDE) for Cas9 wt. The InDels measured in OT-2 come from amplification/sequencing errors, as mutations in the amplicons are not specific to the gRNA matching sequence.

Conclusion

HBA2 deletion in edited β-thalassaemic HUDEP or patient HSCs improves the α-globin precipitation as observed in patient having an α-thalassaemic trait. Thus, hijacking the HBA promoter to produce β-chains restores the α/β imbalance and lead to significant HbA formation. Edited CD34+ (RNP only or RNP+AAV) cells have been successfully transplanted into immunocompromised mice and were able to retain their multilineage potentiality.

To offer a safer editing strategy without DSBs, we applied RNP composed of Nickase D10A and HBA gRNA. We observed a lower targeting integration in HSCs compared to spCas9 but without indels generation and with a lower toxicity. Nickase is a promising strategy but requires optimisation such as delivery methods or used of other Nickases variants. Finally, the analysis of off-target via GUIDE-seq demonstrate the robustness and the safety of strategy as none of them were detected.

6.2 *EX VIVO* EDITING OF HUMAN HSCS FOR ERYTHROID EXPRESSION OF THERAPEUTIC PROTEINS (PAVANI ET AL., 2020)

Introduction

Protein replacement therapy (PRT) becomes a gold standard therapy for many monogenic disorders that requires supplementation of the missing protein such as lysosomal enzyme or blood factors. While lifesaving, PRT consists of weekly intravenous injection of a human recombinant protein that could result in patient to immune response against recombinant protein and remains quite expensive. By insertion of a functional copy of the deficient protein in patient's HSCs, *ex vivo* GT offers a curative alternative for monogenic disorders. In this context, we developed a universal platform to achieve targeted transgene integration into a safe-harbour locus : the α-globin locus (HBA). In HSCs, we induced DSBs in HBA locus with CRISPR-spCas9 and delivered a therapeutic transgene with HA for HBA using AAV6 allowing targeted integration with HDR. The integration of therapeutic transgene into HBA locus leads to high and erythroid specific expression in erythroblasts. Therefore, HBA platform would require minimal transgene integration events in HBA locus to provide sufficient amount of therapeutic proteins reducing as consequence the potential off-target and toxicity due to editing and DNA donor delivery.

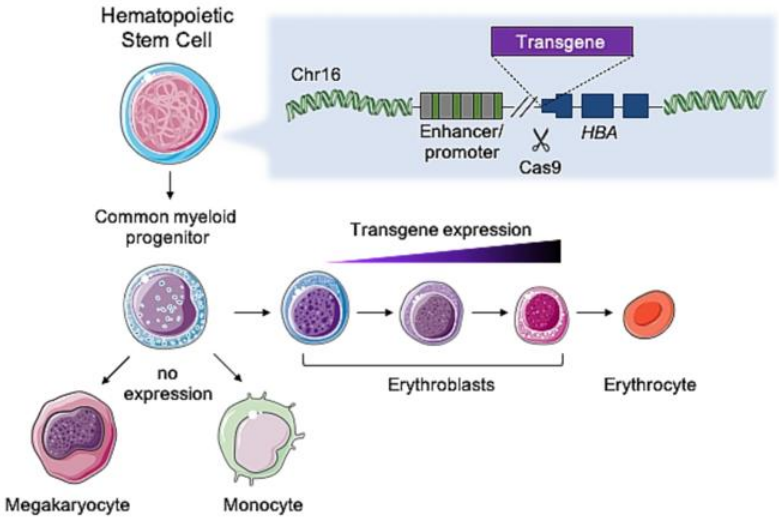

Figure 35) Representation of the HBA-targeted platform for protein expression in erythroid cells (from Community, 2020). The integration of the therapeutic transgene under the control of the endogenous α-globin promoter will allow specific protein expression in erythrocytes.

We first selected gRNA targeting the non-coding 5' untranslated (UTR) region of HBA locus without affecting erythroid differentiation or hemoglobin synthesis. Then, the efficiency of targeting integration in HBA locus was evaluated upon AAV6 delivery of a promoterless GFP template flanked by HBA HA. Finally, potential off-target sites were investigated via IDLV capture analysis to assure the safety and specificity of our Cas9/gRNA strategy. To evaluate the erythroid-based platform for protein secretion, we performed targeted integration of promoterless therapeutic transgenes in HSCs. We tested the strategy on different disease model as hemophilia B (FIX), Mucopolysaccharidosis (Iduronidase, IDUA), Fabry disease (α-galactosidase, GLA), and Wolman disease (Lysosomal acid lipase, LAL) all of them currently treated with PRT. We then differentiated edited HSC, towards the erythroid lineage for 14 days and monitored enzyme secretion. Finally, the engraftment and multilineage reconstitution potency of edited CD34+ was evaluated in immunocompromised (NSG) mice.

Contribution :

I worked on the *in vitro* evaluation of FIX, IDUA, GLA, LAL expression and secretion as well as cross-correction assays in WD fibroblasts. I was also involved in the editing of CD34+ LIPA KI prior NSG transplantation and in the 12-week mice follow up.

Article

nature COMMUNICATIONS

ARTICLE

https://doi.org/10.1038/s41467-020-17552-3 OPEN

Ex vivo editing of human hematopoietic stem cells for erythroid expression of therapeutic proteins

Giulia Pavani[1], Marine Laurent[1], Anna Fabiano[1], Erika Cantelli[1], Aboud Sakkal[1], Guillaume Corre[1], Peter J. Lenting[2], Jean-Paul Concordet[3], Magali Toueille[1], Annarita Miccio[4,5] & Mario Amendola[1✉]

Targeted genome editing has a great therapeutic potential to treat disorders that require protein replacement therapy. To develop a platform independent of specific patient mutations, therapeutic transgenes can be inserted in a safe and highly transcribed locus to maximize protein expression. Here, we describe an ex vivo editing approach to achieve efficient gene targeting in human hematopoietic stem/progenitor cells (HSPCs) and robust expression of clinically relevant proteins by the erythroid lineage. Using CRISPR-Cas9, we integrate different transgenes under the transcriptional control of the endogenous α-globin promoter, recapitulating its high and erythroid-specific expression. Erythroblasts derived from targeted HSPCs secrete different therapeutic proteins, which retain enzymatic activity and cross-correct patients' cells. Moreover, modified HSPCs maintain long-term repopulation and multilineage differentiation potential in transplanted mice. Overall, we establish a safe and versatile CRISPR-Cas9-based HSPC platform for different therapeutic applications, including hemophilia and inherited metabolic disorders.

[1] INTEGRARE, Genethon, UMR_S951 Inserm, Univ Evry, Univ Paris-Saclay, 91002 Evry, France. [2] Laboratory of Hemostasis-Inflammation-Thrombosis, UMR_S1176 Inserm, Univ. Paris-Sud, Université -Saclay, 94276, Le Kremlin-Bicêtre, Orsay, France. [3] National Museum of Natural History, UMR_1154 Inserm, UMR_7196 CNRS, Univ Sorbonne, Paris, France. [4] Imagine Institute, UMR_163 INSERM, Paris, France. [5] Paris Descartes Univ Sorbonne Paris Cité, Paris, France. ✉email: mamendola@genethon.fr

Many diseases require protein replacement therapy (PRT) to supplement a protein that is deficient because of a genetic defect. PRT is approved or under investigation to treat more than 40 inherited disorders, mostly involving blood factors and lysosomal enzymes[1]. Although life saving for some patients, this therapy has several limitations, that lead to treatment failures and limited long-term efficacy[2].

Genome editing technologies have a great therapeutic potential for genetic disorders, as they can fix the underlying disease-causing mutation[3,4]. However, this approach requires the development of countless gene-tailored editing strategies that can hinder clinical translation.

To overcome this issue, a single "safe harbor" or a highly transcribed genomic locus can be exploited to integrate and overexpress different therapeutic transgenes[5]. Previous studies successfully used adeno-associated virus (AAV) for nuclease-mediated targeting of transgenes under the control of the endogenous albumin promoter in liver[6,7]. The striking transcriptional activity of this locus achieved therapeutic protein levels in different preclinical models and thus prompted the first in vivo genome editing trial in humans (NCT03041324). Although promising, this approach is hampered by: (1) presence of pre-existing antibodies against AAV capsid that precludes treatment to a significant portion of patients[8]; (2) long-term expression of synthetic nucleases in vivo, which could result in genotoxicity and trigger immune responses against transduced hepatocytes[9,10]; (3) liver conditions that can alter AAV transduction and hepatic protein expression[11,12].

As therapeutic alternative, hematopoietic stem cells (HSCs) can be harnessed to overexpress transgenes in downstream hematopoietic lineages. Differently from liver, autologous HSCs can be easily accessed for ex vivo gene manipulation and re-administration, thus circumventing immunological issues; however, a suitable locus for transgene integration (knock-in, KI) still needs to be identified.

α-globin genes are expressed by the erythroid lineage at extremely high levels (~1.5 g/day)[13], they are present in 4 copies per cells and the loss of up to 3 α-globin alleles is mostly asymptomatic[14], making this locus a promising candidate for KI in HSCs. In addition, erythroid cells are the most abundant hematopoietic progeny (~2×10^{11} new erythrocytes per day[13]) and can secrete relevant amounts of therapeutic proteins, as previously demonstrated by gene transfer using lentiviral vectors (LV)[15–17].

Here, using CRISPR-Cas9 we integrate therapeutic genes under the transcriptional control of the endogenous α-globin promoter in human HSCs. We aim to combine strong transcription and abundance of transgene-expressing erythroblasts to maximize protein production, reducing the number of integration events required to reach therapeutic levels.

This HSC platform for robust erythroid-specific expression of therapeutic proteins opens possibilities for treating hemophilia and lysosomal storage disorders (LSD), as well as other genetic diseases.

Results

Selection of gRNA targeting the α-globin locus. To generate a DNA double-strand break (DSB) for transgene integration in the α-globin locus, we focused on *Streptococcus pyogenes* (*Sp*)Cas9 nuclease, the only Cas in clinical trials to edit HSCs (NCT03164135; NCT03655678). We designed 14 guide (g)RNAs targeting the non-coding sequences of α-globin genes, in particular the 5′ untranslated region and introns (5′UTR, IVS1 and IVS2 respectively), avoiding known regulatory elements (Fig. 1a and Supplementary Table 1A). gRNA were tested for on-target DNA cleavage (InDels) in K562 erythroleukemic cells constitutively expressing Cas9 (Fig. 1b). For the best candidates for each region we analyzed the indels pattern (Supplementary Fig. 1a) and we assayed their effect on α-globin production. As control, we designed a gRNA (KO) targeting the first exon of *HBA1* and *HBA2* genes, which abrogates α-globin production. In K562, 5′UTR and IVS2 gRNA did not alter α-globin protein level (Supplementary Fig. 1b) and were therefore selected for further investigation.

To evaluate DNA cleavage efficiency in clinically-relevant human HSPCs, cells were transfected with Cas9/gRNA ribonucleoprotein complex (RNP). To control the effects of the editing procedure, we included a gRNA targeting an unrelated genomic locus (AAVS1). We observed efficient editing for 5′UTR and IVS2 gRNA in both erythroid liquid culture and methylcellulose-plated colony-forming cells (CFC) (Fig. 1c), which did not affect HSPC viability and multilineage potential (CFC assay; Fig. 1d and Supplementary Fig. 1c) or altered erythroid differentiation (flow cytometry analysis, Fig. 1e). Remarkably, 5′UTR and IVS2 gRNA did not modify α-globin expression, measured as ratio between α- and β-like globin chains (Fig. 1f and Supplementary Fig. 1d). In accordance with these data, adult hemoglobin (2α+2β globin chains; HbA) remained the predominant hemoglobin form in both 5′UTR and IVS2 erythroblasts, while it strongly decreased in KO controls where alternative homotetramers lacking α-globin chains appeared, as in α-thalassemic patients[14] (Fig. 1g and Supplementary Fig. 1e). Lastly, since the two α-globin genes (*HBA1* and *HBA2*) are the result of evolutionary duplication (96.67% sequence homology, GRCh38), we evaluated if simultaneous cleavage of both genes can induce loss of *HBA2* in edited HSPCs. We observed a reduction of *HBA2* copies per cell to 1.8 ± 0.3 for IVS2 gRNA, which selectively targets *HBA2*, and to 1.4 ± 0.3 for 5′UTR gRNA (Supplementary Fig. 1f); however, these rearrangements had minimal effect on globin production, as shown above. Detection and quantification of *HBA2* inversions was not possible due to technical issues associated with the presence of repetitive sequences and the high GC content of the α-globin locus.

Overall, these results demonstrate that both 5′UTR and IVS2 gRNA efficiently cut α-globin genes without affecting HSPC viability, differentiation potential and hemoglobin expression, thus representing an interesting genomic locus to test KI.

Targeted integration. To evaluate if the α-globin promoter can drive the expression of an integrated heterologous transgene, we generated KI cassettes containing a promoterless GFP (Supplementary Fig. 2a). These cassettes were delivered in K562-Cas9 cells using integrase-defective lentiviral vector (IDLV) and integrated by transfecting a gRNA encoding plasmid. Interestingly, all gRNA/IDLV combinations resulted in GFP expression, which increased upon erythroid differentiation (Supplementary Fig. 2b). In addition, on-target integration by non-homologous end joining was confirmed in GFP positive clones by PCR (Supplementary Fig. 2c) and the presence of a chimeric messenger RNA showed correct splicing of intron traps (Supplementary Fig. 2d). Similar results were obtained upon KI in the β-globin gene, suggesting that KI in globin genes with different expression levels could be a viable strategy to modulate transgene expression (Supplementary Fig. 2e–j).

We further confirmed these α-globin KI data in immortalized human erythroid progenitor cells (HUDEP-2)[18], which can differentiate to reticulocytes. To perform KI, HUDEP-2 cells were transfected with 5′UTR or IVS2 RNP and transduced with an AAV6 carrying the aforementioned expression cassettes flanked by homology arms to favor homologous DNA recombination

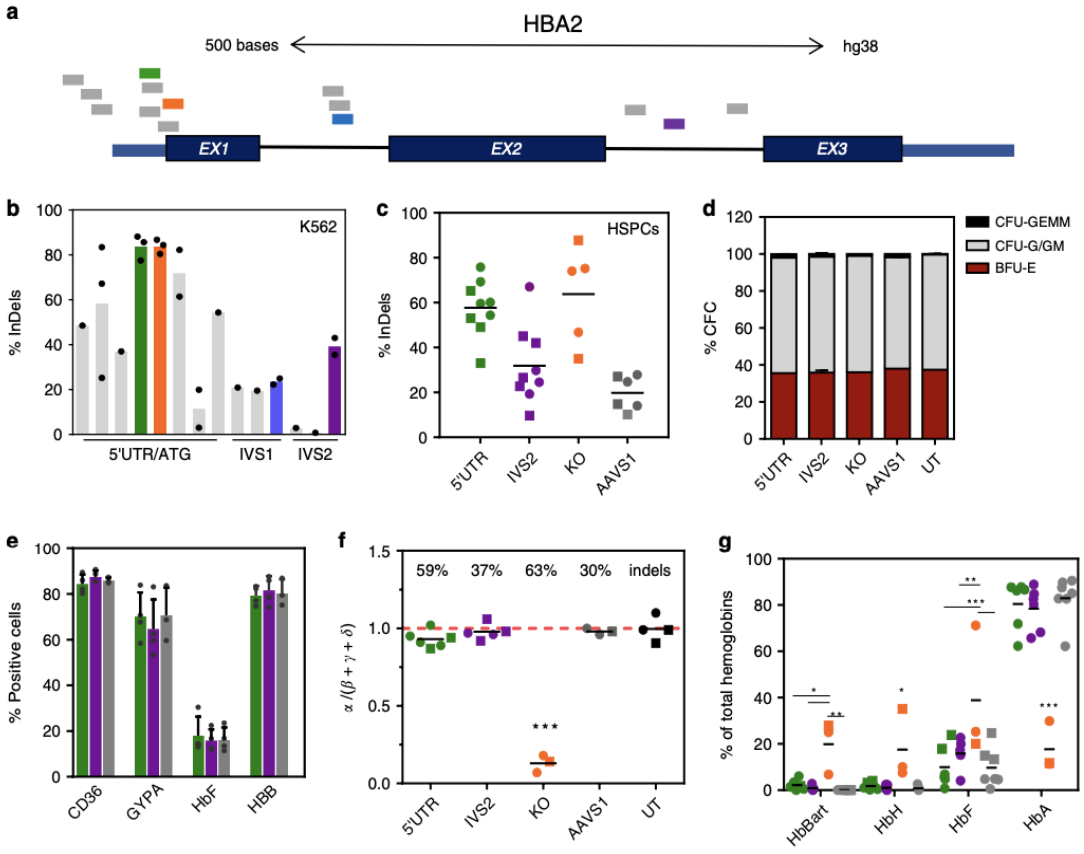

Fig. 1 Editing of selected sites in the α-globin locus minimally affects globin production. a Locations of gRNA on HBA2 gene. All gRNA except 74 (in purple) target both HBA1 and HBA2. Selected gRNA are highlighted. **b** K562-Cas9 screening of gRNA targeting different region of the α-globin locus (5′ untranslated region/start codon (5′UTR/ATG), intron 1 (IVS1) or intron 2 (IVS2)). Each bar is a different gRNA, each dot a different experiment. Editing efficiency is expressed as percentage of modified HBA alleles (bars represent mean; data from 1, 2 or 3 biological replicates). The gRNA selected for each region are highlighted. **c** Editing efficiencies in HSPCs in erythroid liquid culture (circles) or in BFU-E (burst-forming unit-erythroid, squares). Lines show mean (2-4 donors; $n = 5$ KO, $n = 6$ AAVS1, $n = 9$ 5′UTR and IVS2). **d** Colony-forming cell (CFC) frequency in edited HSPCs (mean ± SD; $n = 2$, $n = 4$ for IVS2). CFU-GEMM, granulocyte, erythroid, macrophage, megakaryocyte; BFU-E, burst-forming unit-erythroid; CFU-G/GM, granulocyte-macrophage. **e** Flow-cytometry analysis of erythroid markers upon differentiation of edited HSPCs, day12 (green 5′UTR, purple IVS2 and gray AAVS1). Results are shown as mean ± SD ($n = 3$ biological replicates, 3 different donors; $p = 0.94$, one-way ANOVA Tukey's test). **f** HPLC analysis of hemoglobin monomers of erythroblasts derived from edited HSPCs ($n = 6$ 5′UTR, $n = 5$ IVS2, $n = 3$ KO and AAVS1, $n = 4$ UT; 4 donors). InDels percentage mean is indicated. The ratio α/β-like globins in normal cells is close to 1 (red dashed line). Black lines show mean; BFU-E (squares), erythroid liquid culture (circles) (***$p < 0.001$ vs UT, 5′UTR, IVS2, AAVS1; one-way ANOVA, Tukey's test). **g** HPLC analysis of hemoglobin tetramers of erythroblasts derived from edited HSPCs (same samples as in **f**). Every tetramer is reported as % of total hemoglobins (*$p < 0.05$; **$p < 0.01$, ***$p < 0.001$; two-way ANOVA, Dunnet's test). Black lines show mean; BFU-E (squares), erythroid liquid culture (circles). Hb Bart, γ_4 ($p = 0.017$ 5′UTR, $p = 0.013$ IVS2, $p = 0.006$ AAVS1 vs KO); HbH, β_4 ($p = 0.038$ 5′UTR, $p = 0.035$ IVS2, $p = 0.032$ AAVS1 vs KO); HbF, fetal hemoglobin, $\alpha_2\gamma_2$ ($p < 0.001$ 5′UTR and AAVS1, $p = 0.002$ IVS2 vs KO); HbA, adult hemoglobin, $\alpha_2\beta_2$ ($p < 0.001$ vs KO). Source data are in the Source Data file.

(HDR)[19] (Fig. 2a). After puromycin selection, GFP was expressed from both genomic sites and increased about 100 fold upon differentiation, with 5′UTR integration expressing ~10 fold higher than IVS2 (Fig. 2b, c).

We then performed 5′UTR and IVS2 KI in HSPCs, where HDR was more efficient and no enrichment was required. Again, we observed a similar GFP upregulation after erythroid induction (~100 fold) and a higher expression upon 5′UTR integration (Fig. 2d–f and Supplementary Fig. 2k).

For this reason and considering that DNA targeted integration in IVS2 could result in the expression of a truncated α-globin chain, we selected the 5′UTR region for further investigation. Importantly, even if PCR analysis of individual CFC showed integration in both erythroid and granulocyte-monocyte colonies (Supplementary Fig. 2l), flow cytometry and microscopy data demonstrated that GFP expression was restricted to erythroid progenitors (Fig. 2g, h). Sanger sequencing of PCR products spanning the AAV-genome junction of colonies showed that KI occurred through HDR ($n = 10$; Supplementary Fig. 2l, m) Taken together, these data show that KI into α-globin locus is efficient and results in robust erythroid-specific expression.

Off-targets analysis. We performed off-target analysis for 5′UTR gRNA in K562. Briefly, cells were transfected with RNP for 5′

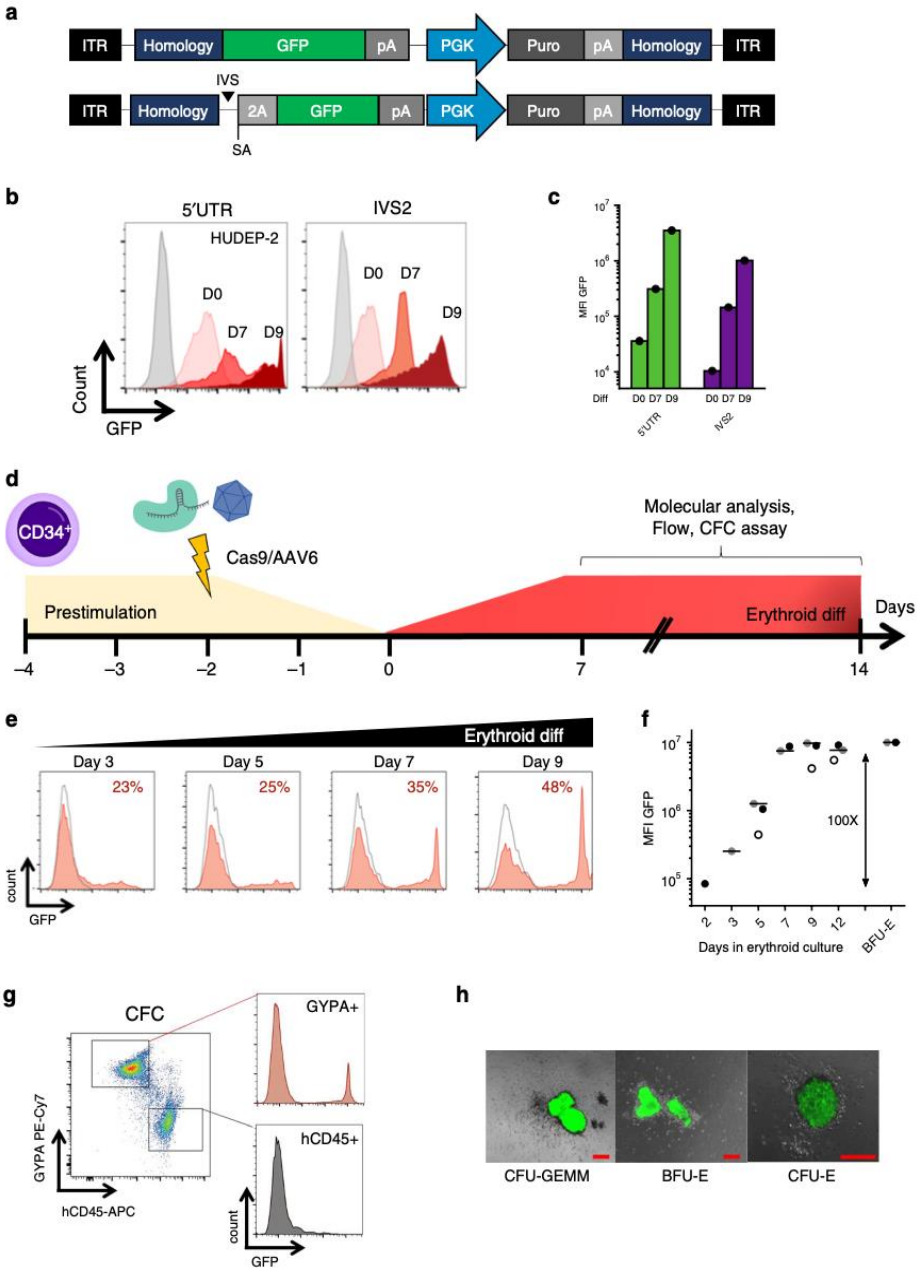

UTR or AAVS1 (negative control), and 29 top-scoring off-targets predicted in silico[20,21] were PCR amplified for InDels quantification. Although on-target activity reached >85%, we could not detect any difference between HBA15 and control AAVS1 gRNA at any of the predicted HBA15 off-target sites (Supplementary Table 2) (with a technical threshold of >2% of TIDE software)[22]. To detect unpredicted off-targets, we also performed an unbiased genome-wide screening by IDLV capture analysis. This method exploits the tendency of IDLV genome to ligate into DSB, thereby stably tagging otherwise undetectable DSB[23,24]. To this purpose, K562 were transduced in triplicate with an IDLV encoding for a constitutively expressed GFP and transfected with 5′UTR or IVS2 RNP. The latter sample was used as positive control, since IVS2 gRNA has a known off-target in *HBA1*. After GFP-based sorting, we identified IDLV clustered integration sites (CLIS) by ligation mediated (LM)-PCR coupled with next generation sequencing[25]. As expected, we observed high on-target activity for both gRNA (92.5% and 91.2% of total reads for 5′UTR and IVS2 gRNA, respectively), and we confirmed integration in the predicted *HBA1* off-target for IVS2 (8.5%), in line with TIDE-based indels analysis (8.5% ± 4.9, $n = 5$) (Supplementary Fig. 3a–c). Remarkably, no unique CLIS and none of the predicted off-targets were

Fig. 2 Transgene integration into the α-globin locus results in robust erythroid-specific expression. a AAV6 donors used for KI experiments in 5′UTR (top) and IVS2 (bottom) of the α-globin genes. Both vectors contain a promoterless GFP with bovine growth hormone polyA (pA), followed by a phosphoglycerate Kinase (PGK) promoter with a puromycin selection marker (puro) and simian virus polyA (pA). This cassette is flanked by 250 bp homology arms (homology) to gRNA target. IVS2 trap also contains a synthetic intron (IVS), a splice acceptor (SA) and a self-cleaving peptide (2A). ITR, Inverted terminal repeats. **b** Representative histograms of GFP expression of HUDEP-2 KI cells at day 0 (light pink), day 7 (red) and day 9 of erythroid differentiation (dark red). Untreated HUDEP-2 are shown in gray ($n = 1$). **c** Barplot of GFP median fluorescent intensity (MFI) as in **b**. **d** Schematic representation of HSPC targeting experiments. **e** Representative histograms of GFP expression of 5′UTR KI (red fill) and AAV6 only HSPCs (gray line) during erythroid differentiation. Percentage of GFP positive cells is indicated ($n = 3$ different donors). **f** GFP median fluorescent intensity (MFI) during differentiation of 5′UTR KI HSPCs (lines indicate mean, $n = 3$ different donors indicated by open, gray and black circles). **g** Representative dot plots showing GFP expression in erythroid (GYPA+) and leukocytes (hCD45+) CFC. **h** Representative overlay images (bright field and GFP channel) of different erythroid progenitor-derived colonies ($n = 24$). Scale bars in red indicate 200 µm. CFU-GEMM, granulocyte, erythroid, macrophage, megakaryocyte; BFU-E, burst-forming unit-erythroid; CFU-E, erythroid. Source data are in the Source Data file.

identified for 5′UTR gRNA after correction for random IDLV integration, further assuring the lack of any predominant off-target for this gRNA.

Hemophilia B. As first therapeutic target, we tested our platform for hemophilia B (OMIM #306900), a disease model for gene-based therapies caused by the absence of functional Factor IX (FIX, *F9*). Initially, HUDEP-2 cells were transfected with 5′UTR RNP and transduced with an AAV6 carrying two 250 bp homology arms flanking a promoterless human FIX-R338L (FIX Padua[26]) and a constitutive GFP reporter to easily track KI cells (Fig. 3a). Concordance between DNA integration and GFP expression analyses before and after GFP sorting confirmed that most integrations were on-target (Fig. 3b), with a preference for *HBA1* integration (Supplementary Fig. 4a). FIX expression was upregulated upon HUDEP-2 erythroid differentiation (Fig. 3c) and its secretion (median 1161 ng/10^6 cells/FIX copy, 769.1-1885, interquartile range) correlated with the number of integrated FIX copies (Fig. 3d).

Editing of HSPCs showed that also in primary cells, without any selection, we could obtain high levels of InDels (Supplementary Fig. 4b) and KI of FIX as measured by GFP (Fig. 3e) and on-target ddPCR (Supplementary Fig. 4c), associated with a reduced number of *HBA2* copies (Supplementary Fig. 4d).

Once more, we could demonstrate that *F9* mRNA and protein secretion increased upon erythroid differentiation (Fig. 3f, g) and that secreted FIX was functional (Fig. 3h; Supplementary Fig. 4e). Interestingly, FIX expression achieved with targeted integration was higher compared to a state-of-the-art LV carrying an artificial β-globin promoter[27] (Fig. 3I, j), highlighting one of the advantages of exploiting endogenous promoters in their chromatin context. Analysis of HSPC derived colonies, confirmed that high KI efficiency in CFC (both erythroid and granulocyte-monocyte colonies, Supplementary Fig. 4f) did not affect HPSC clonogenic differentiation capacity (Supplementary Fig. 4g), although the total number of CFC was lower than control HSPCs due to known AAV toxicity (Supplementary Fig. 4h)[28,29]. In addition, by analyzing KI HSPC derived burst-forming unit-erythroid colonies (BFU-E) we showed that *F9* integrations were mostly monoallelic (Fig. 3k) and HDR-mediated (19/19 colonies; Supplementary Fig. 4i), associated with a reduced number of *HBA2* copies (Supplementary Fig. 4l). Importantly, also BFU-E derived erythroblasts were capable of secreting FIX (Supplementary Fig. 4m).

These results clearly indicate that this platform can express and secrete a functional protein with therapeutic relevance.

Lysosomal storage disorders. In light of these promising findings, we expanded our strategy to other genetic diseases eligible for PRT, such as LSD. These inherited metabolic conditions are characterized by an abnormal build-up of toxic metabolites in lysosomes as a result of enzyme deficiencies[30]. Here we tested three different human transgenes encoding for: α-L-iduronidase (IDUA; Hurler syndrome, OMIM #607014), α-galactosidase (GLA; Fabry disease, OMIM #301500) and lysosomal acid lipase (LAL; Wolman disease, OMIM #278000). To facilitate their detection, each enzyme was tagged with 3 copies of hemagglutinin epitope (HA) and cloned into AAV6 vectors (Fig. 4a). As for *F9*, these transgenes were integrated into the α-globin locus of HUDEP-2 and KI cells were enriched by GFP sorting. Both mRNA and protein analyses confirmed enzymes expression, which substantially increased upon erythroid differentiation (16–171 fold and 2.5–4.5 fold respectively, Fig. 4b, c). For additional experiments in HSPCs we focused on *LAL* transgene, since Wolman disease (WD) is a life-threatening genetic condition with a severe liver phenotype and no gene therapy options available.

Editing of HSPCs showed that, without any selection, we could obtain high levels of InDels (Supplementary Fig. 5a) and KI of *LAL* as measured by GFP (Fig. 4d) and on-target ddPCR (Supplementary Fig. 5b), associated with a reduced number of *HBA2* copies (Supplementary Fig. 5c). In addition, LAL enzyme was strongly expressed and secreted upon erythroid differentiation (Fig. 4e, f) and retained its hydrolytic activity, in accordance with antigen levels (Fig. 4g).

By analyzing KI HSPC derived burst-forming unit-erythroid colonies (BFU-E) we showed that *LAL* integrations were mostly monoallelic (Fig. 4h), associated with a reduced number of *HBA2* copies (Supplementary Fig. 5d). After aggregation of the genotypes of *F9* and *LAL* BFU-E, we established that most of edited BFU-E (87%) had transgene integration and/or *HBA2* deletion and 53% harbored both modifications (Supplementary Fig. 5e, f).

In order to be therapeutically relevant, secreted LAL enzyme should cross-correct LAL deficient cells and reduce pathological cholesterol accumulation in lysosomes. Thus, we exposed WD patient's fibroblasts to conditioned medium from untreated (UT) or KI HSPC derived erythroblasts (LAL). After 3 days we observed LAL uptake in WD fibroblast lysates (Fig. 4i), which correlated with a significant decrease of total cholesterol (Fig. 4j) and lipid deposits (Fig. 4k), clearly showing that the secreted enzyme can ameliorate the metabolic dysfunction. Altogether, we demonstrated that our platform is versatile and can express several functional therapeutic proteins that require post-translational modifications.

In vivo long-term analysis of edited HSPCs. To evaluate if LAL-KI HSPCs maintain their homing, engraftment and multi-lineage potential, we transplanted immunodeficient NOD/SCID/γ[31] (NSG) mice and monitored human cells for 16 weeks (Fig. 5a). All mice showed successful engraftment in bone marrow, spleen and blood (Fig. 5b). GFP positive cells were present at different time points (Fig. 5c, d; Supplementary

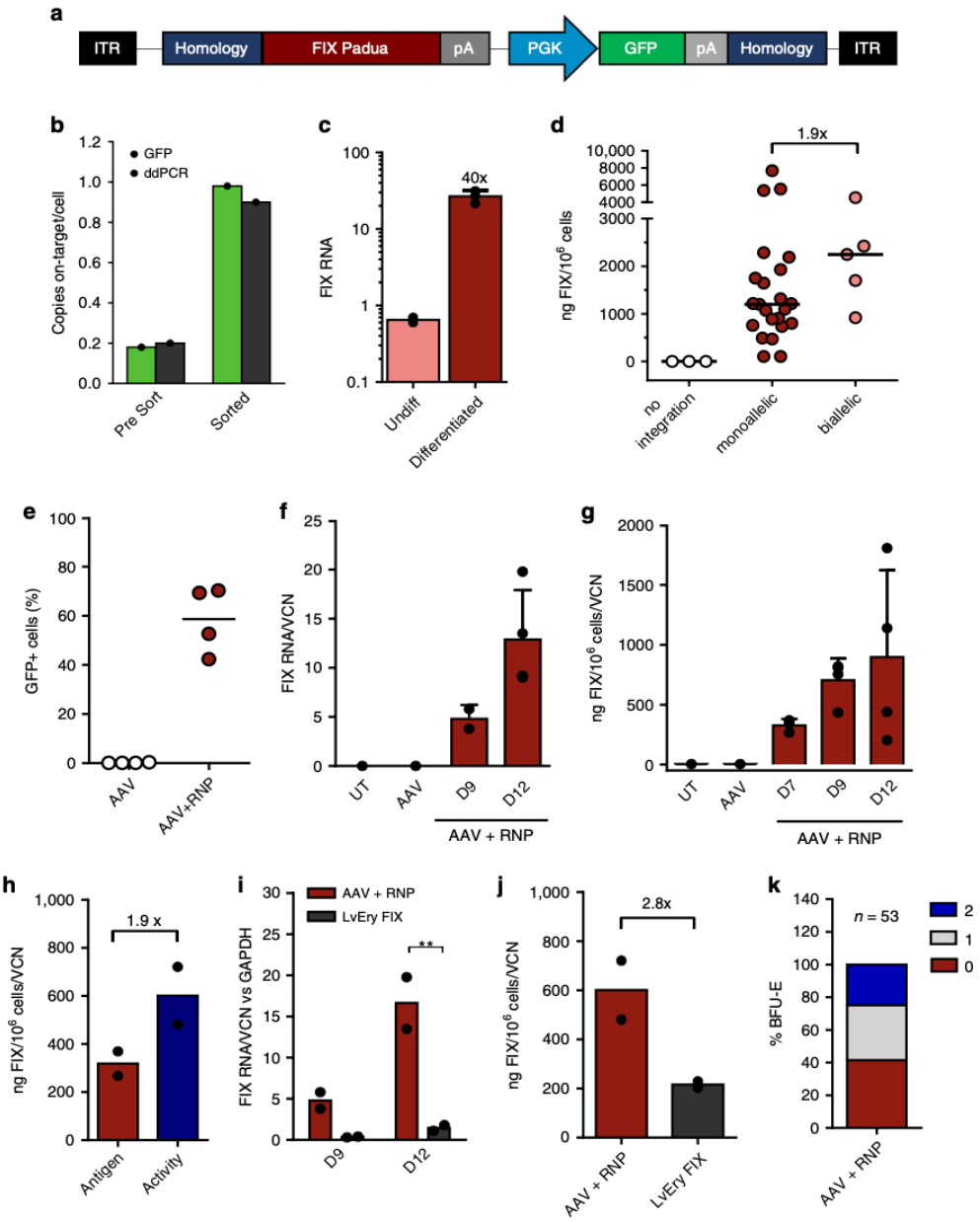

Fig. 3 *F9* KI into the α-globin locus results in expression and secretion of functional enzyme. a AAV6 donor used for KI experiments of FIX Padua. **b** FIX KI efficiency in HUDEP-2 cells was measured by flow cytometry (light green) or ddPCR specific for on-target integration (dark green) before and after sorting ($n = 1$). **c** Quantification of FIX mRNA in KI HUDEP-2 upon differentiation (mean ± SD, $n = 2$ undifferentiated, $n = 3$ differentiated). **d** Quantification of FIX secretion in medium of HUDEP-2 clones ($n = 28$) with monoallelic or biallelic KI (ELISA), as detected by on target ddPCR analysis (AAV-genome junction amplification). Lines represent median. **e** KI efficiency in HSPCs at day 9 of erythroid differentiation. Lines represent mean ($n = 4$). **f**, **g** FIX expression during HSPC differentiation at RNA (**f**, qPCR; $n = 2$ day 9; $n = 4$ day 12) and protein level (**g**, ELISA on supernatants, $n = 3$ day 7; $n = 4$ day 9 and 12; 3 donors). Bars represent mean ± SD. **h** Comparison of FIX antigen (ELISA) and activity (aPTT) in supernatants of KI HSPCs (mean; $n = 2$). **i**, **j** Comparison of FIX RNA at day 9 and 12 of erythroid differentiation (**i**) and protein (**j**) in KI HSPCs (AAV + RNP) vs HSPCs transduced with an erythroid-specific lentiviral vector (LvEry FIX). Bars represent mean (**$p = 0.003$ *t*-test Holm-Sidak correction for RNA at day 12; $p = 0.08$ for protein, $n = 2$). **k** Integration pattern in single BFU-E (2 donors): no integration (0), monoallelic (1) and biallelic KI (2). Source data are in the Source Data file.

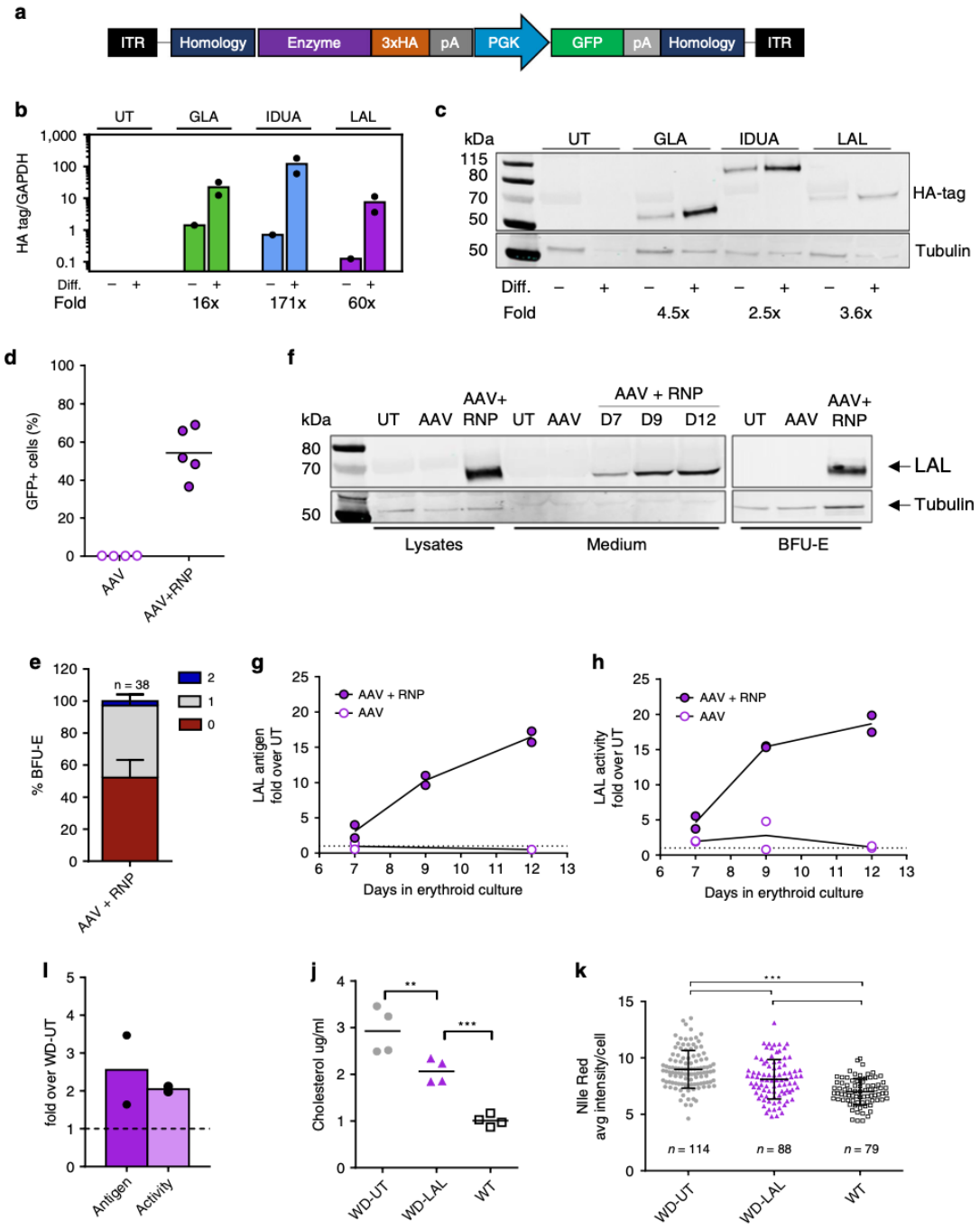

Fig. 6a) and in all cell subsets analyzed (Fig. 5e), including more primitive HSPCs in the bone marrow (Fig. 5f), demonstrating that KI HSCs were able to reconstitute the entire hematopoietic system. However, in accordance with previous reports describing AAV toxicity in HSPCs[28,29], KI HSPCs showed lower engraftment levels compared to unedited HSPCs (Fig. 5b) and a reduction of KI GFP positive cells after transplantation (Fig. 5c).

Since NSG mice do not support human erythroid differentiation[32], we isolated human CD34$^+$ cells from bone marrow of engrafted mice and differentiated them ex vivo. In a CFC assay, KI HSPCs were still able to generate both erythroid and myeloid colonies, to express GFP (Supplementary Fig. 6b) and, most importantly, to produce LAL in erythroblasts (Fig. 5g and Supplementary Fig. 6c). Similar in vivo and ex vivo results were also obtained for FIX (Supplementary Fig. 6d–g).

Fig. 4 Expression and therapeutic potential of different lysosomal enzymes. a AAV6 donor used for KI experiments. All enzymes were tagged with hemagglutinin tag (3xHA). **b** Transcript upregulation of different enzymes in targeted HUDEP-2 upon differentiation (qPCR, $n = 2$, mean). Fold increase is indicated. **c** Representative western blot detecting different enzymes (HA-tag and anti-β tubulin) of targeted HUDEP-2 upon differentiation ($n = 2$). **d** KI efficiency of LAL-AAV6 in HSPCs at day 9 (lines indicate mean; AAV $n = 4$, AAV + RNP $n = 5$). **e** Representative western blot of LAL in HSPC lysates, supernatants and BFU-E in untreated (UT), transduced (AAV) and KI-HSPCs (AAV + RNP). Anti-HA tag and anti-β tubulin antibodies were used. **f** Quantification of secreted LAL during erythroid differentiation. Anti-LAL antibody was used. Data are shown as fold increase over untreated cells (UT, donor=2). **g** LAL activity in HSPC supernatants during erythroid differentiation, data are shown as fold increase over untreated cells (UT, $n = 2$). **h** Integration pattern in single BFU-E: no integration (0), monoallelic (1) and biallelic (2). Mean ± SD, donor = 2). **i** Uptake of erythroid-expressed LAL by WD fibroblasts, measured by western blot or activity assay (mean; $n = 2$). **j** Cholesterol levels in WD fibroblasts after incubation with conditioned medium from untreated (UT) or LAL KI-erythroblasts. WT fibroblasts are shown as control ($n = 4$; $p = 0.003$ WD-UT vs WD-LAL; $p < 0.001$ WD-LAL vs WT; one-way ANOVA, Tukey's test). **k** Nile Red staining in WD fibroblasts after incubation with conditioned medium from untreated (UT) or LAL KI-erythroblasts. WT fibroblasts are shown as control. Black lines indicate mean ± SD; number of fibroblasts analyzed is indicated. (***$p < 0.001$ one-way ANOVA, Tukey's test). Source data are in the Source Data file.

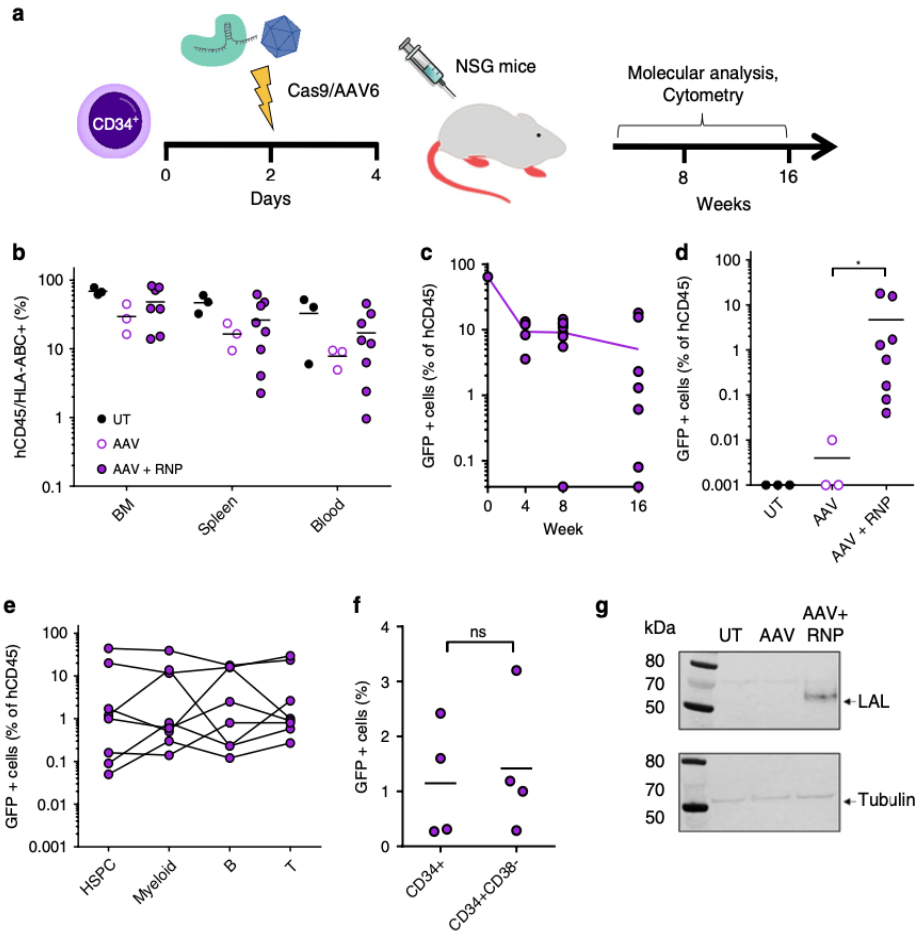

Fig. 5 KI HSPCs engraft NSG mice and express LAL upon erythroid differentiation. a Schematic representation of engraftment experiments. **b** Percentage of human CD45+/HLA-ABC+ cells in hematopoietic organs of mice. BM = bone marrow. (UT and AAV $n = 3$; AAV + RNP $n = 8$). **c** GFP positive cells in peripheral blood of transplanted mice over time. Line indicates mean ($n = 4$ week 4; $n = 8$ week 8 and 16). **d** Edited cells in bone marrow of transplanted mice. GFP is expressed as percentage of CD45+ cells, mean is shown (*$p = 0.012$ AAV vs AAV + RNP, two-tailed Mann–Whitney test). **e** GFP positive cells in HSPCs (CD34), myeloid (CD33), B (CD19) and T (CD3) cells in bone marrow of transplanted mice. Each line represents one animal ($n = 8$). **f** GFP positive cells in HSPCs (CD34) and in a more primitive HSPC subset ($CD34^+CD38^-$) in bone marrow of transplanted mice ($n = 4$; ns: $p = 0.8$, two-tailed Mann Whitney test). **g** Western blot on CD34-derived BFU-E from mice engrafted with untreated (UT), transduced (AAV) or KI HSPCs (AAV + RNP). Anti-HA tag and anti-β tubulin antibodies were used ($n = 2$, BFU-E pooled from 2 mice). Source data are in the Source Data file.

Overall, these data show that KI HSPCs can engraft NSG mice and reconstitute all hematopoietic lineages.

Discussion

We developed an ex vivo platform for efficient gene targeting in human HSCs and robust expression of therapeutic transgenes by the erythroid lineage. By inserting transgenes under the control of the endogenous α-globin gene promoter, we demonstrated that erythroblasts derived from KI HSPCs ex vivo can express and secrete different therapeutic proteins, which retain their enzymatic activity and cross-correct the metabolic defect of patient's cells. In addition, KI HSPCs were able to engraft in vivo and maintained multilineage differentiation potential, we thus expect that our strategy can be used as platform to treat genetic and non-genetic disorders.

We demonstrated that the α-globin locus can be used as a safe harbor for transgene KI in HSCs. In particular, we showed that our selected Cas9/gRNA targeting α-globin 5′ UTR is: (i) efficient in inducing DSB in HSPCs (up to 80%); (ii) safe, as no effect on HSPC multipotency and hemoglobin expression was observed; (iii) specific for α-globin genes, as no predominant off-targets were detected. To further improve the safety profile of this approach, we can envisage the use of Cas9 variants, e.g., high-fidelity[33] or nickase[34]; nonetheless, ad hoc DNA analysis for major chromosomal alterations will be required before moving to clinical testing[35].

Using the described 5′UTR gRNA and an AAV6 vector carrying a promoterless transgene we achieved efficient HDR-based integration in the α-globin locus (above 50%). Although transgene integration will result in knockout of the targeted α-globin allele, this should not be a concern since α-globin genes are redundant and a reduction of 50% of α-globin chain is clinically asymptomatic[14]. In addition, while it is theoretically possible to achieve 4 transgene integrations (1 for each *HBA* gene), KI efficiency is mostly limited to 1 transgene per cell (Figs. 3d, k, 4h), minimizing the risk of causing α-thalassemia.

Transgene expression was limited to the erythroid lineage and increased following erythroid maturation, as expected from the endogenous α-globin promoter. Importantly, we showed that erythroblasts are able to synthetize and secrete different functional enzymes; secreted LAL was uptaken by patient's fibroblast and correctly sorted to lysosomes to reduce pathological cholesterol accumulation, suggesting that secreted enzymes are properly processed to enter the mannose-6-phosphate pathway[36]. Overall, these results show the versatility of our platform and support its application to other LSD.

By transplanting HSPCs in humanized NSG, we demonstrated that KI HSPCs can repopulate the bone marrow and give rise to progenitors and differentiated hematopoietic lineages. Unfortunately, since NSG and other immunodeficient mouse models do not support significant human erythropoiesis and prevent the in vivo assessment of this erythroid-based platform[32,37], we performed ex vivo erythroid differentiation of bone marrow isolated $CD34^+$ cells confirming that HSCs can still differentiate and express the integrated transgene. Future experiment of KI in mouse HSPCs carrying the human α-globin locus will allow in vivo erythroid differentiation and direct assessment of the steady-state expression levels achievable with our strategy[38].

Protein replacement therapies have proven to be a life-saving therapy for patients affected by rare genetic diseases[1]. However, PRT requires frequent costly injections with a peak-and-trough serum kinetics, which reduce patients' compliance to the therapy and efficacy of treatment[39], and it is affected by development of anti-drugs antibodies, which negatively influence drug bioavailability and activity[40]. Instead, gene therapy can provide constant serum level of therapeutic proteins with a single administration and can induce immune tolerance to the expressed transgene[41]. In particular, the idea of integrating a therapeutic transgene in a safe and highly transcribed genomic locus has been already described for the albumin gene[5–7] and is now under clinical evaluation (NCT03041324, NCT02695160). However, this in vivo approach is hampered by pre-existing liver conditions, pre-existing neutralizing antibodies and cell-mediated immune responses against AAV vectors used to deliver transgenes or nucleases, thus severely limiting the number of potentially treatable patients[8]. To avoid these issues, autologous HSCs can be successfully engineered ex vivo by LV to express transgenes in ubiquitous[42,43] or lineage-restricted manner[44–46], including erythroid lineage[15,16,47,48]; however, the semi-random integration pattern of LV is intrinsically associated with the risk of inactivating an oncosuppressor and transactivating an oncogene. Our strategy promises to be a safer option since transgene integration is targeted to a safe locus, no exogenous promoter is required and transgene expression is truly restricted to erythroid cells, which can induce immune tolerance to exogenous proteins[49–52]. In addition, transgene expression achieved by targeted integration outperformed a LV carrying an erythroid-specific promoter[27,53], which can only partially replicate the complex regulation of a genomic locus due to vector capacity limitations and different chromatin context. The benefit associated to our strategy is twofold: (i) need of fewer modified HSPCs; (ii) higher expression potential.

Our approach still requires bone marrow transplantation of HSPCs, but on-going improvements of HSC mobilization and conditioning regimens will facilitate this procedure[54,55]. In addition, we will explore alternative DNA donor delivery system, e.g. IDLV or non-viral vectors[56], or transient p53 inactivation[29] as means to avoid the negative effect of AAV6 on HSPC engraftment potential[28]. Finally, we will have to assess in vivo if over-expression of transgenes in erythroid precursor cells can have an effect on the HSCs niche in the bone marrow or on erythrocyte differentiation, half-life and clearance[57]. Previous experiments using LV to express different proteins from erythrocytes did not show any impact on erythropoiesis[15–17,58]; however, transgene-specific effects should be carefully evaluated.

Finally, we will engineer transgene sequence with blood-brain barrier shuttle peptides[48,59] to treat LSD with central nervous system involvement, a severe limitation of current PRT[60].

In conclusion, we identified the human α-globin gene as a safe genomic locus for transgene KI in HSCs and erythroid-specific overexpression of therapeutic protein. Future in vivo tests will elucidate the therapeutic potential of this CRISPR-Cas9 based HSC-platform for PRT, especially for LSD and hemophilia.

Methods

Plasmids. Different gRNA protospacers were cloned in hU6-gRNA encoding plasmid (Addgene plasmid # 53188) after BbsI digestion[61].

Promoter trap encodes for a promoterless GFP reporter (with bovine growth hormone polyA) followed by a puromycin resistance gene under the control of the human phosphoglycerate kinase 1 (PGK) promoter with a SV40 polyA. For intron traps, we added a synthetic intron with splice acceptor site (adapted from[62] and a self-cleaving peptide from porcine teschovirus-1 (P2A)[63] in frame (+0 or +2) at 5′ of GFP cDNA (Supplementary Fig. 2a and Supplementary Methods). These cassettes were inserted in a standard lentiviral vector (LV) backbone[64] in antisense orientation with respect to its LTR.

According to the experiments, GFP and puromycin sequences were exchanged with enzyme cDNA and GFP respectively. *F9* (Gene ID: 2158, R338L substitution[26], *GLA* (Gene ID: 2717), *IDUA* (Gene ID: 3425) and *LAL* (Gene ID: 3988) cDNA with a C-terminal 3xHA tag (1xHA: TATCCCTATGACGTGCCT GATTACGCC) and arms of homology (250 bp each) were synthetized by Genscript (Piscataway, NJ) and cloned in a standard AAV vector backbone (AAV2) in sense orientation with respect to its ITR. Upon successful HDR, transgene translation starts from the same ATG as the endogenous α-globin ATG for 5′ UTR integration or after translation of a fragment of α-globin chain for IVS2

integration (α-globin-2A-GFP). Homology arms for 5′UTR α-globin integration are: upstream, chr16:172,642-172,892; downstream, chr16:172,893-173,142 (hg38).

Homology arms for IVS2 α-globin integration are: upstream, chr16:173,135-173,385; downstream, chr16:173,386-173,636 (hg38).

Vector productions. LV were produced by transient transfection of 293T using third-generation packaging plasmid pMDLg/p.RRE (or pMDLg/p.RRE.D64V for integrase defective vectors; IDLV), pK.REV, and pseudotyped with the vesicular stomatitis virus glycoprotein G (VSV-G) envelope. LV/IDLV were titrated in HCT116 cells[65] and HIV-1 Gag p24 content was measured by ELISA (Perkin-Elmer) according to manufacturer's instructions.

All recombinant single-stranded AAV2/6 used in this study were produced using an adenovirus-free triple transfection method of HEK293 and purified by two sequential cesium chloride (CsCl) density gradients or by single affinity chromatography (AVB Sepharose; GE Healthcare, Chicago, IL). The final product was formulated in sterile phosphate buffered saline containing 0.001% of pluronic (F68; Sigma Aldrich, Saint Louis, MO), and stored at −80 °C[66,67].

Cell culture and reagents. K562 cells (ATCC® CCL-243) were maintained in RPMI 1640 medium containing 2 mM glutamine and supplemented with 10% fetal bovine serum (FBS, Lonza, Basel, Switzerland), 10 mM HEPES, 1 mM sodium pyruvate and penicillin and streptomycin (100U/ml each; Gibco, Waltham, MA, USA). HUDEP-2 cells[18] were maintained in StemSpan SFEM (StemCell Technologies, Vancouver, BC, Canada) supplemented with 2 mM glutamine, 100U/ml penicillin and streptomycin (Gibco, Waltham, MA, USA), Epo 3 U/ml, SCF 50 ng/ml (PeproTech, Rocky Hill, NJ, USA); 1 µg/ml doxycycline and 1 µM dexamethasone (Sigma Aldrich, St. Louis, MO, USA). Cells were differentiated in Iscove's Modified Dulbecco's Medium (IMDM) with 2 mM glutamine, 100U/ml penicillin and streptomycin (Gibco, Waltham, MA, USA Gibco, Waltham, MA, USA), Epo 3 U/ml, SCF 50 ng/ml (PeproTech, Rocky Hill, NJ, USA), 5% AB human serum (Biowest, Nuaillé, France), 10 µg/ml insulin, 330 µg/ml Holo-Transferrin, 2 U/ml heparin, 1 µg/ml doxycycline (Sigma Aldrich, St. Louis, MO, USA). Doxycycline and SCF were removed after 5 days of differentiation[68]. HUDEP-2 single cell clones were obtained by limiting dilution. Human primary fibroblasts were obtained from the NIGMS Human Genetic Cell Repository at the Coriell Institute for Medical Research: GM 11851 A (Wolman disease fibroblasts) and GM 08333 C (healthy donor fibroblasts). Fibroblasts were maintained in DMEM medium supplemented with 2 mM Glutamax (Gibco, Waltham, MA, USA), 15% of FBS (Lonza, Basel, Switzerland) and 100U/ml of penicillin/Streptomycin (Gibco, Waltham, MA, USA). *Streptococcus pyogenes* (Sp)Cas9 protein (with 2 nuclear localization signals, NLS; provided by J.P. Concordet) was expressed in E. coli strain BL21 Rosetta 2. The protein was purified by a combination of affinity, ion exchange and size exclusion chromatographic steps[69]. tracrRNA and crRNA were purchased from Integrated DNA Technologies, resuspended and annealed by manufacturer's instructions. Chemically modified single guide RNA were purchased from Synthego. Primer and probes for PCR were purchased from Sigma-Aldrich (St. Louis, MI, USA) and Integrated DNA Technologies (Coralville, IA, USA).

Editing experiments in K562. gRNA screening: To generate a stable clone of Cas9-expressing K562 (K562-Cas9), K562 cells were transduced with a lentiviral vector (Addgene #52962) expressing SpCas9 and a blasticidin resistance cassette, selected with blasticidine (10ug/ml; Sigma-Aldrich, St. Louis, MI, USA) and subcloned. 2.5×10^5 K562-Cas9 cells were transfected with 200 ng of gRNA-containing plasmid using NucleofectorAmaxa 4D (Lonza, Basel, Switzerland) with SF Cell Line 4D-Nucleofector Kit, K562 program. 48 hours after transfection, cells were harvested and DNA was extracted for molecular analysis.

Targeted integration: 5×10^5 of K562-Cas9 cells were transduced at multiplicity of infection (MOI) 50 with integrase defective lentiviral vectors (IDLV) containing a promoterless GFP and a constitutively expressed puromycin-resistance gene. After 24 h cells were washed and 2.5×10^5 of transduced cells were transfected with 200 ng of gRNA-containing vector as previously described. Cells were selected with puromycin (5 ug/ml, Sigma-Aldrich, St. Louis, MI, USA) and sorted for GFP positivity using MoFlocell sorter (Beckman Coulter, Pasadena, CA, USA). Erythroid differentiation was induced with 50 µM Hemin (Sigma-Aldrich, St. Louis, MI, USA) and monitored for 4 days. As K562 differentiation is heterogeneous, to determine differentiation status cells were stained with an anti-Glycophorin A (GYPA) antibody (see list) and GFP expression was analyzed by flow cytometry.

CD34$^+$ cell culture, transfection and transduction. Human umbilical cord blood (UCB) samples were provided by Centre Hospitalier Sud-Francilien (CHSF, Evry, France) and processed according to France bioethics laws (declaration DC-2012-1655 to the French Ministry of Higher Education and Research). CD34+ cells were purified by immunomagnetic selection with AUTOMACS PRO (Miltenyi Biotec, Paris, France) after immunostaining with CD34 MicroBead Kit (Miltenyi Biotec, Paris, France). Mobilized peripheral blood (MPB) and UCB CD34+ were also obtained by Cliniscience (Nanterre, France). MPB- or UCB-derived HSPCs were thawed and cultured in prestimulation media for 48 h (StemSpan, Stemregenin-1 0.75uM, StemCell technologies, Vancouver, BC, Canada; rhSCF 300 ng/ml, Flt3-L 300 ng/ml, rhTPO 100 ng/ml and IL-3 20 ng/ml, CellGenix, Freiburg, Germany). Specific crRNA and scaffold tracrRNA were annealed (Integrated DNA Technologies, Coralville, IA, USA) or diluted (Synthego, CA, USA) following manufacturer's instruction and ribonucleoprotein complexes were formed with 30 pmol of spCas9 (ratio 1:1.5). 2.5×10^5 HSPCs per condition were transfected with RNP complex using P3 Primary Cell 4D-Nucleofector kit (CA137 program). In KI experiments, 15 min after transfection HSPCs were transduced with AAV6 vectors for 6 h (MOI 10000-30000), washed and left in prestimulation media for additional 48 h. Lentiviral transduction of HSPCs was performed in retronectin-coated plates (5ug/cm2; Takara, Japan) for 6 h in the presence of 4 µg/ml protamine sulfate (Sanofi Aventis, Paris, France)[65]. After manipulation, HSPCs were cultured in erythroid differentiation medium (StemSpan, StemCell Technologies, Vancouver, BC, Canada; SCF 20 ng/ml, Epo 1 u/ml, IL3 5 ng/ml, Dexamethasone 2 µM and Betaestradiol 1 µM; Sigma-Aldrich, St.Louis, MI, USA) or in semisolid Methocult medium (colony-forming cells (CFC) assay, H4435, StemCell Technologies, Vancouver, BC, Canada) for 14 days. Colonies were counted and identified according to morphological criteria (BFU-E, CFU-G/GM, and CFU-GEMM). In some experiments, BFU-E were picked and cultured in erythroid progenitor expansion medium (StemSpan SFEM, StemCell Technologies, Vancouver, BC, Canada; Epo 20 ng/ml, SCF 100 ng/ml, insulin-like growth factor-1 (IGF-1) 50 ng/ml (PeproTech, Rocky Hill, NJ, USA); and 2 µM dexamethasone (Sigma Aldrich, St. Louis, MO, USA) for 3-5 days[70].

Flow cytometry. Cells were fixed and/or permeabilized using Cytofix/Cytoperm™ (BD Bioscience, San Jose, CA, USA) according to manufacturer's instructions. For live cells analysis, viability was assessed using Zombie Yellow dye (BioLegend, San Diego, CA, USA) as per manufacturers' instructions to exclude dead cells from the analysis. Negative controls were obtained by staining cells only with the isotype control antibodies. For engraftment studies, an Fc Receptor Binding Inhibitor antibody was used to block unspecific binding of mouse Ab to human cells, as per manufacturers' instructions. Cells were analyzed using CytoFLEX S (Beckman Coulter, Pasadena, CA, USA) or SP6800 Spectral Analyzer (Sony, Tokyo, Japan); data were elaborated with CytExpert (Beckman Coulter, Pasadena, CA, USA) or FlowJo software (Tree Star, OR, USA).

We used MoFlocell sorter (Beckman Coulter, Pasadena, CA, USA) to select for live GFP positive cells. See Supplementary Table 4 for antibodies list and Supplementary methods for gating strategy of human engrafted cells.

DNA analysis. Genomic DNA was extracted with QIAamp DNA Micro Kit (Qiagen, Hilden, Germany) or QuickExtract™ DNA Extraction Solution (Lucigen, Middelton, WI, USA).

Quantification of editing efficiency (InDel): 50 ng of genomic DNA were used to amplify the region that spans the cutting site of each gRNA using KAPA2G Fast ReadyMix (Kapa Biosystem, Wilmington, MA, USA). After Sanger sequencing (Genewiz, Takeley, UK), the percentage of Insertions and deletions (InDel) was calculated using TIDE software[22]. See Supplementary Table 3 for primer sequences.

Droplet digital PCR: ddPCR was performed according to manufacturer's instruction using ddPCR Supermix for Probes No dUTP (Biorad, Hercules, CA, US) and 1–50 ng of genomic DNA digested with HindIII (New England Biolabs, Ipswich, MA, USA). Droplets were generated using AutoDG Droplet Generator and analyzed with QX200 droplet reader; data analysis was performed with QuantaSoft (Biorad, Hercules, CA, US).

To quantify HBA2 copy number, primers and probe were designed on the 3′ UTR of HBA2 gene, as it differs significantly from HBA1.

To quantify on-target transgene integration events, primers and probe were designed spanning the donor DNA-genome 3′ junction. Human albumin (ALB) or ZNF843 were used as reference for copy number evaluation (assay ID: dHsaCP2506312, Biorad, Hercules, CA, US). Percentage of on-target integration obtained by ddPCR nicely correlated with GFP values obtained by FACS in KI cells (Supplementary Methods). See Supplementary Table 3 for primer and probe sequences.

RNA extraction and RT-qPCR. Total RNA was purified using RNeasy Micro kit (Qiagen, Hilden, Germany) and reverse-transcribed using Transcriptor First Strand cDNA Synthesis Kit (Roche, Basel, Switzerland). qPCR was performed using Maxima Syber Green/Rox (Life Scientific, Thermo-Fisher Scientific, Waltham, MA, US). Primers and probes were optimized using the standard curve method to reach 100% ± 5% efficiency. The relative expression of each target gene was normalized using human GAPDH as a reference gene (NM_002046.6) and represented as 2^ΔCt for each sample or as fold changes (2^ΔΔCt) relative to the control. See Supplementary Table 3 for primer sequences.

Protein quantification and Western blot. FIX detection: FIX antigen in supernatants was measured with an ELISA assay using a standard curve with known amount of human FIX. A microtiter plate is coated with an anti-human FIX antibody (MA1-43012; Thermo-Fisher Scientific, Waltham, MA, US), blocked with PBS-2% bovine serum albumin (BSA) and incubated with diluted supernatants. Protein is detected with a goat anti-human horseradish peroxidase (HRP)-

conjugated antibody (CL20040APHP; Cedarlane, Burlington, Canada)[71]. Samples were analyzed at different dilutions (1/20, 1/40 and 1/100). FIX activity was measured by activated partial thromboplastin time (aPTT)[26]. Protein concentration in diluted supernatant was calculated using a standard curve containing known quantities of hFIX spiked in FIX-deficient plasma.

Western blot: To detect intracellular proteins cells were lysed in RIPA buffer (Sigma-Aldrich, St.Louis, MI, USA) supplemented with protease inhibitor (Roche, Basel, Switzerland), freezed/thawed and centrifuged 10′ at 14,000 at 4 °C. Total protein was quantified using BCA assay (Thermo-Fisher Scientific, Waltham, MA, US). 5–15 µg of protein or 2.5 ul of cell supernatants were denatured at 90 °C for 10′, run under reducing conditions on a 4–12% Bis-tris gel and transferred to a nitrocellulose membrane using iBlot2 system (Invitrogen, Waltham, MA, US). After Ponceau staining (Invitrogen, Waltham, MA, US) membranes were blocked for 2 h with Odyssey blocking buffer (Odyssey Blocking buffer (PBS), Li-Cor Biosciences, Lincoln, NE, USA) and incubated for 1 h with primary antibodies followed by specific secondary antibodies in PBS:Blocking buffer (see Supplementary Table 5 for antibodies list). β-Tubulin was used as loading control. Blots were imaged at 169 µm with Odyssey imager and analyzed with ImageStudio Lite software (Li-Cor Biosciences, Lincoln, NE, USA). After image background subtraction (average method, top/bottom), band intensities were quantified and normalized with tubulin signal. Antibody concentrations, suppliers and catalog numbers are provided in Supplementary Table 5.

LAL activity assay: Protein activity was detected in supernatants as previously described[72,73] with some modifications. Briefly, samples were incubated 10 min at 37 °C with 42 µM Lalistat-2 (Sigma-Aldrich, St. Louis, MI, USA), a specific competitive inhibitor of LAL, or water. Samples were then transferred to a Optiplate 96 F plate (PerkinElmer) where fluorimetric reactions were initiated with 75 µl of substrate buffer (340 µM 4-MUP, 0.9% Triton X-100 and 220 µM cardiolipin in 135 mM acetate buffer pH 4.0). After 10 min, fluorescence was recorded (35 cycles, 30" intervals, 37 °C) using SPARK TECAN Reader (Tecan, Austria). Kinetic parameters (average rate) were calculated using Magellan Software. LAL activity over untreated samples was quantified using this formula:

$$\frac{\text{Edited sample (without Lalistat} - \text{with Lalistat)}}{\text{Untreated sample (without Lalistat} - \text{with Lalistat)}}$$

LAL uptake assay: Equal amounts of conditioned medium from KI or control HSPCs during erythroid differentiation were collected, concentrated using Amicon® 10 kDa (Merck, Kenilworth, NJ, USA), diluted with opti-MEM to their original volume (Gibco, Waltham, MA, USA) and filtrated with a 0.22 µm filter (Millipore, Burlington, MA, USA). Processed medium were added to 4.5×10^5 WD fibroblasts in a 6-well plate. After 3 days, fibroblasts were harvested and pellets were frozen for LAL and cholesterol quantification.

Cholesterol quantification: Total cholesterol was measured with Amplex red (Thermo-Fisher Scientific, Waltham, MA, US) as per manufacturer's instructions. Fluorescence (endpoint) was recorded with SPARK TECAN Reader (Tecan, Austria) and cholesterol content was quantified with a standard curve.

Nile red staining: 4×10^4 fibroblasts were seeded in a 8−well LAB_TEK coverglass (Nunc, Rochester, NY, USA) and cultured in conditioned medium of KI or UT HSPCs. After 3 days, cell were stained with Nile Red (Nile Red staining kit, Abcam, Cambridge, UK) as per manufacturer's instructions. 8 fields for each condition were randomly acquired with an inverted fluorescence microscope (10x magnification; EVOS imaging system, Thermo-Fisher Scientific, Waltham, MA, US) and average fluorescence intensity per cell was calculated with ImageJ[74] using a custom made macro.

HPLC analysis of globin chains and tetramers. HPLC analysis was performed using a NexeraX2 SIL-30AC chromatograph (Shimadzu, Kyoto, Japan) and analyzed with LC Solution software. HSPC derived erythroblasts were lysed in water and globin chains were separated using a 250 × 4.6 mm, 3.6 µm Aeris Widepore column (Phenomenex, Torrance, CA, USA). Samples were eluted with a gradient mixture of solution A (water/acetonitrile/trifluoroacetic acid, 95:5:0.1) and solution B (water/acetonitrile/trifluoroacetic acid, 5:95:0.1), monitoring absorbance at 220 nm. Hemoglobin tetramers were separated by HPLC using a cation-exchange column (PolyCAT A, PolyLC, Columbia, MD, USA). Samples were eluted with a gradient mixture of solution A (20 mM bis Tris, 2 mM KCN, pH 6.5) and solution B (20 mM bis Tris, 2 mM KCN, 250 mM NaCl, pH 6.8). The absorbance was measured at 415 nm.

In vivo experiments. NOD.Cg-Prkdc^{scid}Il2rg^{tm1Wjl}/SzJ (NSG) mice were purchased from The Jackson Laboratory (strain 005557) and maintained in specific-pathogen-free (SPF) conditions. This study was approved by ethical committee CEEA-51 and conducted according to French and European legislation on animal experimentation (APAFiS#16499-2018071809263257_v4).

48 h after editing, $5–7 \times 10^5$ CD34 + cells were injected intravenously into female NSG mice after sublethal irradiation (150 cGy). Human cell engraftment and KI levels were monitored at different time points in peripheral blood by flow cytometry using anti human CD45 and HLA-ABC antibodies (see Supplementary Table 4). 16 weeks after transplantation, blood, bone marrow and spleen were harvested and analyzed. Peripheral blood was directly stained and red blood cells lysed during sample fixation (VersaLyse Lysing Solution and IOTest3 Fixative solution, Beckman Coulter, Pasadena, CA, USA).

Cell purification and enrichment. Human CD34$^+$ cells were purified from mouse bone marrow by immunomagnetic selection with CD34 MicroBead Kit UltraPure in combination with AUTOMACS PRO (PosselD2 separation program; Miltenyi Biotec, Paris, France). Human CD45 cells from mouse peripheral blood or bone marrow were enriched with CD45 MicroBeads (Possel separation program; Miltenyi Biotec, Paris, France).

Off-target analysis. Off-target candidates were predicted in silico using two different software with the following parameters: up to 4 mismatches and no bulges (CRISPOR)[20]; up to 2 mismatches, 1 insertion and 1 deletion tolerated (COSMID)[21].

K562-Cas9 cells were edited at saturation with multiple rounds of transfection with different gRNA; genomic DNA was amplified at predicted off-target sites, Sanger-sequenced and analyzed with TIDE software.

IDLV capture[24] was used for experimental identification of potential off-target sites. K562 cells were transduced with an IDLV expressing a GFP reporter (MOI 100) and subsequently transfected with 30 pmol of Cas9:gRNA complex (1:2). Two weeks later at least 5×10^4 GFP positive cells were sorted using MoFlocell sorter (Beckman Coulter, Pasadena, CA, USA) and expanded for genomic DNA extraction. LTR vector-genome junctions were amplified by ligation mediated (LM)-PCR as previously described[25]. Briefly, 1 µg genomic DNA was fragmented with Tru91 restriction enzyme (Roche, Basel, Switzerland) and ligated to a TA-protruding double-stranded DNA linker. After SacI digestion (Roche, Basel, Switzerland), multiple nested PCRs were performed with specific primers annealing to the linker and vector LTR. Amplicons ranging from 200 to 500 kb were purified by NucleoSpin Gel and PCR Clean-up kit (Macherey-Nagel, Düren, Germany). 1 µg of the final libraries was subsequently processed with MiSeq Reagent Kit v3 (2 × 300-bp pair-end sequencing) and sequenced to saturation on Illumina MiSeq System (IGA Technology Services, Udine, Italy). Raw reads were processed as previously described, alignments with best scores were kept, and integration sites were identified. IDLV integration sites that mapped within a ±300 bp window were identified as clustered integration sites (CLIS).

Statistical analyses. Statistical analyses were performed using GraphPad Prism version 6.00 for Windows (GraphPad Software, La Jolla, CA, USA, "www.graphpad.com"). One-way or two-way analysis of variance (ANOVA) with Tukey's or Dunnet's multiple comparison post-test for three or more groups was performed as indicated (alpha = 0.05). Values are expressed as mean ± standard deviation (SD) as otherwise indicated.

Reporting summary. Further information on research design is available in the Nature Research Reporting Summary linked to this article.

Data availability

The authors declare that all data supporting the findings of this study are available within the paper and Supplementary Information. The IDLV capture data that support the findings of this study have been deposited in NCBI Gene Expression Omnibus (GEO) under accession number GSE133861. [https://www.ncbi.nlm.nih.gov/geo/query/acc.cgi?acc=GSE133861]. Any other relevant data are available upon reasonable request. Source data are provided with this paper.

Received: 11 December 2019; Accepted: 6 July 2020;
Published online: 29 July 2020

References

1. Gorzelany, J. A. & de Souza, M. P. Protein replacement therapies for rare diseases: a breeze for regulatory approval? *Sci. Transl. Med* **5**, 178fs110 (2013).
2. Concolino, D., Deodato, F. & Parini, R. Enzyme replacement therapy: efficacy and limitations. *Ital. J. Pediatr.* **44**, 120 (2018).
3. Li, H. et al. In vivo genome editing restores haemostasis in a mouse model of haemophilia. *Nature* **475**, 217–221 (2011).
4. Park, C. Y. et al. Functional correction of large factor VIII gene chromosomal inversions in hemophilia A patient-derived iPSCs using CRISPR-Cas9. *Cell Stem Cell* **17**, 213–220 (2015).
5. Barzel, A. et al. Promoterless gene targeting without nucleases ameliorates haemophilia B in mice. *Nature* **517**, 360–364 (2015).
6. Sharma, R. et al. In vivo genome editing of the albumin locus as a platform for protein replacement therapy. *Blood* **126**, 1777–1784 (2015).
7. De Caneva, A. et al. Coupling AAV-mediated promoterless gene targeting to SaCas9 nuclease to efficiently correct liver metabolic diseases. *JCI Insight* **5**, e128863 (2019).

8. Boutin, S. et al. Prevalence of serum IgG and neutralizing factors against adeno-associated virus (AAV) types 1, 2, 5, 6, 8, and 9 in the healthy population: implications for gene therapy using AAV vectors. *Hum. Gene Ther.* **21**, 704–712 (2010).
9. Pien, G. C. et al. Capsid antigen presentation flags human hepatocytes for destruction after transduction by adeno-associated viral vectors. *J. Clin. Invest* **119**, 1688–1695 (2009).
10. Charlesworth, C. T. et al. Identification of preexisting adaptive immunity to Cas9 proteins in humans. *Nat. Med.* **25**, 249–254 (2019).
11. Hosel, M. et al. Hepatitis B virus infection enhances susceptibility toward adeno-associated viral vector transduction in vitro and in vivo. *Hepatology* **59**, 2110–2120 (2014).
12. Sobrevals, L. et al. AAV vectors transduce hepatocytes in vivo as efficiently in cirrhotic as in healthy rat livers. *Gene Ther.* **19**, 411–417 (2012).
13. Dzierzak, E. & Philipsen, S. Erythropoiesis: development and differentiation. *Cold Spring Harb. Perspect. Med.* **3**, a011601 (2013).
14. Vichinsky, E. P. Clinical manifestations of alpha-thalassemia. *Cold Spring Harb. Perspect. Med.* **3**, a011742 (2013).
15. Chang, A. H., Stephan, M. T. & Sadelain, M. Stem cell-derived erythroid cells mediate long-term systemic protein delivery. *Nat. Biotechnol.* **24**, 1017–1021 (2006).
16. Wang, D. et al. Reprogramming erythroid cells for lysosomal enzyme production leads to visceral and CNS cross-correction in mice with Hurler syndrome. *Proc. Natl. Acad. Sci. USA* **106**, 19958–19963 (2009).
17. Montiel-Equihua, C. A. et al. The beta-globin locus control region in combination with the EF1alpha short promoter allows enhanced lentiviral vector-mediated erythroid gene expression with conserved multilineage activity. *Mol. Ther.* **20**, 1400–1409 (2012).
18. Kurita, R. et al. Establishment of immortalized human erythroid progenitor cell lines able to produce enucleated red blood cells. *PLoS ONE* **8**, e59890 (2013).
19. Wang, J. et al. Homology-driven genome editing in hematopoietic stem and progenitor cells using ZFN mRNA and AAV6 donors. *Nat. Biotechnol.* **33**, 1256–1263 (2015).
20. Haeussler, M. et al. Evaluation of off-target and on-target scoring algorithms and integration into the guide RNA selection tool CRISPOR. *Genome Biol.* **17**, 148 (2016).
21. Cradick, T. J., Qiu, P., Lee, C. M., Fine, E. J. & Bao, G. COSMID: a web-based tool for identifying and validating CRISPR/Cas off-target sites. *Mol. Ther. Nucleic Acids* **3**, e214 (2014).
22. Brinkman, E. K., Chen, T., Amendola, M. & van Steensel, B. Easy quantitative assessment of genome editing by sequence trace decomposition. *Nucleic Acids Res.* **42**, e168 (2014).
23. Wang, X. et al. Unbiased detection of off-target cleavage by CRISPR-Cas9 and TALENs using integrase-defective lentiviral vectors. *Nat. Biotechnol.* **33**, 175–178 (2015).
24. Gabriel, R. et al. An unbiased genome-wide analysis of zinc-finger nuclease specificity. *Nat. Biotechnol.* **29**, 816–823 (2011).
25. Poletti, V. et al. Preclinical development of a lentiviral vector for gene therapy of X-linked severe combined immunodeficiency. *Mol. Ther. Methods Clin. Dev.* **9**, 257–269 (2018).
26. Simioni, P. et al. X-linked thrombophilia with a mutant factor IX (factor IX Padua). *N. Engl. J. Med.* **361**, 1671–1675 (2009).
27. Miccio, A. et al. In vivo selection of genetically modified erythroblastic progenitors leads to long-term correction of beta-thalassemia. *Proc. Natl. Acad. Sci. USA* **105**, 10547–10552 (2008).
28. Romero, Z. et al. Editing the sickle cell disease mutation in human hematopoietic stem cells: comparison of endonucleases and homologous donor templates. *Mol. Ther.* **27**, 1389–1406 (2019).
29. Schiroli, G. et al. Precise gene editing preserves hematopoietic stem cell function following transient p53-mediated DNA damage response. *Cell Stem Cell* **24**, 551–565 e558 (2019).
30. Futerman, A. H. & van Meer, G. The cell biology of lysosomal storage disorders. *Nat. Rev. Mol. Cell Biol.* **5**, 554–565 (2004).
31. Ishikawa, F. et al. Development of functional human blood and immune systems in NOD/SCID/IL2 receptor {gamma} chain(null) mice. *Blood* **106**, 1565–1573 (2005).
32. Hu, Z., Van Rooijen, N. & Yang, Y. G. Macrophages prevent human red blood cell reconstitution in immunodeficient mice. *Blood* **118**, 5938–5946 (2011).
33. Vakulskas, C. A. et al. A high-fidelity Cas9 mutant delivered as a ribonucleoprotein complex enables efficient gene editing in human hematopoietic stem and progenitor cells. *Nat. Med.* **24**, 1216–1224 (2018).
34. Ran, F. A. et al. Double nicking by RNA-guided CRISPR Cas9 for enhanced genome editing specificity. *Cell* **154**, 1380–1389 (2013).
35. Cullot, G. et al. CRISPR-Cas9 genome editing induces megabase-scale chromosomal truncations. *Nat. Commun.* **10**, 1136 (2019).
36. Braulke, T. & Bonifacino, J. S. Sorting of lysosomal proteins. *Biochim. Biophys. Acta* **1793**, 605–614 (2009).
37. McDermott, S. P., Eppert, K., Lechman, E. R., Doedens, M. & Dick, J. E. Comparison of human cord blood engraftment between immunocompromised mouse strains. *Blood* **116**, 193–200 (2010).
38. Wallace, H. A. et al. Manipulating the mouse genome to engineer precise functional syntenic replacements with human sequence. *Cell* **128**, 197–209 (2007).
39. Wraith, J. E. Limitations of enzyme replacement therapy: current and future. *J. Inherit. Metab. Dis.* **29**, 442–447 (2006).
40. Wang, J. et al. Neutralizing antibodies to therapeutic enzymes: considerations for testing, prevention and treatment. *Nat. Biotechnol.* **26**, 901–908 (2008).
41. Herzog, R. W. Complexity of immune responses to AAV transgene products - Example of factor IX. *Cell Immunol.* **342**, 103658 (2019).
42. Cartier, N. et al. Hematopoietic stem cell gene therapy with a lentiviral vector in X-linked adrenoleukodystrophy. *Science* **326**, 818–823 (2009).
43. Biffi, A. et al. Lentiviral hematopoietic stem cell gene therapy benefits metachromatic leukodystrophy. *Science* **341**, 1233158 (2013).
44. Chen, Y., Schroeder, J. A., Kuether, E. L., Zhang, G. & Shi, Q. Platelet gene therapy by lentiviral gene delivery to hematopoietic stem cells restores hemostasis and induces humoral immune tolerance in FIX(null) mice. *Mol. Ther.* **22**, 169–177 (2014).
45. Ramezani, A., Zweier-Renn, L. A. & Hawley, R. G. Factor VIII delivered by haematopoietic stem cell-derived B cells corrects the phenotype of haemophilia A mice. *Thromb. Haemost.* **105**, 676–687 (2011).
46. Shi, Q. et al. Platelet gene therapy corrects the hemophilic phenotype in immunocompromised hemophilia A mice transplanted with genetically manipulated human cord blood stem cells. *Blood* **123**, 395–403 (2014).
47. Chang, A. H., Stephan, M. T., Lisowski, L. & Sadelain, M. Erythroid-specific human factor IX delivery from in vivo selected hematopoietic stem cells following nonmyeloablative conditioning in hemophilia B mice. *Mol. Ther.* **16**, 1745–1752 (2008).
48. Wang, D. et al. Engineering a lysosomal enzyme with a derivative of receptor-binding domain of apoE enables delivery across the blood-brain barrier. *Proc. Natl. Acad. Sci. USA* **110**, 2999–3004 (2013).
49. Grimm, A. J., Kontos, S., Diaceri, G., Quaglia-Thermes, X. & Hubbell, J. A. Memory of tolerance and induction of regulatory T cells by erythrocyte-targeted antigens. *Sci. Rep.* **5**, 15907 (2015).
50. Kontos, S., Kourtis, I. C., Dane, K. Y. & Hubbell, J. A. Engineering antigens for in situ erythrocyte binding induces T-cell deletion. *Proc. Natl. Acad. Sci. USA* **110**, E60–E68 (2013).
51. Pishesha, N. et al. Engineered erythrocytes covalently linked to antigenic peptides can protect against autoimmune disease. *Proc. Natl. Acad. Sci. USA* **114**, 3157–3162 (2017).
52. Huang, N. J. et al. Genetically engineered red cells expressing single domain camelid antibodies confer long-term protection against botulinum neurotoxin. *Nat. Commun.* **8**, 423 (2017).
53. Marktel, S. et al. Intrabone hematopoietic stem cell gene therapy for adult and pediatric patients affected by transfusion-dependent ss-thalassemia. *Nat. Med.* **25**, 234–241 (2019).
54. Abadir, E., Bryant, C., Larsen, S. & Clark, G. J. Targeting the niche: depleting haemopoietic stem cells with targeted therapy. *Bone Marrow Transpl.* **54**, 961–968 (2019).
55. Domingues, M. J., Nilsson, S. K. & Cao, B. New agents in HSC mobilization. *Int J. Hematol.* **105**, 141–152 (2017).
56. Lombardo, A. et al. Gene editing in human stem cells using zinc finger nucleases and integrase-defective lentiviral vector delivery. *Nat. Biotechnol.* **25**, 1298–1306 (2007).
57. Theurl, I. et al. On-demand erythrocyte disposal and iron recycling requires transient macrophages in the liver. *Nat. Med* **22**, 945–951 (2016).
58. Wang, H. et al. High-level protein production in erythroid cells derived from in vivo transduced hematopoietic stem cells. *Blood Adv.* **3**, 2883–2894 (2019).
59. Oller-Salvia, B., Sanchez-Navarro, M., Giralt, E. & Teixido, M. Blood-brain barrier shuttle peptides: an emerging paradigm for brain delivery. *Chem. Soc. Rev.* **45**, 4690–4707 (2016).
60. Ebbink, B. J. et al. Classic infantile Pompe patients approaching adulthood: a cohort study on consequences for the brain. *Dev. Med. Child Neurol.* **60**, 579–586 (2018).
61. Kabadi, A. M., Ousterout, D. G., Hilton, I. B. & Gersbach, C. A. Multiplex CRISPR/Cas9-based genome engineering from a single lentiviral vector. *Nucleic Acids Res.* **42**, e147 (2014).
62. Karnan, S. et al. Improved methods of AAV-mediated gene targeting for human cell lines using ribosome-skipping 2A peptide. *Nucleic Acids Res.* **44**, e54 (2016).
63. Kim, J. H. et al. High cleavage efficiency of a 2A peptide derived from porcine teschovirus-1 in human cell lines, zebrafish and mice. *PLoS ONE* **6**, e18556 (2011).
64. Follenzi, A., Ailles, L. E., Bakovic, S., Geuna, M. & Naldini, L. Gene transfer by lentiviral vectors is limited by nuclear translocation and rescued by HIV-1 pol sequences. *Nat. Genet.* **25**, 217–222 (2000).

65. Lattanzi, A. et al. Optimization of CRISPR/Cas9 delivery to human hematopoietic stem and progenitor cells for therapeutic genomic rearrangements. *Mol. Ther.* **27**, 137–150 (2019).
66. Ayuso, E., Mingozzi, F. & Bosch, F. Production, purification and characterization of adeno-associated vectors. *Curr. Gene Ther.* **10**, 423–436 (2010).
67. Rohr, U. P. et al. Fast and reliable titration of recombinant adeno-associated virus type-2 using quantitative real-time PCR. *J. Virol. Methods* **106**, 81–88 (2002).
68. Canver, M. C. et al. BCL11A enhancer dissection by Cas9-mediated in situ saturating mutagenesis. *Nature* **527**, 192–197 (2015).
69. Menoret, S. et al. Homology-directed repair in rodent zygotes using Cas9 and TALEN engineered proteins. *Sci. Rep.* **5**, 14410 (2015).
70. Wen, J., Tao, W., Hao, S. & Zu, Y. Cellular function reinstitution of offspring red blood cells cloned from the sickle cell disease patient blood post CRISPR genome editing. *J. Hematol. Oncol.* **10**, 119 (2017).
71. Meliani, A. et al. Enhanced liver gene transfer and evasion of preexisting humoral immunity with exosome-enveloped AAV vectors. *Blood Adv.* **1**, 2019–2031 (2017).
72. Aguisanda, F. et al. Neural stem cells for disease modeling of Wolman disease and evaluation of therapeutics. *Orphanet. J. Rare Dis.* **12**, 120 (2017).
73. Hamilton, J., Jones, I., Srivastava, R. & Galloway, P. A new method for the measurement of lysosomal acid lipase in dried blood spots using the inhibitor Lalistat 2. *Clin. Chim. Acta* **413**, 1207–1210 (2012).
74. Schneider, C. A., Rasband, W. S. & Eliceiri, K. W. NIH Image to ImageJ: 25 years of image analysis. *Nat. Methods* **9**, 671–675 (2012).

Acknowledgements

We thank Sabine Charier for advices on NGS engraftment, Anna De Cian, Fatima Amor, Anne Chalumeau and Cecile Loubière for technical help. We also thank Samia Martin and Genethon "Vector Core Facility" for vector production, Jeremy Cosette and Genethon "Imaging and Cytometry Core Facility" for image analysis and FACS sorting, Laetitia van Wittenberghe for help with mice experimentation. We gratefully acknowledge the Conseil Général de l'Essonne (ASTRES) and Genopole Research in Evry for financial help for the purchase of equipment. We thank Anne Galy, Giuseppe Ronzitti, Fulvio Mavilio and the whole Amendola's laboratory for fruitful discussion. We thank Ryo Kurita and Yukio Nakamura for proving HUDEP-2 cells under an MTA with Genethon and Feng Zhang and Charles Gersbach for providing plasmids through Addgene. We are grateful to consenting mothers and to Dr Rigonnot and staff of the Maternity at the Centre Hospitalier Sud-Francilien (CHSF; Evry, France) for providing umbilical cord blood samples. This work was supported by grants to G.P., Bayer (Hemophilia Awards Program), and M.A., (AFM-Telethon, Inserm and Genopole (Chaire Fondagen)). G.P. was supported by the European Union's Horizon 2020 (SCIDNET No 666908). A.S. was partially supported by a PhD fellowship from the French Minister of Higher Education, Research and Innovation via University of Evry.

Author contributions

G.P. conceived the study, designed and performed experiments, analyzed data and wrote the manuscript. M.L. performed experiments and analyzed data for LAL. E.K., A.F. and A.S. performed experiments. G.C. performed bioinformatics analysis of Cas9/gRNA specificity. P.L. performed aPTT assay for FIX experiments. J.P.C. provided purified SpCas9 protein. M.T. produced and titrated AAV and LV. A.M. performed and analyzed HPLC. M.A. conceived the study, designed experiments, analyzed data and wrote the manuscript.

Competing interests

G.P. and M.A. are the inventors of a patent describing this HSC-based gene therapy platform (Genetically engineered hematopoietic stem cell as a platform for systemic protein expression; EP18305026.9). The remaining authors declare no competing interests.

Additional information

Supplementary information is available for this paper at https://doi.org/10.1038/s41467-020-17552-3.

Correspondence and requests for materials should be addressed to M.A.

Peer review information *Nature Communications* thanks Pietro Genovese and the other, anonymous, reviewer(s) for their contribution to the peer review of this work. Peer reviewer reports are available.

Reprints and permission information is available at http://www.nature.com/reprints

Publisher's note Springer Nature remains neutral with regard to jurisdictional claims in published maps and institutional affiliations.

Supplementary Information:

Ex vivo editing of human hematopoietic stem cells for erythroid expression of therapeutic proteins

Giulia Pavani[1], Marine Laurent[1], Anna Fabiano[1], Erika Cantelli[1], Aboud Sakkal[1], Guillaume Corre[1], Peter J. Lenting[2], Jean-Paul Concordet[3], Magali Toueille[1], Annarita Miccio[4], Mario Amendola[1*]

1 INTEGRARE, Genethon, UMR_S951 Inserm, Univ Evry, Univ Paris-Saclay, 91002 Evry, France.
2 Laboratory of Hemostasis-Inflammation-Thrombosis, UMR_S 1176 Inserm, Univ. Paris-Sud, Université Paris-Saclay, 94276, Le Kremlin-Bicêtre, France.
3 Museum National D'Histoire Naturelle, UMR_1154 Inserm, UMR_7196 CNRS, Univ Sorbonne, Paris, France.
4 Imagine Institute, UMR_163 INSERM, Paris, France; Paris Descartes, Univ Sorbonne Paris Cite´, Paris, France.
*Corresponding author: mamendola@genethon.fr

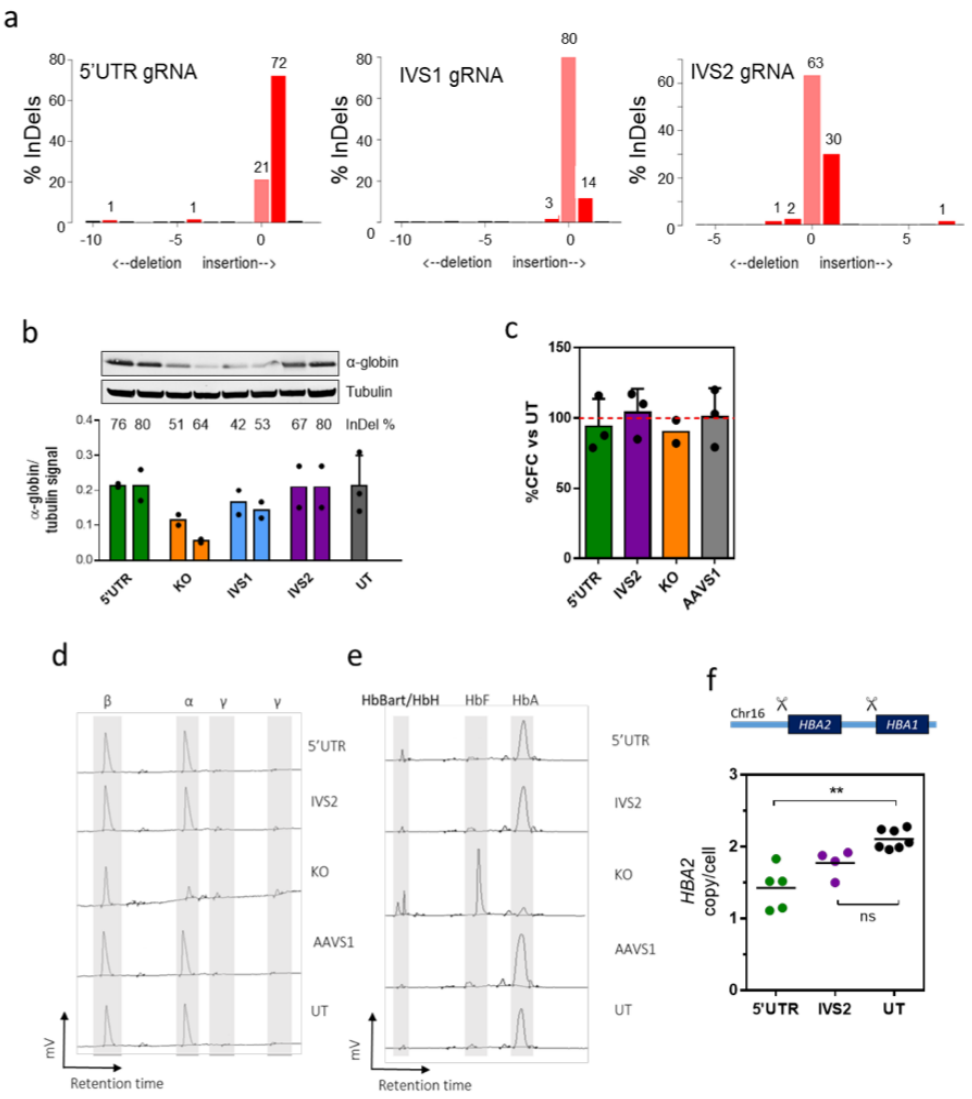

Supplementary Figure 1. (**a**) Representative InDel pattern distribution for 5'UTR, IVS1 and IVS2 HBA gRNAs as assessed by TIDE. (**b**) α-globin expression in K562 cells after genome editing of *HBA*: representative western blot (top) and its quantification (n=2, n=3 for UT; mean ±SD). Percentage of modified *HBA* alleles (indels %) is indicated above bars. Each bar is a different gRNA plasmid transfection, each dot a different analysis. (**c**) CFC numbers expressed as percentage of untreated control (UT). Red dotted line indicates 100%; bars represent mean ±SD (n=3, KO n=2). (**d**) Representative HPLC chromatograms for globin subunit analysis of Figure 1b. (**e**) Representative HPLC chromatograms for globin tetramer analysis of Figure 1d. (**f**) *HBA2* copy number quantification in edited HSPCs by digital droplet PCR (ddPCR) (**, p<0.01; one-way ANOVA, Tukey's test; p=0.008 5'UTR vs UT; n=5 5'UTR, n=4 IVS2, n=7 UT). Schematic representation of *HBA2* deletion is shown above the graph.

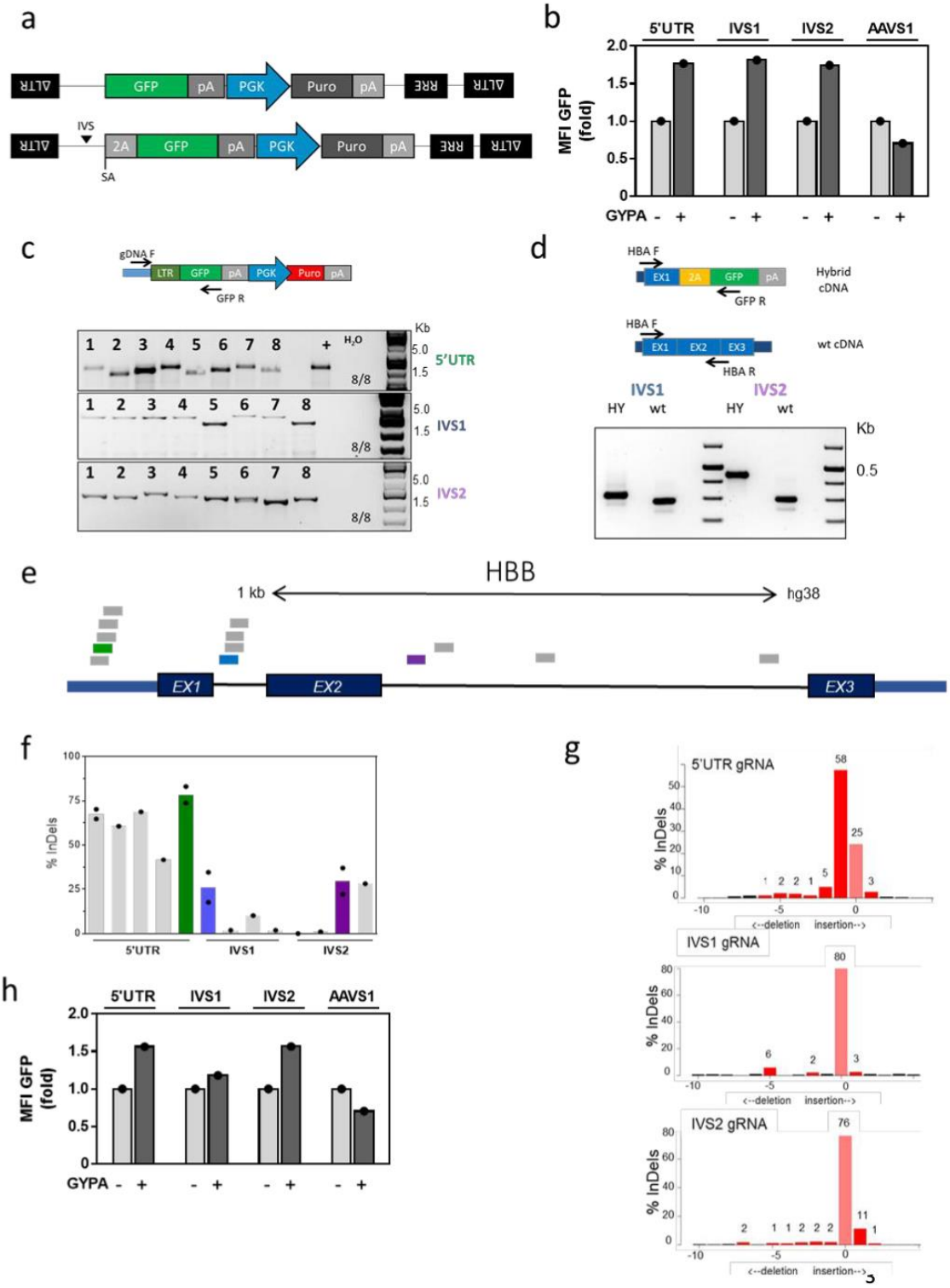
a
ΔLTR
GFP
pA
PGK
Puro
pA
RRE
ΔLTR
IVS
2A
SA
b
5'UTR
IVS1
IVS2
AAVS1
MFI GFP (fold)
GYPA - + - + - + - +
c
gDNA F
LTR
GFP
pA
PGK
Puro
GFP R
Kb
5'UTR
IVS1
IVS2
8/8
d
HBA F
EX1
2A
GFP
pA
Hybrid cDNA
GFP R
EX2
EX3
wt cDNA
HBA R
IVS1
IVS2
HY
wt
Kb
0.5
e
HBB
1 kb
hg38
EX1
EX2
EX3
f
% InDels
5'UTR
IVS1
IVS2
g
5'UTR gRNA
IVS1 gRNA
IVS2 gRNA
% InDels
<--deletion
insertion-->
h
5'UTR
IVS1
IVS2
AAVS1
MFI GFP (fold)
GYPA - + - + - + - +

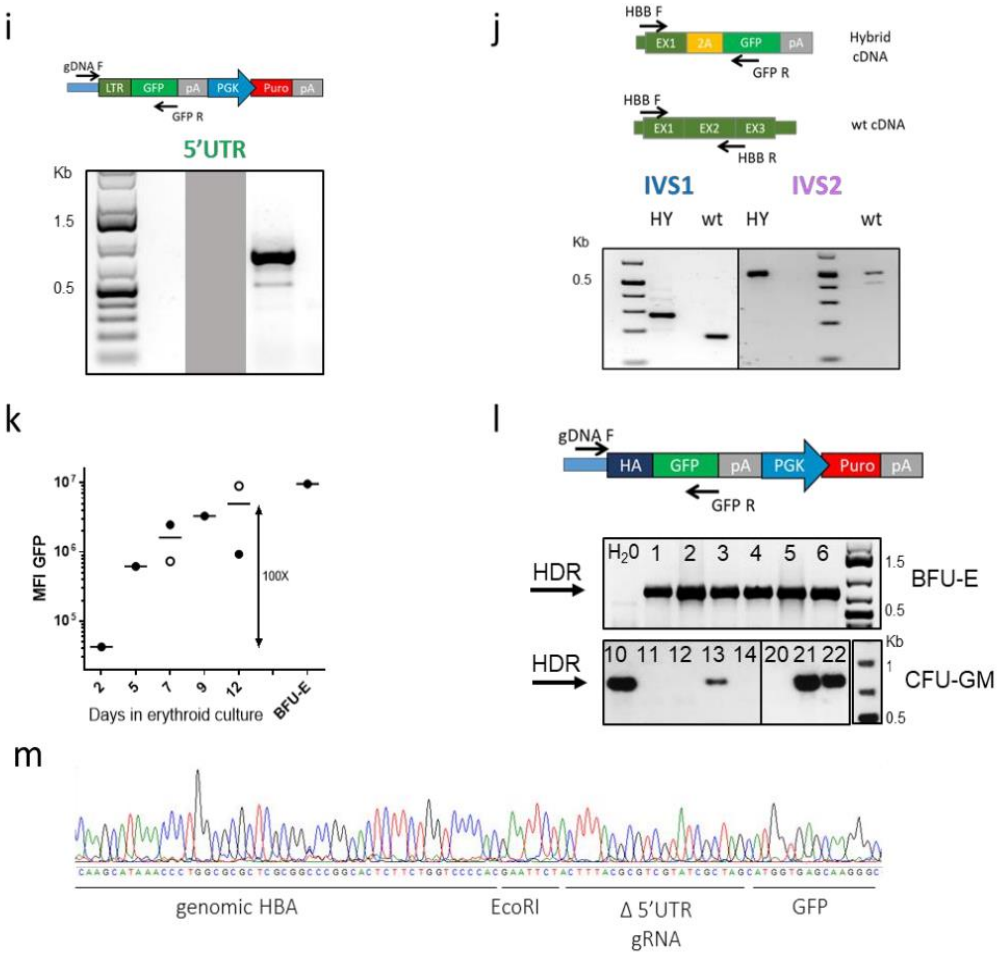

Supplementary Figure 2. (**a**) Proviral form of integrase-defective lentiviral vectors (IDLV) donors used in K562 for KI experiments in 5'UTR (top) and IVS2 (bottom). (**b**) Upregulation of GFP median fluorescent intensity (MFI) in HBA KI K562, upon hemin induction of globin genes. GFP fold increase was calculated in differentiated cells (GYPA+) after normalization of the signal in non-differentiated (GYPA-) cells (n=1). (**c**) PCR analysis of on-target integration in the α-globin locus of K562 KI single-cell clones(24 single-cell clones). A positive control of targeted integration is also shown (+). Schematic representation of the PCR strategy is shown above the graph. (**d**) Detection of the spliced hybrid mRNA (HY), resulting from correct integration and processing of intron traps in IVS1 and IVS2 of HBA(n=1, pooled GFP sorted cells). Schematic representation of the PCR strategy is shown above the graph. WT is the wild type *HBB* mRNA (**e**) Locations of gRNA on *HBB* gene, selected gRNAs are highlighted. (**f**) K562 screening of gRNAs targeting the β-globin locus (5' untranslated region (5'UTR), intron 1 (IVS1) or in intron 2 (IVS2)). Editing efficiency is expressed as percentage of modified *HBB* alleles. Selected gRNAs are highlighted. (n=1, n=2 for

highlighted guides). (**g**) Representative InDel pattern distribution for 5'UTR, IVS1 and IVS2 HBB gRNA as assessed by TIDE. (**h**) Upregulation of GFP median fluorescent intensity (MFI) in *HBB* KI K562, upon hemin induction of globin genes. Same AAVS1 control as in supplementary figure 1b (n=1). (**i**) PCR analysis of on-target integration in the 5'UTR of *HBB* in KI K562 GFP sorted cells (n=1). Schematic representation of the PCR strategy is shown above the graph **(j)** Detection of the spliced hybrid mRNA (HY), resulting from correct integration and processing of intron traps in IVS1 and IVS2 of *HBB* in KI K562 GFP sorted cells (n=1). Schematic representation of the PCR strategy is shown above the graph. WT is the wild type *HBB* mRNA (**k**) GFP median fluorescent intensity (MFI) during differentiation of IVS2 KI HSPCs (bar indicates mean, 2 donors). (**l**) Molecular analysis of single GFP+ BFU-E and random CFU-GM derived from KI HSPCs (n=14). Arrows indicate the amplicon corresponding to the HDR integration of the trap in the 5'UTR of the α-globin locus (n=10). Schematic representation of the PCR strategy is shown above the graph. (**m**) Sanger-sequencing chromatogram of the HDR amplicon (identical for the 10 KI colonies in **l**). Features are indicated below the sequence. Δ5'UTR gRNA indicates the modified sequence in the AAV6 donor to avoid cleavage of the trap after integration.

a

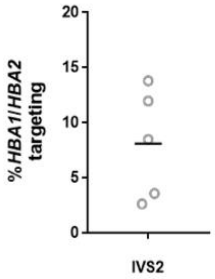

b

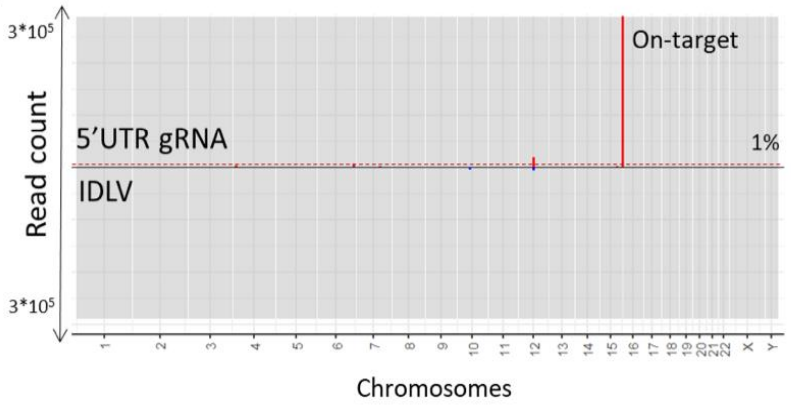

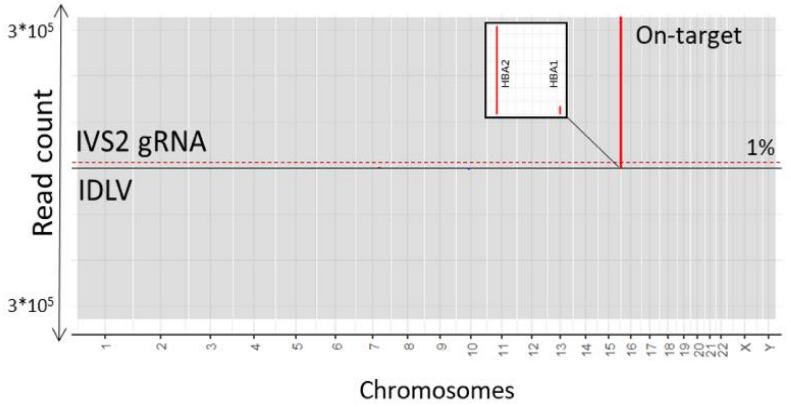

c

Sample		CLIS				Reads					
gRNA	n	total	unique	on-target	gRNA specific*	total	on-target	% on-target	off-target	% off-target	% off-/ on-target
5'UTR	3	19	9	2	2**	601,241	556,159	93	-	-	
IVS2	2	31	25	1	19[$]	360,642	328,800	91.2	30,611[$$]	8.5[$$]	9.3
IDLV	2	6	4	0	-	12,005	-	-	-	-	

* CLIS present in only one gRNA; ** CLIS present in only 1 replicate out of 3

[$] Only 1 CLIS is present in both replicates (*HBA1*); [$$] Data for the *HBA1* main off-target (panel a)

6

Supplementary Figure 3. (**a**) Percentage of HBA1 editing in K562 after transfection with IVS2 gRNA RNP (n=5). (**b**) Clustered integration sites (CLIS) distribution in different chromosomes in K562 for 5'UTR (top) and IVS2 (bottom) gRNA (n=3 replicates for 5'UTR gRNA, n=2 replicates for IVS2 and IDLV control). Y axis is the number of NGS reads. Red dotted lines indicate 1% of reads. Inset shows results in the genomic interval chr16 220000-227000 (hg19). (**c**) Summary Table of CLIS represented in (**b**). Total = sum of all CLIS in each replicates; unique = number of unique CLIS for each gRNA; gRNA specific: number of unique CLIS for each gRNA after subtraction of shared CLIS observed in different conditions (off-targets).

a

FIX copies	Integration		
	HBA1	*HBA2*	*HBA1/ HBA2*
1	19	1	3
2	3		2

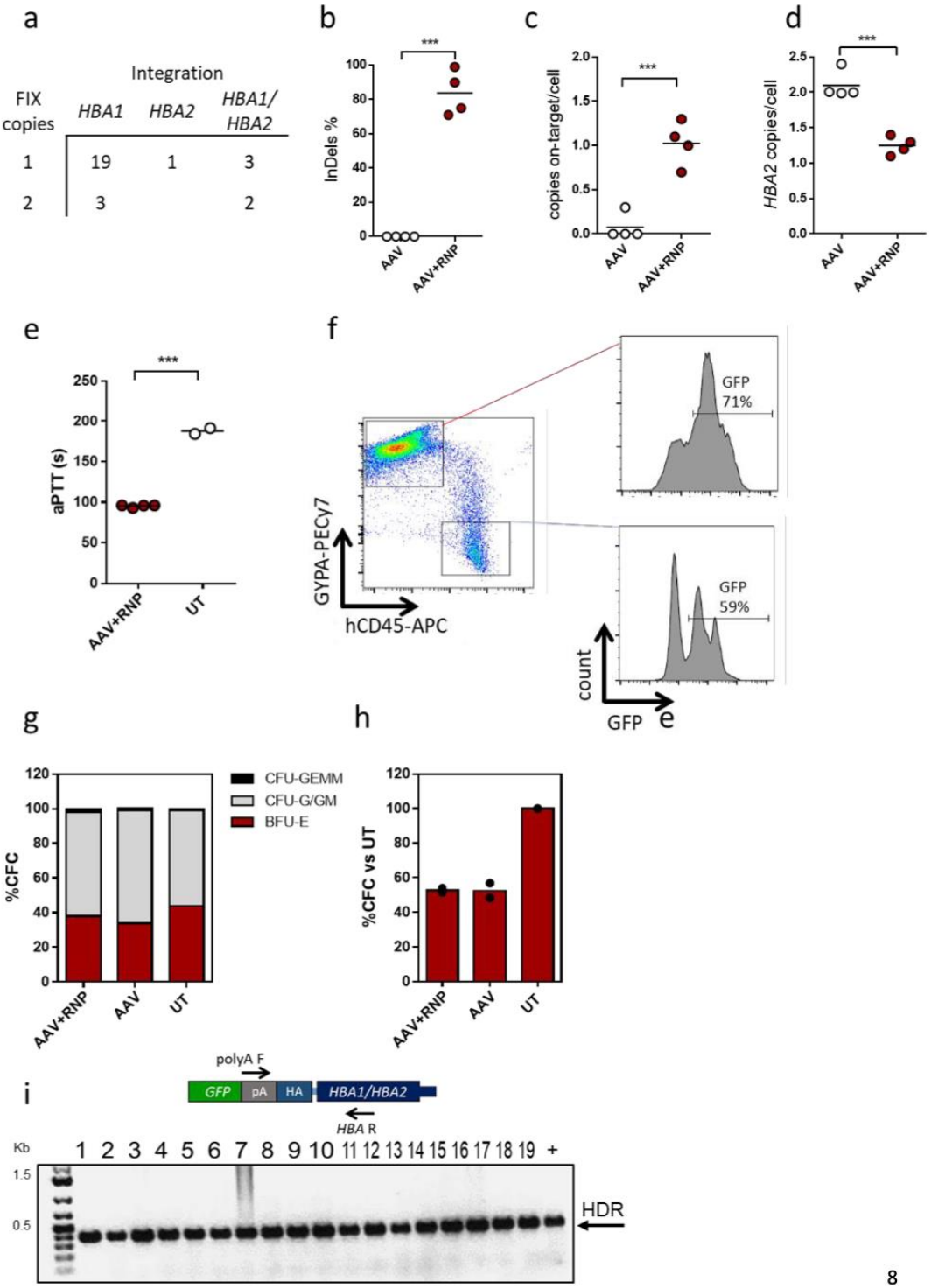

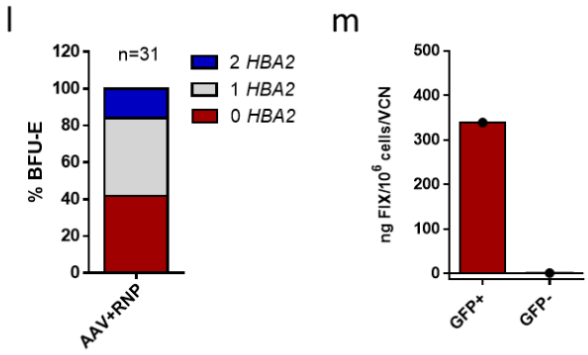

Supplementary Figure 4. (**a**) Characterization of on-target integration of FIX KI HUDEP2 clones shown in Figure 3d. Number of FIX copies integrated and their locations (*HBA1* or *HBA2*) is indicated in the table (n= 28). (**b-d**) Indels quantification (p<0.0001) (**b**), *HBA2* copies (p=0.0004) (**c**) and FIX on-target integration (p=0.0006) (**d**) in edited HSPCs in erythroid liquid culture (n= 4 ; ***: *p* <0.001, two-tailed Student's *t* test). (**e**) Raw clotting times (seconds, s) from supernatants of KI (AAV+RNP) or untreated (UT) HSPC (n= 4 AAV+RNP, n=2 UT; ***: p<0.0001, two-tailed Student's *t* test). (**f**) Representative cytometry dot plots showing GFP expression in red (GYPA+) and white (CD45+) CFC (from 3 biological replicates). (**g**) Colony formation unit (CFU) frequency in KI HSPC. CFU-GEMM, granulocyte, erythroid, macrophage, megakaryocyte; BFU-E, burst-forming unit-erythroid; CFU-G/GM, granulocyte-macrophage. Bars represent mean ±SD (n= 2 AAV+RNP and UT, n=3 AAV). (**h**) CFC number expressed as percentage of untreated control (UT). Bars represent mean ±SD (n=2). (**i**) PCR analysis of single GFP+ BFU-E derived from FIX KI HSPCs. Arrow indicates the amplicon size compatible with HDR mediated integration of the trap in the 5'UTR of *HBA* (n=19). A positive control colony is also shown (+). Schematic representation of the PCR strategy is shown above the graph. (**l**) Quantification of *HBA2* copies in single BFU-E of FIX KI HSPCs. (**m**) FIX expression in supernatants of GFP sorted BFU-E of KI-HSPCs (n=1, pooled from 2 replicates).

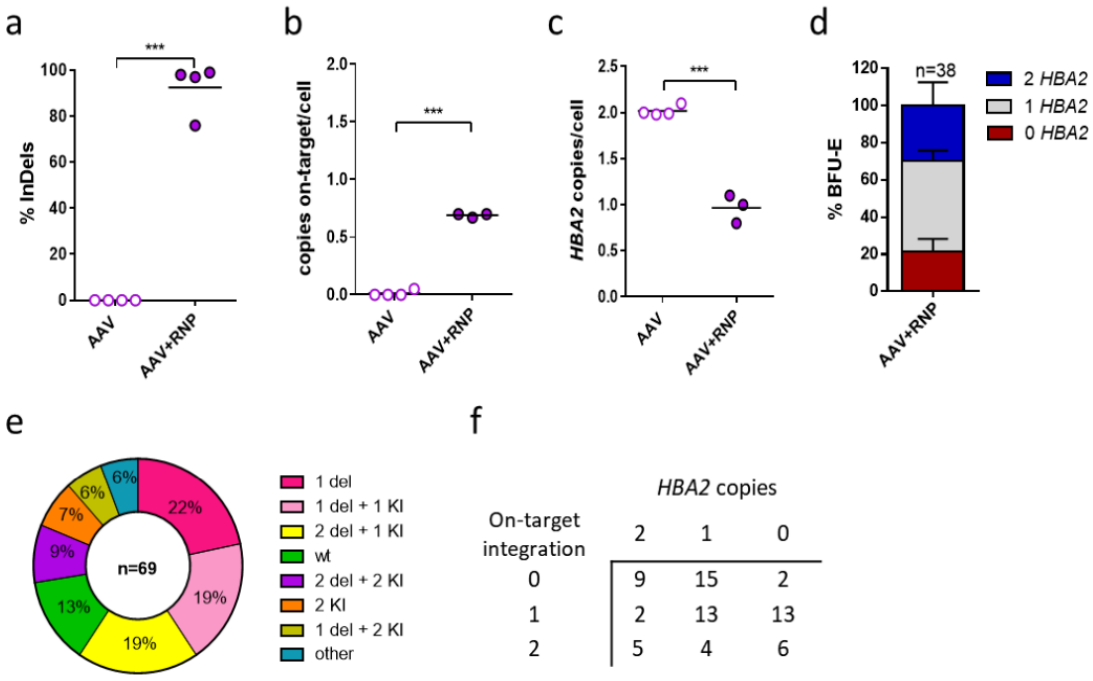

On-target integration	*HBA2* copies 2	1	0
0	9	15	2
1	2	13	13
2	5	4	6

Supplementary Figure 5. Indels quantification (**a**), LAL on-target integration (**b**) and *HBA2* copies (**c**) in edited HSPCs in erythroid liquid culture(n=3-4; ***: p <0.001, Student's t test). (**d**) Quantification of *HBA2* copies in single BFU-E of LAL KI HSPCs. Bars represent mean ±SD (colonies derived from 2 donors). (**e**) Genotypes of BFU-E derived from FIX and LAL KI HSPCs. ("wt", unmodified colonies; "KI", on-target integration; "del", *HBA2* deletion). Percentages are indicated (n=69, 3 donors). (**f**) Colony genotypes shown in (**e**).

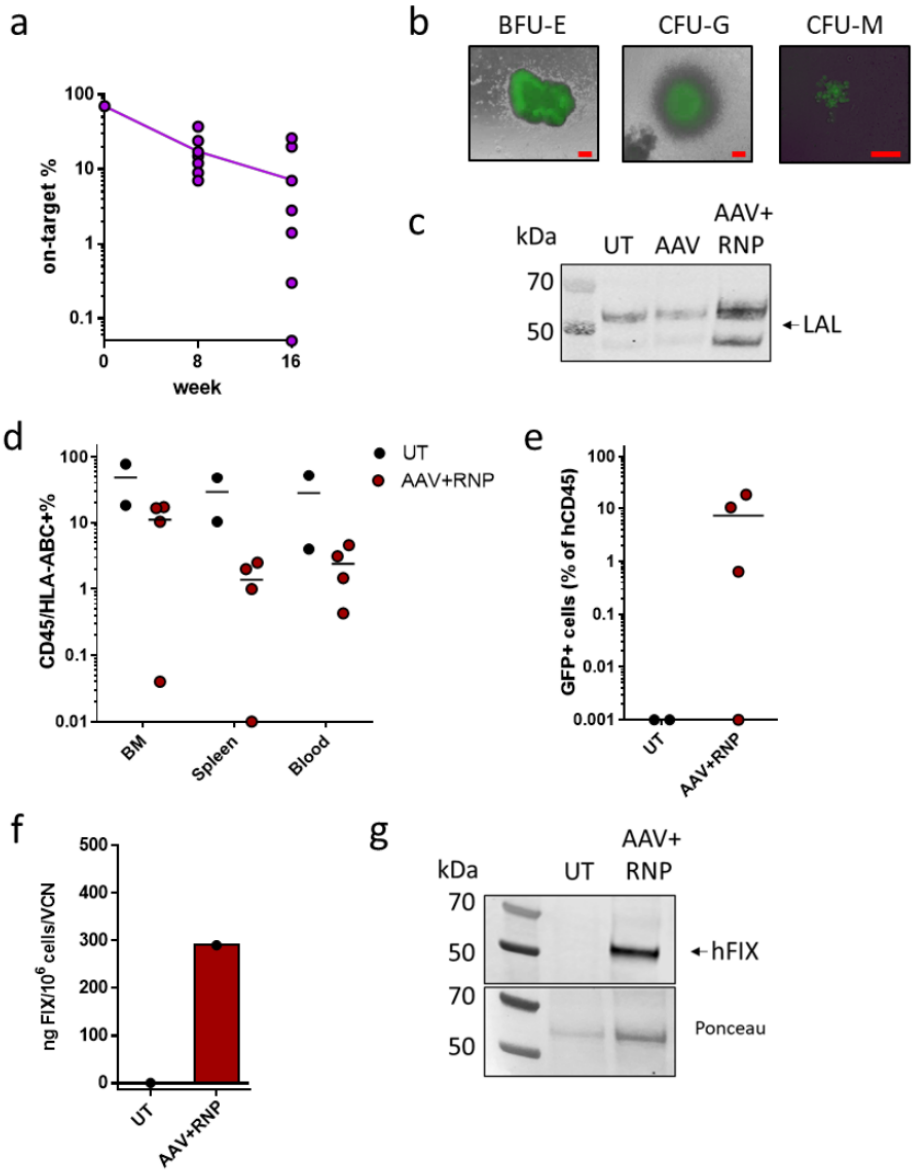
a
on-target %
100
10
1
0.1
0
8
16
week
b
BFU-E
CFU-G
CFU-M
c
kDa
UT
AAV
AAV+ RNP
70
50
LAL
d
CD45/HLA-ABC+%
UT
AAV+RNP
BM
Spleen
Blood
e
GFP+ cells (% of hCD45)
UT
AAV+RNP
f
ng FIX/10^6 cells/VCN
500
400
300
200
100
0
UT
AAV+RNP
g
kDa
UT
AAV+ RNP
70
50
hFIX
70
50
Ponceau

Supplementary Figure 6. (**a**) Percentage of on-target integration in mouse peripheral blood by ddPCR. (**b**) Representative overlay images (bright field and GFP channel) of KI HSPC progenitors recovered from transplanted mice. BFU-E, burst-forming unit-erythroid; CFU-G, granulocyte; CFU-M, monocyte. Scale bars in red indicate 200 µm. (**c**) Western blot of LAL in CD34-derived BFU-E from mice that received untreated (UT) and KI-HSPCs (AAV+RNP). Anti-LAL tag antibody was used. (**d**) Percentage of human CD45+/HLA-ABC+ cells in hematopoietic organs of mice at week 16. BM = bone marrow (n= 4 AAV+RNP, n=2 UT). (**e**) Edited cells in bone marrow of transplanted mice. GFP is expressed as percentage of CD45+ cells, mean is shown (n= 4 AAV+RNP, n=2 UT). (**f**) Human FIX expression in supernatants of CD34-derived BFU-E from mice that engrafted with untreated (UT) or KI-HSPCs (AAV+RNP) (n= 1, pooled from 2 mice). (**g**) Western blot on CD34-derived BFU-E from mice engrafted with untreated (UT) or KI HSPCs (AAV+RNP). Ponceau staining is also shown (n= 1, pooled from 2 mice).

Supplementary table 1: List of gRNAs tested

HBA gRNA name	Protospacer with PAM
HBA 10	GGGTTTATGCTTGGGGCGCG**GGG**
HBA 12	GACTCAGAGAGAACCCACCA**TGG**
HBA 14	TGGGTTCTCTCTGAGTCTGT**GGG**
HBA 19	GCGCGGGGGCACGCCCGGCC**GGG**
HBA 15 (5'UTR)	GGGTTCTCTCTGAGTCTGTG**GGG**
HBA 16 (KO)	GTCGGCAGGAGACAGCACCA**TGG**
HBA 17	GCAGGAGACAGCACCATGGT**GGG**
HBA 20	CATAAACCCTGGCGCGCTCG**CGG**
HBA INT1 73b (IVS1)	CAGGCCACCCTCAACCGTCC**TGG**
HBA INT1 72	TCCGGGGCCAGGACGGTTGA**GGG**
HBA INT1 73	GTCCGGGGCCAGGACGGTTG**AGG**
HBA INT2 13REV	CCCTCGACCCAGATCGCTCC**CGG**
HBA INT2 63	GAAGAGGGTCAGTGCGGCCC**AGG**
HBA INT2 74 (IVS2)	GCGTGATCCTCTGCCCTGAG**AGG**
HBB gRNA name	**Full Sequence with PAM**
HBB 37	GGTTGGCCAATCTACTCCC**AGG**
HBB 49	GGGTTGGCCAATCTACTCCC**AGG**
HBB 53	GGAGTAGATTGGCCAACCCT**AGG**
HBB 54	GATTGGCCAACCCTAGGGTG**TGG**
HBB 77 (5'UTR)	GAGTAGATTGGCCAACCCTA**GGG**
HBB INT 1 36 (IVS1)	TGGTATCAAGGTTACAAGAC**AGG**
HBB INT1 36REV	TCCACATGCCCAGTTTCTAT**TGG**
HBB INT1 47FOR	TTAAGGAGACCAATAGAAAC**TGG**
HBB INT1 48FOR	TAAGGAGACCAATAGAAACT**GGG**
HBB INT2 340FOR	CTGCCTAGTACATTACTATT**TGG**
HBB INT2 797REV	ATTAGCAAAAGGGCCTAGCT**TGG**
HBB INT2 20 (IVS2)	GTTAAGTTCATGTCATAGGA**AGG**
HBB INT2 39	GACGAATGATTGCATCAGTG**TGG**
Control	**Full Sequence with PAM**
AAVS1	GTCCCCTCCACCCCACAGTG**GGG**

Supplementary table 2: 5'UTR gRNA off-targets

Off Target	Sequence	mismatch	deletion	chr	start	end	strand	type	gene	Indel % HBA15 *	Indel % AAVS1*
1	GGGTTTTCCTGAGTCTGTGTGG	1	Del 12	chr6	167624159	167624180	-	intergenic	TCP10L2-UNC93A	0	1
2	GGGTTCCCTCTGATCTGTGGGG	1	Del 7	chr7	57350881	57350902	-	intergenic	LOC105375297-LOC100653233	1	1
3	GGGTTCCTCTGAGGCTGTGAGG	1	Del 14	chr21	35358171	35358192	+	intergenic	LOC101928126-SLC5A3	0	0
4	GGGTTTCTCTGAGTCAGTGTGG	1	Del 15	chr14	38170058	38170079	-	intron	TTC6	0	0
5	GGGTTTCTCTGAGTCTCTGGGG	1	Del 15	chr17	77153181	77153202	-	intron	RBFOX3	0	1
6	GGGTGCTCTCTGAGTCTGGTGGGG	1	Ins 3	chr9	93549548	93549571	-	intergenic	DIRAS2-SYK	0	ND
7	GGGTTCTCTCTGAGCCTGGAGG	1	Del 2	chr2	231805880	231805901	-	intergenic	GPR55-SPATA3-AS1	3	4
8	CGGTTCTCTCTGAGTCTATGAAG	2	0	chr6	169440547	169440569	-	intergenic	RP3-495K2.2-RP3-495K2.1	1	1
9	GGGTTCCCTCTGAGGCTGTGAGG	2	0	chr9	77688205	77688227	-	intron	NMRK1	1	1
10	GGGTTCTCTCTCAGTCTGTGTGT	2	0	chr6	24657192	24657214	-	intron	TDP2	0	0
11	TGATTCTTTCTGAGTCTGTGAGG	3	0	chr2	229878873	229878895	-	intergenic	AC007677.2-PID1	0	0
12	TTGTGCTCTCTGAGTCTGTGTGG	3	0	chr16	58978340	58978362	+	intergenic	RP11-700H13.1-RP11-410D17.2	0	0
13	TGCTTCTCTCTGAGTCTGGGCGA	3	0	chr8	134399964	134399986	-	intergenic	CTC-458A3.1-CTC-369M3.1	1	1
14	GGATTCTGTCTGTGTCTGTGAGA	3	0	chr11	66956537	66956559	-	intergenic	KDM2A-AP001885.1	1	1
15	GGGTTCTTTCTGAGGCTGGGAGG	3	0	chr7	138374829	138374851	-	intergenic	AC020983.5-SVOPL	0	0
16	GGGTTCTCTCTGAGGCTTTCAGG	3	0	chr16	31075849	31075871	-	intron	ZNF668	2	0
17	TGTTTCTATCTGAGTCTGTGGGA	3	0	chr16	54632788	54632810	-	intergenic	AC079412.1-RP11-1136G4.1	0	0
18	TGGTTCTCTCTGAGGCTCTGAGG	3	0	chr8	145594499	145594521	+	intergenic	SLC52A2-ADCK5	ND	ND
19	GGGTTCGTTCTGAGGCTGTGAGG	3	0	chr11	2577287	2577309	+	intron	KCNQ1	1	1
20	GGGTTTGCTCTGAGGCTGTGGGG	3	0	chr4	1392471	1392493	+	intergenic	CRIPAK-NKX1-1	0	1
21	AGATGCTGTCTGAGTCTGTGGGG	4	0	chr12	4038222	4038244	+	intergenic	RP11-664D1.1-RP11-320N7.2	1	0
22	ATGACCTCTCTGAGTCTGTGTGG	4	0	chr3	127328104	127328126	+	intron	MCM2	1	2
23	TGTTTCTGTGTGAGTCTGTGTGG	4	0	chr19	55433833	55433855	-	intergenic	NCR1-NLRP7	ND	ND
24	GATATCTCTGTGAGTCTGTGAGG	4	0	chr3	70751897	70751919	+	intergenic	RP11-231I13.2-COX6CP6	1	0
25	TGGTCCTCTCAGAGTCTGTAAGG	4	0	chr20	3236843	3236865	+	exon	C20orf194	1	2
26	TGATTCTTTCTGAGTATGTGGGG	4	0	chr10	37317185	37317207	+	intergenic	ARL6IP1P2-ANKRD30A	1	0
27	TGATTCTTTCTGAGTATGTGGGG	4	0	chr11	80331104	80331126	-	intergenic	RNU6-544P-ARL6IP1P3	1	0
28	GGGTTTTCTTAGAATCTGTGAGG	4	0	chr11	48672787	48672809	+	intergenic	OR4A44P-RP11-56P9.5	not present in K562	
29	GGGTCTTCCCTCAGTCTGTGTGG	4	0	chr5	154003375	154003397	-	intergenic	MIR3141-MIR1303	0	0

*With a threshold limit of ~2% (TIDE[22])

Supplementary table 3: primer list

PCR		
Gene/amplicon	**name**	**sequence**
HBA 1/2 – IVS1	3820 F	TATCGCCAGAGGGAAAGGGA
	4870 R	CTTGAAGTTGACCGGGTCCA
HBA1/2 sequencing	894 R	TAGGTCTTGGTGGTGGGGAA
HBA2	611 F	GCACTCTTCTGGTCCCCAC
	1512R	GCAGAGAGGTCCTTGGTCTG
HBA1	HBA EX1F	CCGACAAGACCAACGTCAA
	5614 R	CTCTAGGGTCCAGCGTTTTTCC
AAVS1	MA359	CAGCTCAGGTTCTGGGAGAG
	MA360	CTTGTAGGCCTGCATCATCA
HBB 5UTR	HBB9 F	CTGTCTCCACATGCCCAGTT
	HBB9 R	GGAGACGCAGGAAGAGATCC
HBB IVS2	HBB IVS2 F	TTGGACAGCAAGAAAGCGAG
	HBB IVS2 R	GTGAGTCTATGGGACGCTTGA
HBA EX1-2 cDNA	HBA EX1F	CCGACAAGACCAACGTCAA
	4870 R	CTTGAAGTTGACCGGGTCCA
HBA-GFP IVS1 hybrid	HBA EX1F	CCGACAAGACCAACGTCAA
	PPT_EGFP_R	GAACTTCAGGGTCAGCTTGC
HBA EX2-3 cDNA	875 F	GAACTTCAGGGTCAGCTTGC
	HBA EX3 R	CTCACAGAAGCCAGGAACTT
HBA-GFP IVS2 hybrid	875 F	TTCCCCACCACCAAGACCTA
	PPT_EGFP_R	GAACTTCAGGGTCAGCTTGC
On-target 5'junct (5'UTR - IVS1 HBA)	3820 F	TATCGCCAGAGGGAAAGGGA
	PPT_EGFP_R	GAACTTCAGGGTCAGCTTGC
On-target 5'junct (IVS2 HBA)	HBA EX1F	CCGACAAGACCAACGTCAA
	PPT_EGFP_R	GAACTTCAGGGTCAGCTTGC
HBA2 INT	mini PolyA 1F	TGGACAAACCACAACTAGAATGC
	1512R	GCAGAGAGGTCCTTGGTCTG
HBA1 INT	mini PolyA 1F	TGGACAAACCACAACTAGAATGC
	5614 R	CTCTAGGGTCCAGCGTTTTTCC
OFF TARGET 1	OFF-T 1COSF	CTTTAGACACCCAGTGGGAAG
	OFF-T 1COSF	AGCCAGATGCCATAGAGTTTAC
OFF TARGET 2	OFF-T 2COSF	CTGCAACTGAACCCGAGTAATA
	OFF-T 2COSR	GGGAGTAGGCAGCATGATTT
OFF TARGET 3	OFF-T 4COSF	ACCCTCCTCACACCATGTA
	OFF-T 4COSR	ACCTCTGAATGTGGCTTTATGT
OFF TARGET 4	OFF-T 5COSF	CCAAGGCAGGCAGATTACTT
	OFF-T 5COSR	GACAACAGTCTACAGGCATCTC
OFF TARGET 5	OFF-T 6COSF	TTTCATCCCTGGCAAGCTAC
	OFF-T 6COSR	TTTGTGGTCAGTGTCTGTGG
OFF TARGET 6	OFF-T 7COSF	ACCTCTAGGATGAGAGGTAAA
	OFF-T 7COSR	CTATTGGATTAGATAGCATGTTGTG
OFF TARGET 7	OFF-T 8COSF	CCTGCAGGGAGGAATTAAGAAG

	OFF-T 8COSR	CCCTGGGTTCAGGTTCAAAT
OFF TARGET 8	OFF-T HBA15 1F	TAAAGTCCTAATGCCCAGTTCTC
	OFF-T HBA15 1R	CTGCCCAGGTTCAAACAATTC
OFF TARGET 9	OFF-T 9COSF	TCAGCCTTATCACCCATCATC
	OFF-T 9COSR	GCTCTGCAGAACCCATCTAT
OFF TARGET 10	OFF-T HBA15 2F	GAACTGGGTCATAGCTGGGG
	OFF-T HBA15 2R	CATCCTGTCTCCATCGCAGG
OFF TARGET 11	OFF-T 1MIT47 F	CGCAGACACAGACACTCAAA
	OFF-T 1MIT47 R	CTCCTTCACAGAAACCCATCC
OFF TARGET 12	OFF-T 2MIT45F	TATGTGGCTTCCCTTGGTTC
	OFF-T 2MIT45R	TGACCTTTGCTGTGCTTAGT
OFF TARGET 13	OFF-T HBA15 3F	TGTGTAGATGGGTTCTCTACCT
	OFF-T HBA15 3R	CTACCCTTGGAGAACTGTATGC
OFF TARGET 14	OFF-T HBA15 4F	TGCAGTGACCTGAGATTGTG
	OFF-T HBA15 4R	CCCATTGTGGTTGGAGAAGATA
OFF TARGET 15	OFF-T HBA15 5F	TCACAAGGTCAGCAGTTTGA
	OFF-T HBA15 5R	TGCGTGGACACGTGTATTAG
OFF TARGET 16	OFF-T 6bMIT259F	TCACGATTCCTCAAGCTACAC
	OFF-T HBA15 6R	CACGTCTGGGTACACTCTTTATC
OFF TARGET 17	OFF-T HBA15 7F	AAGGTGAAGGAGGAGCAAAG
	OFF-T HBA15 7R	GTGAGGAGGCTGAAACGATAG
OFF TARGET 18	OFF-T HBA15 8F	CTGGCTAACACGGTGAAACT
	OFF-T HBA15 8R	CAGGAGAAGAGAGAGGGAGATT
OFF TARGET 19	OFF-T HBA15 9F	CCTCCCATATGCCCACATTT
	OFF-T HBA15 9R	ATCAGCAGCCAGGTTTGTAG
OFF TARGET 20	OFF-T HBA15 10F	GGATGTGAGTAGATCAGGTTGG
	OFF-T HBA15 10R	TGGCAATGGTGTGCTTCT
OFF TARGET 21	OFF-T 4MIT329F	GCATGTGTGTGCATGTGTATG
	OFF-T 4MIT329R	CTGTGGCCCTAATCCTTTGTAG
OFF TARGET 22	OFF-T 5MIT327F	CAGGATGCTGTGAGAGGATATG
	OFF-T 5MIT327R	GATCTTGAGCCAGGAGTTTGA
OFF TARGET 23	OFF-T 6MIT259F	AGATCACGAGGTCAGGAGAT
	OFF-T 6MIT259R	CTTCTTGGGCCATTTGCTATTT
OFF TARGET 24	OFF-T 7MIT206F	CCCTTTCCACTTTCCTGGTAAC
	OFF-T 7MIT206R	GCAAGCGAAGGAGGTCATTTA
OFF TARGET 25	OFF-T 1CFD355F	CCAGTCCTTGATGCTGTCTT
	OFF-T 1CFD355R	TGTTCCTCTCTGTCTCTCTCTC
OFF TARGET 26	OFF-T 3CFD353F	CCGGTTGCTATCTGTGGAAATA
	OFF-T 3CFD353R	CTAGGAGAGACAATCACCATGC
OFF TARGET 27	OFF-T 4CFD354F	CACCATGATTTCGGGAGTTTG
	OFF-T 4CFD354R	CAGACACTGCTCTACACTATCC

OFF TARGET 28	OFF-T 5CFD352F	GTTAGGGATGTGGGCATTCA
	OFF-T 5CFD352R	GGTTTCTCAGAGAGCTTCCTTC
OFF TARGET 29	OFF-T 6CFD351F	GTGGTGGTACTCTCCTGTAGT
	OFF-T 6CFD351R	CCTGCTGTGTTCCTTCCTTT
ddPCR		
On-target 3'junction	3'HBA INT F	TGGACAAACCACAACTAGAATGC
	3'HBA INT 3 R	AAGTGCGGGAAGTAGGTCTT
	3'HBA INT PRB	56-FAM/CTGTCTCCTGCCGACAAGACCAAC
HBA2	HBA2 3' F	GCCCTTCCTGGTCTTTGAATA
	HBA2 3' R	ACCTCCATTGTTGGCACAT
	HBA2 3' PRB	56-FAM/TGTGTGTGCCTGGGTTCTCTCTAT
ALB	ALB F	GCTGTCATCTCTTGTGGGCTGT
	ALB R	ACTCATGGGAGCTGCTGGTTC
	ALB P	CCTGTCATGCCCACACAAATCTCTCC
qPCR		
Human FIX	hFIX 1F	AAGCGGTACAACTCAGGCAA
	hFIX 1R	CTTCCAGAACTCGGTGGTCC
HA-tag	HATAG 1F	TGATTACGCCGGCACAG
	HATAG 1R	ATCAGGCACATCATAAGGGTATC
GAPDH	GAPDH F	CTTCATTGACCTCAACTACATGGTTT
	GAPDH R	TGGGATTTCCATTGATGACAAG

F=forward; R=reverse, PRB=probe.

Supplementary table 4: Antibodies for flow cytometry

Name	Fluorochrome	Clone	Company	Catalog Number	Dilution
human Fc Receptor binding inhibitor polyclonal antibody			eBioscience	16-9161-73	1:50
anti-human Fetal Hemoglobin	APC		Life Technologies	MHF05	Per manufacturer's instructions
anti-human Hemoglobin β	PE	37-8	Santa Cruz Biotechnology	sc-21757	1:50
anti-human HLA-ABC	PE	G46-2.6	BD Bioscience	555553	Per manufacturer's instructions
anti-human CD36	FITC	C836	BD Bioscience	555454	Per manufacturer's instructions
anti-human CD235a (GYPA)	PE-Cy7	GA-R2	BD Bioscience	563666	Per manufacturer's instructions
anti-human CD71	APC	M-A712	BD Bioscience	551374	Per manufacturer's instructions
anti-human CD45	APC	HI30	BD Bioscience	555485	Per manufacturer's instructions
anti-human CD45	PB	J.33	Beckman Coulter	A74765	Per manufacturer's instructions
anti-human CD33	BV421	P67.6	BD Bioscience	744761	1:100
anti-human CD19	BV605	HIB19	BD Bioscience	740394	1:100
anti-human CD3	BB700	SK7	BD Bioscience	566575	1:10
anti-human CD34	PE	AC136	Miltenyi Biotec	130-113-179	1:50
anti-human CD38	APC	REA671	Miltenyi Biotec	130-110-244	1:25
IgG1, κ isotype control	APC		Life Technologies	MG105	Per manufacturer's instructions
IgG1, κ isotype control	APC		BD Bioscience	550854	Per manufacturer's instructions
IgG1, κ isotype control	BV421		BD Bioscience	562438	1:100
IgG1, κ isotype control	BV605	X40	BD Bioscience	562652	1:100
IgG1, κ isotype control	BB700	X40	BD Bioscience	566404	1:100

IgG2a, κ isotype control	APC	G155-178	BD Bioscience	551414	Per manufacturer's instructions
IgG2a, κ isotype control	PE		BD Bioscience	555574	Per manufacturer's instructions
IgG2a, κ isotype control	PE	S43.10	Miltenyi Biotec	130-113-272	1:50
IgG2b, κ isotype control	PE-Cy7		BD Bioscience	560542	1:100

All antibodies were mouse monoclonal antibodies, unless differently specified.

Supplementary table 5: Antibodies for western Blot

Target	host	Fluorochrome	Clone	Company	Dilution
anti-human LAL	Mouse	-	9G7F12, 7G6D7	Thermo-Fisher	1:1000
HA-TAG	Mouse	-	16B12	Eurogentec	1:1000
anti-human α-globin	Goat	-	D-16	Santa Cruz Biotechnology	1:200
anti-human FIX	Rabbit	-	Polyclonal	Invitrogen	1:500
anti-human β-tubulin	Rabbit	-	Polyclonal	Li-Cor Biosciences	1:1000
Anti-mouse IgG (H+L)	Goat	800CW	Polyclonal	Li-Cor Biosciences	1:15000
Anti-mouse IgG (H+L)	Donkey	680LT	Polyclonal	Li-Cor Biosciences	1:15000
Anti-rabbit IgG (H+L)	Goat	680LT	Polyclonal	Li-Cor Biosciences	1:15000
Anti-goat IgG (H+L)	Donkey	800CW	Polyclonal	Li-Cor Biosciences	1:15000

Conclusion and follow-up studies

The erythroid-based platform shows efficient gene targeting in the HBA locus leading to robust expression of therapeutic transgenes upon erythroid differentiation. In fact, the secreted LAL enzyme from LIPA KI erythroblasts was able to cross-correct the lipid accumulation in WD fibroblasts putting in light the therapeutic benefit of this strategy. Transplantation of edited CD34+ in immunocompromised mice was successful with a maintain of the multilineage differentiation potential. Unfortunately, immunocompromised mice do not support human erythroid differentiation preventing us from *in vivo* assessment of erythroid platform. To overcome this limitation, we are currently evaluating the strategy using a humanized mouse model for HBA locus (Wallace et al., 2007).

To achieve higher protein expression and secretion of LAL upon erythroid differentiation, we performed several LIPA transgene optimization (Described in Result part 6.3.1). For that, we designed different LVVs encoding LIPA cDNA under control of the GLOBE erythroid specific promoter. LVVs have been tested on HSCs and would allow us to screen easily different LIPA constructions.

Finally, we performed multimodal cytometry approach in order to further investigate lipid accumulation in LAL-D and improve the discrimination between WT, WD, and treated fibroblasts (Described in Result part 6.3.2).

6.3 LAL-D : Optimization of LIPA cDNA and characterization of the lipid phenotype

Introduction :

LAL-D is LSD caused by mutation(s) in LIPA gene and triggers fatal lipid accumulation, hepatomegaly, splenomegaly, and difficulties to thrive. As consequence, WD leads to a premature death in first year after birth without treatment. The only symptomatic treatment consists of ERT that requires weekly administration of the recombinant human LAL. Here, we exploited LV-based *ex vivo* GT to optimize LIPA cDNA to maximize the expression and erythroid secretion of the therapeutic LAL enzyme (Described in Result part 6.3.1).

Then, we also developed a multi-modal cytometry-based approach to better characterize the LAL-D phenotype and offers for patient of follow-up pipeline. With this approach, we were able to better discriminate between WT and WD population based on the lipid accumulation and to assess therapeutic effects of LV insertion of LIPA gene into WD fibroblasts (Described in Result part 6.3.2).

6.3.1 Optimisation of LIPA transgene

We have optimized LIPA transgenes using LVVs as they are easier and cheaper to implement compared to targeting integration, in addition to offering a curative approach for LAL-D as LV-based correction is already in the clinic for other LSDs. The LV particle designed encodes for *LIPA* gene under the control of the GLOBE erythroid promoter (Miccio et al., 2008) to ensure the LAL expression in erythroid-specific cells. Therefore, RBCs would serve as vesicle to deliver therapeutic enzyme in circulation and LAL would take advantage of the cross-correction effect to treat affected tissues. As control of our erythroid-based GT, we will use LV particle encoding LIPA under the control of an ubiquitous promoter already in clinical for LSD : phosphoglycerate kinase promoter (PGK). In order to be able to follow the exogenous LAL, we added an HA-tag cassette into the 3' of the LIPA transgene sequence.

To maximize the secretion of enzyme out of mature erythroid population, we designed LVVs encoding LIPA gene with several signal peptide coming from other secreted enzyme. We restricted the selection of signal peptides based on two papers that optimized GAA transgene secretion for pompe disease (Puzzo et al., 2017) and that engineered Chinese hamster ovary cells for optimal recombinant antibodies secretion (Kober et al., 2013). Therefore, we constructed 7 LVVs encoding LIPA transgenes different signal peptide (SP) sequences :

Signal peptide (SP)	Abbreviation	Protein sequence	Ref
WT LIPA	SP1	MKMRFLGLVVCLVLWTLHSEGSG	Unitprot
a-1 antitrypsin	SP2	MPSSVSWGILLLAGLCCLVPVSLA	(Puzzo et al., 2017)
Iduronate 2-sulfatase	SP6	MPPPRTGRGLLWLGLVLSSVCVALG	
Chymotrypsinogen B2	SP7	MAFLWLLSCWALLGTTFG	
Plasma protease inhibitor	SP8	MASRLTLLTLLLLLLAGDRASS	
Serum albumin preprotein	SP9	MKWVTFISLLFLFSSAYS	(Kober et al., 2013)
Azurocidin preprotein	SP10	MTRLTVLALLAGLLASSRA	

Table 7) Different signal peptides used with their protein sequences and references

6.3.1.1 Signal peptide optimization in K562 cells

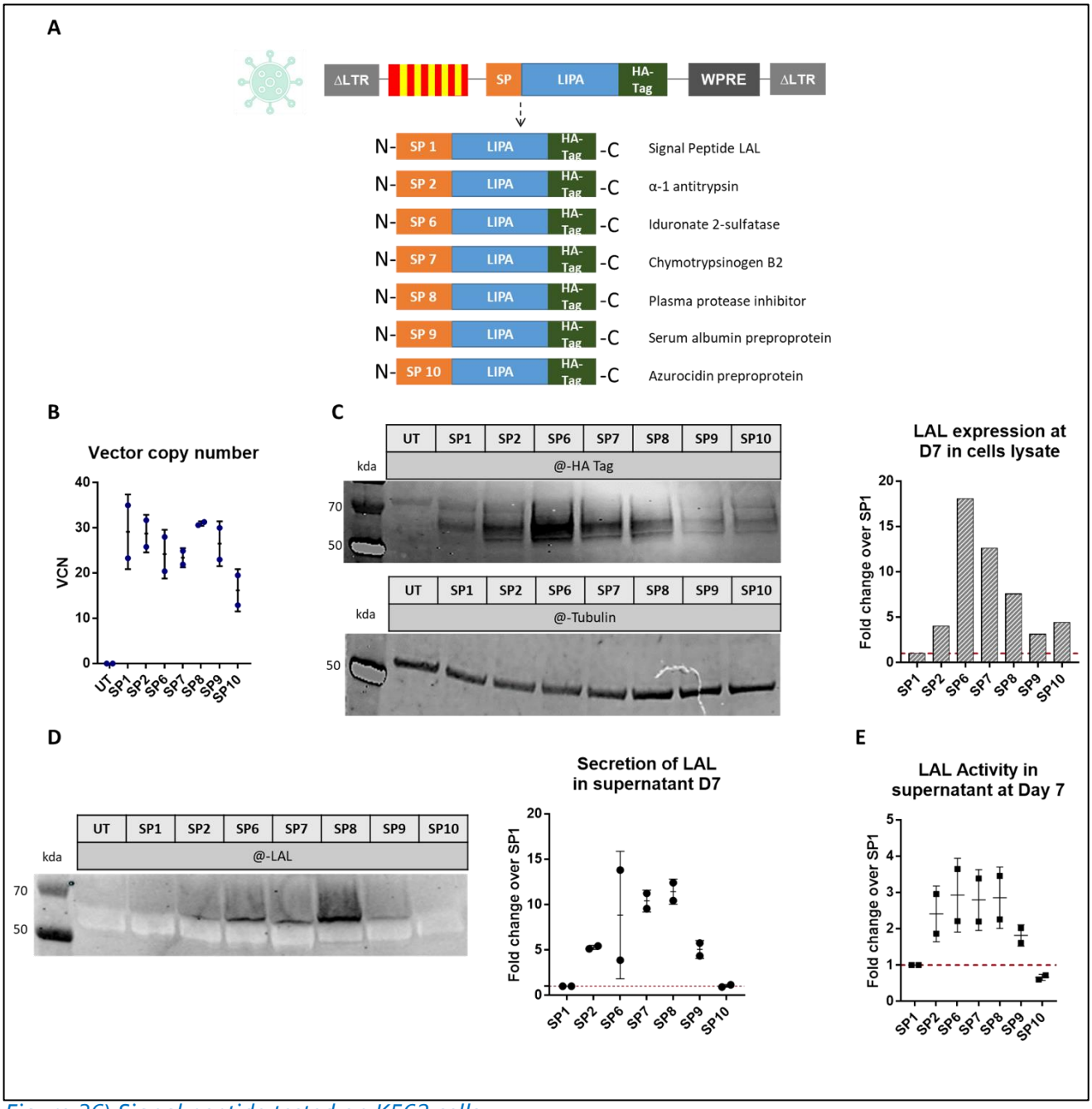

Figure 36) Signal peptide tested on K562 cells.

***A**. Representation of lentiviral constructions & signal peptides used to optimize the secretion of the LAL enzyme. **B**. Vector copy number at day 7 after the transduction of K562 with the different lentivirus. **C**. Western blot (WB) of the K562 lysate at day 7 labelled with @-HA-tag & @-Tubulin and analysis of the LAL signal over LAL WT signal peptide (SP1), normalized on Tubulin and VCNs. **D**. WB of K562 supernatant & analysis of the LAL signal over LAL WT signal peptide and normalized on the volume of supernatant and VCNs. **E.** Ratio of LAL activity in supernatant over LAL WT signal peptide and normalized on VCNs.*

We initially transduced K562 cells with the 7 LVVs encoding LIPA transgenes (Figure 36.A). We achieved efficient LVV integration 7 days after transduction with all the constructions (VCN around 25 copies, Figure 36.B). Upon LVV integration, we observed stable expression of LAL protein for the 7 LIPA constructions on WB. Nonetheless, the amount of LAL expression varies according to the SP used. In fact, SP6, SP7 and SP8 provide the strongest LAL expression in K562 with an increase around 10-fold normalized to SP1 (Figure 36.C). SP2, SP 9 & SP10 provide ~5-fold increase of LAL expression (Figure 36.C).

The increase of LAL expression leads to an improvement of enzyme secretion in the culturing medium as measured on WB. We observed a good correlation between LAL expression and secretion. Thus, SP6, SP7 and SP8 also provide the strongest LAL secretion while SP10 does not provide any LAL secretion advantage (Figure 36.D). We confirmed that the addition of signal peptide did not impact the activity of LAL enzyme and observed an increase up to 3-fold of LAL activity in supernatant with SP6, SP7 and SP8 (Figure 36.E). The LAL activity remains lower than the expression and secretion that could indicated secretion of the non-active LAL form.

In K562 cells, SP6, SP7 and SP8 contribute to better production and secretion of active LAL compared to WT SP (SP1). To confirm this result, we tested these SPs into human CD34+ HSCs.

6.3.1.2 Signal peptide optimization in CD34+ cells

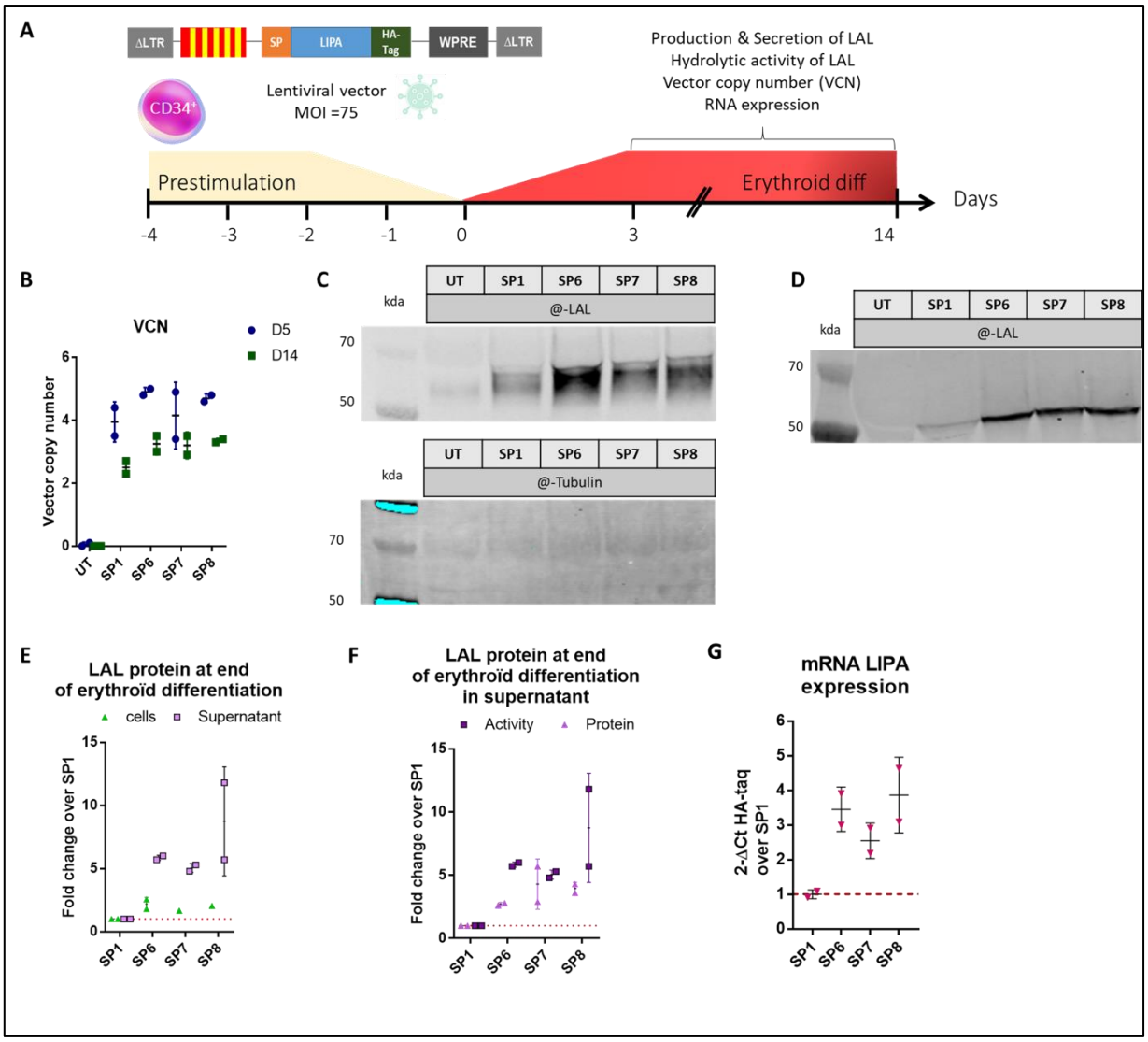

Figure 37) Signal peptide in CD34+

A. *Experimental layout of the viral infection of CD34+ and the erythroid differentiation* ***B.*** *Vector copy number at day 5 and 14 erythroid differentiation of transduced CD34+.* ***C.*** *WB of the CD34+ lysate in the end of differentiation (day 14) labelled with @-LAL & @-Tubulin* ***D.*** *WB of CD34+ supernatant during erythroid differentiation marked with LAL.* ***E.*** *Fold change of LAL protein in the end of differentiation in CD34+ lysates or supernatant over SP1* ***F.*** *Fold change of LAL protein & activity in the end of differentiation in CD34+ supernatant over SP1 treated cells* ***G.*** *Quantification mRNA of LIPA with HA-tag primer on hGAPDH in the end of differentiation (D14).*

We transduced CD34+ HSCs with LVVs encoding SP6, SP7 and SP8 LIPA transgene. 2 days after transduction, we initiated CD34+ erythroid differentiation for 14 days to measure the LAL expression and secretion in erythroid differentiated population (Figure 37.A). We observed stable integration of the LVV into CD34+ genome with around 3 copies per cells in the end of erythroid differentiation (Days 14) (Figure 37.B). We measured the LAL expression in cell lysate and secretion in culturing medium by WB using detecting LAL-antibody (Figure 37.C & D). In erythroid differentiated population, the loading control (Tubulin) was not detected, and we used the visible band at 70 kDa as normalizer. We observed 2-fold increase of LAL expression (Figure 37.E) in line with the 2-fold increase of LIPA transcription (Figure 37.G) measured by RT-qPCR. The LAL secretion in culturing medium increased up to 5-fold (Figure 37.E). Erythroid secreted LAL conserves its hydrolytic activity thus we observed a good correlation between LAL protein detected by WB and the LAL activity (Figure 37.F). In CD34+, SP8 results in the strongest LAL expression upon erythroid differentiation. Then, we performed a codon optimization on SP8 LIPA construction that use synonymous codon more accessible into the cells to increase the protein expression.

6.3.1.3 Codon optimization of SP8 LIPA construction on CD34+

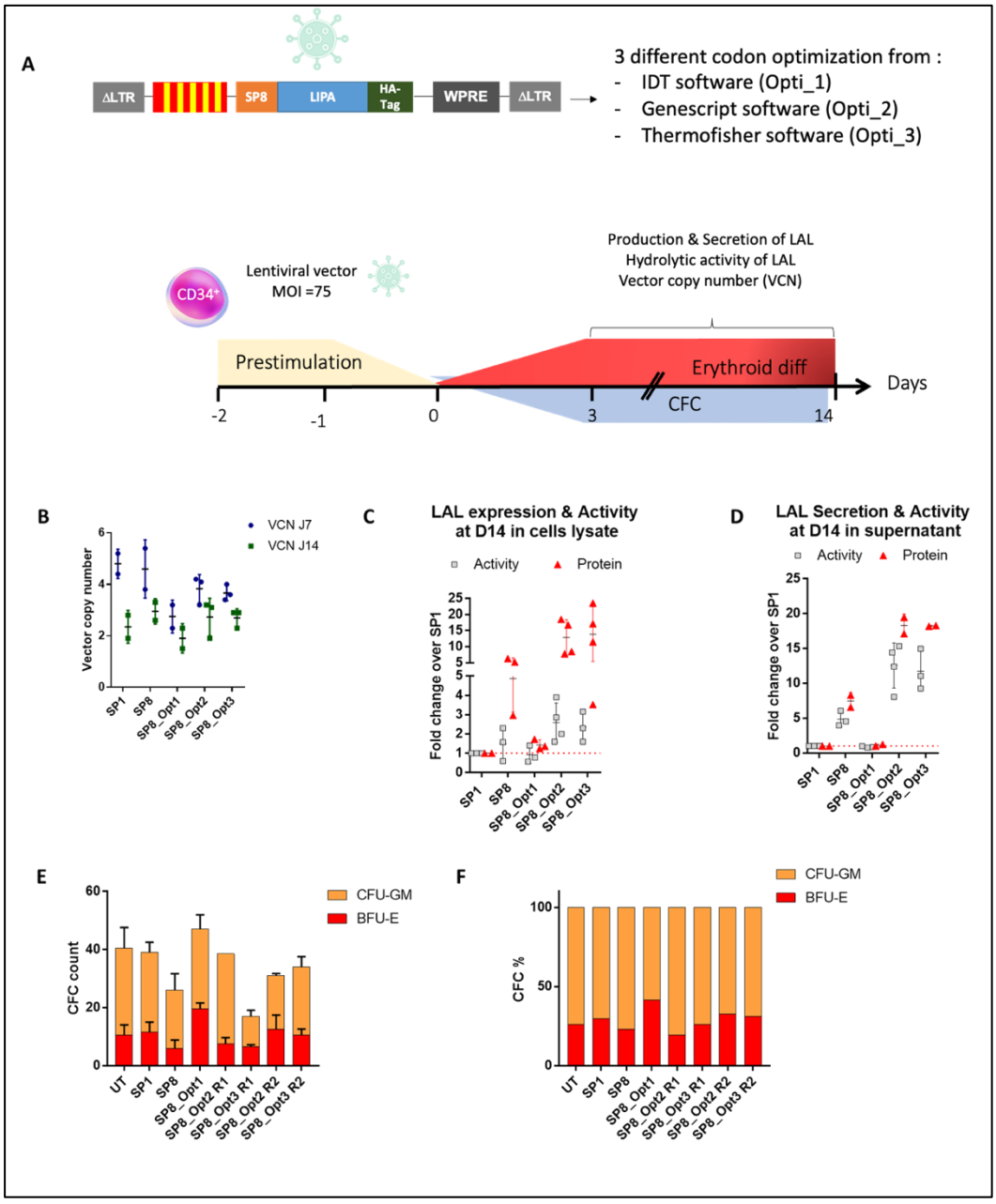

Figure 38) Codon optimization of SP8 LIPA in CD34+

A. *Experimental layout of the viral infection of CD34+ and the erythroid differentiation* ***B.*** *Vector copy number at day 7 and 14 erythroid differentiation of transduced CD34+.* ***C.*** *LAL expression & activity in the cells lysate at the end of erythroid differentiation (D14)* ***D.*** *LAL expression & activity in the supernatant at the end of erythroid differentiation (D14)* ***F&G.*** *CFC count and percentage in untreated and LV transduced CD34+*

We performed codon optimization of SP8 construction using 3 online software to maximize protein expression. We transduced hCD34+ HSCs with either SP1, SP8 or the 3-codon optimized SP8 LVVs. 2 days after transduction, we initiated erythroid differentiation, and we performed colony forming units (CFU) to assure the multilineage potency of LV-transduced HSCs (Figure 38.A). We achieved a stable LV transduction in HSCs with around 3 copies per cells. The integration of LIPA construction leads to a strong LAL expression in cell lysate that is augmented with Optimization 2 & 3. In fact, we reached 15-fold more LAL protein which is twice more than with SP8. and 2-3-fold of LAL activity compared to SP1 (Figure 38.C). Nonetheless, the codon optimizations 2 & 3 lead to a 15-fold increase of LAL secretion and activity in erythroid culturing medium indicating that the LAL erythroid secreted conserves its hydrolytic activity while optimization 1 doesn't enhance LAL secretion.

Transduction of CD34+ with LIPA LVVs induced a minimal toxicity on lineage reconstitution for SP8, Optimization 1 & 3 constructions as observed in the CFU experiment (Figure 38.E) without changing the proportion of white or red colonies (Figure 38.F). With Optimization 2 construction, the lineage reconstitution was variable between replicates and lower compared to UT population (Figure 38.E) although the proportion white or red colonies remains unchanged (Figure 38.F). Therefore, erythroid expression of LAL remains a safe strategy that doesn't affect the multilineage potential of hCD34+.

Conclusion

Both the signal peptide and the codon optimization result in a 15-fold increase of LAL functional secretion on erythroid differentiated hCD34+. It also highlights the importance of the proper transgene design to maximize its expression thus the therapeutic strategy. The optimization of the LIPA transgene gave rise to a French and international patent (EP 20 306524.8).

6.3.2 Novel cytometry-based characterization of lysosomal storage disease affected patient's cells

Introduction

To further investigate the lipid accumulation in WD fibroblasts, we developed a multi-modal cytometry-based approach. With this approach, we also assessed GT for LAL-D via LVV delivery of a functional LIPA gene into WD patients' fibroblasts. The lipids and lysosome accumulation of WD patients' fibroblasts was investigated through fluorescence microscopy and confocal microscopy upon neutral lipid staining (Nile Red) and lysosome staining (LysoGreen). Using flow cytometry, we explored the granularity changes caused by lipid accumulation. Then, we took advantage of the IFC to analyze fluorescent signal and quantify fluorescent vesicle per cells. We validated the cytometry pipeline on engineered LIPA KO human blood cell line and on peripheral blood mononuclear cells (PBMCs) from LIPA KO mouse model.

Novel cytometry-based characterization of lysosomal storage disease affected patient's cells

Marine LAURENT 1, 2 (*), Jérémie COSETTE 1 (*), Giulia PAVANI 1,2, Sarah BAYOL 1,2, Daniel STOCKHOLM 1,3, and Mario AMENDOLA

1. Genethon, 91000, Evry, France
2. Université Paris-Saclay, Univ Evry, Inserm, Genethon, Integrare research unit UMR_S951, 91000, Evry, France
3. Ecole Pratique des Hautes Etudes, PSL Research University, Paris, France

Key Words: Wolman disease, lysosomal acid lipase, lysosomal storage disorder, flow cytometry, imaging cytometry, gene therapy, CRISPR/Cas9

Abstract

Wolman disease (WD) is a severe lysosomal storage disorder (LSD) characterized by fatal lipid accumulation and caused by deficiency of the lipid metabolic enzyme, Lysosomal Acid Lipase (LAL), involved in the lysosomal hydrolysis of cholesterols and triglycerides. Due to the imbalance of lipids homeostasis, Wolman patient suffers from hepatosplenomegaly, hepatic failure and adrenal calcification resulting in a premature infant death within the first year of age (Kohli et al., 2020; Aguisanda et al., 2017a). In this work, we explored different cytometry modalities to fully characterize the phenotype of LAL deficient cells. In particular, we analysed WD patient's fibroblasts stained with Nile Red (NR), marker of intracellular lipid droplets, and Lysogreen (LG), marker of lysosomes, on fluorescence wide field microscope, confocal microscope, conventional and image flow cytometer. To ensure that lipid homeostasis imbalance is coming from the LAL- deficiency (LAL-D) itself, we integrated a functional version of the *LIPA* gene into WD fibroblasts.

We observed that WD fibroblasts have a higher fluorescence intensity and granularity as well as an increased number of lipids droplets and LG spots than healthy cells. Using 3-d dimension confocal, we observed that the higher intensity of LG is due to an increase in the number of lysosomes.

Finally, since fibroblasts are not easily accessible cells, we investigated the lipids deposits in engineered LIPA KO white blood cell lines to mimic easily accessible peripheral blood mononuclear cells (PBMC) and on PBMCs from LAL-D mouse model.

Overall, these analyses can help to diagnose the disease and to monitor over time the phenotype progression and correction upon treatment. We expect that this sensitive analysis pipeline could be used to evaluate the success of gene correction strategies and implemented to study and diagnose other lysosomal storage disorder (LSD).

Introduction

Lysosomal Storage Disorders (LSD) are inborn metabolism errors caused by defective lysosome function that results in toxic metabolites accumulation in various organs and tissues (Rajkumar and Dumpa, 2022). Among these disorders, lysosomal acid lipase deficiency (LAL-D) is caused by mutations in the lipase A (*LIPA*) gene encoding for the LAL enzyme involved in the lysosomal hydrolysis of neutral lipids into cholesterol ester (CE) and triglyceride (TG). The phenotypic spectrum of LAL-D depends on the residual enzymatic activity and ranges from the severe infantile-onset (Wolman disease, WD) to milder later-onset forms (cholesteryl ester storage disease, CESD). Wolman patients represent ~1/300,000 live births with less than 5 % of functional LAL enzyme and suffer from hepatomegaly, splenomegaly and hepatic failure leading, without treatment, to premature infant death in the first year of life (Li and Zhang, 2019; Aguisanda et al., 2017a; Pericleous et al., 2017)

In physiological conditions, the excess of circulating neutral lipids is stored in cells within structure called lipid droplets (LD) involved in diverse functions as cell survival, lipid cell homeostasis and protein storage (Cohen, 2018; Fujimoto et al., 2008). In LAL-D patients instead, both lysosomes and LDs tend to accumulate and prevent cells from having a normal metabolism impairing the whole organ function (Dubland and Francis, 2015).

Enzyme replacement therapy (ERT) is the only available supportive treatment and consists in the injection of the missing LAL enzyme to restore lipid homeostasis (Potter et al., 2021; Pastores and Hughes, 2020; Erwin, 2017). LAL-D diagnosis relies on symptoms appearance in the first week of life, on LAL enzymatic activity evaluation on a blood dried sample, and on the identification of the underlying *LIPA* mutations (Kohli et al., 2020; Lukacs et al., 2017). While precise and quantitative, these methods struggle to assess the lipid phenotype and disease progression.

Improving patient care and developing curative approaches for LAL-D require both a better characterization of the disorder and a pipeline to follow-up the treatment and its therapeutic effects overtime. Here, we describe a multi-modal cytometry approach aiming to better discriminate the phenotype of WD and healthy cells and to evaluate the outcome of gene therapy by restoring LAL enzymatic activity via the integration of a functional LIPA gene into WD patients' fibroblasts.

We first investigated lipids and lysosome accumulation in WD fibroblasts through fluorescence microscopy and confocal microscopy as previously described (Aguisanda et al., 2017b; Pham et al., 2005; Greenspan et al., 1985). Then, we analyzed WD fibroblasts granularity changes

caused by lipid accumulation using flow cytometry to increase the number of acquired events and the speed of the analysis.

To combine fluorescence microscopy with the statistical power of cytometry, WD fibroblasts were analyzed with an imaging flow cytometer (IFC), which enables the acquisition of an image of each cell in bright field and fluorescent channels. Combined together, single-cell fluorescence imaging and image processing allowed us to localize and count the fluorescent spots in each cell.

Finally, paving the way towards blood sample analyses, we used our analysis workflow to investigate the lipids deposits in engineered LIPA KO white blood cell lines mimicking easily accessible peripheral blood mononuclear cells (PBMC) and on PBMCs from LAL-D mouse model.

Materials and methods

Cells and reagents

Cell culture and transduction

Cell culture

Human primary fibroblasts were obtained from the NIGMS Human Genetic Cell Repository at the Coriell Institute for Medical Research: GM 11851 and GM06124 (Wolman disease fibroblasts) and GM 08333 and GM 00041 (healthy donor fibroblasts). Fibroblasts were maintained in Dulbecco's Modified Eagle Medium (DMEM) medium supplemented with 2mM Glutamax (Gibco by Life Technology), 15% of FBS (FBS, BioWhittaker, Lonza) and 100U/ml of penicillin/Streptomycin (Gibco).
K562 cells (ATCC® CCL-243, erythroleukemia cells) and Jurkat (ATCC® TIB-152, Lymphoblasts) were maintained in RPMI 1640 medium containing 2mM glutamine and supplemented with 10% fetal bovine serum (FBS, Lonza, Basel, Switzerland), 10mM HEPES, 1mM sodium pyruvate and penicillin and streptomycin (100U/ml each; Gibco, Waltham, MA, USA).

LV vector cloning and production

The WT LIPA cDNA was cloned into a standard lentiviral vector (LV) backbone (Follenzi et al., 2000) in antisense orientation with respect to its LTR. The cassette was inserted under the control of human β-globin promotor (Montiel-Equihua et al., 2012) and with the posttranscriptional regulatory element of woodchuck hepatitis virus (WPRE) sequence in the 3′ untranslated region of coding sequences.

LV were produced by transient transfection of 293T using third-generation packaging plasmid pMDLg/p.RRE, pK.REV, and pseudotyped with the vesicular stomatitis virus glycoprotein G (VSV-G) envelope. LV were titrated in HCT116 cells65 and HIV-1 Gag p24 content was measured by ELISA (Perkin- Elmer) according to manufacturer's instructions. The final product was formulated in sterile X-vivo 20 (Lonza, Basel, Switzerland) and stored at −80 °C.

Fibroblasts transduction

3 x 10^6 fibroblasts were seeded and cultured in a 6-well plate (Nunclon Delta Surface, Thermofisher). Cells were transduced, 1 day after seeding, at a MOI of 100 with a VSG-pseudotyped lentiviral vector encoding the human LIPA gene.

LIPA KO cell lines:

Editing

3 LIPA gRNAs (Gene Knockout kit V2, Synthego, CA, USA) were diluted following manufactuer's instruction and ribonucleoprotein complexes were formed with 30 pmol of SpCas9 (ratio 1:2), kindly provided by Dr. J.P. Concordet, and 30 µM of Alt-R Cas9 Electroporation Enhancer (1075915, IDT). 250 000 of Jurkat and K562 cells were electroporated with 3 µL RNP complex and 18 µL of Amaxa buffer solution : SE cell line 4D-Nucleofector kit (Electroporation program: FF-120) and SF cell line 4D-Nucleofector kit (Electroporation program: FF-120) respectively according to manufacturer's instructions (Lonza, Basel, Switzerland). The day after electroporation cells were washed once in sterile PBS and resuspended in 500 µL of fresh medium.

Quantification of the KO:

Genomic DNA was extracted with QuickExtract™ DNA Extraction Solution (Lucigen, Middelton, WI, USA). Genomic DNA were amplified next to cutting site of gRNAs (Sequence Forwad: TCACTGCTACCTTGCCAGTG; Sequence Reverse: CCTTACTGCTAGTCATTAAATTCCTAGC) using KAPA2G Fast ReadyMix (Kapa Biosystem, Wilmington, MA, USA). Upon genomic edition, three bands were expected: undeleted one at 571bps (no-gRNA cutting: WT sequence or single gRNA cutting), deleted band at 500 bps (deletion with 2 gRNAs :either 1&2 gRNAs or 2&3 gRNAs) and another deleted band at 432 (deletion with 2 gRNAs : 1&3 gRNAs) (Fig 4.A). PCR products were loaded in a 1% agarose gel and the three bands were quantified using ImageJ. The ratio of each band in percentage was calculated with the following formula:

$$Ratio\ (\%) = \frac{Mean\ bands\ intensity}{Single\ band\ intensity} * 100$$

The % of editing in the undeleted bands (571 bps) was quantified after sequencing with TIDE analysis (Synthego, ICE). The final % of editing was calculated as follow:

$$Total\ editing\ (\%) = \%\ ratio_{500bps} + \%\ ratio_{432bps} + (\%\ ratio_{571bps} X\ \%\ editing_{571bps})$$

LAL-D mPBMCs analysis:

LAL-D mouse model:

The LIPA KO mouse model has a deletion of the exon 4 in the murine LIPA gene and were kindly provided by Dr. Kratky, University of Graz, Austria. Mice were maintained in a specific pathogen-free (SPF) environment with a regular light-dark (12 h/12 h) cycle and ad libitum access to food and water This study was approved by ethical committee CEEA-51 and conducted according to French and European legislation on animal experimentation (APAFiS#24477-201912230940416 v1). 6-months LAL-D and WT littermates were used for the blood processing.

Blood processing:

Blood of LAL-D and WT mice were collected after Isoflurane anaesthesia (IsoFlurin, Axience) from the retro-orbital veins with heparinized capillary and collected into 3, 8% citrate Eppendorf tube. Then, red blood cells (RBCs) were lysed using ACK solution (Thermo-Fisher Scientific, Waltham, MA, US) according to manufacturer's instructions. mPBMCs were either resuspended in PBS and analyzed unstained or stained with NR : mPBMCs were incubated 30 min at 37°C with 1:1000 diluted NR. After staining, cells were washed once in sterile PBS and resuspended in PBS solution prior flow cytometry and image flow cytometry analysis.

Biochemical analyses

Western blot

To detect intracellular proteins, fibroblasts were lysed in RIPA buffer (Sigma-Aldrich, St.Louis, MI, USA) supplemented with protease inhibitor (Roche, Basel, Switzerland), freezed/thawed and centrifuged 10 minutes at 14,000 rcf at 4 °C. Total protein was quantified using BCA assay (Thermo-Fisher Scientific, Waltham, MA, US). 30 µg of protein were denatured at 90 °C for 10 minutes, run under reducing conditions on a 4–12% Bis-tris gel and transferred to a nitrocellulose membrane using iBlot2 system (Invitrogen, Waltham, MA, US). After Ponceau staining (Invitrogen, Waltham, MA, US), membranes were blocked for 2 h with Odyssey blocking buffer (Odyssey Blocking buffer (PBS), Li-Cor Biosciences, Lincoln, NE, USA) and incubated for 1 h with primary antibodies: mouse anti-hLAL (Thermofisher, 9G7F12, 7G6D7, dilution 1:2000) followed by specific secondary antibodies in PBS:Blocking buffer : goat anti-mouse IgG (H+L) at 800CW (Li-Cor Biosciences, dilution 1:15 000). α-actinin (sc-17829, mouse monoclonal, Santa Cruz Biotechnology) was used as loading control. Blots were imaged at 169 µm with Odyssey imager and analysed with ImageStudio Lite software (Li-Cor Biosciences, Lincoln, NE, USA). After image background subtraction (average method, top/bottom), band intensities were quantified and normalized with α-actinin signal.

LAL activity assay:

Protein activity was detected in supernatants as previously described (Aguisanda et al., 2017b; Hamilton et al., 2012) with some modifications. Samples were incubated 10 minutes at 37 °C with 42 µM Lalistat-2 (Sigma-Aldrich, St. Louis, MI, USA), a specific competitive inhibitor of LAL, or with water. Samples were then transferred to a Optiplate 96 F plate (PerkinElmer) where fluorimetric reactions were initiated with 75 µl of substrate buffer (340 µM of 4-Methylumbelliferyl phosphate (4-MUP), 0.9% Triton X-100 and 220 µM cardiolipin in 135mM acetate buffer pH 4.0). After 10 minutes, fluorescence was recorded (35 cycles, 30 seconds intervals, 37 °C) using SPARK TECAN Reader (Tecan, Austria). Kinetic parameters (average rate, RFU/min) were calculated using Magellan Software and the relative LAL activity was calculated as follow:

$$Relative\ LAL\ activity = \frac{Signal\ \ without\ Lalistat}{Signal\ \ with\ Lalistat}$$

Cytometry

Flow cytometry

3 x 10^5 fibroblasts were detached with TrypLE (Gibco, Waltham, MA, USA) or 3 x 10^5 LIPA KO cell lines were spun down (500 rpm 5 min) and stained with Nile Red (dilution 1:1000, NR) or LysoGreen (dilution 1:1000, LG) (Abcam, Cambridge, UK) as per manufacturer's instructions. Then, cells were washed once and resuspended with sterile PBS. Cells were analyzed using CytoFLEX S after laser calibration with Daily QC Fluorospheres (Beckman Coulter, Pasadena, CA, USA). Live cells were gated using forward and side scatter and about 9 000 cells were analysed. Unstained cells were used as negative controls. Data were elaborated with FlowJo software (Tree Star, OR, USA) or Kaluza (Beckman Coulter, Pasadena, CA, USA).

Image Flow Cytometry

Stained cells, as above, were acquired using an Image Stream X MKII (Amnis, Luminex, USA) with INSPIRE software (Amnis, Luminex, USA). Analyses were performed using IDEAS 6.1 software (Amnis, Luminex, USA). A first histogram of gradient root mean square (RMS) was plotted to exclude cells out of focus. A common Area vs Aspect Ratio dot plot allowed us to exclude cell doublets. Then, in the population of single cells, we analysed four parameters: the staining (NR or LG) fluorescence intensity and spot count per cell, the SSC (side scatter) autofluorescence intensity and spot count per cell. For SSC and NR, a spot is detected when its mean intensity reaches 20 times the average cell background ratio. For LG, a spot is detected when its mean intensity reaches 15 times the average cell background ratio. On average, 5 000 cells were analysed per experiment.

Image acquisition

Fluorescence Microscopy

8 x 10^4 fibroblasts were seeded and cultured in a 6-well plate (Nunc). After 5 days, cells were stained with Nile Red (Dilution 1:1000, Nile Red staining kit, Abcam) or with Lysogreen (Dilution 1:700, Lysosomal staining kit-Green Fluorescence, Abcam) as per manufacturer's instructions. 8 fields for each condition were randomly acquired with an inverted fluorescence microscope (EVOS, Life Technologies, USA - 10X magnification) and average fluorescence intensity per cell was calculated with a custom-made ImageJ plugin.

Confocal Microscopy

3 x 10^4 fibroblasts were seeded and cultured in a MatTEK (MatTek corporation, 35 mm Glass bottom, USA). After 3 days, cells were first stained with Lysogreen (20 min at 37°C) and cells washed once Dulbecco's phosphate-buffered saline (DPBS, Gibco). Then, fibroblasts were stained for 15 min at 37°C with 5 µM Draq5 (Abcam), 10 µM Wheat Germ Agglutinin (WGA, Thermofisher) that binds non-specifically to cell membranes and washed in Hanks' Balanced Salt Solution (HBSS , Gibco). Plates were acquired with a LEICA TCS SP8 confocal microscope (LEICA, Germany) using a HC PL APO CS2 63X 1.4NA oil immersion objective. For each field of view, a stack of the whole cell layer was acquired (1 image every 0.4 µm). Several fields were acquired and quantified per condition.

Image analysis

Fluorescence Microscopy

Fluorescence images of fibroblast were quantified using a custom-made ImageJ plugin. Images were first segmented using a manual threshold, which is chosen to optimize cell contour detection. Once thresholded, an area corresponding to the cell is automatically detected and the mean fluorescence intensity inside the cell is measured using the Analyze Particle feature.

Confocal Microscopy

3-Dimensional images of fibroblasts were reconstructed and quantified using Imaris Sofware (Oxford Instruments, UK). The total number spot was measured using the spot feature of Imaris, with an

estimated spot diameter set at 400 nm. The total number of spots was divided by the number of cells in the field of view, counted as the number of nucleus, to finally obtain the average number of spot per cell in a the field of view.

Statistical analysis

Statistical analyses were performed using GraphPad Prism version 6.00 for Windows (GraphPad Software, La Jolla, CA, USA, "www.graphpad.com"). One-way or two-way analysis of variance (ANOVA) with Dunn's or Dunnet's multiple comparison post-test were performed as indicated (alpha = 0.05). Values are expressed as mean ± standard error of mean (SEM) as otherwise indicated.

Results

We obtained and characterized primary fibroblasts from two heathy donors (HD) and two WD patients. First, we confirmed that LAL protein (Fig 1.A) and enzymatic activity (Fig 1.B) were strongly reduced in patient's cells. Then, we analyzed the phenotype of fibroblasts by fluorescence microscopy. Cells were stained either with Nile red (NR), a marker of neutral lipids, or with LysoGreen (LG), a lysosomal dye. NR mean intensity in WD fibroblasts was about 2.3-fold more intense than HD fibroblasts (mean 5.75 ± 0.8 and 13.2 ± 5.7respectively), which confirms lipid accumulation in impaired cells (Fig 1. C-D). The intensity of the lysosome staining (LG) increases along with NR, showing higher intensity in WD fibroblasts than HD (mean 9.35 ± 2 and 7.9 ± 2.3 respectively), although cellular heterogeneity was more important (Fig 1. C-E). To confirm that the WD fibroblast phenotype is due to the absence of LAL and can be corrected with gene therapy, we introduced a hLAL functional transgene by LV mediated gene addition (WD3_LV). LV treated WD fibroblasts show a significant reduction of the lipids deposit compared to the untreated counterpart (Fig 1. C-D, mean NR intensity: 6.1 ± 1.1) and lysosome mean fluorescence intensity (Fig 1. C, E, mean LG intensity: 7.4 ± 1.6). The observed higher LG signal in WD fibroblasts could be due to an increase in the number and/or size of lysosomes. Using confocal microscopy, we could localize LG signal inside the cytoplasm compartment, as expected (Fig1.F) and we counted lysosomal vesicles by 3D images reconstruction. WD fibroblasts exhibited around 1.7 more lysosomal vesicles compared to HD or WD_LV fibroblasts (Fig 1. F-G, mean vesicles count per cell: 391 ± 86.5 for WD; 149.2 for HD ± 27.3; 155 ± 66.9 for WD_LV).

Overall, analyses of lipid content and lysosomal vesicles using microscopy allows the investigation of WD fibroblasts phenotype. Confocal microscopy provides more information, but it is time-consuming in both acquisition and analysis of images, thus limiting the number of cells that can be analyzed.

Flow cytometry is the gold standard method for analyzing and phenotyping high amount of cells in a short amount of time (Hasegawa et al., 2013). We therefore measured the fluorescence signals from fibroblasts stained with LG or NR by flow cytometry (Fig 2). NR intensity of WD fibroblasts was about 2.5 ± 0.4 fold higher compared to healthy ones (Fig 2.A) confirming the cell lipid accumulation observed with microscope analysis. Surprisingly, LG signal did not change between WD and healthy fibroblast (Fig 2.B) and could indicate a loss of information with LG staining in fibroblasts detached with enzymatic treatment. Interestingly, Side scatter signal (SSC), which measures the internal complexity as granularity of a cell, of

WD fibroblasts remains higher that healthy ones (Fig 2.C) indicating that the accumulation of LDs increases the granularity of WD fibroblasts. Insertion of a functional copy of LIPA gene decreased the lipids accumulation by 1.8 ± 0.8 fold compared to WD fibroblasts without achieving a normal lipid content (Fig 2.A-C).

In order to combine speed of analysis and statistic power of flow cytometry with precise vesicle quantification offered by microscopy, we took advantage of image flow cytometry (IFC), which allows measuring fluorescence intensity as well as localizing and counting the fluorescent spots per cell (Holzner et al., 2021). We used IFC to analyze NR, LG and SSC intensity as well as spot counting per cell. Fluorescence intensity follows the same tendency observed with conventional flow cytometry.

WD fibroblasts accumulate lipids (WD NR mean intensity 3.7± 1.7 Fig 3.A-B) and surprisingly, the counting of fluorescent NR spots per cells emphasized the fold change between healthy and patient donors by 100-fold while lysosomal vesicles spot counting does not exhibit such a strong difference compared to healthy donor (Fig 3.C).While, the difference between LG intensity and spot count in WD fibroblasts remains similar, and does not provide a clear distinction between WD and HD fibroblasts. As before, LV treatment partially corrected cell phenotype and reduced the lipid accumulation. IFC provides not only a SSC signal but also a SSC image, permitting to localize and quantify the spots of higher granularity (Marina et al., 2012). As observed with flow cytometry, the SSC intensity pattern discriminates the different phenotypes. Moreover, counting the spots of higher granularity appear to be more efficient for discriminating WD fibroblast from healthy fibroblast: 3± 1 fold for intensity and 127- fold ± 83 for spot counting (Fig 3.C), making SSC spot counting an interesting method for label free discrimination of phenotypes.

At this stage, analysis of lipid vesicles with cytometry methods appears to be a promising way to confirm the underlying diagnosis or to assess the efficiency of treatment. Nevertheless, access to WD fibroblasts require patient's skin biopsies, therefore we decided to test our analysis on blood cells. Due to lack of patients' blood cells, LIPA KO cell lines were engineered to mimic peripheral blood mononuclear cells (PBMC).

From two PBMC well-known cell lines, K562 and Jurkat, we generated *LIPA* KO cell lines by deleting the exon 4 of the *LIPA* gene using the CRISPR-Cas9 system. We combined three different gRNAs and we quantified the deletion efficiency via PCR (Fig. 4A). For the undeleted band, we performed a TIDE analysis to quantify the indel causing a frameshift

mutation. The KO efficiency of 95% and 83%, for K562 and Jurkat respectively, was calculated by considering both the deletion and the indel efficiency (Fig. 4A). We confirmed the generation of LAL KO cell lines by measuring the enzymatic activity. While in Jurkat cell lines the deletion of exon 4 of *LIPA* gene completely abolished the LAL enzymatic activity, in K562 cell line no activity was detected in both wild type and KO cells, suggesting that these cells do not express LIPA and were therefore used as negative control (Fig 4.B).

The lipid and lysosomal vesicles accumulation was monitored using the SSC signal as well as NR and LG labelled population with classic flow cytometry and image flow cytometry. In Jurkat *LIPA* KO cell line, an increase in all three parameters with both cytometry methods was observed, indicating an increase in lipids and lysosomes content (Fig 4.C). Interestingly, the spot counting with IFC strongly enhanced the differences between WT and KO Jurkat cells, by 9 ± 0.5 -fold for lipid content and 4 ± 3-fold for lysosomes and granularity (Fig 4.D).
In line with the absence of LAL activity, K562 KO population does not exhibit accumulation in lipid nor lysosome vesicles and behaves similarly to K562 WT cells (Fig 4.C-D).

To validate the feasibility of analysis pipeline on blood sample with take advance of mouse model having a deletion in Exon 4 of LIPA gene resulting in a total loss of LAL activity in homozygote mice for the deletion (Fig 4.E). Murine PBMCs (mPBMCs) from whole blood of LIPA KO mouse model has been stained with NR and analysed with conventional or image flow cytometry. Analysing LAL-D mouse in conventional flow cytometry shows a lipid accumulation in mPBMCs (Mean NR: 1.7± 0.3 Fig 4.F) resulting in an increase of granularity of cells (Mean SSC: 2.1 ± 0.04 Fig 4.F). While, the intensity of NR in IFC remains lower and variable than conventional flow cytometry and may be caused by the small amount of analysed cells (N=885 cells). Nonetheless, spot count on LIPA KO mPBMCs NR stained reinforces the difference with WT population by 6.5 ± 3 fold (Fig 4.G). Lipid accumulation on LIPA KO mPBMCs results in fold increase of granularity both observed in SSC signal (2.2 ±0.7 Fig. 4.G) and Spot count (2.3 ±0.7, Fig. 4.G).

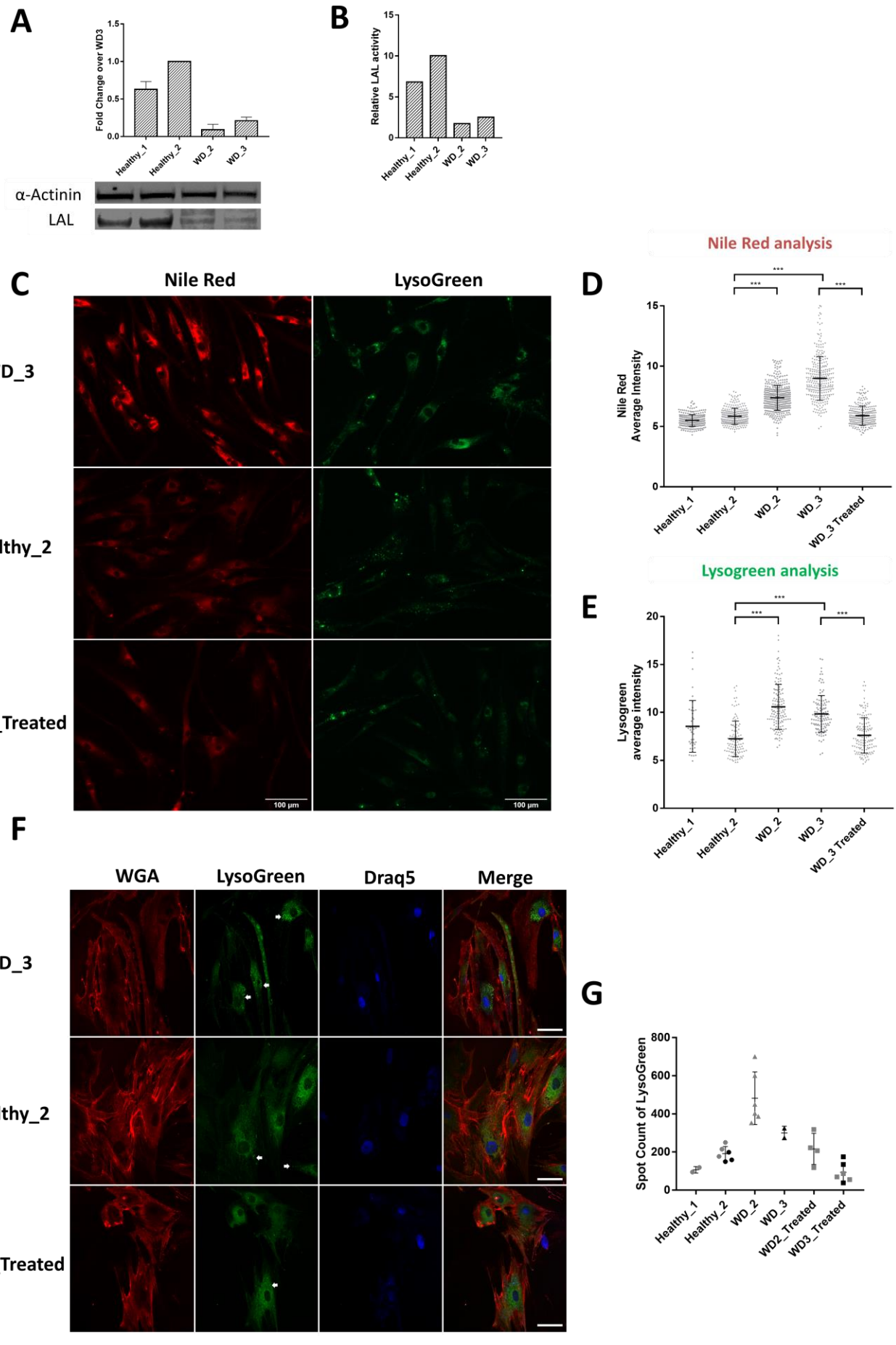
A
Fold Change over WD3
1.5
1.0
0.5
0.0
Healthy_1
Healthy_2
WD_2
WD_3
α-Actinin
LAL
B
Relative LAL activity
15
10
5
0
Healthy_1
Healthy_2
WD_2
WD_3
C
Nile Red
LysoGreen
WD_3
Healthy_2
WD3_Treated
100 µm
100 µm
D
Nile Red analysis
Nile Red
Average Intensity
15
10
5
0
***
***
***
Healthy_1
Healthy_2
WD_2
WD_3
WD_3 Treated
E
Lysogreen analysis
Lysogreen
average intensity
20
15
10
5
0
***
***
***
Healthy_1
Healthy_2
WD_2
WD_3
WD_3 Treated
F
WGA
LysoGreen
Draq5
Merge
WD_3
Healthy_2
WD3_Treated
G
Spot Count of LysoGreen
800
600
400
200
0
Healthy_1
Healthy_2
WD_2
WD_3
WD2_Treated
WD3_Treated

Figure 1: Biochemical and microscopic characterization of Wolman patients' fibroblasts. A: Western blot of LAL and α-actinin proteins **B:** LAL relative enzymatic activity in donor fibroblasts. **C:** Fluorescence microscopy images of fibroblasts stained with Nile Red (left panel) or Lysogreen (right panel). **D-E**: Quantification of mean fluorescence intensity (MFI) per cell of Nile Red (NR) (Kruskal-Wallis Test p***<0.0001; Healthy 1 = 270 cells, Healthy 2= 258 cells, WD_2 = 438 cells, WD_3 =288 cells, WD3_Treated = 253 cells) and Lysogreen (LG) (Kruskal-Wallis Test p***<0.0001; Healthy 1 = 42 cells, Healthy 2= 105 cells, WD_2 = 134 cells, WD_3 =113 cells, WD3_Treated = 134 cells). **F**: Confocal microscopy acquisition of fibroblasts stained with Wheat Germ Agglutinin (WGA) for cell membranes, Lysogreen for lysosome, Draq5 for the nucleus, and merge (X60). Scale bar 50 µm; White arrows indicate the lysosomal vesicles **G:** Quantification of the Lysogreen spot per cells based on confocal microscopy 3D acquisition. Each dot represents the analysis on one z-stack. Total analyzed cells: Healthy 1 = 21 cells, Healthy 2=87 cells, WD_2 = 94 cells, WD_3 =69 cells, WD2_Treated = 62 cells, WD3_Treated = 18 cells; black & gray dots represent experimental replicates.

Nile Red analysis

A

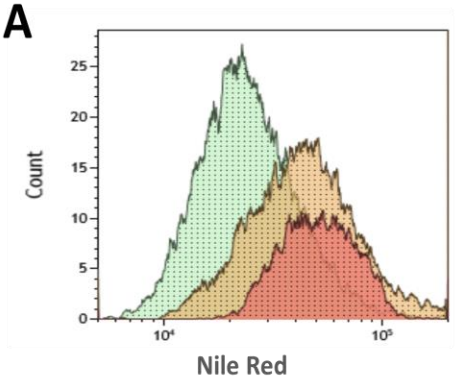

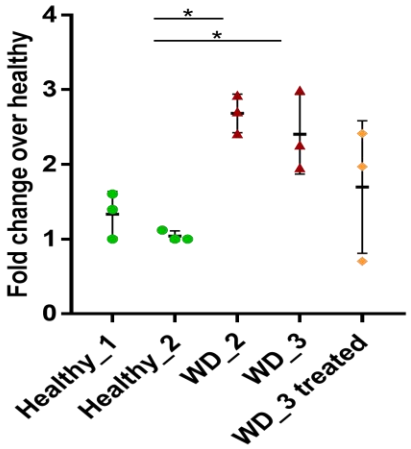

Lysogreen analysis

B

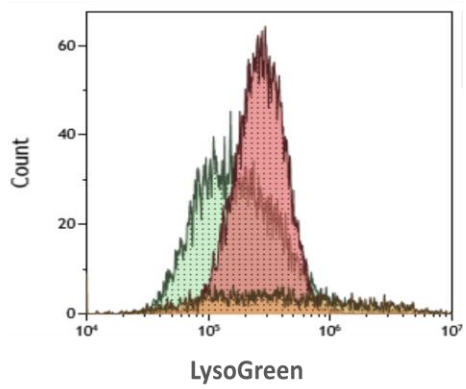

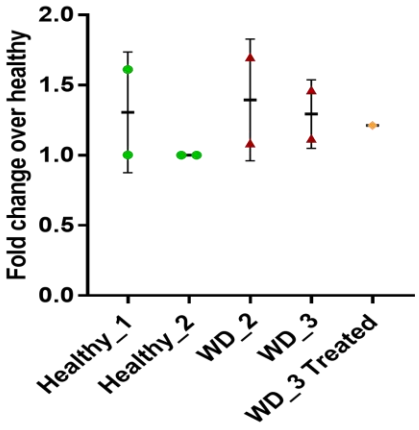

Side Scatter analysis

C

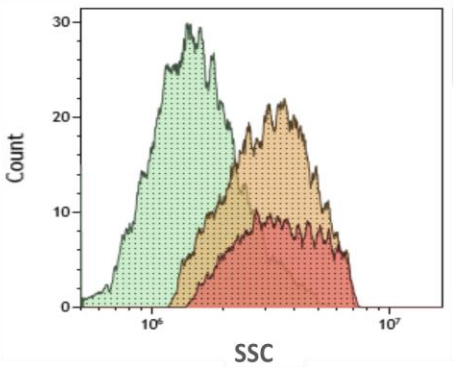

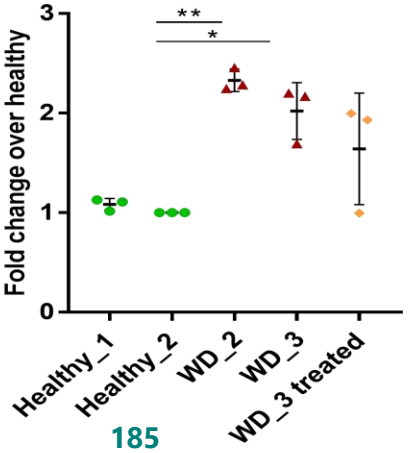

Figure 2: **Conventional flow cytometry analysis of donor fibroblasts'.** Each dot represents an experimental replicate. Statistic tests are two-way Annova with α: 0, 05. **A:** Fluorescence intensity histograms and fold change compared to Healthy_2 for NR staining. **B:** Fluorescence intensity histograms and fold change compared to Healthy_2 for LG staining. **C:** Side scatter intensity histograms and fold change compared to Healthy_2.

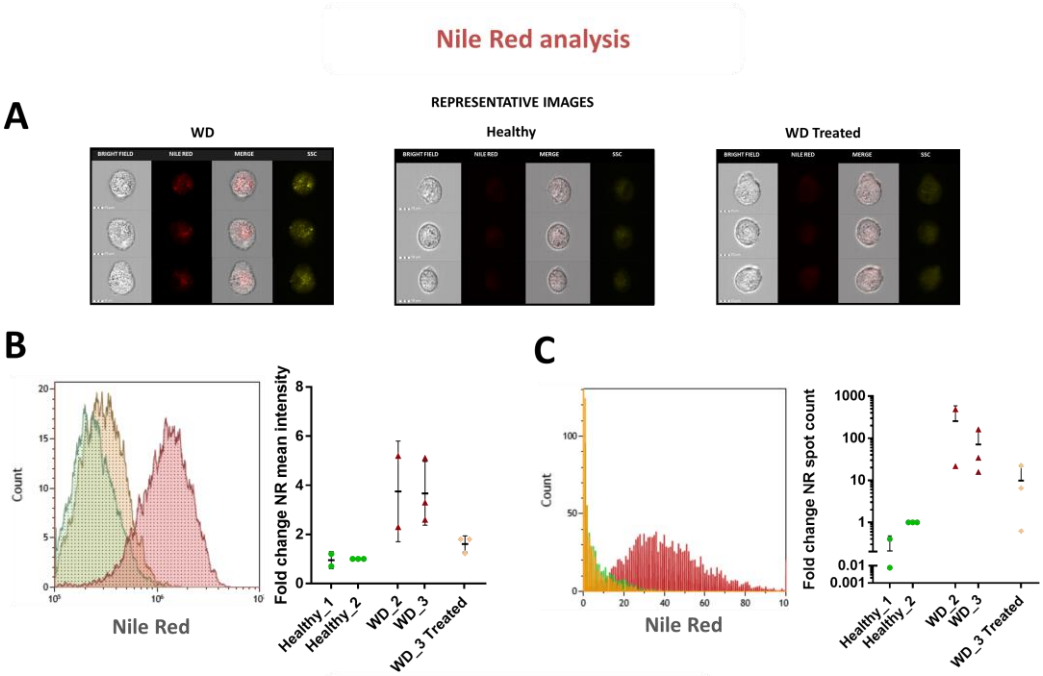
Nile Red analysis
A
REPRESENTATIVE IMAGES
WD
Healthy
WD Treated
BRIGHT FIELD
NILE RED
MERGE
SSC
B
C
Count
Nile Red
Fold change NR mean intensity
Fold change NR spot count
Healthy_1
Healthy_2
WD_2
WD_3
WD_3 Treated
Lysogreen analysis
D
REPRESENTATIVE IMAGES
WD
Healthy
WD Treated
BRIGHT FIELD
LYSOGREEN
MERGE
E
F
LysoGreen
Fold change LG mean intensity
Fold change LG spot count
Side Scatter analysis
G
H
SSC
Fold change SSC mean intensity
Fold change SSC Spot count

Figure 3: **Image flow cytometry of donor fibroblasts**. Each dot represents an experimental replicate. **A:** Representative image of NR stained fibroblasts on image flow cytometry. **B:** Fold change over Healthy_2 of NR mean intensity. **C:** Fold change over Healthy_2 of Nile Red mean spot count per cell **D:** Representative image of LG stained fibroblasts on image flow cytometry. **E:** Fold change over Healthy_2 of LG mean intensity **F:** Fold change of over Healthy_2 LG mean spot count per cell **G:** Fold change over Healthy 2 of SSC mean intensity **H:** Fold change over Healthy 2 of SSC spot count per cells.

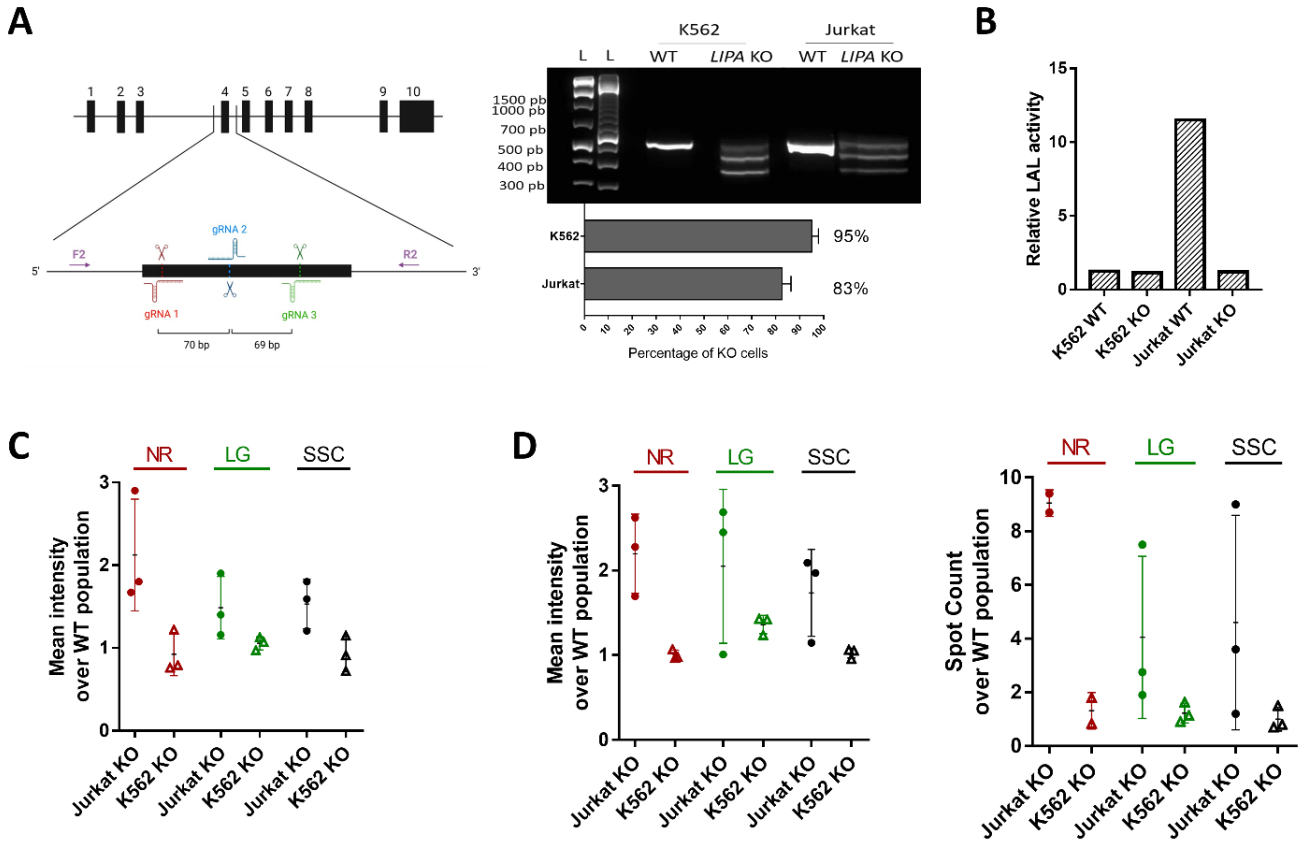
A
1 2 3 4 5 6 7 8 9 10
gRNA 2
F2
R2
5'
3'
gRNA 1
gRNA 3
70 bp
69 bp
K562
Jurkat
L L WT LIPA KO WT LIPA KO
1500 pb
1000 pb
700 pb
500 pb
400 pb
300 pb
K562
95%
Jurkat
83%
Percentage of KO cells
B
Relative LAL activity
K562 WT
K562 KO
Jurkat WT
Jurkat KO
C
NR
LG
SSC
Mean intensity over WT population
Jurkat KO
K562 KO
D
NR
LG
SSC
Mean intensity over WT population
Spot Count over WT population
E
LIPA gene
FRT
lacZ
loxP
SA
pA
LAL-D mouse model
LAL activity in liver 6 months
LAL activity (RFU/min)
WT
LAL-D
F
NR mean intensity Fold change over WT population
SSC mean intensity Fold change over WT population
G
Nile Red analysis
Side Scatter analysis
MFI NR Fold over WT
NR Spot count Fold over WT
SSC MFI Fold over WT
SSC Spot count Fold over WT

Figure 4: Characterization of LIPA KO cell lines: Jurkat and K562, and mPBMCs from LAL-D mice. A: Editing strategy with the percentage of KO generated and **B:** the LAL enzymatic activity in function of the cell lines. **C:** Fold change of NR, LG and SSC of stained cells in function of the WT population with conventional flow cytometry. Each dot represents an experimental replicate. **D:** Fold change of NR, LG & SSC mean intensity & spot count in function of the WT population acquired with image flow cytometry. Each dot represents an experimental replicate. **E:** LAL activity on the liver of 6 months-old LAL-D mice **F:** NR and SSC MFI fold change over WT mouse acquired with flow cytometry. Each dot represents one analysed mouse. **G:** Fold change of NR and SSC mean intensity as well as spot count in function of the WT mouse acquired with image flow cytometry. Each dot represents an analysed mouse.

Discussion

In this present study, we explored the lipid deposits, lysosomal content and granularity of Wolman disease patients' derived fibroblasts with a combination of different cytometry methods: fluorescence wide field microscopy, confocal microscopy, conventional flow cytometry and image flow cytometry. A clear phenotype is well observed for LAL-D with all cytometry methods used. WD fibroblasts have a lipid vesicle accumulation compared to healthy donor, as it was already described (Pham et al., 2005; Fukumoto and Fujimoto, 2002; Brown et al., 1988; Greenspan et al., 1985). In line with an increase of lipid content, we observed with both confocal and fluorescence microscopy a higher intensity of lysosome staining (LG) in Wolman patient cells than in healthy ones (Aguisanda et al., 2017b). It suggests that lipid deposit increases the number of lysosome as an overcompensation mechanism for the loss of LAL function (Xu et al., 2012).

To confirm that the phenotypic observation was due to impaired LAL function, we inserted in WD fibroblasts a functional copy of the LIPA gene. Corrected WD fibroblasts show a significant reduction of the lipids deposit and absolute count of lysosomal vesicles indicating that LAL is the main cause of the phenotype and that gene therapy is an option to rebalance lipids homeostasis (Fig 1-3).

Although widely used to investigate the lipids content in WD, wide-field fluorescence microscopy (Aguisanda et al., 2017b; Pham et al., 2005; Brown et al., 1988) allows the processing and analysis of a limited number of cells doesn't allow a precise intracellular localization of the signal. In comparison, confocal microscopy provides 3-Dimensional reconstructed images of WD fibroblasts allowing precisely counting and confirming the expected cytoplasmic localization of the lysosomal vesicles (Fig 1. F-G). Nevertheless, confocal microscopy remains time-consuming and limited in terms of number of analyzed cells. To overcome these limitations, we analyzed WD fibroblasts via conventional flow cytometry and imaging flow cytometry (Fig 2-3). Both cytometry methods allows the analysis of a high number of cells in short time. Furthermore, together with labelling quantification, they allow measurement of the granularity change (SSC parameter) due to vesicle accumulation without any staining. IFC has the additional benefit of acquiring an image of each cell allowing to quantify the number and localize lipids and lysosomal vesicles within the cell. This spot counting feature allows refining the characterization of the disease's phenotype. In fact, we could observe a difference of ~100-fold in spots based on NR staining or granularity parameter (Fig 3 C, H). Since the number of LD increases more that their intensity, we can hypothesize

that cells respond to the metabolic stress by generating more lipids deposits rather than enlarging them.

Nevertheless, in our experiments LG signal appears variable among WD fibroblasts (Fig 1. C-E) or even does not provide a clear distinction between WD and HD fibroblasts (Fig 3. E-F). Here, we have assumed that LysoGreen only stains lysosomes, however, LysoGreen may not be too specific. Its fluorescence intensity increases with acidification, which occurs in several acidic cellular organelles including the Golgi apparatus, lysosomes and secretory vesicles (Demaurex, 2002). Therefore, while lysosomes are expected to exhibit the strongest fluorescence, other organelles may have contributed to the fluorescence of LysoGreen (Marina et al., 2012). Besides, fibroblasts undergo enzymatic treatment to detach them from culture dishes for cytometry analyses that could overall influence the cell pH and therefore the LG staining. Also, lysosomes are not only involved in the lipid accumulation (Schultz et al., 2011) and therefore may not be the best readout to characterize the LAL-D and to monitor overtime the disease progression.

To evaluate if the observed phenotype could be generalized to other cells, we analysed additional LAL-D cell lines. We choose hematopoietic cell lines to mimic PBMCs, as they are easily accessible material and could be used to monitor patients' disease progression and treatment. Since WD is a rare disease and to reduce patients' variability, we used CRISPR/Cas9 to generate isogenic LAL KO cell lines.

In particular, Jurkat cells, an immortalized line of human T lymphocyte cells, have been impacted by the KO of LAL enzyme and mimics the WD fibroblasts: accumulation of lipid vesicles and slight increase of lysosomal content (Fig 4. C-D). Finally, the difference is less that observed in WD fibroblasts, and could be explained by the smaller size of Jurkat cells compared to fibroblasts. We investigated the lipid accumulation also in mPBMCs from whole blood of LIPA KO mouse model and the NR spot count analysis demonstrate an increase similar to engineered Jurkat cells confirming the feasibility of analysis pipeline on blood sample (Fig 4. E-G). Previously, the lipid accumulation of LAL-D murine macrophage has been co-localized within lysosomes without increasing the lipid droplet markers (Schlager et al., 2017). Later, the co-localization of lysosomes and lipids would be investigated in our mPBMCs from LAL-D using Image flow cytometry. Overall, the proposed IFC analysis offers a fast and precise evaluation of LAL-D phenotype in patient PBMCs to complement the diagnosis or to follow-up the disease and its ERT treatments. Further, these methods of analysis could be used to develop new therapeutic option or applied on other LSD that suffers also from toxic accumulation as Pompe disease, Niemman Pick disease … (Platt et al., 2018; Xu et al., 2014)

References

Aguisanda, F., Thorne, N., Zheng, W., 2017a. Targeting Wolman disease and cholesteryl ester storage disease: disease pathogenesis and therapeutic development. Curr. Chem. Genomics Transl. Med. 11, 1.

Aguisanda, F., Yeh, C.D., Chen, C.Z., Li, R., Beers, J., Zou, J., Thorne, N., Zheng, W., 2017b. Neural stem cells for disease modeling of Wolman disease and evaluation of therapeutics. Orphanet J. Rare Dis. 12, 120. https://doi.org/10.1186/s13023-017-0670-9

Brown, W.J., Warfel, J., Greenspan, P., 1988. Use of Nile red stain in the detection of cholesteryl ester accumulation in acid lipase-deficient fibroblasts. Arch. Pathol. Lab. Med. 112, 295–297.

Cohen, S., 2018. Chapter Three - Lipid Droplets as Organelles, in: Galluzzi, L. (Ed.), International Review of Cell and Molecular Biology. Academic Press, pp. 83–110. https://doi.org/10.1016/bs.ircmb.2017.12.007

Demaurex, N., 2002. pH Homeostasis of cellular organelles. News Physiol. Sci. Int. J. Physiol. Prod. Jointly Int. Union Physiol. Sci. Am. Physiol. Soc. 17, 1–5. https://doi.org/10.1152/physiologyonline.2002.17.1.1

Dubland, J.A., Francis, G.A., 2015. Lysosomal acid lipase: at the crossroads of normal and atherogenic cholesterol metabolism. Front. Cell Dev. Biol. 3, 3.

Erwin, A.L., 2017. The role of sebelipase alfa in the treatment of lysosomal acid lipase deficiency. Ther. Adv. Gastroenterol. 10, 553–562.

Follenzi, A., Ailles, L.E., Bakovic, S., Geuna, M., Naldini, L., 2000. Gene transfer by lentiviral vectors is limited by nuclear translocation and rescued by HIV-1 pol sequences. Nat. Genet. 25, 217–222. https://doi.org/10.1038/76095

Fujimoto, T., Ohsaki, Y., Cheng, J., Suzuki, M., Shinohara, Y., 2008. Lipid droplets: a classic organelle with new outfits. Histochem. Cell Biol. 130, 263–279. https://doi.org/10.1007/s00418-008-0449-0

Fukumoto, S., Fujimoto, T., 2002. Deformation of lipid droplets in fixed samples. Histochem. Cell Biol. 118, 423–428. https://doi.org/10.1007/s00418-002-0462-7

Greenspan, P., Mayer, E.P., Fowler, S.D., 1985. Nile red: a selective fluorescent stain for intracellular lipid droplets. J. Cell Biol. 100, 965–973. https://doi.org/10.1083/jcb.100.3.965

Hamilton, J., Jones, I., Srivastava, R., Galloway, P., 2012. A new method for the measurement of lysosomal acid lipase in dried blood spots using the inhibitor Lalistat 2. Clin. Chim. Acta 413, 1207–1210. https://doi.org/10.1016/j.cca.2012.03.019

Hasegawa, D., Bugarin, C., Giordan, M., Bresolin, S., Longoni, D., Micalizzi, C., Ramenghi, U., Bertaina, A., Basso, G., Locatelli, F., Biondi, A., te Kronnie, G., Gaipa, G., 2013. Validation of flow cytometric phospho-STAT5 as a diagnostic tool for juvenile myelomonocytic leukemia. Blood Cancer J. 3, e160–e160. https://doi.org/10.1038/bcj.2013.56

Holzner, G., Mateescu, B., van Leeuwen, D., Cereghetti, G., Dechant, R., Stavrakis, S., deMello, A., 2021. High-throughput multiparametric imaging flow cytometry: toward diffraction-limited sub-cellular detection and monitoring of sub-cellular processes. Cell Rep. 34, 108824. https://doi.org/10.1016/j.celrep.2021.108824

Kohli, R., Ratziu, V., Fiel, M.I., Waldmann, E., Wilson, D.P., Balwani, M., 2020. Initial assessment and ongoing monitoring of lysosomal acid lipase deficiency in children and

adults: Consensus recommendations from an international collaborative working group. Mol. Genet. Metab. 129, 59–66. https://doi.org/10.1016/j.ymgme.2019.11.004
Li, F., Zhang, H., 2019. Lysosomal Acid Lipase in Lipid Metabolism and Beyond. Arterioscler. Thromb. Vasc. Biol. 39, 850–856. https://doi.org/10.1161/ATVBAHA.119.312136
Lukacs, Z., Barr, M., Hamilton, J., 2017. Best practice in the measurement and interpretation of lysosomal acid lipase in dried blood spots using the inhibitor Lalistat 2. Clin. Chim. Acta 471, 201–205. https://doi.org/10.1016/j.cca.2017.05.027
Marina, O.C., Sanders, C.K., Mourant, J.R., 2012. Correlating light scattering with internal cellular structures. Biomed. Opt. Express 3, 296–312. https://doi.org/10.1364/BOE.3.000296
Montiel-Equihua, C.A., Zhang, L., Knight, S., Saadeh, H., Scholz, S., Carmo, M., Alonso-Ferrero, M.E., Blundell, M.P., Monkeviciute, A., Schulz, R., Collins, M., Takeuchi, Y., Schmidt, M., Fairbanks, L., Antoniou, M., Thrasher, A.J., Gaspar, H.B., 2012. The β-Globin Locus Control Region in Combination With the EF1α Short Promoter Allows Enhanced Lentiviral Vector-mediated Erythroid Gene Expression With Conserved Multilineage Activity. Mol. Ther. 20, 1400–1409. https://doi.org/10.1038/mt.2012.50
Pastores, G.M., Hughes, D.A., 2020. Lysosomal Acid Lipase Deficiency: Therapeutic Options. Drug Des. Devel. Ther. Volume 14, 591–601. https://doi.org/10.2147/DDDT.S149264
Pericleous, M., Kelly, C., Wang, T., Livingstone, C., Ala, A., 2017. Wolman's disease and cholesteryl ester storage disorder: the phenotypic spectrum of lysosomal acid lipase deficiency. Lancet Gastroenterol. Hepatol. 2, 670–679.
Pham, N.-A., Gal, M.R., Bagshaw, R.D., Mohr, A.J., Chue, B., Richardson, T., Callahan, J.W., 2005. A comparative study of cytoplasmic granules imaged by the real-time microscope, Nile Red and Filipin in fibroblasts from patients with lipid storage diseases. J. Inherit. Metab. Dis. 28, 991–1004. https://doi.org/10.1007/s10545-005-0117-7
Platt, F.M., d'Azzo, A., Davidson, B.L., Neufeld, E.F., Tifft, C.J., 2018. Lysosomal storage diseases. Nat. Rev. Dis. Primer 4, 1–25. https://doi.org/10.1038/s41572-018-0025-4
Potter, J.E., Petts, G., Ghosh, A., White, F.J., Kinsella, J.L., Hughes, S., Roberts, J., Hodgkinson, A., Brammeier, K., Church, H., Merrigan, C., Hughes, J., Evans, P., Campbell, H., Bonney, D., Newman, W.G., Bigger, B.W., Broomfield, A., Jones, S.A., Wynn, R.F., 2021. Enzyme replacement therapy and hematopoietic stem cell transplant: a new paradigm of treatment in Wolman disease. Orphanet J. Rare Dis. 16, 235. https://doi.org/10.1186/s13023-021-01849-7
Rajkumar, V., Dumpa, V., 2022. Lysosomal Storage Disease, in: StatPearls. StatPearls Publishing, Treasure Island (FL).
Schlager, S., Vujic, N., Korbelius, M., Duta-Mare, M., Dorow, J., Leopold, C., Rainer, S., Wegscheider, M., Reicher, H., Ceglarek, U., Sattler, W., Radovic, B., Kratky, D., 2017. Lysosomal lipid hydrolysis provides substrates for lipid mediator synthesis in murine macrophages. Oncotarget 8, 40037–40051. https://doi.org/10.18632/oncotarget.16673
Schultz, M.L., Tecedor, L., Chang, M., Davidson, B.L., 2011. Clarifying lysosomal storage diseases. Trends Neurosci. 34, 401–410. https://doi.org/10.1016/j.tins.2011.05.006
Xu, M., Liu, K., Swaroop, M., Porter, F.D., Sidhu, R., Finkes, S., Ory, D.S., Marugan, J.J., Xiao, J., Southall, N., Pavan, W.J., Davidson, C., Walkley, S.U., Remaley, A.T., Baxa, U., Sun, W., McKew, J.C., Austin, C.P., Zheng, W., 2012. Type C1 and Wolman Cholesterol Storage Disorders*□S 287, 12.
Xu, M., Liu, K., Swaroop, M., Sun, W., Dehdashti, S.J., McKew, J.C., Zheng, W., 2014. A Phenotypic Compound Screening Assay for Lysosomal Storage Diseases. J. Biomol. Screen. 19, 168–175. https://doi.org/10.1177/1087057113501197

Conclusion

In fluorescent microscopy, WD patients' fibroblasts have a significant lipids and lysosomes accumulation that are restored upon LIPA copy insertion. Flow cytometry analysis confirmed the lipid accumulation and correction upon GT measurable also with Side scatter (SSC) parameter representing the granularity of cells. It suggests that WD phenotype could then studied without labelling. The lysosome signal in flow cytometry remains close between WD and WT fibroblasts suggesting a loss of information in suspended fibroblasts. The IFC allows the quantification of the lipid vesicles both upon NR stain or on SSC parameter and highlights a 100-fold of difference between WD and WT fibroblasts. Fibroblasts are not an easily accessible materials, therefore we engineered LIPA KO white blood cell to mimic PBMCs and we used PBMCs from LIPA to validate the cytometry pipeline. Both, LIPA KO Jurkat and mPBMCS from LIPA KO mice recapitulate the lipid accumulation observed in WD fibroblasts. To further validate the strategy, we plan to use WD patient PBMCs in a near future from Necker institute.

Discussion and Conclusion

7 DISCUSSION AND CONCLUSION

This work was focus on the development of a universal erythroid platform for secretion of therapeutic proteins in circulation or expression of β-globin chains in RBCs. In particular, I was involved in the assessment of HBA targeting platform for β-thalassemia. In fact, our CRISPR-Cas 9 system results in HBA 2 deletion in the HBA locus that could be benefit for β-thalassemia as α- gene deletion improve the $\frac{\alpha}{\beta}$ imbalance and the thalassemic traits (Cavazzana et al., 2017). We tested this hypothesis on β-thalassemic HUDEP-2 (HUDEP-2 β0) and observed that mono or biallelic deletion of HBA 2 restore the $\frac{\alpha}{\beta}$ imbalance and α-precipitation through normal. To further improve the β-thalassemic pattern, we targeted β-globin AS3 transgene into HBA locus using AAV6 delivery in HUDEP-2 β0. The combination of HBA2 deletion and β-globin AS3 results in significant HbA formation. We assessed the feasibility and the safety of the strategy on healthy HSCs and observed mainly in 1 copy deletion of HBA2 and 1 copy insertion of β-globin AS3 that are efficiently transcript in edited CD34+. Thus, injection of edited CD34+ into lethally irradiated immunocompromised mice lead to successful engraftment and full reconstitution of hematologic population in BM, SP and PB indicating that edited CD34+ cells conserve their multilineages ability.

To assess the therapeutic potential of the strategy in a relevant model, we edited β-thalassemic patient HSCs with our CRISPR-Cas9 systems and β-globin AS3 transgene and compared the benefit with the current *ex vivo* GT for β-thalassemia : LVV particle encoding β-globin AS3 transgene upon GLOBE promoter (NC702453477). In β-thalassemic patient HSCs, we achieved efficient editing in HBA locus with 1 copy deletion of HBA2 and 1 copy of β-globin AS3 integration. In comparison, LVV results in 1,5 copy of β-globin AS3 integration efficiently transcript. Interestingly, the targeting integration in HBA locus results in comparable or better $\frac{\alpha}{\beta}$ imbalance than LVV insertion. To further improve the safety of the editing, we tested the Nickase D10A instead spCas9 in RNP to prevent DSB. In our hand, Nickase provides less efficient KI than spCas9 but improves cell viability. Alternative delivery systems as nanoparticle or used of Nickase variant could ameliorate the KI in HSCs (Tran et al., 2022).

Here, we provide a proof of principle that hijacking the endogenous HBA promoter to produce β-globin chain results in a significant improvement of β-thalassemic trait. Moreover, the deletion of HBA2 could also be interesting for SCD since α-thalassemic trait ameliorates the patient phenotype (Cavazzana et al., 2017). Thus, the expression of anti-sickling HBB could reduce the HbS polymerization and the progression of the disorder. Another strategy has been developed for SCD based on the replacement of mutated exon using CRISPR-cas9 and AAV6 donor template (Dever et al., 2016) and tested into humanized globin-cluster SCD mouse of the underlying mutation (Wilkinson et al., 2021). KI of the correct exon results in HbA formation normalizing the RBCs feature in SCD mouse blood confirming the therapeutic potential of KI HSCs strategy for hemoglobinopathies. Integration of the corrective β-globin gene or sequence under the control of the endogenous erythroid specific promoter provide expression of the β-globin chain at a physiological level in the proper and restricted erythroid population. Therefore, gene editing for β-hemoglobinopathies would provide strong and sufficient β-globin chains to fully restore the disease phenotype paving the way of a complete and long-term correction of the disorders. Nonetheless, *ex vivo* GT for hemoglobinopathies requires myeloablation of patient's BM that remains toxic and HSCs culturing and transplantation that could decrease the HSCs engraftment and treatment efficacy. To overcome these issues, *in vivo* HSCs transduction has been applied to reactivate γ-globin expression in a SCD mouse model (Li et al., 2021) or introduce a copy of γ-globin in nonhuman primates using helper-dependent adenovirus (HDAd5/35++) vectors (Li et al., 2022). Both experiments restore HbA formation and fully correct phenotype without inducing genotoxicity (Li et al., 2022).

During my thesis, I was also involved in the evaluation of the HBA targeting integration and erythroid expression of clotting factors and lysosomal enzymes. This work provides proof of principle that erythroid secreted enzymes are active and able to cross-correct the metabolic dysfunction of patient fibroblasts. It also confirms that mature erythrocytes are capable of post-translational modification as M6P necessary for enzyme uptake in defective cells. Therefore, erythroid secretion of therapeutic protein appears to be a worthy strategy to treat disorder that requires PRT. As LAL-D is a monogenic disorder without curative treatment, I stress out my thesis journey on the characterization of LAL-D phenotype and on the development of an optimized *ex vivo* GT for treatment of LAL-D based on the secretion of therapeutic enzyme in bloodstream.

We tested HBA locus as a safe harbor locus for integration of therapeutic transgenes in the attempt to hijack the superactive HBA promoter to produce the proteins of interest in an high and erythroid-specific manner. To this end, we used both CRISPR-cas9 system to cleave the 5' of UTR region of HBA locus and HDR DNA reparair mechanism to integrate transgene under endogenous HBA promoter. Editing occurred upon RNP electroporation and DNA template was delivered using AAV6 vector encoding HA for HBA locus, a promoterless transgene sequence and PGK GFP reporter cassette. The HBA locus is composed of 2 HBA genes (HBA 2 and HBA1) highly homologue, our gRNA cleaves both in 5'UTR of HBA 2 and HBA1 genes resulting in either a unique cut in one of the two genes or double cut inducing HBA2 deletion. In our experiment, we observed mainly 1 deletion of HBA that do not impair Hb formation. In fact, deletion of up to 3 out of the 4 α-globins are well tolerated in α-thalassemia (Chonat and Quinn, 2017). We analyzed potential off-target site with IdLV capturing and sequencing to assure the safety and specificity of our Cas9/gRNA strategy. None of the predicted off-target site was confirmed supporting the safety of our gRNA. Recently, DSBs induced by CRISPR-cas9 have been linked to chromosomal rearrangement (Cullot et al., 2019) that should be evaluated with our gRNA strategy. Different strategies could be employed for chromosomal rearrangement analysis as chromosomal aberration analysis by single targeted linker-mediated PCR sequencing (CAST-Seq (Turchiano et al., 2021))

The targeting integration of DNA template results mainly in 1 copy insertion under endogenous HBA promoter. Using GFP as a DNA template, we found that GFP expression is specific to erythroid population and increases during erythroid maturation. We applied the platform for Hemophilia B using a template encoding FIX cDNA and compared the KI HSCs with classical LVV FIX insertion in HSCs. The erythroid platform over-performs even LVV based HSCs. In fact, we achieved 2,8-fold more FIX expression in KI HSCs compared to LV-corrected HSCs in the end of erythroid differentiation. We tested the platform for metabolic enzymes involved in LSD as α-Iduronidase (IDUA), α-galactosidase (GLA) or Lysosomal acid lipase (LAL) that results in toxic accumulation of substrate in lysosomes. Upon erythroid differentiation, KI HSCs were able to produce all the metabolic enzymes. Erythroid secreted LAL conserves its hydrolytic activity and cross-correct WD fibroblasts leading to a decrease of toxic lipid accumulation. Therefore, erythroid cells should be able to correctly perform M6P post-translational modification required for enzyme uptake via M6P-R. To further validate this hypothesis,

we could perform competition uptake with a gradient of M6P residues and our erythroid secreted enzyme. If the cross-correction on patient fibroblast depends on the M6P-R entry, then the increasing amount of M6P residue should prevent from uptake and decrease the treatment efficiency (Kleinig and Cox, 1998).

Although we quantified the targeting copy with ddPCR, we didn't quantify AAV concatemerization in HBA site that could be observed upon nuclease DSB (Hanlon et al., 2019). In the lab, concatemers of AAV integrated in HBA are currently under investigation using long-read sequencing on the full length of HBA locus. Moreover, AAV vector has been widely described as episomal but random viral integration could occurs into the host genome and give raise to insertional mutagenesis (Deyle and Russell, 2009). Alternative delivery systems could be employed as IdLV preventing random genome insertion and appears less toxic than AAV6 (Romero et al., 2019) or as plasmids that have used in HITI strategy already applied in murine HSCs in IL2R locus (Byambaa et al., 2021).

Lastly, we evaluated the engraftment efficiency of unmodified or modified CD34+ (RNP only or RNP + AAV6) in immunocompromised mice. We observed a good engraftment in BM, spleen and blood for all population although edited cells engraft less than non-modified cells. In fact, editing and gene transfer in HSCs cause p53 activation that results in apoptosis and decrease engraftment efficiency (Schiroli et al., 2019). To improve the engraftment, inhibitor of p53 can be used (Schiroli et al., 2019) or alternative delivery strategies could be employed either for the DNA templates (IdLV, plasmids) or the CRISPR-cas9 complex as nanoparticle (El-Kharrag et al., 2022). Engrafted CD34+ cells were able to re-generate all the hematopoietic cells and we achieved a significant expression of GFP reporter cassette in all blood lineage cells. KI HSCs maintain their homing and multilineage potency. Nonetheless, immunocompromised mice can't perform human erythropoiesis preventing us from *in vivo* assessment of the erythroid platform. We will take advantage of a transgenic mice encoding the human HBA locus to further evaluate *in vivo* the platform. In fact, heterozygote mice for the human HBA locus show a strong globin chains (30% in HPLC analysis on blood samples) expression in erythroid population (Wallace et al., 2007). Here, we plan to collect murine HSCs from heterozygote HBA humanized mouse model and apply our editing strategy. Upon transplantation of edited mHSCs

either in WT or LAL-D mice, we will be able to follow in bloodstream the expression of our transgene of interest as well as the cross-correction effect on the metabolic defect. It would allow us to evaluate both the safety of hijacking HBA promoter on the hemoglobin synthesis and the corrective potential of the platform.

Hijacking HBA promoter to express therapeutic transgenes in erythroid lineage represent a universal platform for secretory proteins using a unique gRNA and delivery template. The absence of both an off-target site and an exogenous promoter to prevent gene transactivation make the erythroid based platform safe. Compared to ERT, the HBA platform offers a long-term curative treatment able to constantly deliver missing protein in affected organs allowing a better enzyme perfusion and providing a higher corrective approach. Thus, engineered erythrocytes to deliver therapeutic compound have been described to provide immune tolerance against the secreted enzyme that would decrease the risk of immune reaction against circulative enzyme compared to ERT (Grimm et al., 2015; Villa et al., 2016). Nonetheless, HBA targeted platform requires myeloablation and BM transplantation that could result in negative outcome in patient. Also, to further evaluate the safety of the strategy, a particular focus needs to be conduct on the impact on the overexpression of transgenes in erythroid precursors and on the α-globin deletion on hemoglobin synthesis and oxygen transport to prevent from the possibility of α-thalassemia induction. Finally, erythroid secreted enzymes are not able to cross the blood brain barrier limiting the employment of the strategies for disorder with CNS involvement. To overcome this issues, engineered blood brain barrier shuttle peptide could be added on the transgene sequence (Zhou et al., 2021).

Due to the unmet medical of curative treatment for LAL-D, I participated in the development of LVV-based *ex vivo* strategy using LVV encoding LIPA sequences under the control of an erythroid promoter. We aimed to produced LAL enzyme in erythroid mature cells that can be secreted into bloodstream to cross-correct affected tissues and organs. As for the HBA targeted platform, the LVV-based correction would allow constant delivery of missing LAL protein in affected organs allowing a better enzyme perfusion with a lower immune reaction due to the immune tolerance induced by engineered erythrocytes compared to ERT (Grimm et al., 2015; Villa et al., 2016). Nonetheless, protein

expression in erythroid progenitors either in bloodstream or BM must be evaluated in order to assure that transgene expression would not be toxic for progenitors or BM niche microenvironment. Compared to our CRISPR mediated HBA targeting strategy, LVV-HSCs correction offers the advantage to be already in clinical trials for other LSDs and be easier and cheaper to produce and assess. Thus, the exogenous erythroid promoter supports the production and secretion of LAL enzyme into bloodstream and could be applied for disorder requiring PRT with the limitation that erythroid secreted enzyme cannot cross the blood brain barrier. A limitation that could be overcome by using blood brain barrier shuttle peptide (Zhou et al., 2021).

We tested different LIPA constructions encoding 7 different signal peptides to maximize the export of LAL enzyme out of the cells. Then, we codon-optimized the construction with the best signal peptide to further increase LAL expression. We assessed the LIPA transgenes on K562 cells line and human HSCs upon LVV transduction. We achieved efficient gene integration with all constructs in both cell types, whereas HSCs are more difficult to transduce and have a lower VCN than K562. The primary screening in K562 allows us to select 3 LIPA constructions (SP6, SP7 and SP8) providing the optimal enzyme secretion that have been further assessed in human HSCs. In HSCs, the signal peptide 8 coming from plasma protein inhibitor led to the highest LAL secretion (7-fold over WT LIPA sequence) in erythroid differentiated CD34+. Interestingly, the signal peptide seems to slightly increase the LAL expression by 2-3-fold that is confirmed by the mRNA quantification. Moreover, LAL activity signal in supernatant appears higher than the LAL protein that may be explained by the difference of sensitivity of the two assays.

The further codon optimization of SP8 LIPA transgene results in an increase up to 15-fold of LAL expression and secretion compared to WT LIPA for the construction 2 and 3. Nonetheless, the LAL activity in cell lysate is lower than the LAL protein quantification that could indicate that some enzymes were not fully functional/process upon LAL activity assays. Whereas in the supernatant, we observed that the optimized LAL conserves its hydrolytic activity and correlates with LAL protein quantification. The codon optimization 1 doesn't provide any advantage as the protein expression and secretion is similar to the LAL WT. This result highlights the importance of the codon sequence

for transgene expression. We evaluated the cross-correction of secreted LAL into WD patient fibroblasts. Although LAL cross-corrects the lipid accumulation we could not see any difference between LAL WT and optimized one due to the low fold change (2-fold) between WT and WD fibroblast preventing from discrimination of LIPA construction. LV-transduction of HSCs are not cytotoxic as count of CFC is similar among untreated cells and transduced one and doesn't affect the multilineage potency of HSCs.

The next step of this project consists of evaluating *in vivo* the therapeutic potential of erythroid secreted LAL. To this end, we recently obtained from Dr. Kratky a mouse model deficient for LAL enzyme due to deletion of Exon 4 of the LIPA gene. In our experiment, the LAL-/- mouse shown lipid accumulation in liver, intestine and spleen mimicking the WD phenotype. Analysis of blood parameters confirms the modification of immunological parameters with an increase number of granulocytes and monocytes/macrophages and a decrease in lymphoid population (both Lymphocytes T and B) (Qu et al., 2010, 2009). We plan to evaluate the LV-based *ex vivo* GT into this LAL-D mouse model. In this purpose, we aim to collect HSCs from WT mice, transduced them with LVV particles and transplanted them back after myeloablation into LAL-/- mice that will consist of lethal irradiation. Neither the toxicity of myeloablation nor its impact on HSCs engraftment and BM niches have been studied on LAL-D mouse and will require further investigation to determine the proper irradiation dose as well as the required number of HSCs to provide successful engraftment and correct the BM environment. Moreover, transplantation of WT HSCs may offer a curative effect on LAL-D mouse that could be over-performed with LV-HSCs. As erythroid promoter is not under evaluation in clinical trials for LSDs, we plan to compare the efficiency of correction using a ubiquitous PGK promoter.

The modification of immunological parameters in blood could be an interesting readout to assess the therapeutic effect on our LV- *ex vivo* GT but could also limit the efficiency of gene therapy since the micro-environment of BM is impaired in LAL-/- mice (Qu et al., 2009, 2010). In fact, mice display a dysregulation in BM progenitor differentiation with an increase of HSCs population (Lin- Sca-1+ c-kit+, LSK) and an expansion of myeloid cells especially MDSC population that interferes on T cell

development and maturation (Qu et al., 2011, 2010). The BM environment of LAL-/- mouse has been restored by either Doxycline inducible expression of LAL in myeloid population (Qu et al., 2011) or by injection of mammalian target of rapamycin (mTOR) pharmacologic inhibitors (Ding et al., 2014). Both strategies display a decrease of myeloid, MDSCs and granulocyte-monocyte progenitor (GMP) expansion. mTOR injection could be a strategy to enhance our LVV-based GT. Thus, we could also take advantage to the proliferation of LSK population in BM to develop an alternative GT consisting to correct HSCs in vivo using HDAd5/35++ injection (Wang et al., 2018). In this strategy, the mHSCs (LSK) are mobilized using G-CSF and transduced by HDAd5/35++ upon direct vector injection in bloodstream. Two Ad5/35++ vectors are required : one containing sleeping beauty transposase system to integrate sequence into host genome and the other the sequence of interest flacking by inverted transposon repeats sequences. This system offers the advantage to get rid from myeloablation, HSCs culturing and transplantation but result in random transgene integration that could lead to transactivation of pro-oncogene (Wang et al., 2018).

Finally, to evaluate the cross-correction ability of our erythroid secreted LAL, we cultivated primary fibroblasts from 2 WD patients with supernatant of edited or transduced HSCs. Then, we used WD fibroblasts to further characterize the disorder and set up an easy-to-implement analysis pipeline to assess toxic lipid deposits and their correction by gene therapy. Biochemical analysis confirms the loss of LAL protein and activity in both WD donor fibroblasts. We first investigated the lipid accumulation upon Nile Red staining (neutral lipids, NR) and the effect on lysosome using LysoGreen (LG) staining on fluorescent microscopy. The quantification of signal intensity per cells upon NR or LG staining out ≈ 2-fold change between WT and WD fibroblasts. Insertion of a functional copy of LIPA gene upon LVV transduction inverts the toxic lipid accumulation and decreases lysosome signal. Then, we observed LG stained fibroblasts upon confocal microscopy and the quantification of LG spot demonstrates an increase of the number of lysosomes in WD fibroblasts compared to WT donors that is corrected upon LIPA gene insertion.

In order to increase both the speed of analysis and the number of analyzed cells, we decided to analyze WD fibroblasts using flow cytometry. With NR staining, we obtained 2-fold increase of lipids

content as observed under microscope, while the LG signal provides heterogenous result. We hypothesized that the detachment of fibroblasts upon TrypLE treatment may result in a loss of information on lysosome content. Thus, LG stains acidic organelles as lysosome but could also labelled Golgi apparatus or secretory vesicle that may contribute to fluorescence signal (Demaurex, 2002; Marina et al., 2012). Flow cytometry provides information on the cell complexity as granularity observed on the SSC. We observe an increase by 2-fold of granularity in WD population compared to healthy one suggesting vesicle accumulation measurable without staining. Gene correction of WD fibroblasts tends to decrease the lipid content and restore the normal morphology of fibroblasts.

Finally, we decided to analyze WD fibroblasts with IFC to combine the speed of analysis of flow cytometry with precise quantification of vesicles provided by microscopy. With IFC, we recapitulated the increase of NR staining and SSC intensity : around 4-fold change. The spot count function allows us to increase the discrimination between WD and WT fibroblasts by a 100-fold making possible to assess our different GT constructions. However, the LG staining reveals heterogenous signal and spot count as observed with flow cytometry. Analysis lipids droplets accumulation in WD appears to be an efficient way to monitor the LAL-D and its treatment. Nonetheless, fibroblasts are not an easily accessible material and patient PBMCs are difficult to obtain. Therefore, we generated LIPA KO hematopoietic cell lines that mimic PBMCs. In particular, LIPA KO Jurkat cells recapitulate the WD phenotype with an increase of lipids content observed in flow cytometry and IFCs caused by the loss of LAL activity. In contrast, K562 KO LIPA was not affected by the deletion of LIPA sequences, mainly due to the low baseline LAL activity in the K562 WT population. We also took advantage of PBMCs from our LAL-/- mouse model to confirm the increase of signal NR and spot count in LAL-deficient living model. The toxic lipid accumulation is monitorable and quantifiable directly on blood either with NR or no staining (SSC parameter). The spot count fold change observed in LAL LIPA KO Jurkat or LAL-/- PBMCs were lower than in fibroblasts and could be explain by the lower cell surface of hematopoietic cells compared to fibroblasts. The lysosome analysis provide heterogenous signal in suspended fibroblasts but not under microscopy and has been already applied for drug screening (Xu et al., 2012; Aguisanda et al., 2017). On this project, we planned to investigate the LAL-D phenotype on WD patient PBMCs in the future. Such cytometry-based pipeline could be employed to better characterize other LSD as Pompe disease and assess the therapeutic potency of gene

therapy or the efficiency of viral slot production. Moreover, we could employ other microscopy approaches to investigate and quantify the lipids deposits as Nanolive (https://www.nanolive.ch/) to produce 3-D label-free image of our fibroblasts or holographic microscopy on living cells using quantitative phase imaging to discriminate lipid accumulation from other cytoplasm contents. To go further and confirm the toxic accumulation, we could also use different lipid probes as BODIPY that present a lower background signal and a higher LD specify compared to NR (Fam et al., 2018).

COMMUNICATIONS AND PUBLICATIONS

8 COMMUNICATIONS AND PUBLICATIONS

8.1 COMMUNICATION (CHRONOLOGICAL ORDER)

- Congress: Cold Genome Engineering: CRISPR Frontiers cold spring harbor laboratory, 18-20/08/20221, virtual

Virtual poster: *Ex vivo* editing of human hematopoietic stem cells for erythroid expression of therapeutic proteins
Authors : Giulia Pavani, Marine Laurent, Anna Fabiano, Erika Cantelli, Aboud Sakkal, Guillaume Corre, Peter Lenting, Jean-Paul Concordet, Magali Toueille, Annarita Miccio, Mario Amendola

- Congress : association française de cytométrie (AFC), 06-08/10/2021, Strasbourg

Oral and poster presentations : Cytométrie multimodale pour la caractérisation de cellules déficientes en acide lipase lysosomale
Authors : Marine Laurent, Giulia Pavani, Anna Fabiano, Daniel Stockolm, Jérémie Cosette et Mario Amendola
Finalist for the young cytometer prize, Wednesday 6th October 2021

- Congress : European Society of Gene and Cell Therapy (ESGCT), 19-21/10/2022, virtual

Virtual poster : *Ex vivo* editing of human hematopoietic stem cells for LAL-D therapy
Autors : Marine Laurent, Giulia Pavani, Christine Jenny, Anna Fabiano, Mario Amendola

- Congress : American Society of Gene and Cell Therapy (ASGCT), 15-19/05/2022, Washington DC

Oral presentation : *Ex Vivo* Editing of Hematopoietic Stem Cells for Erythroid Expression of Therapeutic Proteins *In Vivo* for LAL-D Therapy;
Tuesday 17th May 2022 **session** : Tool and approaches for inborn errors of metabolism.
Authors : Marine Laurent, Giulia Pavani, Christine Jenny, Anna Fabiano, Mario Amendola
Meritorious abstract travel award

Poster : Novel cytometry based characterization of lysosomal disease affected and gene corrected patient's cells.
Authors : Marine Laurent, Giulia Pavani, Sarah Bayol, Daniel Stockholm, Jérémie Cosette and Mario Amendola

8.2 PUBLICATIONS :

Pavani, G., Laurent, M., Fabiano, A., Cantelli, E., Sakkal, A., Corre, G., Lenting, P.J., Concordet, J.-P., Toueille, M., Miccio, A., Amendola, M., 2020. Ex vivo editing of human hematopoietic stem cells for erythroid expression of therapeutic proteins. Nat Commun 11, 3778. https://doi.org/10.1038/s41467-020-17552-3

Pavani, G., Fabiano, A., Laurent, M., Amor, F., Cantelli, E., Chalumeau, A., Maule, G., Tachtsidi, A., Concordet, J.-P., Cereseto, A., Mavilio, F., Ferrari, G., Miccio, A., Amendola, M., 2021. Correction of β-thalassemia by CRISPR/Cas9 editing of the α-globin locus in human hematopoietic stem cells. Blood Adv 5, 1137–1153. https://doi.org/10.1182/bloodadvances.2020001996

Amendola, M., Bedel, A., Buj-Bello, A., Carrara, M., Concordet, J.P., Frati, G., Gilot, D., Giovannangeli, C., Gutierrez-Guerrero, A., Laurent, M. and Miccio, A., 2021. Recent Progress in Genome Editing for Gene Therapy Applications: The French Perspective. Human Gene Therapy, 32(19-20), pp.1059-1075.

8.3 PATENT

EP 20 306524.8 "lysosomal acid lipase variants and uses thereof" (International reference : PCT N° EP2021/084929).

8.4 STUDENTS SUPERVISION

Febuary 2021-July 2021 : "Multi-modal cytometry for quantifying lipid content in blood cells lines deficient in Lysosomal Acid Lipase", Sarah Bayol, Master 2 in Cell and molecular biology of microenvironment (M2 BioC2M), University of Cergy

Juin 2022-Septembre 2022 : "Characterisation of a mouse model deficient for the acid lysosomal lipase", Lucie Laur, Master 1 in National Institute of Applied Sciences of Toulouse

Bibliography

9 BIBLIOGRAPHY

Aguisanda, F., Yeh, C.D., Chen, C.Z., Li, R., Beers, J., Zou, J., Thorne, N., Zheng, W., 2017. Neural stem cells for disease modeling of Wolman disease and evaluation of therapeutics. Orphanet J Rare Dis 12, 120. https://doi.org/10.1186/s13023-017-0670-9

Ahmed, M.H., Ghatge, M.S., Safo, M.K., 2020. Hemoglobin: Structure, Function and Allostery. Subcell Biochem 94, 345–382. https://doi.org/10.1007/978-3-030-41769-7_14

Alnasser, S.M., 2021. Review on mechanistic strategy of gene therapy in the treatment of disease. Gene 769, 145246. https://doi.org/10.1016/j.gene.2020.145246

Ameis, D., Merkel, M., Eckerskorn, C., Greten, H., 1994. Purification, characterization and molecular cloning of human hepatic lysosomal acid lipase. Eur J Biochem 219, 905–914. https://doi.org/10.1111/j.1432-1033.1994.tb18572.x

Antoniou, P., Miccio, A., Brusson, M., 2021. Base and Prime Editing Technologies for Blood Disorders. Front Genome Ed 3, 618406. https://doi.org/10.3389/fgeed.2021.618406

Anzalone, A.V., Randolph, P.B., Davis, J.R., Sousa, A.A., Koblan, L.W., Levy, J.M., Chen, P.J., Wilson, C., Newby, G.A., Raguram, A., Liu, D.R., 2019. Search-and-replace genome editing without double-strand breaks or donor DNA. Nature 576, 149–157. https://doi.org/10.1038/s41586-019-1711-4

Arabi, F., Mansouri, V., Ahmadbeigi, N., 2022. Gene therapy clinical trials, where do we go? An overview. Biomedicine & Pharmacotherapy 153, 113324. https://doi.org/10.1016/j.biopha.2022.113324

Atkins, A., Chung, C.-H., Allen, A.G., Dampier, W., Gurrola, T.E., Sariyer, I.K., Nonnemacher, M.R., Wigdahl, B., 2021. Off-Target Analysis in Gene Editing and Applications for Clinical Translation of CRISPR/Cas9 in HIV-1 Therapy. Frontiers in Genome Editing 3.

Azhagiri, M.K.K., Babu, P., Venkatesan, V., Thangavel, S., 2021. Homology-directed gene-editing approaches for hematopoietic stem and progenitor cell gene therapy. Stem Cell Res Ther 12, 500. https://doi.org/10.1186/s13287-021-02565-6

Banasik, M.B., McCray, P.B., 2010. Integrase-defective lentiviral vectors: progress and applications. Gene Ther 17, 150–157. https://doi.org/10.1038/gt.2009.135

Becker, S., Boch, J., 2021. TALE and TALEN genome editing technologies. Gene and Genome Editing 2, 100007. https://doi.org/10.1016/j.ggedit.2021.100007

Belisário, A.R., Rodrigues, C.V., Martins, M.L., Silva, C.M., Viana, M.B., 2010. Coinheritance of α-Thalassemia Decreases the Risk of Cerebrovascular Disease in a Cohort of Children with Sickle Cell Anemia. Hemoglobin 34, 516–529. https://doi.org/10.3109/03630269.2010.526003

Bergamaschi, G., Perfetti, V., Tonon, L., Novella, A., Lucotti, C., Danova, M., Glennie, M.J., Merlini, G., Cazzola, M., 1996. Saporin, a ribosome-inactivating protein used to prepare immunotoxins, induces cell death via apoptosis. Br J Haematol 93, 789–794. https://doi.org/10.1046/j.1365-2141.1996.d01-1730.x

Bernstein, D.L., Lobritto, S., Iuga, A., Remotti, H., Schiano, T., Fiel, M.I., Balwani, M., 2018. Lysosomal acid lipase deficiency allograft recurrence and liver failure- clinical outcomes of 18 liver transplantation patients. Mol Genet Metab 124, 11–19. https://doi.org/10.1016/j.ymgme.2018.03.010

Biffi, A., Montini, E., Lorioli, L., Cesani, M., Fumagalli, F., Plati, T., Baldoli, C., Martino, S., Calabria, A., Canale, S., Benedicenti, F., Vallanti, G., Biasco, L., Leo, S., Kabbara, N., Zanetti, G., Rizzo, W.B., Mehta, N.A.L., Cicalese, M.P., Casiraghi, M., Boelens, J.J., Del Carro, U., Dow, D.J., Schmidt, M., Assanelli, A., Neduva, V., Di Serio, C., Stupka, E., Gardner, J., von Kalle, C., Bordignon, C., Ciceri, F., Rovelli, A., Roncarolo, M.G., Aiuti, A., Sessa, M., Naldini, L., 2013. Lentiviral Hematopoietic Stem Cell Gene Therapy Benefits Metachromatic Leukodystrophy. Science 341, 1233158. https://doi.org/10.1126/science.1233158

Boitano, A.E., Wang, J., Romeo, R., Bouchez, L.C., Parker, A.E., Sutton, S.E., Walker, J.R., Flaveny, C.A., Perdew, G.H., Denison, M.S., Schultz, P.G., Cooke, M.P., 2010. Aryl Hydrocarbon Receptor Antagonists Promote the Expansion of Human Hematopoietic Stem Cells. Science 329, 1345–1348. https://doi.org/10.1126/science.1191536

Brandt, S.J., Koury, M.J., 2009. Regulation of LMO2 mRNA and protein expression in erythroid differentiation. Haematologica 94, 447–448. https://doi.org/10.3324/haematol.2008.005140

Braulke, T., Bonifacino, J.S., 2009. Sorting of lysosomal proteins. Biochimica et Biophysica Acta (BBA) - Molecular Cell Research 1793, 605–614. https://doi.org/10.1016/j.bbamcr.2008.10.016

Brendel, C., Williams, D.A., 2020. Current and future gene therapies for hemoglobinopathies. Current Opinion in Hematology 27, 149–154. https://doi.org/10.1097/MOH.0000000000000581

Burton, B.K., Feillet, F., Furuya, K.N., Marulkar, S., Balwani, M., 2022. Sebelipase alfa in children and adults with lysosomal acid lipase deficiency: Final results of the ARISE study. Journal of Hepatology 76, 577–587. https://doi.org/10.1016/j.jhep.2021.10.026

Byambaa, S., Uosaki, H., Ohmori, T., Hara, H., Endo, H., Nureki, O., Hanazono, Y., 2021. Non-viral ex vivo genome-editing in mouse bona fide hematopoietic stem cells with CRISPR/Cas9. Molecular Therapy - Methods & Clinical Development 20, 451–462. https://doi.org/10.1016/j.omtm.2021.01.001

Callahan, P., Leonard, Me., Powell, M.S., 2020. Lipid Transport, Storage, and Utilization.

Cantú, I., Philipsen, S., 2014. Flicking the switch: adult hemoglobin expression in erythroid cells derived from cord blood and human induced pluripotent stem cells. Haematologica 99, 1647–1649. https://doi.org/10.3324/haematol.2014.116483

Capecchi, M.R., 2005. Gene targeting in mice: functional analysis of the mammalian genome for the twenty-first century. Nat Rev Genet 6, 507–512. https://doi.org/10.1038/nrg1619

Capotondo, A., Milazzo, R., Garcia-Manteiga, J.M., Cavalca, E., Montepeloso, A., Garrison, B.S., Peviani, M., Rossi, D.J., Biffi, A., 2017. Intracerebroventricular delivery of hematopoietic progenitors results in rapid and robust engraftment of microglia-like cells. Sci Adv 3, e1701211. https://doi.org/10.1126/sciadv.1701211

Caulier, A.L., Sankaran, V.G., 2022. Molecular and cellular mechanisms that regulate human erythropoiesis. Blood 139, 2450–2459. https://doi.org/10.1182/blood.2021011044

Cavazzana, M., Antoniani, C., Miccio, A., 2017. Gene Therapy for β-Hemoglobinopathies. Molecular Therapy 25, 1142–1154. https://doi.org/10.1016/j.ymthe.2017.03.024

Cavazzana-Calvo, M., Payen, E., Negre, O., Wang, G., Hehir, K., Fusil, F., Down, J., Denaro, M., Brady, T., Westerman, K., Cavallesco, R., Gillet-Legrand, B., Caccavelli, L., Sgarra, R., Maouche-Chrétien, L., Bernaudin, F., Girot, R., Dorazio, R., Mulder, G.-J., Polack, A., Bank, A., Soulier, J., Larghero, J., Kabbara, N., Dalle, B., Gourmel, B., Socie, G., Chrétien, S., Cartier, N., Aubourg, P., Fischer, A., Cornetta, K., Galacteros, F., Beuzard, Y., Gluckman, E., Bushman, F., Hacein-Bey-Abina, S., Leboulch, P., 2010. Transfusion independence and HMGA2 activation after gene therapy of human β-thalassaemia. Nature 467, 318–322. https://doi.org/10.1038/nature09328

Cebrian-Serrano, A., Davies, B., 2017. CRISPR-Cas orthologues and variants: optimizing the repertoire, specificity and delivery of genome engineering tools. Mamm Genome 28, 247–261. https://doi.org/10.1007/s00335-017-9697-4

Chandel, N.S., 2021. Lipid Metabolism. Cold Spring Harb Perspect Biol 13, a040576. https://doi.org/10.1101/cshperspect.a040576

Chang, A.H., Stephan, M.T., Sadelain, M., 2006. Stem cell–derived erythroid cells mediate long-term systemic protein delivery. Nature biotechnology 24, 1017.

Charlesworth, C.T., Deshpande, P.S., Dever, D.P., Camarena, J., Lemgart, V.T., Cromer, M.K., Vakulskas, C.A., Collingwood, M.A., Zhang, L., Bode, N.M., Behlke, M.A., Dejene, B., Cieniewicz, B., Romano, R., Lesch, B.J., Gomez-Ospina, N., Mantri, S., Pavel-Dinu, M., Weinberg, K.I., Porteus, M.H., 2019. Identification of preexisting adaptive immunity to Cas9 proteins in humans. Nat Med 25, 249–254. https://doi.org/10.1038/s41591-018-0326-x

Chhabra, A., Ring, A.M., Weiskopf, K., Schnorr, P.J., Gordon, S., Le, A.C., Kwon, H.-S., Ring, N.G., Volkmer, J., Ho, P.Y., Tseng, S., Weissman, I.L., Shizuru, J.A., 2016. Hematopoietic stem cell transplantation in immunocompetent hosts without radiation or chemotherapy. Sci Transl Med 8, 351ra105. https://doi.org/10.1126/scitranslmed.aae0501

Chiabrando, D., Mercurio, S., Tolosano, E., 2014. Heme and erythropoieis: more than a structural role. Haematologica 99, 973–983. https://doi.org/10.3324/haematol.2013.091991

Chonat, S., Quinn, C.T., 2017. Current Standards of Care and Long Term Outcomes for Thalassemia and Sickle Cell Disease, in: Malik, P., Tisdale, J. (Eds.), Gene and Cell Therapies for Beta-Globinopathies, Advances in Experimental Medicine and Biology. Springer, New York, NY, pp. 59–87. https://doi.org/10.1007/978-1-4939-7299-9_3

Ciurea, S.O., Andersson, B.S., 2009. Busulfan in Hematopoietic Stem Cell Transplantation. Biology of Blood and Marrow Transplantation 15, 523–536. https://doi.org/10.1016/j.bbmt.2008.12.489

Clarke, G.M., Higgins, T.N., 2000. Laboratory Investigation of Hemoglobinopathies and Thalassemias: Review and Update. Clinical Chemistry 46, 1284–1290. https://doi.org/10.1093/clinchem/46.8.1284

Community, N.P.B., 2020. REDit: Engineering erythroid cells for therapeutic applications [WWW Document]. Nature Portfolio Bioengineering Community. URL http://bioengineeringcommunity.nature.com/posts/redit-engineering-erythroid-cells-for-therapeutic-applications (accessed 8.1.22).

Concordet, J.-P., Haeussler, M., 2018. CRISPOR: intuitive guide selection for CRISPR/Cas9 genome editing experiments and screens. Nucleic Acids Res 46, W242–W245. https://doi.org/10.1093/nar/gky354

Copelan, E.A., 2006. Hematopoietic Stem-Cell Transplantation. The New England Journal of Medicine 14.

Cullot, G., Boutin, J., Toutain, J., Prat, F., Pennamen, P., Rooryck, C., Teichmann, M., Rousseau, E., Lamrissi-Garcia, I., Guyonnet-Duperat, V., Bibeyran, A., Lalanne, M., Prouzet-Mauléon, V., Turcq, B., Ged, C., Blouin, J.-M., Richard, E., Dabernat, S., Moreau-Gaudry, F., Bedel, A., 2019. CRISPR-Cas9 genome editing induces megabase-scale chromosomal truncations. Nat Commun 10, 1136. https://doi.org/10.1038/s41467-019-09006-2

Czechowicz, A., Kraft, D., Weissman, I.L., Bhattacharya, D., 2007. Efficient Transplantation via Antibody-based Clearance of Hematopoietic Stem Cell Niches. Science 318, 1296–1299. https://doi.org/10.1126/science.1149726

Dailey, H.A., Meissner, P.N., 2013. Erythroid Heme Biosynthesis and Its Disorders. Cold Spring Harb Perspect Med 3, a011676. https://doi.org/10.1101/cshperspect.a011676

de Lima, M., McNiece, I., Robinson, S.N., Munsell, M., Eapen, M., Horowitz, M., Alousi, A., Saliba, R., McMannis, J.D., Kaur, I., Kebriaei, P., Parmar, S., Popat, U., Hosing, C., Champlin, R., Bollard, C., Molldrem, J.J., Jones, R.B., Nieto, Y., Andersson, B.S., Shah, N., Oran, B., Cooper, L.J.N., Worth, L., Qazilbash, M.H., Korbling, M., Rondon, G., Ciurea, S., Bosque, D., Maewal, I., Simmons, P.J., Shpall, E.J., 2012. Cord-Blood Engraftment with Ex Vivo Mesenchymal-Cell Coculture. New England Journal of Medicine 367, 2305–2315. https://doi.org/10.1056/NEJMoa1207285

Demaurex, N., 2002. pH Homeostasis of cellular organelles. News Physiol Sci 17, 1–5. https://doi.org/10.1152/physiologyonline.2002.17.1.1

Dever, D.P., Bak, R.O., Reinisch, A., Camarena, J., Washington, G., Nicolas, C.E., Pavel-Dinu, M., Saxena, N., Wilkens, A.B., Mantri, S., Uchida, N., Hendel, A., Narla, A., Majeti, R., Weinberg, K.I., Porteus, M.H., 2016. CRISPR/Cas9 β-globin gene targeting in human haematopoietic stem cells. Nature 539, 384–389. https://doi.org/10.1038/nature20134

DeWitt, M.A., Magis, W., Bray, N.L., Wang, T., Berman, J.R., Urbinati, F., Heo, S.-J., Mitros, T., Muñoz, D.P., Boffelli, D., Kohn, D.B., Walters, M.C., Carroll, D., Martin, D.I.K., Corn, J.E., 2016. Selection-free genome editing of the sickle mutation in human adult hematopoietic stem/progenitor cells. Sci Transl Med 8, 360ra134. https://doi.org/10.1126/scitranslmed.aaf9336

Deyle, D.R., Russell, D.W., 2009. Adeno-associated virus vector integration. Curr Opin Mol Ther 11, 442–447.

Ding, X., Du, H., Yoder, M.C., Yan, C., 2014. Critical Role of the mTOR Pathway in Development and Function of Myeloid-Derived Suppressor Cells in lal−/− Mice. The American Journal of Pathology 184, 397–408. https://doi.org/10.1016/j.ajpath.2013.10.015

Doudna, J.A., Charpentier, E., 2014. The new frontier of genome engineering with CRISPR-Cas9. Science 346, 1258096. https://doi.org/10.1126/science.1258096

Drysdale, C.M., Nassehi, T., Gamer, J., Yapundich, M., Tisdale, J.F., Uchida, N., 2021. Hematopoietic Stem Cell-Targeted Gene-Addition and Gene-Editing Strategies for β-hemoglobinopathies. Cell Stem Cell 28, 191–208. https://doi.org/10.1016/j.stem.2021.01.001

Du, H., 1998. Targeted disruption of the mouse lysosomal acid lipase gene: long-term survival with massive cholesteryl ester and triglyceride storage. Human Molecular Genetics 7, 1347–1354. https://doi.org/10.1093/hmg/7.9.1347

Du, H., Heur, M., Duanmu, M., Grabowski, G.A., Hui, D.Y., Witte, D.P., Mishra, J., 2001. Lysosomal acid lipase-deficient mice: depletion of white and brown fat, severe hepatosplenomegaly, and shortened life span 12.

Dzierzak, E., Philipsen, S., 2013. Erythropoiesis: Development and Differentiation. Cold Spring Harb Perspect Med 3, a011601. https://doi.org/10.1101/cshperspect.a011601

Eaton, W.A., Bunn, H.F., 2017. Treating sickle cell disease by targeting HbS polymerization. Blood 129, 2719–2726. https://doi.org/10.1182/blood-2017-02-765891

El-Kharrag, R., Berckmueller, K.E., Madhu, R., Cui, M., Campoy, G., Mack, H.M., Wolf, C.B., Perez, A.M., Humbert, O., Kiem, H.-P., Radtke, S., 2022. Efficient polymer nanoparticle-mediated delivery of gene editing reagents into human hematopoietic stem and progenitor cells. Molecular Therapy 30, 2186–2198. https://doi.org/10.1016/j.ymthe.2022.02.026

Ellison, S.M., Liao, A., Wood, S., Taylor, J., Youshani, A.S., Rowlston, S., Parker, H., Armant, M., Biffi, A., Chan, L., Farzaneh, F., Wynn, R., Jones, S.A., Heal, P., Gaspar, H.B., Bigger, B.W., 2019. Pre-clinical Safety and Efficacy of Lentiviral Vector-Mediated Ex Vivo Stem Cell Gene Therapy for the Treatment of Mucopolysaccharidosis IIIA. Mol Ther Methods Clin Dev 13, 399–413. https://doi.org/10.1016/j.omtm.2019.04.001

Ezgu, F., 2016. Chapter Seven - Inborn Errors of Metabolism, in: Makowski, G.S. (Ed.), Advances in Clinical Chemistry. Elsevier, pp. 195–250. https://doi.org/10.1016/bs.acc.2015.12.001

Fam, T.K., Klymchenko, A.S., Collot, M., 2018. Recent Advances in Fluorescent Probes for Lipid Droplets. Materials (Basel) 11, 1768. https://doi.org/10.3390/ma11091768

Feingold, K.R., 2000. Introduction to Lipids and Lipoproteins, in: Feingold, K.R., Anawalt, B., Boyce, A., Chrousos, G., de Herder, W.W., Dhatariya, K., Dungan, K., Hershman, J.M., Hofland, J., Kalra, S., Kaltsas, G., Koch, C., Kopp, P., Korbonits, M., Kovacs, C.S., Kuohung, W., Laferrère, B., Levy, M., McGee, E.A., McLachlan, R., Morley, J.E., New, M., Purnell, J., Sahay, R., Singer, F., Sperling, M.A., Stratakis, C.A., Trence, D.L., Wilson, D.P. (Eds.), Endotext. MDText.com, Inc., South Dartmouth (MA).

Ferrari, G., Thrasher, A.J., Aiuti, A., 2021. Gene therapy using haematopoietic stem and progenitor cells. Nat Rev Genet 22, 216–234. https://doi.org/10.1038/s41576-020-00298-5

Ferrari, S., Jacob, A., Cesana, D., Laugel, M., Beretta, S., Varesi, A., Unali, G., Conti, A., Canarutto, D., Albano, L., Calabria, A., Vavassori, V., Cipriani, C., Castiello, M.C., Esposito, S., Brombin, C., Cugnata, F., Adjali, O., Ayuso, E., Merelli, I., Villa, A., Di Micco, R., Kajaste-Rudnitski, A., Montini, E., Penaud-Budloo, M., Naldini, L., 2022. Choice of template delivery mitigates the genotoxic risk and adverse impact of editing in human hematopoietic stem cells. Cell Stem Cell 29, 1428-1444.e9. https://doi.org/10.1016/j.stem.2022.09.001

Ferrari, S., Vavassori, V., Canarutto, D., Jacob, A., Castiello, M.C., Javed, A.O., Genovese, P., 2021. Gene Editing of Hematopoietic Stem Cells: Hopes and Hurdles Toward Clinical Translation. Frontiers in Genome Editing 3.

Fischer, A., Hacein-Bey-Abina, S., Cavazzana-Calvo, M., 2010. 20 years of gene therapy for SCID. Nat Immunol 11, 457–460. https://doi.org/10.1038/ni0610-457

Frangoul, H., Altshuler, D., Cappellini, M.D., Chen, Y.-S., Domm, J., Eustace, B.K., Foell, J., de la Fuente, J., Grupp, S., Handgretinger, R., Ho, T.W., Kattamis, A., Kernytsky, A., Lekstrom-Himes, J., Li, A.M., Locatelli, F., Mapara, M.Y., de Montalembert, M., Rondelli, D., Sharma, A., Sheth, S., Soni, S., Steinberg, M.H., Wall, D., Yen, A., Corbacioglu, S., 2021. CRISPR-Cas9 Gene Editing for Sickle Cell Disease and β-Thalassemia. New England Journal of Medicine 384, 252–260. https://doi.org/10.1056/NEJMoa2031054

Frati, G., Miccio, A., 2021. Genome Editing for β-Hemoglobinopathies: Advances and Challenges. Journal of Clinical Medicine 10, 482. https://doi.org/10.3390/jcm10030482

Fricker, S.P., 2013. Physiology and Pharmacology of Plerixafor. Transfus Med Hemother 40, 237–245. https://doi.org/10.1159/000354132

Fumagalli, F., Calbi, V., Sora, M.G.N., Sessa, M., Baldoli, C., Rancoita, P.M.V., Ciotti, F., Sarzana, M., Fraschini, M., Zambon, A.A., Acquati, S., Redaelli, D., Attanasio, V., Miglietta, S., Mattia, F.D., Barzaghi, F., Ferrua, F., Migliavacca, M., Tucci, F., Gallo, V., Carro, U.D., Canale, S., Spiga, I., Lorioli, L., Recupero, S., Fratini, E.S., Morena, F., Silvani, P., Calvi, M.R., Facchini, M., Locatelli, S., Corti, A., Zancan, S., Antonioli, G., Farinelli, G., Gabaldo, M., Garcia-Segovia, J., Schwab, L.C., Downey, G.F., Filippi, M., Cicalese, M.P., Martino, S., Serio, C.D., Ciceri, F., Bernardo, M.E., Naldini, L., Biffi, A., Aiuti, A., 2022. Lentiviral haematopoietic stem-cell gene therapy for early-onset metachromatic leukodystrophy: long-term results from a non-randomised, open-label, phase 1/2 trial and expanded access. The Lancet 399, 372–383. https://doi.org/10.1016/S0140-6736(21)02017-1

Gabriel, R., Lombardo, A., Arens, A., Miller, J.C., Genovese, P., Kaeppel, C., Nowrouzi, A., Bartholomae, C.C., Wang, J., Friedman, G., Holmes, M.C., Gregory, P.D., Glimm, H., Schmidt, M., Naldini, L., von Kalle, C., 2011. An unbiased genome-wide analysis of zinc-finger nuclease specificity. Nat Biotechnol 29, 816–823. https://doi.org/10.1038/nbt.1948

Gasiunas, G., Young, J.K., Karvelis, T., Kazlauskas, D., Urbaitis, T., Jasnauskaite, M., Grusyte, M.M., Paulraj, S., Wang, P.-H., Hou, Z., Dooley, S.K., Cigan, M., Alarcon, C., Chilcoat, N.D., Bigelyte, G., Curcuru, J.L., Mabuchi, M., Sun, Z., Fuchs, R.T., Schildkraut, E., Weigele, P.R., Jack, W.E., Robb, G.B., Venclovas, Č., Siksnys, V., 2020. A catalogue of biochemically diverse CRISPR-Cas9 orthologs. Nat Commun 11, 5512. https://doi.org/10.1038/s41467-020-19344-1

Gentner, B., Tucci, F., Galimberti, S., Fumagalli, F., De Pellegrin, M., Silvani, P., Camesasca, C., Pontesilli, S., Darin, S., Ciotti, F., Sarzana, M., Consiglieri, G., Filisetti, C., Forni, G., Passerini, L., Tomasoni, D., Cesana, D., Calabria, A., Spinozzi, G., Cicalese, M.-P., Calbi, V., Migliavacca, M., Barzaghi, F., Ferrua, F., Gallo, V., Miglietta, S., Zonari, E., Cheruku, P.S., Forni, C., Facchini, M., Corti, A., Gabaldo, M., Zancan, S., Gasperini, S., Rovelli, A., Boelens, J.-J., Jones, S.A., Wynn, R., Baldoli, C., Montini, E., Gregori, S., Ciceri, F., Valsecchi, M.G., la Marca, G., Parini, R., Naldini, L., Aiuti, A., Bernardo, M.-E., 2021. Hematopoietic Stem- and Progenitor-Cell Gene Therapy for Hurler Syndrome. New England Journal of Medicine 385, 1929–1940. https://doi.org/10.1056/NEJMoa2106596

Ghobadi, A., Rettig, M.P., Cooper, M.L., Holt, M.S., Ritchey, J.K., Eissenberg, L., DiPersio, J.F., 2014. Bortezomib is a rapid mobilizer of hematopoietic stem cells in mice via modulation of the VCAM-1/VLA-4 axis. Blood 124, 2752–2754. https://doi.org/10.1182/blood-2014-08-595967

Ghobadi, A., Rettig, M.P., Holt, M.S., Ritchey, J.K., Kennerly, K., Chendamarai, E., Eissenberg, L., DiPersio, J.F., 2018. Ixazomib, an oral proteasome inhibitor, induces rapid mobilization of hematopoietic progenitor cells in mice. Blood 131, 2594–2596. https://doi.org/10.1182/blood-2017-10-811620

Ghosh, S., Brown, A.M., Jenkins, C., Campbell, K., 2020. Viral Vector Systems for Gene Therapy: A Comprehensive Literature Review of Progress and Biosafety Challenges. Applied Biosafety 25, 7–18. https://doi.org/10.1177/1535676019899502

Gomaraschi, M., Bonacina, F., Norata, G.D., 2019. Lysosomal Acid Lipase: From Cellular Lipid Handler to Immunometabolic Target. Trends in Pharmacological Sciences 40, 104–115. https://doi.org/10.1016/j.tips.2018.12.006

Gomez-Ospina, N., Scharenberg, S.G., Mostrel, N., Bak, R.O., Mantri, S., Quadros, R.M., Gurumurthy, C.B., Lee, C., Bao, G., Suarez, C.J., Khan, S., Sawamoto, K., Tomatsu, S., Raj, N., Attardi, L.D., Aurelian, L., Porteus, M.H., 2019. Human genome-edited hematopoietic stem cells phenotypically correct Mucopolysaccharidosis type I. Nat Commun 10, 4045. https://doi.org/10.1038/s41467-019-11962-8

Grigg, A.P., Roberts, A.W., Raunow, H., Houghton, S., Layton, J.E., Boyd, A.W., McGrath, K.M., Maher, D., 1995. Optimizing dose and scheduling of filgrastim (granulocyte colony-stimulating factor) for mobilization and collection of peripheral blood progenitor cells in normal volunteers. Blood 86, 4437–4445.

Grimm, A.J., Kontos, S., Diaceri, G., Quaglia-Thermes, X., Hubbell, J.A., 2015. Memory of tolerance and induction of regulatory T cells by erythrocyte-targeted antigens. Sci Rep 5, 15907. https://doi.org/10.1038/srep15907

Haapaniemi, E., Botla, S., Persson, J., Schmierer, B., Taipale, J., 2018. CRISPR-Cas9 genome editing induces a p53-mediated DNA damage response. Nat Med 24, 927–930. https://doi.org/10.1038/s41591-018-0049-z

Hacein-Bey-Abina, S., Pai, S.-Y., Gaspar, H.B., Armant, M., Berry, C.C., Blanche, S., Bleesing, J., Blondeau, J., de Boer, H., Buckland, K.F., Caccavelli, L., Cros, G., De Oliveira, S., Fernández, K.S., Guo, D., Harris, C.E., Hopkins, G., Lehmann, L.E., Lim, A., London, W.B., van der Loo, J.C.M., Malani, N., Male, F., Malik, P., Marinovic, M.A., McNicol, A.-M., Moshous, D., Neven, B., Oleastro, M., Picard, C., Ritz, J., Rivat, C., Schambach, A., Shaw, K.L., Sherman, E.A., Silberstein, L.E., Six, E., Touzot, F., Tsytsykova, A., Xu-Bayford, J., Baum, C., Bushman, F.D., Fischer, A., Kohn, D.B., Filipovich, A.H., Notarangelo, L.D., Cavazzana, M., Williams, D.A., Thrasher, A.J., 2014. A Modified γ-Retrovirus Vector for X-Linked Severe Combined Immunodeficiency. N Engl J Med 371, 1407–1417. https://doi.org/10.1056/NEJMoa1404588

Hamilton, J., Jones, I., Srivastava, R., Galloway, P., 2012. A new method for the measurement of lysosomal acid lipase in dried blood spots using the inhibitor Lalistat 2. Clinica Chimica Acta 413, 1207–1210. https://doi.org/10.1016/j.cca.2012.03.019

Hanlon, K.S., Kleinstiver, B.P., Garcia, S.P., Zaborowski, M.P., Volak, A., Spirig, S.E., Muller, A., Sousa, A.A., Tsai, S.Q., Bengtsson, N.E., Lööv, C., Ingelsson, M., Chamberlain, J.S., Corey, D.P., Aryee, M.J., Joung, J.K., Breakefield, X.O., Maguire, C.A., György, B., 2019. High levels of AAV vector integration into CRISPR-induced DNA breaks. Nat Commun 10, 4439. https://doi.org/10.1038/s41467-019-12449-2

Hastie, E., Cataldi, M., Marriott, I., Grdzelishvili, V.Z., 2013. Understanding and altering cell tropism of vesicular stomatitis virus. Virus Res 176, 10.1016/j.virusres.2013.06.003. https://doi.org/10.1016/j.virusres.2013.06.003

Hattangadi, S.M., Wong, P., Zhang, L., Flygare, J., Lodish, H.F., 2011. From stem cell to red cell: regulation of erythropoiesis at multiple levels by multiple proteins, RNAs, and chromatin modifications. Blood 118, 6258–6268. https://doi.org/10.1182/blood-2011-07-356006

Hawley, R.G., RAMEZANI, A., HAWLEY, T.S., 2006. Hematopoietic Stem Cells. Methods Enzymol 419, 149–179. https://doi.org/10.1016/S0076-6879(06)19007-2

Hoggatt, J., Singh, P., Tate, T.A., Chou, B.-K., Datari, S.R., Fukuda, S., Liu, L., Kharchenko, P.V., Schajnovitz, A., Baryawno, N., Mercier, F.E., Boyer, J., Gardner, J., Morrow, D.M., Scadden, D.T., Pelus, L.M., 2018. Rapid Mobilization Reveals a Highly Engraftable Hematopoietic Stem Cell. Cell 172, 191-204.e10. https://doi.org/10.1016/j.cell.2017.11.003

Huang, J., Khan, A., Au, B.C., Barber, D.L., López-Vásquez, L., Prokopishyn, N.L., Boutin, M., Rothe, M., Rip, J.W., Abaoui, M., Nagree, M.S., Dworski, S., Schambach, A., Keating, A., West, M.L., Klassen, J., Turner, P.V., Sirrs, S., Rupar, C.A., Auray-Blais, C., Foley, R., Medin, J.A., 2017. Lentivector Iterations and Pre-Clinical Scale-Up/Toxicity Testing: Targeting Mobilized CD34+ Cells for Correction of Fabry Disease. Mol Ther Methods Clin Dev 5. https://doi.org/10.1016/j.omtm.2017.05.003

Jang, Y., Kim, Y.-S., Wielgosz, M.M., Ferrara, F., Ma, Z., Condori, J., Palmer, L.E., Zhao, X., Kang, G., Rawlings, D.J., Zhou, S., Ryu, B.Y., 2020. Optimizing lentiviral vector transduction of hematopoietic stem cells for gene therapy. Gene Ther 27, 545–556. https://doi.org/10.1038/s41434-020-0150-z

Jiang, F., Doudna, J.A., 2017. CRISPR-Cas9 Structures and Mechanisms. Annu Rev Biophys 46, 505–529. https://doi.org/10.1146/annurev-biophys-062215-010822

Kalra, A., Yetiskul, E., Wehrle, C.J., Tuma, F., 2022. Physiology, Liver, in: StatPearls. StatPearls Publishing, Treasure Island (FL).

Kanafi, M.M., Tavallaei, M., 2022. Overview of advances in CRISPR/deadCas9 technology and its applications in human diseases. Gene 830, 146518. https://doi.org/10.1016/j.gene.2022.146518

Kanter, J., Tisdale, J.F., Mapara, M.Y., Kwiatkowski, J.L., Krishnamurti, L., Schmidt, M., Miller, A.L., Pierciey, F.J., Huang, W., Ribeil, J.-A., Thompson, A.A., Walters, M.C., 2019. Resolution of Sickle Cell Disease Manifestations in Patients Treated with Lentiglobin Gene Therapy: Updated Results from the Phase 1/2 Hgb-206 Group C Study. Blood 134, 990. https://doi.org/10.1182/blood-2019-128894

Katsumura, K.R., DeVilbiss, A.W., Pope, N.J., Johnson, K.D., Bresnick, E.H., 2013. Transcriptional Mechanisms Underlying Hemoglobin Synthesis. Cold Spring Harbor Perspectives in Medicine 3, a015412–a015412. https://doi.org/10.1101/cshperspect.a015412

Khan, A., Barber, D.L., Huang, J., Rupar, C.A., Rip, J.W., Auray-Blais, C., Boutin, M., O'Hoski, P., Gargulak, K., McKillop, W.M., Fraser, G., Wasim, S., LeMoine, K., Jelinski, S., Chaudhry, A., Prokopishyn, N., Morel, C.F., Couban, S., Duggan, P.R., Fowler, D.H., Keating, A., West, M.L., Foley, R., Medin, J.A., 2021. Lentivirus-mediated gene therapy for Fabry disease. Nat Commun 12, 1178. https://doi.org/10.1038/s41467-021-21371-5

Kim, A., Dean, A., 2012. Chromatin Loop Formation in the β-Globin Locus and Its Role in Globin Gene Transcription. Mol Cells 34, 1–5. https://doi.org/10.1007/s10059-012-0048-8

Kleinig, M., Cox, J., 1998. A Quantitative Mannose 6-Phosphate Receptor-Basedin VitroAssay for Recombinant HumanN-Acetylgalactosamine-4-sulfatase. Analytical Biochemistry 260, 128–134. https://doi.org/10.1006/abio.1998.2699

Kober, L., Zehe, C., Bode, J., 2013. Optimized signal peptides for the development of high expressing CHO cell lines. Biotechnology and Bioengineering 110, 1164–1173. https://doi.org/10.1002/bit.24776

Kohn, D.B., Booth, C., Shaw, K.L., Xu-Bayford, J., Garabedian, E., Trevisan, V., Carbonaro-Sarracino, D.A., Soni, K., Terrazas, D., Snell, K., Ikeda, A., Leon-Rico, D., Moore, T.B., Buckland, K.F., Shah, A.J., Gilmour, K.C., De Oliveira, S., Rivat, C., Crooks, G.M., Izotova, N., Tse, J., Adams, S., Shupien, S., Ricketts, H., Davila, A., Uzowuru, C., Icreverzi, A., Barman, P., Campo Fernandez, B., Hollis, R.P., Coronel, M., Yu, A., Chun, K.M., Casas, C.E., Zhang, R., Arduini, S., Lynn, F., Kudari, M., Spezzi, A., Zahn, M., Heimke, R., Labik, I., Parrott, R., Buckley, R.H., Reeves, L., Cornetta, K., Sokolic, R., Hershfield, M., Schmidt, M., Candotti, F., Malech, H.L., Thrasher, A.J., Gaspar, H.B., 2021. Autologous Ex Vivo Lentiviral Gene Therapy for Adenosine Deaminase Deficiency. New England Journal of Medicine 384, 2002–2013. https://doi.org/10.1056/NEJMoa2027675

Kosicki, M., Tomberg, K., Bradley, A., 2018. Repair of double-strand breaks induced by CRISPR-Cas9 leads to large deletions and complex rearrangements. Nat Biotechnol 36, 765–771. https://doi.org/10.1038/nbt.4192

Langford-Smith, A., Wilkinson, F.L., Langford-Smith, K.J., Holley, R.J., Sergijenko, A., Howe, S.J., Bennett, W.R., Jones, S.A., Wraith, J., Merry, C.L., Wynn, R.F., Bigger, B.W., 2012. Hematopoietic stem cell and gene therapy corrects primary neuropathology and behavior in mucopolysaccharidosis IIIA mice. Mol Ther 20, 1610–1621. https://doi.org/10.1038/mt.2012.82

Lattanzi, A., Meneghini, V., Pavani, G., Amor, F., Ramadier, S., Felix, T., Antoniani, C., Masson, C., Alibeu, O., Lee, C., Porteus, M.H., Bao, G., Amendola, M., Mavilio, F., Miccio, A., 2019. Optimization of CRISPR/Cas9 Delivery to Human Hematopoietic Stem and Progenitor Cells for Therapeutic Genomic Rearrangements. Molecular Therapy 27, 137–150. https://doi.org/10.1016/j.ymthe.2018.10.008

Lawrence, R.E., Zoncu, R., 2019. The lysosome as a cellular centre for signalling, metabolism and quality control. Nat Cell Biol 21, 133–142. https://doi.org/10.1038/s41556-018-0244-7

Levasseur, D.N., Ryan, T.M., Reilly, M.P., McCune, S.L., Asakura, T., Townes, T.M., 2004. A Recombinant Human Hemoglobin with Anti-sickling Properties Greater than Fetal Hemoglobin*. Journal of Biological Chemistry 279, 27518–27524. https://doi.org/10.1074/jbc.M402578200

Li, C., Samulski, R.J., 2020. Engineering adeno-associated virus vectors for gene therapy. Nat Rev Genet 21, 255–272. https://doi.org/10.1038/s41576-019-0205-4

Li, C., Wang, H., Georgakopoulou, A., Gil, S., Yannaki, E., Lieber, A., 2021. In Vivo HSC Gene Therapy Using a Bi-modular HDAd5/35++ Vector Cures Sickle Cell Disease in a Mouse Model. Mol Ther 29, 822–837. https://doi.org/10.1016/j.ymthe.2020.09.001

Li, C., Wang, H., Gil, S., Germond, A., Fountain, C., Baldessari, A., Kim, J., Liu, Z., Georgakopoulou, A., Radtke, S., Raskó, T., Pande, A., Chiang, C., Chin, E., Yannaki, E., Izsvák, Z., Papayannopoulou, T., Kiem, H.-P., Lieber, A., 2022. Safe and efficient in vivo hematopoietic stem cell transduction in nonhuman primates using HDAd5/35++ vectors. Molecular Therapy - Methods & Clinical Development 24, 127–141. https://doi.org/10.1016/j.omtm.2021.12.003

Li, F., Zhang, H., 2019. Lysosomal Acid Lipase in Lipid Metabolism and Beyond. ATVB 39, 850–856. https://doi.org/10.1161/ATVBAHA.119.312136

Li, H., Haurigot, V., Doyon, Y., Li, T., Wong, S.Y., Bhagwat, A.S., Malani, N., Anguela, X.M., Sharma, R., Ivanciu, L., Murphy, S.L., Finn, J.D., Khazi, F.R., Zhou, S., Paschon, D.E., Rebar, E.J., Bushman, F.D., Gregory, P.D., Holmes, M.C., High, K.A., 2011. In vivo genome editing restores haemostasis in a mouse model of haemophilia. Nature 475, 217–221. https://doi.org/10.1038/nature10177

Lian, X., Yan, C., Yang, L., Xu, Y., Du, H., 2004. Lysosomal acid lipase deficiency causes respiratory inflammation and destruction in the lung. American Journal of Physiology-Lung Cellular and Molecular Physiology 286, L801–L807. https://doi.org/10.1152/ajplung.00335.2003

Liang, S., Moghimi, B., Yang, T.P., Strouboulis, J., Bungert, J., 2008. Locus control region mediated regulation of adult β-globin gene expression. J Cell Biochem 105, 9–16. https://doi.org/10.1002/jcb.21820

Lis, R., Karrasch, C.C., Poulos, M.G., Kunar, B., Redmond, D., Duran, J.G.B., Badwe, C.R., Schachterle, W., Ginsberg, M., Xiang, J., Tabrizi, A.R., Shido, K., Rosenwaks, Z., Elemento, O., Speck, N.A., Butler, J.M., Scandura, J.M., Rafii, S., 2017. Conversion of adult endothelium to immunocompetent haematopoietic stem cells. Nature 545, 439–445. https://doi.org/10.1038/nature22326

Liu, G., Lin, Q., Jin, S., Gao, C., 2022. The CRISPR-Cas toolbox and gene editing technologies. Molecular Cell, Focus on technology 82, 333–347. https://doi.org/10.1016/j.molcel.2021.12.002

Liu, Y., Luo, Y., Xia, L., Qiu, B., Zhou, T., Feng, M., Xue, F., Chen, X., Han, L., Zhang, J., Xia, Q., 2019. The Effects of Liver Transplantation in Children With Niemann-Pick Disease Type B. Liver Transplantation 25, 1233–1240. https://doi.org/10.1002/lt.25457

Magrin, E., Miccio, A., Cavazzana, M., 2019. Lentiviral and genome-editing strategies for the treatment of β-hemoglobinopathies. Blood 134, 1203–1213. https://doi.org/10.1182/blood.2019000949

Mak, C.M., Lee, H.-C.H., Chan, A.Y.-W., Lam, C.-W., 2013. Inborn errors of metabolism and expanded newborn screening: review and update. Critical Reviews in Clinical Laboratory Sciences 50, 142–162. https://doi.org/10.3109/10408363.2013.847896

Marina, O.C., Sanders, C.K., Mourant, J.R., 2012. Correlating light scattering with internal cellular structures. Biomed Opt Express 3, 296–312. https://doi.org/10.1364/BOE.3.000296

Marktel, S., Scaramuzza, S., Cicalese, M.P., Giglio, F., Galimberti, S., Lidonnici, M.R., Calbi, V., Assanelli, A., Bernardo, M.E., Rossi, C., Calabria, A., Milani, R., Gattillo, S., Benedicenti, F., Spinozzi, G., Aprile, A., Bergami, A., Casiraghi, M., Consiglieri, G., Masera, N., D'Angelo, E., Mirra, N., Origa, R., Tartaglione, I., Perrotta, S., Winter, R., Coppola, M., Viarengo, G., Santoleri, L., Graziadei, G., Gabaldo, M., Valsecchi, M.G., Montini, E., Naldini, L., Cappellini, M.D., Ciceri, F., Aiuti, A., Ferrari, G., 2019. Intrabone hematopoietic stem cell gene therapy for adult and pediatric patients affected by transfusion-dependent ß-thalassemia. Nat Med 25, 234–241. https://doi.org/10.1038/s41591-018-0301-6

Martínez-Molina, E., Chocarro-Wrona, C., Martínez-Moreno, D., Marchal, J.A., Boulaiz, H., 2020. Large-Scale Production of Lentiviral Vectors: Current Perspectives and Challenges. Pharmaceutics 12, 1051. https://doi.org/10.3390/pharmaceutics12111051

Meier, A.F., Fraefel, C., Seyffert, M., 2020. The Interplay between Adeno-Associated Virus and Its Helper Viruses. Viruses 12, 662. https://doi.org/10.3390/v12060662

Mendel, G., 1886. Versuche über Pflanzen-Hybriden. Verh. Naturforsch. Ver. Brünn 4: 3–47 (1866)(Article in German).

Miccio, A., Cesari, R., Lotti, F., Rossi, C., Sanvito, F., Ponzoni, M., Routledge, S.J., Chow, C.-M., Antoniou, M.N., Ferrari, G., 2008. In vivo selection of genetically modified erythroblastic progenitors leads to long-term correction of β-thalassemia. Proceedings of the National Academy of Sciences.

Mochalova, E.N., Kotov, I.A., Lifanov, D.A., Chakraborti, S., Nikitin, M.P., 2022. Imaging flow cytometry data analysis using convolutional neural network for quantitative investigation of phagocytosis. Biotechnology and Bioengineering 119, 626–635. https://doi.org/10.1002/bit.27986

Montiel-Equihua, C.A., Zhang, L., Knight, S., Saadeh, H., Scholz, S., Carmo, M., Alonso-Ferrero, M.E., Blundell, M.P., Monkeviciute, A., Schulz, R., Collins, M., Takeuchi, Y., Schmidt, M., Fairbanks, L., Antoniou, M., Thrasher, A.J., Gaspar, H.B., 2012. The β-Globin Locus Control Region in Combination With the EF1α Short Promoter Allows Enhanced Lentiviral Vector-mediated Erythroid Gene Expression With Conserved Multilineage Activity. Molecular Therapy 20, 1400–1409. https://doi.org/10.1038/mt.2012.50

Morgan, R.A., Gray, D., Lomova, A., Kohn, D.B., 2017. Hematopoietic Stem Cell Gene Therapy – Progress and Lessons Learned. Cell Stem Cell 21, 574–590. https://doi.org/10.1016/j.stem.2017.10.010

Morris, K.T., Khan, H., Ahmad, A., Weston, L.L., Nofchissey, R.A., Pinchuk, I.V., Beswick, E.J., 2014. G-CSF and G-CSFR are highly expressed in human gastric and colon cancers and promote carcinoma cell proliferation and migration. Br J Cancer 110, 1211–1220. https://doi.org/10.1038/bjc.2013.822

Mullard, A., 2020. Gene-editing pipeline takes off. Nature Reviews Drug Discovery 19, 367–372. https://doi.org/10.1038/d41573-020-00096-y

Munley, J.A., Kelly, L.S., Mohr, A.M., 2022. Adrenergic Modulation of Erythropoiesis After Trauma. Front. Physiol. 0. https://doi.org/10.3389/fphys.2022.859103

Nagree, M.S., Scalia, S., McKillop, W.M., Medin, J.A., 2019. An update on gene therapy for lysosomal storage disorders. Expert Opin Biol Ther 19, 655–670. https://doi.org/10.1080/14712598.2019.1607837

Nakade, S., Tsubota, T., Sakane, Y., Kume, S., Sakamoto, N., Obara, M., Daimon, T., Sezutsu, H., Yamamoto, T., Sakuma, T., Suzuki, K.T., 2014. Microhomology-mediated end-joining-dependent integration of donor DNA in cells and animals using TALENs and CRISPR/Cas9. Nat Commun 5, 5560. https://doi.org/10.1038/ncomms6560

Naldini, L., 2019. Genetic engineering of hematopoiesis: current stage of clinical translation and future perspectives. EMBO molecular medicine 11, e9958.

Nguyen, P., Leray, V., Diez, M., Serisier, S., Bloc'h, J.L., Siliart, B., Dumon, H., 2008. Liver lipid metabolism. Journal of Animal Physiology and Animal Nutrition 92, 272–283. https://doi.org/10.1111/j.1439-0396.2007.00752.x

Okimoto, T., Friedmann, T., Miyanohara, A., 2001. VSV-G Envelope Glycoprotein Forms Complexes with Plasmid DNA and MLV Retrovirus-like Particles in Cell-free Conditions and Enhances DNA Transfection. Molecular Therapy 4, 232–238. https://doi.org/10.1006/mthe.2001.0443

Omer-Javed, A., Pedrazzani, G., Albano, L., Ghaus, S., Latroche, C., Manzi, M., Ferrari, S., Fiumara, M., Jacob, A., Vavassori, V., Nonis, A., Canarutto, D., Naldini, L., 2022. Mobilization-based chemotherapy-free engraftment of gene-edited human hematopoietic stem cells. Cell 185, 2248-2264.e21. https://doi.org/10.1016/j.cell.2022.04.039

Ou, L., DeKelver, R.C., Rohde, M., Tom, S., Radeke, R., St. Martin, S.J., Santiago, Y., Sproul, S., Przybilla, M.J., Koniar, B.L., Podetz-Pedersen, K.M., Laoharawee, K., Cooksley, R.D., Meyer, K.E., Holmes, M.C., McIvor, R.S., Wechsler, T., Whitley, C.B., 2019. ZFN-Mediated In Vivo Genome Editing Corrects Murine Hurler Syndrome. Molecular Therapy 27, 178–187. https://doi.org/10.1016/j.ymthe.2018.10.018

Parenti, G., Medina, D.L., Ballabio, A., 2021. The rapidly evolving view of lysosomal storage diseases. EMBO Molecular Medicine 13, e12836. https://doi.org/10.15252/emmm.202012836

Pavani, G., Amendola, M., 2020. Targeted Gene Delivery: Where to Land. Front Genome Ed 2, 609650. https://doi.org/10.3389/fgeed.2020.609650

Pavani, G., Fabiano, A., Laurent, M., Amor, F., Cantelli, E., Chalumeau, A., Maule, G., Tachtsidi, A., Concordet, J.-P., Cereseto, A., Mavilio, F., Ferrari, G., Miccio, A., Amendola, M., 2021. Correction of β-thalassemia by CRISPR/Cas9 editing of the α-globin locus in human hematopoietic stem cells. Blood Adv 5, 1137–1153. https://doi.org/10.1182/bloodadvances.2020001996

Pavani, G., Laurent, M., Fabiano, A., Cantelli, E., Sakkal, A., Corre, G., Lenting, P.J., Concordet, J.-P., Toueille, M., Miccio, A., Amendola, M., 2020. Ex vivo editing of human hematopoietic stem cells for erythroid expression of therapeutic proteins. Nat Commun 11, 3778. https://doi.org/10.1038/s41467-020-17552-3

Piel, F.B., Steinberg, M.H., Rees, D.C., 2017. Sickle Cell Disease. New England Journal of Medicine 376, 1561–1573. https://doi.org/10.1056/NEJMra1510865

Piras, G., Montiel-Equihua, C., Chan, Y.-K.A., Wantuch, S., Stuckey, D., Burke, D., Prunty, H., Phadke, R., Chambers, D., Partida-Gaytan, A., Leon-Rico, D., Panchal, N., Whitmore, K., Calero, M., Benedetti, S., Santilli, G., Thrasher, A.J., Gaspar, H.B., 2020. Lentiviral Hematopoietic Stem Cell Gene Therapy Rescues Clinical Phenotypes in a Murine Model of Pompe Disease. Molecular Therapy - Methods & Clinical Development 18, 558–570. https://doi.org/10.1016/j.omtm.2020.07.001

Pittman, R.N., 2011. Oxygen Transport, Regulation of Tissue Oxygenation. Morgan & Claypool Life Sciences.

Platt, F.M., Boland, B., van der Spoel, A.C., 2012. Lysosomal storage disorders: The cellular impact of lysosomal dysfunction. Journal of Cell Biology 199, 723–734. https://doi.org/10.1083/jcb.201208152

Platt, F.M., d'Azzo, A., Davidson, B.L., Neufeld, E.F., Tifft, C.J., 2018. Lysosomal storage diseases. Nat Rev Dis Primers 4, 1–25. https://doi.org/10.1038/s41572-018-0025-4

Poletti, V., Mavilio, F., 2018. Interactions between Retroviruses and the Host Cell Genome. Molecular Therapy - Methods & Clinical Development 8, 31–41. https://doi.org/10.1016/j.omtm.2017.10.001

Potter, J.E., Petts, G., Ghosh, A., White, F.J., Kinsella, J.L., Hughes, S., Roberts, J., Hodgkinson, A., Brammeier, K., Church, H., Merrigan, C., Hughes, J., Evans, P., Campbell, H., Bonney, D., Newman, W.G., Bigger, B.W., Broomfield, A., Jones, S.A., Wynn, R.F., 2021. Enzyme replacement therapy and hematopoietic stem cell transplant: a new paradigm of treatment in Wolman disease. Orphanet J Rare Dis 16, 235. https://doi.org/10.1186/s13023-021-01849-7

Prakash, V., Moore, M., Yáñez-Muñoz, R.J., 2016. Current Progress in Therapeutic Gene Editing for Monogenic Diseases. Mol Ther 24, 465–474. https://doi.org/10.1038/mt.2016.5

Pugach, E.K., Feltes, M., Kaufman, R.J., Ory, D.S., Bang, A.G., 2018. High-content screen for modifiers of Niemann-Pick type C disease in patient cells. Human Molecular Genetics 27, 2101–2112. https://doi.org/10.1093/hmg/ddy117

Puzzo, F., Colella, P., Biferi, M.G., Bali, D., Paulk, N.K., Vidal, P., Collaud, F., Simon-Sola, M., Charles, S., Hardet, R., 2017. Rescue of Pompe disease in mice by AAV-mediated liver delivery of secretable acid α-glucosidase. Science translational medicine 9, eaam6375.

Qamar Saeed, M., Dufour, N., Bartholmae, C., Sieranska, U., Knopf, M., Thierry, E., Thierry, S., Delelis, O., Grandchamp, N., Pilet, H., Ravassard, P., Massonneau, J., Pflumio, F., von Kalle, C., Lachapelle, F., Bemelmans, A.-P., Schmidt, M., Serguera, C., 2014. Comparison Between Several Integrase-defective Lentiviral Vectors Reveals Increased Integration of an HIV Vector Bearing a D167H Mutant. Mol Ther Nucleic Acids 3, e213. https://doi.org/10.1038/mtna.2014.65

Qu, P., Du, H., Wilkes, D.S., Yan, C., 2009. Critical Roles of Lysosomal Acid Lipase in T Cell Development and Function. The American Journal of Pathology 174, 944–956. https://doi.org/10.2353/ajpath.2009.080562

Qu, P., Shelley, W.C., Yoder, M.C., Wu, L., Du, H., Yan, C., 2010. Critical Roles of Lysosomal Acid Lipase in Myelopoiesis. Am J Pathol 176, 2394–2404. https://doi.org/10.2353/ajpath.2010.091063

Qu, P., Yan, C., Blum, J.S., Kapur, R., Du, H., 2011. Myeloid-Specific Expression of Human Lysosomal Acid Lipase Corrects Malformation and Malfunction of Myeloid-Derived Suppressor Cells in lal−/− Mice. The Journal of Immunology 187, 3854–3866. https://doi.org/10.4049/jimmunol.1003358

Rai, R., Romito, M., Rivers, E., Turchiano, G., Blattner, G., Vetharoy, W., Ladon, D., Andrieux, G., Zhang, F., Zinicola, M., Leon-Rico, D., Santilli, G., Thrasher, A.J., Cavazza, A., 2020. Targeted gene correction of human hematopoietic stem cells for the treatment of Wiskott - Aldrich Syndrome. Nat Commun 11, 4034. https://doi.org/10.1038/s41467-020-17626-2

Ramakrishna, S.H., Kasala, M.B., Perumal, K., Malleeswaran, S., Patcha, R.V., Varghese, J., 2022. Living-Donor Liver Transplantation for Late-Onset Lysosomal Acid Lipase Deficiency. Journal of Clinical and Experimental Hepatology 12, 672–676. https://doi.org/10.1016/j.jceh.2021.06.022

Ribeil, J.-A., Hacein-Bey-Abina, S., Payen, E., Magnani, A., Semeraro, M., Magrin, E., Caccavelli, L., Neven, B., Bourget, P., El Nemer, W., Bartolucci, P., Weber, L., Puy, H., Meritet, J.-F., Grevent, D., Beuzard, Y., Chrétien, S., Lefebvre, T., Ross, R.W., Negre, O., Veres, G., Sandler, L., Soni, S., de Montalembert, M., Blanche, S., Leboulch, P., Cavazzana, M., 2017. Gene Therapy in a Patient with Sickle Cell Disease. N Engl J Med 376, 848–855. https://doi.org/10.1056/NEJMoa1609677

Romero, Z., Lomova, A., Said, S., Miggelbrink, A., Kuo, C.Y., Campo-Fernandez, B., Hoban, M.D., Masiuk, K.E., Clark, D.N., Long, J., Sanchez, J.M., Velez, M., Miyahira, E., Zhang, R., Brown, D., Wang, X., Kurmangaliyev, Y.Z., Hollis, R.P., Kohn, D.B., 2019. Editing the Sickle Cell Disease Mutation in Human Hematopoietic Stem Cells: Comparison of Endonucleases and Homologous Donor Templates. Molecular Therapy 27, 1389–1406. https://doi.org/10.1016/j.ymthe.2019.05.014

Rumaney, M.B., Ngo Bitoungui, V.J., Vorster, A.A., Ramesar, R., Kengne, A.P., Ngogang, J., Wonkam, A., 2014. The Co-Inheritance of Alpha-Thalassemia and Sickle Cell Anemia Is Associated with Better Hematological Indices and Lower Consultations Rate in Cameroonian Patients and Could Improve Their Survival. PLoS One 9, e100516. https://doi.org/10.1371/journal.pone.0100516

Saif, M.A., Bigger, B.W., Brookes, K.E., Mercer, J., Tylee, K.L., Church, H.J., Bonney, D.K., Jones, S., Wraith, J.E., Wynn, R.F., 2012. Hematopoietic stem cell transplantation improves the high incidence of neutralizing allo-antibodies observed in Hurler's syndrome after pharmacological enzyme replacement therapy. Haematologica 97, 1320–1328. https://doi.org/10.3324/haematol.2011.058644

Sakuma, T., Takenaga, M., Kawabe, Y., Nakamura, T., Kamihira, M., Yamamoto, T., 2015. Homologous Recombination-Independent Large Gene Cassette Knock-in in CHO Cells Using TALEN and MMEJ-Directed Donor Plasmids. International Journal of Molecular Sciences 16, 23849–23866. https://doi.org/10.3390/ijms161023849

Scharenberg, S.G., Poletto, E., Lucot, K.L., Colella, P., Sheikali, A., Montine, T.J., Porteus, M.H., Gomez-Ospina, N., 2020. Engineering monocyte/macrophage−specific glucocerebrosidase expression in human hematopoietic stem cells using genome editing. Nat Commun 11, 3327. https://doi.org/10.1038/s41467-020-17148-x

Schiroli, G., Conti, A., Ferrari, S., della Volpe, L., Jacob, A., Albano, L., Beretta, S., Calabria, A., Vavassori, V., Gasparini, P., Salataj, E., Ndiaye-Lobry, D., Brombin, C., Chaumeil, J., Montini, E., Merelli, I., Genovese, P., Naldini, L., Di Micco, R., 2019. Precise Gene Editing Preserves Hematopoietic Stem Cell Function following Transient p53-Mediated DNA Damage Response. Cell Stem Cell 24, 551-565.e8. https://doi.org/10.1016/j.stem.2019.02.019

Shamshirgaran, Y., Liu, J., Sumer, H., Verma, P.J., Taheri-Ghahfarokhi, A., 2022. Tools for Efficient Genome Editing; ZFN, TALEN, and CRISPR. Methods Mol Biol 2495, 29–46. https://doi.org/10.1007/978-1-0716-2301-5_2

Sinn, P.L., Sauter, S.L., McCray, P.B., 2005. Gene Therapy Progress and Prospects: Development of improved lentiviral and retroviral vectors – design, biosafety, and production. Gene Ther 12, 1089–1098. https://doi.org/10.1038/sj.gt.3302570

Skulimowska, I., Sosniak, J., Gonka, M., Szade, A., Jozkowicz, A., Szade, K., 2021. The biology of hematopoietic stem cells and its clinical implications. The FEBS Journal n/a. https://doi.org/10.1111/febs.16192

Smith, A.R., Schiller, G.J., Vercellotti, G.M., Kwiatkowski, J.L., Krishnamurti, L., Esrick, E.B., Williams, D.A., Miller, W.P., Woolfson, A., Walters, M.C., 2019. Preliminary Results of a Phase 1/2 Clinical Study of Zinc Finger Nuclease-Mediated Editing of BCL11A in Autologous Hematopoietic Stem Cells for Transfusion-Dependent Beta Thalassemia. Blood 134, 3544. https://doi.org/10.1182/blood-2019-125743

Stoye, J.P., 2012. Studies of endogenous retroviruses reveal a continuing evolutionary saga. Nat Rev Microbiol 10, 395–406. https://doi.org/10.1038/nrmicro2783

Sugimura, R., Jha, D.K., Han, A., Soria-Valles, C., da Rocha, E.L., Lu, Y.-F., Goettel, J.A., Serrao, E., Rowe, R.G., Malleshaiah, M., Wong, I., Sousa, P., Zhu, T.N., Ditadi, A., Keller, G., Engelman, A.N., Snapper, S.B., Doulatov, S., Daley, G.Q., 2017. Haematopoietic stem and progenitor cells from human pluripotent stem cells. Nature 545, 432–438. https://doi.org/10.1038/nature22370

Suzuki, K., Tsunekawa, Y., Hernandez-Benitez, R., Wu, J., Zhu, J., Kim, E.J., Hatanaka, F., Yamamoto, M., Araoka, T., Li, Z., Kurita, M., Hishida, T., Li, M., Aizawa, E., Guo, S., Chen, S., Goebl, A., Soligalla, R.D., Qu, J., Jiang, T., Fu, X., Jafari, M., Esteban, C.R., Berggren, W.T., Lajara, J., Nuñez-Delicado, E., Guillen, P., Campistol, J.M., Matsuzaki, F., Liu, G.-H., Magistretti, P., Zhang, Kun, Callaway, E.M., Zhang, Kang, Belmonte, J.C.I., 2016. In vivo genome editing via CRISPR/Cas9 mediated homology-independent targeted integration. Nature 540, 144–149. https://doi.org/10.1038/nature20565

Taher, A.T., Musallam, K.M., Cappellini, M.D., 2021. β-Thalassemias. New England Journal of Medicine 384, 727–743. https://doi.org/10.1056/NEJMra2021838

Taleei, R., Nikjoo, H., 2013. Biochemical DSB-repair model for mammalian cells in G1 and early S phases of the cell cycle. Mutation Research/Genetic Toxicology and Environmental Mutagenesis, From DNA Damage to Chromosomal Aberrations 756, 206–212. https://doi.org/10.1016/j.mrgentox.2013.06.004

Tasan, I., Zhao, H., 2017. Targeting Specificity of the CRISPR/Cas9 System. ACS Synth Biol 6, 1609–1613. https://doi.org/10.1021/acssynbio.7b00270

Thompson, A.A., Walters, M.C., Kwiatkowski, J., Rasko, J.E.J., Ribeil, J.-A., Hongeng, S., Magrin, E., Schiller, G.J., Payen, E., Semeraro, M., Moshous, D., Lefrere, F., Puy, H., Bourget, P., Magnani, A., Caccavelli, L., Diana, J.-S., Suarez, F., Monpoux, F., Brousse, V., Poirot, C., Brouzes, C., Meritet, J.-F., Pondarré, C., Beuzard, Y., Chrétien, S., Lefebvre, T., Teachey, D.T., Anurathapan, U., Ho, P.J., von Kalle, C., Kletzel, M., Vichinsky, E., Soni, S., Veres, G., Negre, O., Ross, R.W., Davidson, D., Petrusich, A., Sandler, L., Asmal, M., Hermine, O., De Montalembert, M., Hacein-Bey-Abina, S., Blanche, S., Leboulch, P., Cavazzana, M., 2018. Gene Therapy in Patients with Transfusion-Dependent β-Thalassemia. N Engl J Med 378, 1479–1493. https://doi.org/10.1056/NEJMoa1705342

Tolar, J., Petryk, A., Khan, K., Bjoraker, K., Jessurun, J., Dolan, M., Kivisto, T., Charnas, L., Shapiro, E., Orchard, P., 2009. Long-term metabolic, endocrine, and neuropsychological outcome of hematopoietic cell transplantation for Wolman disease. Bone marrow transplantation 43, 21.

Tornabene, P., Ferla, R., Llado-Santaeularia, M., Centrulo, M., Dell'Anno, M., Esposito, F., Marrocco, E., Pone, E., Minopoli, R., Iodice, C., Nusco, E., Rossi, S., Lyubenova, H., Manfredi, A., Di Filippo, L., Iuliano, A., Torella, A., Piluso, G., Musacchia, F., Surace, E.M., Cacchiarelli, D., Nigro, V., Auricchio, A., 2022. Therapeutic homology-independent targeted integration in retina and liver. Nat Commun 13, 1963. https://doi.org/10.1038/s41467-022-29550-8

Tran, N.T., Danner, E., Li, X., Graf, R., Lebedin, M., de la Rosa, K., Kühn, R., Rajewsky, K., Chu, V.T., 2022. Precise CRISPR-Cas–mediated gene repair with minimal off-target and unintended on-target mutations in human hematopoietic stem cells. Science Advances 8, eabm9106. https://doi.org/10.1126/sciadv.abm9106

Trefts, E., Gannon, M., Wasserman, D.H., 2017. The liver. Curr Biol 27, R1147–R1151. https://doi.org/10.1016/j.cub.2017.09.019

Tsai, S.Q., Zheng, Z., Nguyen, N.T., Liebers, M., Topkar, V.V., Thapar, V., Wyvekens, N., Khayter, C., Iafrate, A.J., Le, L.P., Aryee, M.J., Joung, J.K., 2015. GUIDE-seq enables genome-wide profiling of off-target cleavage by CRISPR-Cas nucleases. Nat Biotechnol 33, 187–197. https://doi.org/10.1038/nbt.3117

Turchiano, G., Andrieux, G., Klermund, J., Blattner, G., Pennucci, V., el Gaz, M., Monaco, G., Poddar, S., Mussolino, C., Cornu, T.I., Boerries, M., Cathomen, T., 2021. Quantitative evaluation of chromosomal rearrangements in gene-edited human stem cells by CAST-Seq. Cell Stem Cell 28, 1136-1147.e5. https://doi.org/10.1016/j.stem.2021.02.002

Uchida, N., Li, L., Nassehi, T., Drysdale, C.M., Yapundich, M., Gamer, J., Haro-Mora, J.J., Demirci, S., Leonard, A., Bonifacino, A.C., Krouse, A.E., Linde, N.S., Allen, C., Peshwa, M.V., De Ravin, S.S., Donahue, R.E., Malech, H.L., Tisdale, J.F., 2021. Preclinical evaluation for engraftment of CD34+ cells gene-edited at the sickle cell disease locus in xenograft mouse and non-human primate models. Cell Reports Medicine 2, 100247. https://doi.org/10.1016/j.xcrm.2021.100247

Uchida, N., Li, L., Nassehi, T., Yapundich, M., Gamer, J., Drysdale, C., Haro-Mora, J.J., Demirci, S., Bonifacino, A., Krouse, A., Linde, N.S., Allen, C., De Ravin, S.S., Donahue, R.E., Malech, H.L., Peshwa, M., Tisdale, J.F., 2019. Preclinical Evaluation for Engraftment of Gene-Edited CD34+ Cells with a Sickle Cell Disease Mutation in a Rhesus Transplantation Model. Blood 134, 609. https://doi.org/10.1182/blood-2019-122727

Uddin, F., Rudin, C.M., Sen, T., 2020. CRISPR Gene Therapy: Applications, Limitations, and Implications for the Future. Frontiers in Oncology 10.

Urnov, F.D., Rebar, E.J., Holmes, M.C., Zhang, H.S., Gregory, P.D., 2010. Genome editing with engineered zinc finger nucleases. Nat Rev Genet 11, 636–646. https://doi.org/10.1038/nrg2842

Vakulskas, C.A., Dever, D.P., Rettig, G.R., Turk, R., Jacobi, A.M., Collingwood, M.A., Bode, N.M., McNeill, M.S., Yan, S., Camarena, J., Lee, C.M., Park, S.H., Wiebking, V., Bak, R.O., Gomez-Ospina, N., Pavel-Dinu, M., Sun, W., Bao, G., Porteus, M.H., Behlke, M.A., 2018. A high-fidelity Cas9 mutant delivered as a ribonucleoprotein complex enables efficient gene editing in human haematopoietic stem and progenitor cells. Nat Med 24, 1216–1224. https://doi.org/10.1038/s41591-018-0137-0

Vichinsky, E.P., 2013. Clinical Manifestations of α-Thalassemia. Cold Spring Harb Perspect Med 3, a011742. https://doi.org/10.1101/cshperspect.a011742

Vijay, S., Brassier, A., Ghosh, A., Fecarotta, S., Abel, F., Marulkar, S., Jones, S.A., 2020. Long-Term Survival With Sebelipase Alfa Enzyme Replacement Therapy in Infants With Rapidly Progressive Lysosomal Acid Lipase Deficiency Final Results From 2 Open-Label Studies (preprint). In Review. https://doi.org/10.21203/rs.3.rs-45422/v2

Vijayraghavan, S., Kantor, B., 2017. A Protocol for the Production of Integrase-deficient Lentiviral Vectors for CRISPR/Cas9-mediated Gene Knockout in Dividing Cells. J Vis Exp 56915. https://doi.org/10.3791/56915

Villa, C.H., Anselmo, A.C., Mitragotri, S., Muzykantov, V., 2016. Red blood cells: Supercarriers for drugs, biologicals, and nanoparticles and inspiration for advanced delivery systems. Advanced Drug Delivery Reviews, Biologically-inspired drug delivery systems 106, 88–103. https://doi.org/10.1016/j.addr.2016.02.007

Wagner, D.L., Amini, L., Wendering, D.J., Burkhardt, L.-M., Akyüz, L., Reinke, P., Volk, H.-D., Schmueck-Henneresse, M., 2019. High prevalence of Streptococcus pyogenes Cas9-reactive T cells within the adult human population. Nat Med 25, 242–248. https://doi.org/10.1038/s41591-018-0204-6

Wallace, H.A.C., Marques-Kranc, F., Richardson, M., Luna-Crespo, F., Sharpe, J.A., Hughes, J., Wood, W.G., Higgs, D.R., Smith, A.J.H., 2007. Manipulating the Mouse Genome to Engineer Precise Functional Syntenic Replacements with Human Sequence. Cell 128, 197–209. https://doi.org/10.1016/j.cell.2006.11.044

Walters, M.C., Smith, A.R., Schiller, G.J., Esrick, E.B., Williams, D.A., Gogoleva, T., Rouy, D., Cockroft, B.M., Vercellotti, G.M., 2021. Updated Results of a Phase 1/2 Clinical Study of Zinc Finger Nuclease-Mediated Editing of BCL11A in Autologous Hematopoietic Stem Cells for Transfusion-Dependent Beta Thalassemia. Blood 138, 3974. https://doi.org/10.1182/blood-2021-147907

Wang, D., Tai, P.W.L., Gao, G., 2019. Adeno-associated virus vector as a platform for gene therapy delivery. Nat Rev Drug Discov 18, 358–378. https://doi.org/10.1038/s41573-019-0012-9

Wang, D., Zhang, W., Kalfa, T.A., Grabowski, G., Davies, S., Malik, P., Pan, D., 2009. Reprogramming erythroid cells for lysosomal enzyme production leads to visceral and CNS cross-correction in mice with Hurler syndrome. Proceedings of the National Academy of Sciences 106, 19958–19963. https://doi.org/10.1073/pnas.0908528106

Wang, H., Richter, M., Psatha, N., Li, C., Kim, J., Liu, J., Ehrhardt, A., Nilsson, S.K., Cao, B., Palmer, D., Ng, P., Izsvák, Z., Haworth, K.G., Kiem, H.-P., Papayannopoulou, T., Lieber, A., 2018. A Combined In Vivo HSC Transduction/Selection Approach Results in Efficient and Stable Gene Expression in Peripheral Blood Cells in Mice. Mol Ther Methods Clin Dev 8, 52–64. https://doi.org/10.1016/j.omtm.2017.11.004

Wang, X., Wang, Yebo, Wu, X., Wang, J., Wang, Yingjia, Qiu, Z., Chang, T., Huang, H., Lin, R.-J., Yee, J.-K., 2015. Unbiased detection of off-target cleavage by CRISPR-Cas9 and TALENs using integrase-defective lentiviral vectors. Nat Biotechnol 33, 175–178. https://doi.org/10.1038/nbt.3127

Wang, Yebo, Wang, Yingjia, Chang, T., Huang, H., Yee, J.-K., 2017. Integration-defective lentiviral vector mediates efficient gene editing through homology-directed repair in human embryonic stem cells. Nucleic Acids Res 45, e29. https://doi.org/10.1093/nar/gkw1057

Watson, J.D., Crick, F.H.C., 1953. Molecular Structure of Nucleic Acids: A Structure for Deoxyribose Nucleic Acid. Nature 171, 737–738. https://doi.org/10.1038/171737a0

Wen, W., Zhang, X.-B., 2022. CRISPR–Cas9 gene editing induced complex on-target outcomes in human cells. Experimental Hematology 110, 13–19. https://doi.org/10.1016/j.exphem.2022.03.002

Wilkinson, A.C., Dever, D.P., Baik, R., Camarena, J., Hsu, I., Charlesworth, C.T., Morita, C., Nakauchi, H., Porteus, M.H., 2021. Cas9-AAV6 gene correction of beta-globin in autologous HSCs improves sickle cell disease erythropoiesis in mice. Nat Commun 12, 686. https://doi.org/10.1038/s41467-021-20909-x

Wilkinson, A.C., Ishida, R., Kikuchi, M., Sudo, K., Morita, M., Crisostomo, R.V., Yamamoto, R., Loh, K.M., Nakamura, Y., Watanabe, M., Nakauchi, H., Yamazaki, S., 2019. Long-term ex vivo haematopoietic-stem-cell expansion allows nonconditioned transplantation. Nature 571, 117–121. https://doi.org/10.1038/s41586-019-1244-x

Witeck, C. da R., Schmitz, A.C., Oliveira, J.M.D. de, Porporatti, A.L., Canto, G.D.L., Pires, M.M. de S., 2022. Lysosomal acid lipase deficiency in pediatric patients: a scoping review. J. Pediatr. (Rio J.) 98, 04–14. https://doi.org/10.1016/j.jped.2021.03.003

Worgall, S., Crystal, R.G., 2014. Chapter 34 - Gene Therapy, in: Lanza, R., Langer, R., Vacanti, J. (Eds.), Principles of Tissue Engineering (Fourth Edition). Academic Press, Boston, pp. 657–686. https://doi.org/10.1016/B978-0-12-398358-9.00034-3

Woud, W.W., van der Pol, E., Mul, E., Hoogduijn, M.J., Baan, C.C., Boer, K., Merino, A., 2022. An imaging flow cytometry-based methodology for the analysis of single extracellular vesicles in unprocessed human plasma. Commun Biol 5, 1–14. https://doi.org/10.1038/s42003-022-03569-5

Xu, M., Liu, K., Swaroop, M., Porter, F.D., Sidhu, R., Finkes, S., Ory, D.S., Marugan, J.J., Xiao, J., Southall, N., Pavan, W.J., Davidson, C., Walkley, S.U., Remaley, A.T., Baxa, U., Sun, W., McKew, J.C., Austin, C.P., Zheng, W., 2012. δ-Tocopherol Reduces Lipid Accumulation in Niemann-Pick Type C1 and Wolman Cholesterol Storage Disorders. J Biol Chem 287, 39349–39360. https://doi.org/10.1074/jbc.M112.357707

Yang, C., Wang, X., 2021. Lysosome biogenesis: Regulation and functions. Journal of Cell Biology 220, e202102001. https://doi.org/10.1083/jcb.202102001

Yanik, M., Ponnam, S.P.G., Wimmer, T., Trimborn, L., Müller, C., Gambert, I., Ginsberg, J., Janise, A., Domicke, J., Wende, W., Lorenz, B., Stieger, K., 2018. Development of a Reporter System to Explore MMEJ in the Context of Replacing Large Genomic Fragments. Molecular Therapy - Nucleic Acids 11, 407–415. https://doi.org/10.1016/j.omtn.2018.03.010

Yao, X., Wang, Xing, Liu, J., Hu, X., Shi, L., Shen, X., Ying, W., Sun, X., Wang, Xin, Huang, P., Yang, H., 2017. CRISPR/Cas9 – Mediated Precise Targeted Integration In Vivo Using a Double Cut Donor with Short Homology Arms. EBioMedicine 20, 19–26. https://doi.org/10.1016/j.ebiom.2017.05.015

Yi, Y., Noh, M.J., Lee, K.H., 2011. Current advances in retroviral gene therapy. Curr Gene Ther 11, 218–228. https://doi.org/10.2174/156652311795684740

Zhou, X., Smith, Q.R., Liu, X., 2021. Brain penetrating peptides and peptide–drug conjugates to overcome the blood–brain barrier and target CNS diseases. WIREs Nanomedicine and Nanobiotechnology 13, e1695. https://doi.org/10.1002/wnan.1695

Zschenker, O., 2004. Lysosomal Acid Lipase as a Preproprotein. Journal of Biochemistry 136, 65–72. https://doi.org/10.1093/jb/mvh093

Annexe : Résumé en Français

10 ANNEXE : RÉSUMÉ EN FRANÇAIS

10.1 THERAPIE GENIQUE *EX VIVO* BASE SUR L'UTILISATION DES LENTIVIRUS POUR LES MALADIES GENETIQUES

La thérapie génique (TG) est définie comme une modification génétique basée sur l'insertion d'un gène thérapeutique ou la délétion, modification d'un gène maladie dans le but de corriger un défaut génétique dans le cas de maladies héréditaires ou d'activer la réponse immunitaire pour tuer dans le cadre d'un traitement contre le cancer. Les deux principales thérapies géniques sont : 1) la thérapie génique *ex vivo* basée sur la modification des cellules souches hématopoïétiques (HSCs) du patient dans le cadre de maladie génétique ou de Lymphocytes T dans le cadre de thérapie contre le cancer et 2) la thérapie génique *in vivo* qui repose sur l'injection directe chez le patient de vecteurs codant la séquence d'ADN (Alnasser, 2021). Aujourd'hui, la thérapie génique est appliquée à un large éventail de maladies monogéniques, des maladies métaboliques aux maladies neuromusculaires. Les troubles monogéniques sont des mutations héréditaires rares d'un seul gène entraînant une morbidité et pouvant induire un décès prématuré pendant l'enfance. Désormais, environ 5000 à 8000 maladies monogéniques ont été identifiées, tel que la mucoviscidose, la drépanocytose, la dystrophie musculaire de Duchenne... (Prakash et al., 2016). Tous ces troubles entraînent une synthèse anormale des protéines qui altère l'homéostasie cellulaire et le fonctionnement des organes. La compréhension et le traitement des troubles monogéniques ont fait l'objet de recherches scientifiques importantes au cours de la dernière décennie. Le développement du séquençage du génome permet d'identifier le ou les gènes mutés et donc le mécanisme cellulaire altéré. Au fil du temps, des options thérapeutiques ont été développées pour contrebalancer le phénotype, comme la transplantation d'organes, la transfusion sanguine ou la transplantation allogénique de cellules souches hématopoïétiques (HSCT). Les greffes de cellules souches hématopoïétiques (HSCs) ont permis de gérer avec succès la maladie en améliorant la qualité ou la durée de vie dans différent troubles monogéniques tels que les hémoglobinopathies et les troubles métaboliques. Le traitement consiste à remplacer les HSCs du patient par des cellules saines provenant d'un donneur (Copelan, 2006). Les CSH sont des cellules multipotentes capables de reconstituer un système sanguin sain et de délivrer

les protéines manquantes aux tissus affectés. Chez l'homme, les cellules souches et progénitrices hématopoïétiques (HSPCs) sont situées dans le microenvironnement de la moelle osseuse appelé niche. La niche de la moelle osseuse offre l'environnement approprié pour la différenciation ou l'auto-renouvellement des HSCs. Les HSPCs sont composées de HSCs à long terme, de HSCs à court terme et de progéniteurs multipotents. Les HSCs à long terme sont les cellules souches multipotentes capables de générer toutes les populations de la lignée sanguine : les globules blancs des lignées myéloïdes et lymphoïdes, les globules rouges et les plaquettes, et d'auto-renouveler leur propre population. Alors que les HSCs à court terme et de progéniteurs multipotents ont un potentiel différentiel mais aucune capacité d'auto-renouvellement (Skulimowska et al., 2021 ; Hawley et al., 2006). Bien qu'elles soient thérapeutiques pour certains troubles monogéniques, les HSCT sont limitées par la disponibilité d'un donneur approprié et la réaction immunitaire induite par les lymphocytes du donneur contre le receveur (maladie du greffon contre l'hôte, GAVHD) (Skulimowska et al., 2021 ; Hawley et al., 2006). Récemment, l'autogreffe de HSCs de patients génétiquement corrigés, définie comme une thérapie génique *ex vivo*, est apparue comme une alternative curative prometteuse. En effet, la thérapie génique *ex vivo* permet de contourner l'exigence d'un donneur compatible et offre donc la possibilité de traiter pratiquement tous les patients (Morgan et al., 2017).

Dans le cadre de la GT *ex vivo*, les HSCs du patient sont récupérées et isolées du sang périphérique ou de la moelle osseuse, génétiquement modifiées et transplantées chez le patient. Après la prise de greffe, les HSCs modifiées seront capables de restaurer un système hématopoïétique sain capable de produire les protéines thérapeutiques à un niveau supérieur au niveau physiologique dans un large type de cellules hématopoïétiques allant des globules blancs (lymphocytes, monocytes, cellules tueuses naturelles) aux plaquettes et aux globule rouges (Morgan et al., 2017 ; Naldini, 2019). La correction des HSCs peut prendre différentes formes, de l'insertion d'une copie fonctionnelle du gène muté à l'édition de la ou des mutations sous-jacentes à l'aide de nucléases. Les deux stratégies impliquent la modification du génome des CSH du patient et nécessitent le transport de la séquence d'ADN dans le noyau à l'aide d'un vecteur viral comme un rétrovirus ou de vecteurs non viraux comme des nanoparticules. Le thérapie génique *ex vivo* a été initialement développé en utilisant des vecteurs viraux pour délivrer des gènes thérapeutiques.

Parmi tous les virus, les rétrovirus ont été utilisés avec succès comme véhicule viral. Le vecteur lentiviral (LVV) issu du virus de l'immunodéficience humaine (HIV) et le vecteur γ-rétroviral (γ-RV) issu du virus de la leucémie murine (MLV) sont les principaux vecteurs viraux utilisés pour la thérapie génique *ex vivo* dans les essais cliniques en raison de leur capacité à intégrer l'ADN double brin dans le génome de l'hôte et de leur grande capacité d'encapsulation des transgènes (7-10kb) (Worgall et Crystal, 2014 ; Poletti et Mavilio, 2018). Afin d'utiliser le vecteur viral comme véhicule pour la livraison du transgène, la machinerie réplicative du génome du rétrovirus a été retirée afin d'éviter toute réplication et propagation des vecteurs modifiés. Aussi, le tropisme des vecteurs RV peut être modifié afin d'augmenter l'efficacité de la transduction pour les HSCs puisque, par exemple, le VIH infecte que les lymphocytes T. Dans ce but, le gène encodant la protéine de l'enveloppe du RV non réplicative est composé des glycoprotéines G du virus de la stomatite vésiculaire (VSV-G). Les RV non réplicatifs pseudotypés avec VSV-G ont un tropisme pour un large éventail de types de cellules, sont plus faciles à produire (Okimoto et al., 2001), et la protéine VSV-G n'a pas d'immunité humaine préexistante (Hastie et al., 2013).

Les γ-RV non réplicatifs mis au point ont été utilisés dans des essais cliniques pour traiter le déficit immunitaire combiné sévère lié au chromosome X (SCID-X) causé par une déficience du récepteur de l'interleukine 2 entraînant une immunodéficience chez le patient. Bien que les TG *ex vivo* aient réussi à restaurer l'immunité des patients, 25% d'entre eux développent une leucémie causée par la transactivation du pro-oncogène par le γ-RV (Fischer et al., 2010 ; G. Ferrari et al., 2021). Malgré ces limites, les essais cliniques se poursuivent avec le γ-RV (NCT01129544) et le premier traitement par γ-RV, Strimvelis, pour l'immunodéficience combinée sévère par déficit en adénosine désaminase (ADA-SCID) a été approuvé par la Food and Drug Administration (FDA) en 2016 (NCT04959890).

Néanmoins, cet événement indésirable a conduit au développement de vecteurs inactivés dans lesquels le promoteur naturel du rétrovirus a été supprimé pour empêcher la transactivation du pro-oncogène (Sinn et al., 2005 ; Hacein-Bey-Abina et al., 2014). La suppression du promoteur naturel a nécessité l'utilisation d'un promoteur exogène qui doit être ajouté avant la séquence du transgène. De plus, le LVV semble être moins génotoxique que le γ-RV, c'est pourquoi les LVV sont maintenant

préférentiellement utilisés dans les TGs *ex vivo* (G. Ferrari et al., 2021).

10.2 EDITION DU GENOME DES HSCS POUR LES MALADIES GENETIQUES

La TG *ex vivo* donne lieu à une greffe hématopoïétique stable et sûre à long terme, capable de reconstituer le système sanguin complet tout en produisant la protéine thérapeutique pour un large éventail de troubles tels que les hémoglobinopathies et les anomalies métaboliques (Naldini, 2019 ; G. Ferrari et al., 2021). L'édition du génome est le saint graal de la TG car elle permet d'effectuer une modification précise de la ou des mutations sous-jacentes du patient ou de cibler l'intégration d'un gène fonctionnel dans un locus spécifique. L'édition du génome repose sur deux événements séquentiels : le clivage de la nucléase sur le locus d'intérêt et la réparation précise de l'ADN pour introduire la modification souhaitée. Dans cette tentative, trois générations de nucléases programmables (Nucléases à doigt de zinc : ZFNs, Nucléases effectrices de type activateur de transcription : TALENs, et Courtes répétitions palindromiques groupées et régulièrement espacées CRISPR- associé à une protéine : Cas) ont été développées et sont maintenant évaluées dans des essais cliniques (Shamshirgaran et al., 2022). Alors que le ZFN et le TALEN nécessitent une ingénierie des protéines pour l'interaction avec l'ADN, le système CRISPR-Cas est une endonucléase ADN guidée par l'ARN et ne nécessite qu'une modification de la séquence d'ARN pour cibler différents locus génomiques. Le système CRISPR-Cas a été divisé en deux classes : la classe 1 est composée des types I, III et V qui utilisent plusieurs protéines Cas pour cliver l'ADN étranger tandis que la classe 2 comprend les types II, V et VI qui utilisent une seule protéine Cas pour les cassures double brin (DSB). Le système CRISPR-Cas le plus répandu est un système de classe II, la nucléase Cas9 de *Streptococcus pyogenes* (SpCas9). La nucléase Cas9 est composée de 2 domaines nucléasiques : HNH et RuVC capables de cliver le brin ciblé de l'ARN et le brin complémentaire pour induire un cassure double brin. Initialement, le système CRISPR-Cas était constitué d'une protéine spCas9 couplée à un duplex d'ARN tracrRNA:crRNA capable respectivement d'interagir avec la protéine Cas9 et de lier l'ADN double brin (ds-DNA). Actuellement, un ARN guide fusionné (gRNA) a été conçu avec la séquence complémentaire de l'ARN 5' pour le site cible de l'ADN (« spacer » de 20 nucléotides (nts)) et une structure de liaison Cas9-ARN en 3'. Pour la reconnaissance des gARN, le site cible de l'ADN doit contenir une courte séquence de 3 nts de motif proto-spacer-adjacent (PAM) spécifique au Cas

utilisé tel que le motif NGG (N = A, T, C, ou G) pour spCas9 et un site cible de 20 nts d'ADN. Enfin, le complexe ARN/Cas9 reconnaît les séquences PAM et du « spacer » lie les séquences complémentaires de l'ADN de 20 nts. Ensuite, la nucléase Cas9 induit un cassure double brin 3 base paires (bps) en amont de la séquence PAM. En cas de cassure double brin, trois voies principales de réparation de l'ADN peuvent être mises en œuvre :

- La jonction des extrémités non homologues (NHEJ) est une voie sujette aux erreurs qui entraîne l'insertion et/ou la délétion (indels) de quelques nucléotides au niveau du site de clivage.
- La réparation dirigée par homologie (HDR) vise à insérer ou à remplacer de manière ciblée une séquence d'intérêt par recombinaison homologue. En fait, la HDR s'appuie sur un ADN donneur contenant un site de clivage entouré d'un large bras d'homologie (HA) pour insérer précisément une séquence d'ADN. Lors de l'édition CRISPR-cas9, des oligodéoxynucléotides simple brin (ssODN) ou de l'ADN double brin, délivrés par des vecteurs viraux, des vecteurs non viraux ou des méthodes de transfection, peuvent être utilisés comme ADN donneur dans le locus génomique ciblé.
- La jonction terminale médiée par la microhomologie (MMEJ) aboutit également à l'intégration ou à la correction de la séquence d'ADN en utilisant HA minimal (5-25bps) autour du site de coupe et entraîne la génération d'indels sur le site ciblé (Yanik et al., 2018).

Le mécanisme de réparation des cellules après une double brin dépend des phases du cycle cellulaire qui est composé de 4 phases : la phase S correspondant à la phase de réplication de l'ADN, la phase de mitose (M) conduisant à la division des cellules et 2 interphases : G1 et G2. Le NHEJ est principalement actif pendant l'interphase, tandis que le HDR est préférentiellement utilisé pendant les phases S et G2, ce qui explique le faible nombre d'événements HDR dans les cellules non-divisées telles que les HSCs. Enfin, le mécanisme de réparation MMEJ est impliqué pendant les phases G1 et S (Taleei et Nikjoo, 2013).

La technologie CRISPR-Cas 9 a un large éventail d'applications allant de la perturbation d'un gène pour étudier sa fonction à l'insertion d'une séquence d'ADN dans le site de rupture via la réparation HDR ou MMEJ. Cette dernière représente l'une des approches prometteuses pour traiter les troubles monogénétiques (S. Ferrari et al., 2021).

Pour traiter un trouble monogénique, une copie fonctionnelle du gène muté peut être ciblée soit dans son locus naturel sous le contrôle de son promoteur physiologique, soit sous le contrôle d'un promoteur superactif, soit dans un locus refuge (Pavani et Amendola, 2020). Dans l'ensemble, ces stratégies visent à produire des protéines thérapeutiques à un niveau physiologique ou supraphysiologique pour corriger le trouble monogénique. Le développement de telles stratégies en TG *ex vivo* nécessite à la fois une édition efficace dans le locus cible et la livraison du donneur d'ADN dans le noyau des HSCs. La méthode la plus adoptée pour l'édition *ex vivo* consiste en l'électroporation du complexe ribonucléoprotéique (RNP) de Cas9 et du gARN, qui permet une édition efficace avec une cytotoxicité raisonnable dans les HSCs. Les méthodes de délivrance d'ADN sur les sites de coupures sont basées sur deux approches : virale ou non virale et reposent principalement sur l'intégration basée sur la HDR (Drysdale et al., 2021).

La méthode d'HDR à base virale repose sur la transduction des HScs avec un virus adéno associé (AAV) ou un LV intégratif déficient (IdLV). L'infection des cellules par l'AAV dépend de la reconnaissance des récepteurs glycosylés de la surface cellulaire qui entraînent l'endocytose du virus. Le système cytosquelettique assure le trafic de l'endosome viral à travers le noyau pour délivrer le génome viral. Lors de l'infection par l'AAV, le génome viral peut s'intégrer dans le locus site d'intégration 1 de l'AAV (*AAVS1*). Pour être utilisés comme vecteurs de TG, les AAV ont été modifiés pour éviter la réplication virale. Dans le cadre de la thérapie génique *ex vivo*, la capside AAV6 présente le tropisme le plus élevé pour les HSCs et a été utilisée pour l'insertion ciblée de gènes d'intérêt. Pour assurer une HDR efficace, l'AAV6 a été conçu pour coder le transgène d'intérêt avec de longs bras d'homologie (300-800bps) pour le locus ciblé (Azhagiri et al., 2021). Le donneur HDR AAV6 a été testé pour corriger le X-SCID (Rai et al., 2020) et les défauts métaboliques (Gomez-Ospina et al., 2019 ; Scharenberg et al., 2020). Néanmoins, l'infection par l'AAV6 entraîne une cytotoxicité

qui réduit la repopulation des HSCs dans la moelle ossuese et limite leur emploi (Romero et al., 2019). Par conséquent, d'autres modèles d'administration plus sûrs sont actuellement à l'étude, notamment le vecteur IdLV.

Les IdLV ont une intégrase déficiente en raison de la mutation D116 qui perturbe le domaine catalytique de l'intégrase et ont été développés initialement pour éviter la mutagenèse insertionnelle (Banasik et McCray, 2010 ; Azhagiri et al., 2021). Les IdLV sont principalement utilisés dans la stratégie HDR en raison de leur potentiel de chargement jusqu'à ~ 10 kbs. Romero et al, 2019 compare les modèles donneurs IdLV et AAV6 après édition ZNF ou CRISPR-Cas9 sur la drépanocytose (SCD) et montre que IdLV est moins cytotoxique mais avec une efficacité HDR limitée par rapport à AAV6.

Durant ma thèse, nous sommes intéressées à la thérapie génique *ex vivo* pour les hémoglobinopathies et les maladies héréditaires métaboliques.

10.3 HEMOGLOBINOPATHIES ET THERAPIE GENIQUE :

Les 2 principales β-hémoglobinopathies sont la drépanocytose (SCD) et la β-thalassémie, toutes deux entraînant une anémie du patient et représentant chaque année 400 000 naissances affectées (Frati et Miccio, 2021).

La SCD est causée par une mutation ponctuelle de A à T dans le gène de la β-globine, qui entraîne une substitution d'acides aminés E6V dans les chaînes de la β-globine (β^S), formant l'hémoglobine S (HbS). En condition désoxygénée, les HbS se polymérisent endommageant les érythrocytes en formant des globules rouges falciformes inflexibles (Cavazzana et al., 2017). En conséquence, les globules rouges falciformes provoquent une anémie hémolytique et une vaso-occlusion qui entraîne des dommages ischémiques aux tissus, déclenchant des douleurs et une défaillance des organes. Au fil du temps, des complications chroniques peuvent survenir sous la forme d'une vasculopathie (hypertension pulmonaire, maladie vasculaire cérébrale...) ou d'un dysfonctionnement progressif des organes (lésions hépatiques, insuffisance rénale...). La gravité de la SCD dépend de la polymérisation

de l'HbS et donc de la quantité d'Hb dans les GR. Les patients souffrant de SCD peuvent présenter différents traits améliorant leur phénotype comme l'expression de l'hémoglobine fœtal (HbF) ou les traits de l'α-thalassémie. Dans l'α-thalassémie, 1 ou 2 copies des 4 gènes de l'α-globine sont supprimées, ce qui diminue la production d'α-globine et donc la formation d'Hb. La réduction de l'Hb chez les patients atteints de SCD présentant des traits α-thalassémie entraîne une diminution de la polymérisation de l'HbS et de la gravité de la maladie et augmente la survie des patients (Belisário et al., 2010 ; Rumaney et al., 2014 ; Piel et al., 2017).

La β-thalassémie est le résultat d'un large éventail de mutations dans les gènes de l'α-globine, allant d'une mutation ponctuelle à de grandes délétions, qui touchent 1,5 % de la population mondiale. Les mutations dans les gènes de l'α-globine entraînent une diminution de la production de la chaine α-globine et donc de la quantité d'HbA. La gravité des phénotypes dépend de la mutation sous-jacente : β+ indique une ou plusieurs mutations légères avec une diminution relative de l'expression des chaînes de -globine ; β0 correspond à une ou plusieurs mutations sévères entraînant l'abrogation complète de la synthèse des chaînes de β-globine. L'absence de chaînes de β-globine entraîne la précipitation des chaînes d'α-globine dans les précurseurs érythroïdes et les érythrocytes, ce qui est associé à une altération de l'érythropoïèse et de l'hémolyse des globules rouges (Cavazzana et al., 2017 ; Taher et al., 2021). Comme la SCD, deux conditions peuvent réduire la quantité de chaînes d'α-globine libres : l'α-thalassémie qui diminuent la gravité de la maladie causée par la précipitation des chaînes d'α-globine et l'expression des HbF qui remplacent la β-globine et réduisent le déséquilibre entre les chaînes d'α- et β-globines et améliorent le phénotype (Taher et al., 2021 ; Magrin et al., 2019 ; Cavazzana et al., 2017).

Afin d'offrir un traitement curatif pour la SCD et de la β-thalassémie, des approches de GT *ex vivo* ont été développées et se concentrent principalement sur l'insertion d'un gène fonctionnel de la β-globine ou sur la synthèse de l'HbF. En effet, l'insertion d'une copie fonctionnelle du gène sain de l' β-globine (HBB) dans les HSCs de patient offre la possibilité de produire des chaînes d' β-globine saines, corrigeant ainsi la précipitation de l'HbS dans la SCD et ajustant la synthèse normale de l'HbA dans l' β-thalassémie. D'autres solutions de correction des HSCs ont été proposées, basées sur

l'édition de gènes pour améliorer la production d'HbF ou la correction de la mutation sous-jacente de la β-globine.

10.4 TROUBLE HEREDITAIRE DU METABOLISME ET THERAPIE GENIQUE :

Les erreurs innées du métabolisme (IEM) sont causées par un défaut génétique sur une voie métabolique qui entraîne une déficience de la fonction métabolique et perturbe l'homéostasie. Aujourd'hui, environ 1000 IEMs ont été décrites avec une incidence cumulée d'environ 1/800. Les IEMS sont classées en fonction du groupe d'enzymes défectueuses, des substrats toxiques accumulés ou des organites affectés. Par conséquent, les IEMS sont des groupes hétérogènes de maladies comprenant les troubles des acides aminés, les maladies de l'oxydation des acides gras, les dysfonctionnements mitochondriaux, les maladies du stockage des lipides et les troubles du stockage lysosomal (LSD). Les défauts génétiques peuvent être causés par des mutations ponctuelles, des délétions, des insertions ou des réarrangements chromosomiques qui entraînent la perte d'une enzyme active, d'un transporteur ou d'un cofacteur, ce qui provoque un dysfonctionnement des voies métaboliques ou une accumulation toxique de métabolites. Le diagnostic repose donc sur des tests génétiques et des dosages enzymatiques qui sont disponibles dans le cadre du dépistage néonatal ou du diagnostic prénatal. La prise en charge de la IEM comprend un régime alimentaire spécifique, un traitement enzymatique substitutif (ERT), l'inhibition du substrat ou même la transplantation d'organes ou HSCs (Mak et al., 2013 ; Ezgu, 2016).

Les maladies lysosomales (LSD) sont une sous-famille des IMEs, à l'origine d'environ 70 maladies monogéniques à transmission autosomique récessive ou liée à l'X. Les LSDs sont le résultat d'une ou plusieurs mutations dans des gènes codant pour des protéines lysosomales (nucléase, lipase, glucosidase...) ou des transporteurs membranaires qui génèrent une accumulation de substrats toxiques (lipides, protéines, glucides) altérant la fonction normale du lysosome. En raison de son rôle dans la dégradation des molécules complexes, le foie est souvent affecté par le LSD même si la sévérité de l'atteinte dépend du produit génique déficient. Les macrophages jouent également un rôle central dans l'élimination des débris cellulaires et des produits métaboliques déficients, ce qui entraîne un dysfonctionnement de cette population immunitaire dans les LSDs pouvant déclencher

une inflammation et aggraver la progression de la maladie (Parenti et al., 2021 ; Platt et al., 2018 ; Ezgu, 2016). Globalement, l'incidence des LSDs est d'environ 1:5000 naissances vivantes, mais en prenant individuellement l'incidence des troubles monogéniques sont rares : 1:50000 - 1:250 000 naissances vivantes (Platt et al., 2012, 2018). Les LSDs sont des troubles hétérogènes mais des phénotypes cliniques communs ont été décrits chez les patients tel que : hépatomégalie et splénomégalie. La gravité de la maladie dépend principalement de la ou des mutations qui provoquent soit un début précoce de la maladie chez les patients pédiatriques (forme sévère), soit un début tardif chez les jeunes ou les adultes (forme légère à asymptomatique) (Platt et al, 2018 ; Ezgu, 2016). Dans les LSDs causés par un déficit en hydrolase, la gravité des maladies correspond à l'activité enzymatique résiduelle. Pour le LSD, il existe 2 stratégies thérapeutiques principales :

- La thérapie de remplacement d'enzyme (ERT) est un traitement courant pour le LSD causé par une déficience en hydrolase et consiste en une injection intraveineuse de l'enzyme recombinante manquante visant à dégrader l'accumulation toxique lysosomale. Chez le patient, l'enzyme délivrée par voie sanguine est absorbée par le récepteur M6P-R présent à la surface de nombreux types de cellules et cibler les lysosomes pour remplacer la fonction enzymatique manquante. Le traitement améliore le phénotype clinique du patient et augmente sa durée de vie, mais il reste assez coûteux et nécessite une administration hebdomadaire tout au long de la vie du patient. L'ERT est limité par le développement d'une réponse immunitaire contre l'enzyme recombinante qui peut diminuer l'efficacité du traitement et entraîner un choc anaphylactique. L'ERT n'est pas non plus capable de traverser la barrière hémato-encéphalique pour corriger l'atteinte neurologique et est inaccessible pour certains organes comme le système cardiovasculaire ou la fonction oculaire (Platt et al., 2018).
- HSCT : Le principe est similaire à celui de l'ERT ; au lieu de l'injection d'enzyme, ce sont des cellules saines de donneur qui vont produire la protéine manquante. En fait, lors d'une HSCT, les cellules dérivées de la moelle osseuse d'un donneur sain peuvent produire une enzyme fonctionnelle qui peut corriger les tissus affectés via une correction croisée. Malgré l'amélioration des caractéristiques cliniques, la production de l'enzyme manquante lors d'une HSCT reste faible et n'atteint pas un niveau correctif pour les patients (Nagree et al., 2019 ; Platt et al., 2018).

Le développement de nouvelles options thérapeutiques peut également tirer parti du criblage cellulaire pour identifier les molécules candidates au LSD (Parenti et al., 2021). L'utilisation de ce type de test cellulaire pour quantifier les lysosomes et leur contenu à l'aide de sondes spécifiques a été employée dans différentes LSDs afin de trouver des traitements thérapeutiques ou de suivre le phénotype de la maladie (Xu et al., 2012a ; Aguisanda et al., 2017b). La quantification des vésicules basée sur l'image des cellules peut également tirer parti de la cytométrie en flux d'image (IFC) récemment développée pour améliorer encore la spécificité et la précision de la mesure. En effet, l'IFC combine la cytométrie en flux qui permet l'analyse unitaire du signal de fluorescence ou de la diffraction lumineuse des cellules en suspension avec l'imagerie par microscopie qui prend une image réelle des cellules acquises. Enfin, l'algorithme IFC permet de visualiser et de quantifier la localisation et le nombre d'événements de fluorescence dans les cellules acquises. L'IFC a été récemment employée pour l'analyse de la phagocytose des macrophages (Mochalova et al., 2022), ou l'analyse des vésicules extracellulaires dans le plasma humain (Woud et al., 2022) ouvrant la voie à l'utilisation de l'IFC comme diagnostic ou pipeline de découverte de médicaments pour le LSD.

Parmi les LSDs, nous nous sommes concentrés sur la déficience en lipase acide lysosomale (LAL). La LAL est une enzyme impliquée dans la dégradation des triglycérides (TGs) et des esters de cholestérol (CEs) dans les lysosomes de presque tous les types de cellules, notamment les macrophages et les hépatocytes. La LAL est activée par un pH acide et hydrolyse les CE et les TG en cholestérol libre (FC) et en acides gras libres (FFA) qui servent de source d'énergie par oxydation des acides gras, ou à la formation de membranes ou biosynthèse de composés dérivés du cholestérol (Li et Zhang, 2019). Le LAL est codé par le gène de la lipase A (LIPA) (10q23.2-23.3, 10 exons). 120 mutations de LIPA ont été identifiées et sont associées à la déficience en LAL (LAL-D), un LSD autosomique récessif. Le LAL-D déclenche l'accumulation de CEs et de TGs dans les tissus et les organes, en particulier dans le foie, la rate, l'intestin et les macrophages, ce qui entraîne une défaillance de plusieurs organes. La gravité de la maladie dépend de la quantité restante d'enzyme fonctionnelle. Deux formes ont été caractérisées : le trouble du stockage des esters de cholestérol (CESD, prévalence 1/40 000 naissances

vivantes), moins grave et à apparition tardive, avec environ 2-12% d'enzyme fonctionnelle ; la maladie de Wolman (WD, prévalence 1/100 000 naissances vivantes), forme grave du trouble à apparition précoce, avec moins de 2% d'enzyme LAL fonctionnelle. Les patients atteints de LAL-D souffrent d'hépatomégalie, de splénomégalie et d'hyperlipidémie sans atteinte du système nerveux central. Les patients atteints de WD présentent des difficultés à se développer, une malabsorption intestinale et une calcification des glandes surrénales, le tout conduisant à un décès prématuré dans la première année suivant la naissance si non traités. Les patients atteints de la maladie de CESD présentent un tableau clinique plus bénin avec une athérosclérose et une affection cardiaque prématurées qui pourraient entraîner la mort dans l'enfance ou l'adolescence si elles ne sont pas traitées (Witeck et al., 2022). L'ERT est le traitement standard après le diagnostic du LAL-D et consiste en l'administration intraveineuse hebdomadaire d'une enzyme recombinante du LAL appelée Sebelipase (Kanuma®, Alexion Pharmaceuticals, Inc.). Ce traitement non curatif améliore la durée de vie des patients et les caractéristiques cliniques, principalement la fonction hépatique. Néanmoins, l'ERT a été associé au développement d'anticorps contre l'enzyme recombinante chez 9% des patients traités, il reste très coûteux et son efficacité à long terme est en cours d'évaluation (Burton et al., 2022 ; Vijay et al., 2020). La greffe de cellules souches hématopoïétiques peut également être utilisée pour le LAL-D et montre une normalisation de la fonction hépatique, mais elle est associée à une morbidité élevée et est limitée par l'aptitude du donneur ou la maladie du greffon contre l'hôte (Tolar et al., 2009 ; Potter et al., 2021).

Pour traiter les LSDs, il existe plusieurs stratégies de GT qui ciblent soit les hépatocytes par GT *in vivo*, soit les HSCs par GT *ex vivo*. Les deux stratégies sont basées sur le remplacement, l'ajout ou la correction classique de gènes à l'aide du LVV, de l'AAV ou de l'édition du génome. Le principal avantage de la TG *ex vivo* pour le LSD provient de la capacité de l'enzyme produite par les cellules corrigées à être sécrétée et à être absorbée via la reconnaissance du M6P-R pour corriger même les cellules non modifiées.

10.5 OBJECTIVES DE THESE ET RESULTATS :

Dans la TG *ex vivo*, l'intégration ciblée d'une copie fonctionnelle d'un gène muté dans un locus sûr constitue une thérapie appropriée pour traiter un large éventail de troubles monogéniques. Dans ce contexte, nous avons exploité le locus de l'α-globine (HBA) comme un locus sûr pour développer une plateforme universelle pour l'expression et la sécrétion de protéines thérapeutiques dans les cellules érythroïdes. En effet, le locus HBA exprime fortement la chaîne de α-globine (environ 1,5g/jour) et la perte de 3 des 4 gènes HBA est asymptotique (Vichinsky, 2013). Par conséquent, le détournement du promoteur HBA devrait entraîner une expression élevée du transgène sans interférer avec la formation normale de l'Hémoglobine. La correction LV des HSCs à l'aide du promoteur érythroïde a démontré la capacité des cellules érythroïdes à produire des chaînes de l'α-globine et à soutenir la sécrétion de protéines fonctionnelles comme le facteur de coagulation (Chang et al., 2006) ou l'enzyme métabolique comme l'IDUA pour le syndrome de Hurler (Wang et al., 2009)). En raison de l'abondance des cellules érythroïdes chez l'homme ($5X10^6$ globules rouges/microlitre de sang) et de la forte expression de HBA dans la population érythroïde, la plateforme ciblant HBA nécessiterait un minimum d'événements d'édition et d'intégration pour maximiser la production et la sécrétion de la protéine dans la circulation sanguine, réduisant ainsi l'effet hors-cible induit par CRISPR-cas 9 et la toxicité dus à l'édition et à la livraison du donneur d'ADN. Au cours de ma thèse, j'ai participé à l'évaluation du KI basé sur CRISPR dans le locus HBA pour la β-thalassémie qui combinait la réduction de l'expression de la α-globine causée par la délétion de HBA 2 et l'insertion du gène de la β -globine dans le locus HBA pour restaurer le déséquilibre α/β. La délétion de l'HBA2 dans une lignée cellulaire β-thalassémique éditée ou dans des HSCs de patient améliore la précipitation de la α-globine comme observé chez le patient ayant un trait α-thalassémique. Ainsi, le détournement des promoteurs de l'HBA pour produire des chaînes β restaure le déséquilibre α/β et conduit à une formation significative d'hémoglobine adulte. Les cellules CD34+ modifiées ont été transplantées avec succès chez des souris immunodéprimées et ont pu conserver leur potentialité à générer toutes les lignées sanguines.

Ensuite, nous avons appliqué la plateforme ciblée du locus HBA pour l'expression érythroïde et la sécrétion de protéines thérapeutiques comme les facteurs de coagulation IX responsables de l'hémophilie B et différentes enzymes lysosomales comme la α-galactosidase (GLA) responsable de la maladie de Fabry, l'Iduronidase (IDUA) responsable de la mucopolysaccharidose et la lipase acide

lysosomale (LAL) responsable de la maladie de Wolman (WD). La plateforme montre une édition efficace des gènes dans le locus HBA, ce qui conduit à une expression robuste des transgènes thérapeutiques lors de la différenciation érythroïde. En effet, l'enzyme LAL sécrétée par les érythroblastes LIPA KI a été capable de corriger l'accumulation de lipides dans les fibroblastes de la maladie de Wolman, mettant en lumière le bénéfice thérapeutique de cette stratégie. La transplantation de CD34+ édités chez des souris immunodéprimées a été réussie avec un maintien du potentiel de différenciation.

Nous nous sommes ensuite concentrés sur l'optimisation du transgène de la LIPA en utilisant des LVVs pour améliorer l'expression et la sécrétion de la LAL. À cette fin, j'ai développé des LVVs codant pour la séquence LIPA sous le promoteur érythroïde afin de produire du LAL dans des cellules érythroïdes matures. Le transgène LIPA optimisé servira à la TG *ex vivo* basée sur les LVVs et à notre plateforme ciblée HBA dans le but d'améliorer l'expression du LAL tout en minimisant les événements d'intégration dans le locus HBA nécessaires pour corriger complètement le LAL-D. L'optimisation du peptide signal et des codons d'usage entraînent tous deux une augmentation de 15 fois de la sécrétion fonctionnelle de LAL sur les HSCs différenciés érythroïdes.

Enfin, nous avons mis en place une approche cytométrique multimodale utilisant la cytométrie en flux et la cytométrie en flux d'images (IFC) pour mieux caractériser le phénotype LAL-D et évaluer la puissance thérapeutique de la TG. Nous avons évalué cette approche sur des fibroblastes de patients atteints de WD, sur des cellules Jurkat modifiées par LIPA KO et sur des PBMC pour le modèle de souris LAL-D. L'IFC permet de quantifier les vésicules lipidiques aussi bien sur la coloration Nile Red que sur le paramètre SSC et met en évidence une différence d'un facteur 100 entre les fibroblastes WD et WT. Les Jurkat LIPA KO et les mPBMCS des souris LIPA KO récapitulent l'accumulation de lipides observée dans les fibroblastes WD. Afin de valider davantage cette stratégie, nous prévoyons d'utiliser prochainement les PBMCs de patients atteints de LAL-D provenant de l'institut Necker. Cette approche pourrait être appliquée comme pipeline de suivi pour les patients atteints de LAL-D ou pour évaluer l'effet thérapeutique de la construction virale ou les lots de production.